Global Genome Nucleotide Excision Repair Factors and The Ubiquitin-Proteasome System Regulate The DNA Damage Response in *Saccharomyces cerevisiae*

Department of Pathology
Cardiff University

Neil Humphryes

UMI Number: U518562

UMI U518562

Declaration

This work has not previously been accepted in substance for any degree and is not concurrently in candidature for any degree.

Signed ....(Candidate) Date ......9/11/10...

STATEMENT 1:

This thesis is being submitted in partial fulfilment of the requirements for the degree of PhD.

Signed ....(Candidate) Date 9/11/10
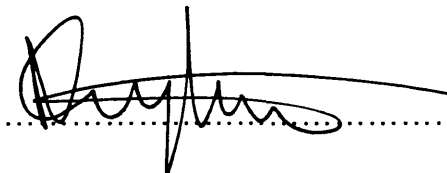
STATEMENT 2:

This thesis is the result of my own independent work/investigation, except where otherwise stated. Other sources are acknowledged by explicit references.
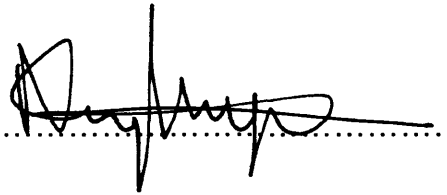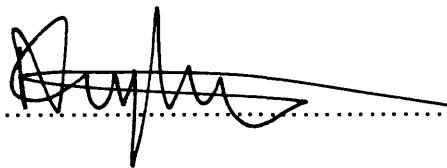
Signed ....(Candidate) Date 9/11/10

STATEMENT 3:

I hereby give consent for my thesis, if accepted, to be available for photocopying and for inter-library loan, and for the title and summary to be made available to outside organisations.

Signed ....(Candidate) Date 9/11/10

STATEMENT 4: PREVIOUSLY APPROVED BAR ON ACCESS

I hereby give consent for my thesis, if accepted, to be available for photocopying and for inter-library loans **after expiry of a bar on access approved previously by the Graduate Development Committee.**

Signed ....(Candidate) Date ....

Acknowledgements

Summary

The DNA damage response triggers a complex regulatory network to protect genomic integrity and promote cell survival by inducing effects such as cell cycle arrest, upregulation of dNTP synthesis and DNA repair. The Nucleotide Excision Re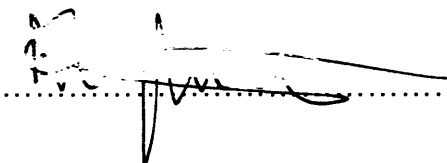pair (NER) pathway removes a broad array of DNA lesions by excising the damage with surrounding DNA and resynthesising the DNA using the undamaged strand as the template. NER consists of two sub-pathways that remove lesions from transcribed DNA (TC-NER), or from the rest of the genome (GG-NER). It has been proposed more recently that NER factors have additional regulatory roles in the DNA damage response.

The initial aim of the study was to identify a possible regulatory interaction between the Abf1 protein and the 19S proteasome. *abf1* and *sug* (proteasome) mutant alleles were employed to identify a functional interaction between the factors but a significantly altered mutant phenotype could not be identified.

The study proceeded to investigate a regulatory role of the Rad4-Rad23 NER complex in the DNA damage response via Rad7-dependent ubiquitination of Rad4. Previous evidence suggested that post-UV Rad4 ubiquitination has a regulatory role in DNA damage-responsive transcription.

Global analysis of gene expression revealed that genes involved in dNTP synthesis, including the Ribonucleotide Reductase (RNR) pathway, were misregulated in a strain unable to ubiquitinate Rad4. The study progressed to investigate the function of the Rad4-Rad23 complex in regulation of the RNR pathway.

It was discovered that constitutive activation or expression of the RNR pathway could suppress the UV sensitivity of the E3 ligase-defective strain, thus suggesting that the Rad7-E3 ligase has a role in regulating cellular dNTP levels in response to DNA damage. The Rad4-Rad23 complex binds at the *DUN1* promoter, a positive regulator of the RNR pathway.

E3 ligase-defective mutant strains were also found to exhibit defective cell cycle progression in the presence and absence of DNA damage. This defective cell cycle progression is suppressed by upregulating the RNR pathway. This further supports a role of the Rad7 E3 ligase in regulation of cellular dNTP levels.

These results indicate a role of the Rad7 E3 ubiquitin ligase in regulation of cellular dNTP levels in the DNA damage response.

Abbreviations

19S – 19S Proteasome Regulatory Complex

20S – 20S Proteasome Core Particle

6-4 PP – Pyrimidine-Pyrimidone 6-4 Photoproduct

6-AU – 6-Azauracil

AAA – ATPases Associated with Diverse Cellular Activities

ATP – Adenosine Triphosphate

BER – Base Excision Repair

bp – base pairs

ChIP – Chromatin Immunoprecipitation

CPD – Cyclobutane Pyrimidine Dimer

DBD – DNA-Binding Domain

DDR – DNA Damage Response

DNA – Deoxyribonucleic Acid

dNDP – Deoxyribonucleotide Diphosphate

dNTP – Deoxyribonucleotide Triphosphate

dsb – Double-Strand Break

dsDNA – Double-Stranded DNA

fc – Fold Change

GAL – Galactose-inducible

HAT – Histone Acetyltransferase

HDAC – Histone Deacetylase

MMR – Mismatch Repair

NER – Nucleotide Excision Repair

ORF – Open Reading Frame

PIKK – Phosphatidylinositol 3' Kinase-like Kinase

RNR – Ribonucleotide Reductase

ROS – Reactive Oxygen Species

RPA – Replication Protein A

RT – Room Temperature

SAGA – Spt-Ada-Gcn5-Acetyltransferase

ssb – Single-Strand Break

ssDNA – Single-Stranded DNA

SUG – Suppressor for Galactose

TLS – Translesion Synthesis

UAS – Upstream Activating Sequence

UPS – Ubiquitin Proteasome System

UV – Ultra-violet (light)

WT – Wild-Type

YDB – Yeast Dialysis Buffer

Contents

1 Introduction

The study of biological pathways within cells aspires to elucidate the complex interactions required for cellular metabolism and survival. Although these pathways can be studied as separate entities, the subtle interplay between distinct biological pathways is of paramount importance, and with the emergence of global techniques to study genetic regulation the complex network of inter-regulated pathways is being revealed. This study aims to investigate specific aspects of several cellular pathways that respond to UV radiation, and how they function together in the DNA damage response to maintain cellular integrity.

1.1 *Saccharomyces cerevisiae* as a Model Organism

Saccharomyces cerevisiae, also known as budding yeast is a single-celled eukaryotic organism that has been used extensively as a convenient and powerful genetic tool. Many human genes were first discovered as yeast homologues, including regulators of the cell cycle, signalling proteins and factors involved in DNA repair. Yeast has also allowed significant progression in the understanding of processes such as regulatory mechanisms of transcriptional control and cellular metabolism.

Budding yeast cells replicate in an asynchronous manner, a process known as budding. This involves formation of the daughter cell as a protrusion on the surface of the mother cell during DNA replication. The process of budding and the yeast cell cycle is discussed in Section 1.6.

The *S. cerevisiae* genome consists of approximately 12 156 677 bp, containing about 6 000 genes, and organised into 16 linear chromosomes. The yeast genome was the first eukaryotic genome to be fully sequenced, and is thought to be approximately 23% homologous to the human genome (en.wikipedia.org/wiki/Saccharomyces_cerevisiae).

1.2 DNA Damage

Cells are constantly being exposed to environmental damaging agents that can compromise the integrity of biological macromolecules. The damage can result from endogenous sources, such as the production of reactive oxygen species during normal cellular respiration, or environmental sources such as chemical mutagens or electromagnetic radiation. These can inflict damages upon polypeptides, lipids and nucleic acids, including the cell's molecular blueprint, DNA. It is the damage of DNA that can be most detrimental, as damage replication can result in harmful mutagenesis, possibly causing metabolic defects or death in unicellular organisms and genomic instability leading to loss of genetic information in more complex multicellular organisms. This process of DNA damage leading to mutagenesis has a role in molecular evolution, and therefore affects genetic variation to some extent. A subtle equilibrium is required to allow genetic variation to develop, which drives natural selection, whilst maintaining the genomic integrity and stability of the organism, which requires repair of damage. In the absence of environmental damaging agents, a typical human cell must repair 10 000 damage events per day in its DNA, caused mainly by reactive oxygen species, a by-product of cellular respiration, and misincorporation of bases during DNA replication, recombination, or repair leading to spontaneous base changes (Friedberg 2001; Peterson and Cote 2004).

DNA damage can adopt many different forms, ranging from slight molecular alterations at a single base to a double-strand break (dsb), whereby the backbone of both DNA strands are severed. These damages include deamination of cytosine, adenine, guanine or 5-methylcytosine, creating uracil, hypoxanthine, xanthine and thymine respectively. It should be noted that some of these products are not alien in normal DNA, so detection becomes more difficult and mismatching can occur during DNA synthesis (Friedberg 2005b; Lindahl 1993). Reactive oxygen species (ROS) and alkylating agents from endogenous sources can cause adducts such as 8-oxoguanine and O6-methyldeoxyguanosine (Hasty et al. 2003). Whereas some agents act as direct carcinogens, molecules such as benzopyrenes can

become a threat to DNA when metabolised by endogenous enzymes, which increase the solubility of the compound to facilitate excretion. However, this allows the compound to attack and attach itself to DNA, causing a helix-distorting bulky adduct (DeMarini 2004; Friedberg 2005b, 2006; Lindahl 1993). The above-mentioned damages all cause distortion of the DNA double helix. Damaging agents such as ionising radiation, ROS and collapsed replication forks can cause single- or double-stranded breaks (ssb/dsb) which can cause more severe genome instability and chromosomal rearrangements.

1.2.1 UV Radiation and DNA Damage

The damaging effect of UV radiation on DNA has been recognised and utilised as an experimental tool for many decades. It was discovered in the 1930s that although UV radiation posed a threat to living cells, they could survive through relatively large doses, however two groups introduced the notion of DNA damage/repair in the late 1940s (Dulbecco 1949; Kelner 1949). More specifically, this marked the discovery of photoreactivation, whereby the repair was dependent on post-damage exposure to a light source to activate the enzyme responsible. The UV radiation spectrum is categorised into three wavelengths; UV-A (400-320nm), UV-B (320-290nm) and UV-C (290-100nm). Most organisms are subjected to UV radiation on a daily basis from the sun, however solar UV radiation reaching the Earth's surface mainly consists of UV-A and UV-B, as the shorter wavelengths are filtered out by the ozone layer. DNA maximally absorbs UV at 260nm, so a 254nm germicidal lamp is used in laboratory irradiation to have optimum DNA damaging effects. UV radiation predominantly induces two major lesions, which are defined as cyclobutane pyrimidine dimers (CPDs), which constitute ~75% of total damage inflicted after UV-C exposure, or pyrimidine-pyrimidone (6-4) photoproducts (6-4 PPs), which account for ~20% of total damage inflicted after UV-C exposure. Both lesions involve the covalent linking of adjacent pyrimidines (Mitchell 1988). Other UV-induced damage includes purine/pyrimidine hydrates, thymine glycols, DNA cross-links and strand breaks (Friedberg 1995; Ichihashi et al. 2003).

CPDs are frequently formed in DNA exposed to UV radiation and involve two adjacent pyrimidines becoming covalently attached by a cyclobutyl ring formed by saturation of the C5=C6 double bond (Figure 1.1A). This stable conformation causes a distortion of the DNA double helix and is defined as a bulky adduct. The thymine dimer CPD was first discovered in the 1960s, and was found to be induced by exposure of cells to sunlight and a hindrance to DNA metabolic processes such as replication and transcription (Setlow and Carrier 1964). The thymine dimer was later discovered to be the most frequently occurring CPD, which are found in the following ratio; T-T: C-T: T-C: C-C = 68:13:16:3 (Mitchell et al. 1992). CPD induction is greatly influenced by nucleotide sequence. A 5' pyrimidine enhances the probability of CPD formation at adjacent thymines (Gordon and Haseltine 1982). CPD induction is also highly dependent on conformation and organisation of chromatin. The arrangement of DNA within and between nucleosomes can greatly influence CPD formation in both a positive and negative manner (Thoma 1999).
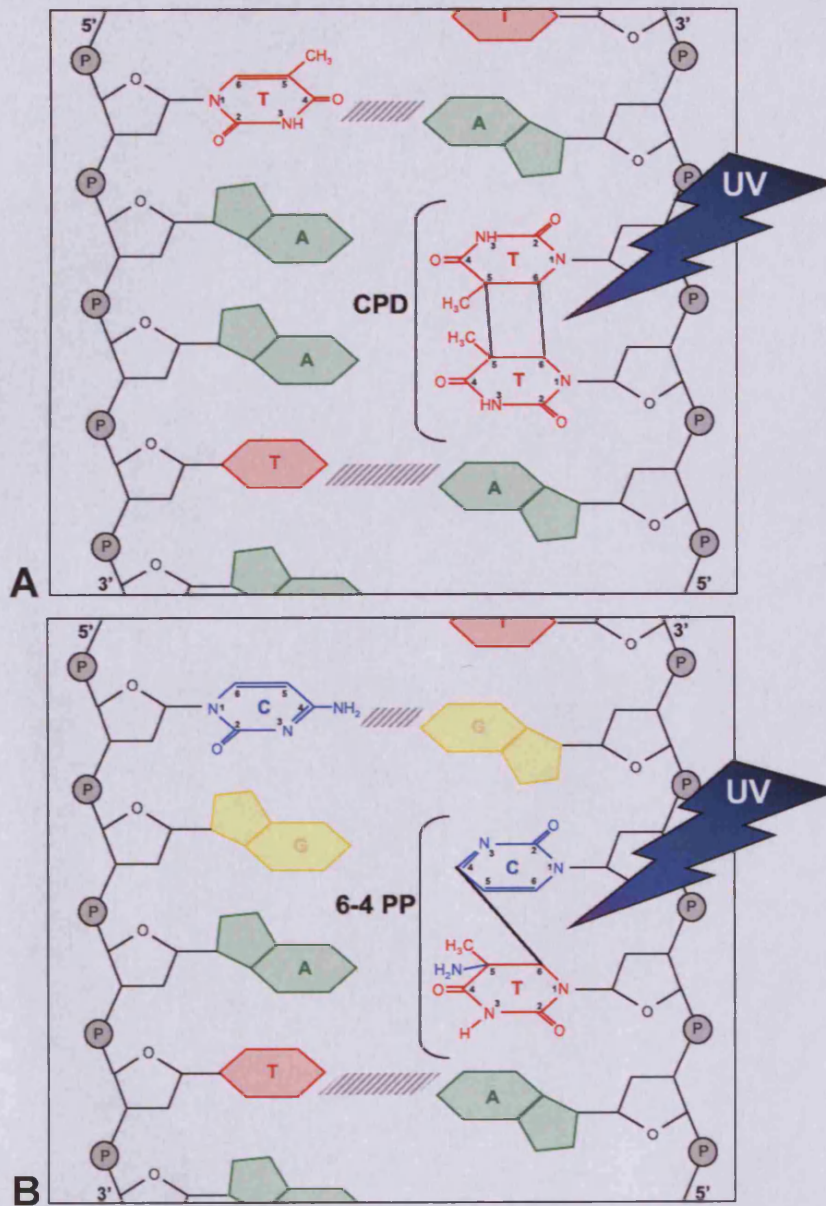
Figure 1.1 - Molecular Structure and Conformation of a UV-induced CPD and 6-4 PP A. UV radiation causes two adjacent pyrimidines to form a cyclobutane dimer by denaturing the C5=C6 bonds. B. UV radiation causes a heterodimer to form between an adjacent Cytosine (at C4) and Thymine (at C6). Figure adapted from (Friedberg 2005b).

Pyrimidine-pyrimidone (6-4) photoproducts (6-4 PP) are also UV-induced lesions formed between adjacent pyrimidines, and are rather less common than the aforementioned CPDs. 6-4 PPs account for 15-30% of UV induced lesions (Mitchell and Nairn 1989). 6-4 PPs most commonly form at cytosine bases located 3' to a pyrimidine. The most abundant 6-4 PP forms between T-C adjacent bases, which occurs much more frequently than C-C and T-T bonds (Mitchell et al. 1990). UV irradiation causes formation of a covalent bond between C6 of the 5' cytosine and C4 of the 3' thymine (Figure 1.1B). This crosslink causes a major helical distortion to the DNA, resulting in a bend of 44°, a far greater disturbance than that inflicted by a CPD (Pearlman et al. 1985). Unlike CPDs, 6-4 PPs are mostly found in linker regions, and inhibited by nucleosomal DNA as suitable bending cannot be achieved.

1.3 DNA Repair

To cope with the plethora of possible DNA lesions, an extensive range of DNA repair mechanisms have evolved. These repair systems each deal with a subset of lesions, allowing very specialised and DNA efficient repair to occur. DNA repair pathways can be divided into two main categories based on their molecular mechanism; direct repair and excision repair. Direct repair acts on the damaged DNA to simply reverse the lesion, retaining the original DNA components, whereas excision repair machinery removes a stretch of ssDNA flanking the lesion either at the base or nucleotide level, and synthesises new DNA in its place. Some repair mechanisms require a dsDNA template from a homologous chromosome to function so can only occur after DNA replication but before mitosis in haploid organisms, whereas other mechanisms can occur at any stage of the cell cycle. Most operate best when the cell cycle is arrested and checkpoint activation facilitates this.

1.3.1 Direct DNA Repair

The most primitive method of DNA repair is simply to directly reverse the offending lesion. Three systems of direct repair are photoreactivation, repair of alkylation damage and removal of single-strand breaks.

Photoreactivation is a mechanism for removing UV-induced CPDs and 6-4 PPs using energy from visible light. It is utilised by many species, excluding humans but including yeast, plants, some bacteria and some mammals such as marsupials (Yasui et al. 1994). A range of photolyases exist, each enzyme specific for a certain lesion, which use energy derived from blue light to separate dimerised pyrimidines, thus correcting DNA helical distortion (Weber 2005).

Minor alkylation of DNA can also be repaired by direct reversal, a pathway evolutionarily conserved from bacteria to humans. Products of the mutagenic agent N-methyl-N'-nitro-N-nitrosoguanidine, which include O6-alkylguanine, can be repaired by the O6-alkylguanine-DNA alkyltransferases, which can remove alkyl groups ranging from methyl to benzyl. The O6-methylguanine-DNA methyltransferase enyzyme operates by transferring a methyl group from guanine in DNA to a cysteine residue within the enzyme (Olsson and Lindahl 1980; Pegg 2000). The proteins that facilitate this type of repair cannot be considered true enzymes as they become permanently inactivated once repair has been catalysed. This class of proteins are also known as 'suicide enzymes'. These alkyltransferases have been found to repair both DNA and RNA.

In the event of a single strand break in the DNA backbone, which can be a result of exposure to ionising radiation, a nick can form whereby no nucleotides are removed. This can be reversed by religation of the 3' hydroxyl and 5' phosphate by a DNA ligase (Friedberg 2005b). However, if the nick progresses to loss of nucleotides or a more severe lesion, additional repair apparatus is required.

1.3.2 Excision Repair

Lesions that disrupt the DNA structure more severely cannot be simply reversed, and require a suitable repair system. Several excision repair pathways exist to deal with a wide variety of damages, however all pathways

include the following stages of repair: lesion detection, invasion and excision, and DNA synthesis and ligation. In general, rather than just undoing the damage, excision repair removes the offending DNA containing the lesion, and resynthesises new DNA using the non-damaged strand as a template. The 3 main excision repair pathways are mismatch repair (MMR), base excision repair (BER) and nucleotide excision repair (NER).

1.3.3 Mismatch Repair

The semi-conservative replication of DNA can on occasions introduce mistakes in nucleotide matching to the template strand. This results in mismatched bases, which if replicated are a source of mutagenesis. Certain DNA sequences are more prone to introduction of mismatched bases during replication or recombination due to the presence of repetative or palindromic nucleotide tracts, which can form secondary structures and pose a challenge to the replicative machinery (Friedberg 2005b). Mismatched bases can also be the result of base damage. Deamination of 5-methyl cytosine, a common base variant in silenced DNA, produces thymine, thus creating a T-G mismatch. MMR can also recognise victims of base oxidation and methylation (Modrich and Lahue 1996). MMR systems require highly sensitive detection systems, as they do not identify bulky chemical adducts or major helical distortions, but they must detect mispaired bases and discriminate which base is incorrectly paired. Once damage is identified, excision and resynthesis can occur in a similar manner to other excision repair pathways (Brown 1999; Friedberg 2005b; Jiricny 2006; Jun et al. 2006). MMR is conserved from prokaryotes to eukaryotes, however the complexity and number of proteins involved has increased dramatically over evolutionary time (Jiricny 2006). Eukaryotes use the MSH and MLH proteins to conduct MMR, whereby the MSH proteins bind to mismatches and promote ATP-dependent repair, and MLH proteins form heterodimers with a variety of proteins to activate MSH proteins. Defective MMR in humans has been implicated in hereditary nonpolyposis colorectal cancer (Kunkel and Erie 2005).

1.3.4 Base Excision Repair

BER acts upon bases with non-bulky chemical adducts. The first stage of BER requires removal of the inappropriate base to produce an abasic site. Specific DNA glycosylases are employed for this, which each recognise and cleave a certain type of damaged base. Some damages are fairly common, for example the presence of uracil, xanthine, hypoxanthine or the oxidation products 8-oxo-7,8-dihydroguanine and 5-hydroxycytosine, so relatively few DNA glycosylases are required to remove the majority of damaged bases, however many different DNA glycosylases exist (Fromme et al. 2004; Seeberg et al. 1995). Following cleavage of the damaged base, the abasic site is removed by specialised nucleases, and the DNA is resynthesised and ligated (Friedberg 2005b).

1.3.5 Nucleotide Excision Repair

Bulky DNA adducts cannot be repaired using MMR or BER so nucleotide excision repair (NER) is employed, which is able to correct a far broader range of lesions, including BER-repairable lesions. The extensive array of lesions NER can repair is due to its mode of damage recognition. Instead of detecting the damage itself, NER is thought to identify distortion in the DNA structure to indirectly detect damage, which allows repair of many diverse lesions using relatively few enzymes (Nouspikel 2009). NER in eukaryotes involves the combined effort of more than 30 peptide factors on naked DNA *in vitro*, and most of these factors are highly conserved across species. Defects in the genes involved in NER are responsible for several human cancer-susceptibility syndromes, including Xeroderma Pigmentosum (XP), Cockayne's Syndrome (CS) and Trichothiodystrophy (TTD).

1.3.5.1 NER in Prokaryotes

NER in bacteria was first discovered in the 1960s, when DNA lesions were found to be removed, along with a short flanking region, and the region was resynthesised following excision (Boyce and Howard-Flanders 1964; Hanawalt and Haynes 1965; Setlow and Carrier 1964). Genetic studies soon

identified the genes involved in the repair process as *uvrA*, *uvrB* and *uvrC* (Howard-Flanders et al. 1966). *uvrA* and *B* are known to be induced by the SOS response (Janion 2001) (Figure 1.7). The multi-step prokaryotic NER reaction requires the ATP-dependent formation of an UvrA dimer (Mazur and Grossman 1991), which proceeds to form a complex with UvrB. This complex recognises, and loads UvrB onto sites of DNA damage (DellaVecchia et al. 2004). UvrC is recruited to DNA- and ATP-bound UvrB and performs the 3' and 5' incisions, then dissociates from the damage site. UvrD (DNA Helicase II) is required to remove the 12-13-base oligonucleotide, and DNA polymerase I fills the resulting gap (Caron et al. 1985; Husain et al. 1985). The repair process is concluded by ligation by DNA ligase. Although very little sequence homology is present between the *uvrABC* genes and eukaryotic NER machinery, the overall molecular mechanism and range of identifiable and repairable damage are strikingly similar (Truglio et al. 2006).

The NER pathway has two distinct sub-pathways, one operates on damage in transcribed DNA, and the other addresses damage in non-transcribed DNA including silenced DNA, and the untranscribed strand of gene ORFs. This division allows prioritised repair of transcribed DNA thus minimising synthesis of defective mutant proteins. Evidence of these separate pathways can be seen in prokaryotes. Transcription-coupled NER (TC-NER) requires the mutation frequency decline (MFD) factor, which uses a DNA-dependent ATPase activity to dissociate stalled RNA pol II at DNA damage. Once the transcription complex is disrupted, MFD aids recruitment of the UvrABC complex (Selby and Sancar 1993).

10

1.4 NER in Eukaryotes – *Saccharomyces cerevisiae*

The factors involved in yeast NER can be organised into three main categories:

1. Core Factors: *RAD1*, *2*, *4*, *10*, *23* and *33*, and components of the TFIIH complex(*RAD3*, *TFB1*, *2*, *3*, *4*, *SSL1* and *2*). Deletion of any of these factors produces mutants that are completely defective in NER, and produces a moderate to severe UV sensitivity.

2. TC-NER Factors: *RAD26*, *DEF1* and *RAD34* (for TC-NER of Pol1-transcribed genes only). Deletion mutants are only defective in TC-NER. *RAD28* has also been implicated in TC-NER.

3. GG-NER Factors: *RAD7*, *RAD16* and *ABF1*. Mutants in these genes are defective in GG-NER.

Mutants defective in either TC-NER or GG-NER generally exhibit less sensitivity to UV radiation than core factor mutants. The NER factors can be isolated in distinct complexes.

Similar to *E coli*, NER in yeast also involves progressive recruitment of proteins to DNA damage loci in an organised, ordered fashion to allow efficient damage removal and repair, however eukaryotic NER is more complex and involves over 30 proteins. It can be separated into 5 distinct steps: damage recognition, open complex formation whereby DNA helicases form a 'bubble' structure, dual incision, excision of damage, and repair synthesis and ligation.

1.4.1 Damage Recognition

Damage recognition is an important and varied stage in NER, due to the wide range of DNA lesions, each inflicting varying degrees of helical distortion. It is the damage recognition stage that differs most between TC-NER and GG-NER, as TC-NER recognition factors identify stalled RNA polymerase to initiate repair, whereas GG-NER detects the damage itself, most likely by detecting DNA helix distortion. As previously described in prokaryotes, TC-NER occurs at a significantly faster rate than GG-NER in order to

preferentially maintain the integrity of transcribed DNA and to recover RNA synthesis that is generally shut-down in response to DNA damage.

1.4.1.1 RNA Polymerase-Independent Damage Recognition

Recognition of DNA damage in GG-NER is thought to require the Rad4-Rad23 recognition complex, Rad14 and RPA. Rad4 has been found to preferentially bind to DNA containing NER-repairable lesions, which is thought to be the first, and rate-limiting step of NER (Friedberg 2005b). Rad4 stably binds the non damaged strand of DNA and flips out the damaged nucleotide by insertion of a β hairpin structure (Min and Pavletich 2007). Virtually all cellular Rad4 is bound to Rad23, whereas Rad23 exists in a >10 fold excess over Rad4, so can function alone, or in combination with other factors in other cellular processes via interaction with the proteasome (Dantuma et al. 2009; Ghaemmaghami et al. 2003). It is thought that the initial binding of the Rad4-Rad23 complex facilitates recruitment of NER factors, however the process of damage recognition and NER activation is not well understood.

It is also known that Rad4 becomes ubiquitinated by the Rad7-Elc1-Cul3 E3 ubiquitin ligase complex, and subsequently degraded following DNA damage induction, however the role of Rad4 degradation in NER activation or the DDR is not yet understood (Gillette et al. 2006). The human homologue of Rad4, XPC is also ubiquitinated in response to DNA damage, however it is not degraded (Bergink et al. 2007; Sugasawa 2006). It appears that Rad4 ubiquitination, and not Rad4 degradation is required for its role in the DNA damage response, as Rad4 stability does not affect UV survival (Gillette et al. 2006). The role of the GG-NER complex is further explored below (Section 1.4.6). Another factor thought to be involved in DNA damage recognition is Rad33, a proposed homologue of human Centrin2. Rad33 has been implicated in both TC-NER and GG-NER by binding to and modifying Rad4 (Figure 1.2) (den Dulk et al. 2008).

1.4.1.2 Transcription-Coupled Damage Recognition

Recognition of damage in TC-NER requires recruitment of TC-NER specific factors to the site of stalled RNA polymerase however the process of factor recruitment is poorly understood. TC-NER in humans requires CSA and CSB, for which the yeast homologue of CSB; Rad26 has been identified (van Gool et al. 1994). CSA and CSB recruit NER factors to the stalled polymerase, and once the damage has been repaired transcription can resume. The mechanism in yeast is not as well understood, however it is known that Rad26 recruits Def1, which brings about Rbp1 ubiquitination (Figure 1.2).

In order to access the damaged DNA the transcriptional machinery must be disassembled, which is seen through targeted degradation of Rbp1, the largest subunit of RNA polymerase II (Malik et al. 2008), however it is not clear if RNA polymerase degradation is necessary for TC-NER to occur. Identification of E3 ubiquitin ligase complexes that targeted Rpb1 allowed two distinct pathways to be identified; TC-NER and Rpb1 ubiquitination. It is thought that Rpb1 degradation may occur to ensure DNA repair when TC-NER fails or is delayed (Svejstrup 2007). Rpb1 ubiquitination may be a general mechanism to manage any stalled transcriptional polymerase rather than a DNA damage-specific response. Another explanation is the idea that elongation of the ubiquitin chain provides a time frame for TC-NER to occur. When the ubiquitin chain reaches the critical length, Rbp1 is degraded and GG-NER must occur instead (Daulny and Tansey 2009).

Rad26 becomes phosphorylated by the checkpoint kinase Mec1 in response to DNA damage and this is required for efficient TC-NER to occur. This provides a link between DNA repair and the DNA damage checkpoint response (Taschner et al.).

TC-NER has been observed in both RNA pol II and RNA pol I-transcribed genes in yeast (Verhage et al. 1996). Rad4 is only involved in TC-NER in RNA pol II transcribed genes, however a gene that shows homology to Rad4, termed Rad34, has been implicated in pol I TC-NER. This suggests that the

two proteins act on different parts of the genome, however they cannot compensate for each other as shown in *rad34* mutants (den Dulk et al. 2005).

1.4.2 Open Complex Formation

Following damage recognition the surrounding DNA is unwound to form an open complex or bubble structure. This allows the repair machinery to access the damaged region. TFIIH, recruited by the Rad4-Rad23 complex or stalled polymerase, is responsible for DNA unwinding. The Rad3 and Rad25 subunits have 5'-3' and 3'-5' helicase activity respectively. Both genes are essential, and are also known to have a role in transcription via their helicase activities (Guzder et al. 1994; Higgins et al. 1983; Naumovski and Friedberg 1983; Park et al. 1992; Qiu et al. 1993). The bubble structure spans across approximately 30 nucleotides, and is stabilised by RPA, Rad14 and Rad2 proteins (Prakash and Prakash 2000) (Figure 1.2).

1.4.3 Dual Incision

The boundaries between ssDNA and dsDNA provide targets for the incision machinery, aided by the RPA and Rad14 proteins. Rad14 has been isolated in a complex with the Rad1-Rad10 nuclease, which is thought to help target the nuclease complex to target the damage (Guzder et al. 2006) (Figure 1.2). Both Rad2 and Rad1-Rad10 complexes possess endonuclease activities. The first incision is conducted by Rad2 3' of the damage, followed by 5' incision by Rad1-Rad10. The typical length of the excised oligonucleotide is 25-32 bases. Rad1-Rad10 also has a role in mitotic recombination, separate from their role in NER (Rattray and Symington 1995).

1.4.4 DNA Excision

Excision of the damaged fragment requires further enzymic activity, which is thought to occur in GG-NER by the Rad16 subunit of the Rad7-Rad16-Abf1 trimeric GG-NER complex (Figure 1.2). Rad16 has been found to generate superhelical torsion in an ATP-dependent manner, which is thought to facilitate displacement of the excised strand (Yu et al. 2004).

1.4.5 Repair Synthesis and Ligation

Following excision of the damaged strand, the genomic DNA is left with a stretch of ssDNA, which would leave the genome vulnerable to nuclease attack if not refilled. Repair synthesis requires the formation of another protein complex involving the DNA polymerases δ and ϵ, along with the accessory factors PCNA, Replication Factor C (RFC) and RPA. The repair process proceeds like normal DNA synthesis, using the non-damaged strand as a template. Finally the gaps are sealed by the Cdc9 DNA ligase, thus restoring intact dsDNA (Wu et al. 1999) (Figure 1.2).
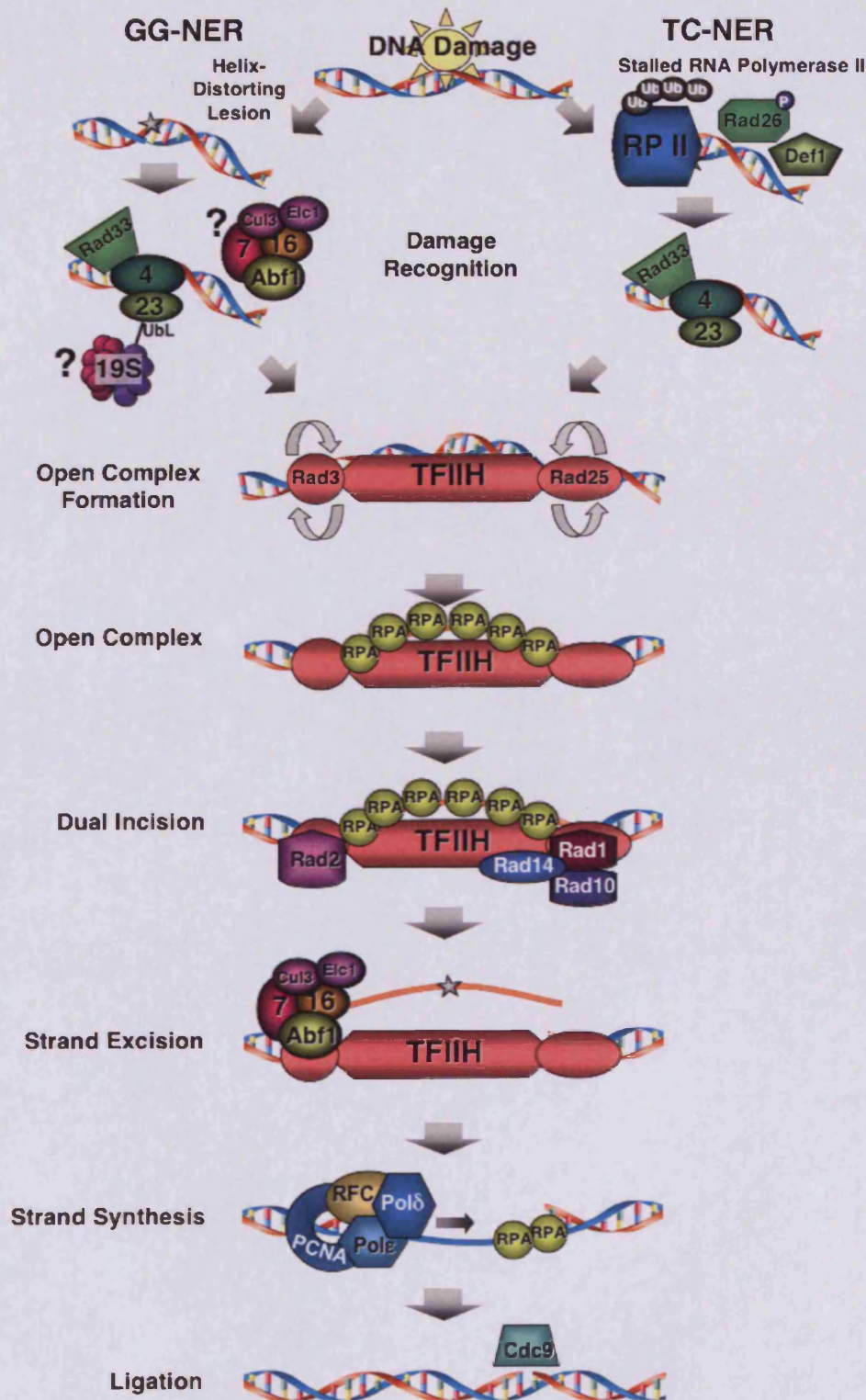
Figure 1.2 - Nucleotide Excision Repair in *S. cerevisiae* NER in yeast requires the sequential recruitment of factors to the site of damage in order to maintain intact DNA. Following production of bulky lesions the damage must be identified. Damage recognition occurs differently in transcribed (TC-NER) and non-transcribed (GG-NER) DNA. Following damage recognition the DNA is unwound, the damaged strand denatured and excised, then repair synthesis and ligation occurs to provide intact dsDNA. Modified from (Dantuma et al. 2009).

16

1.4.6 The Role of the GG-NER Complex

The role of the Rad7-Rad16-Abf1 GG-NER complex in NER is only partially characterised. It is known to have a role in post-incision events of NER (Reed et al. 1998) and in excision of the damaged DNA strand via Rad16's SNF2-like ATPase activity (Yu et al. 2004). The complex is also thought to have a role in DNA damage recognition (Guzder et al. 1997, 1998), and in other cellular processes such as UV-dependent histone H3 acetylation (Teng et al. 2008) and chromatin remodelling via Rad16's ATPase activity.

The GG-NER complex forms an E3 ubiquitin ligase complex that ubiquitinates Rad4 in response to UV and triggers its degradation (Gillette et al. 2006; Ramsey et al. 2004). Although no human homologues of the yeast GG-NER complex factors exist, XPC (the human homologue of Rad4) becomes ubiquitinated by an E3 ligase complex known as UV-DDB containing the human NER factors DDB1 and 2, Cull4a and Roc1. This complex binds to chromatin following UV irradiation, is involved in GG-NER, and has been observed to facilitate post-UV reversible ubiquitination of XPC, revealing a non-proteolytic regulatory activity of XPC ubiquitination. (Pintard et al. 2004; Sugasawa 2006; Willems et al. 2004). The UV-DDB complex is also known to target histones H2A, H3 and H4, which has been suggested to have a role in NER activation. (Kapetanaki et al. 2006; Wang et al. 1997b)

The DNA-binding component of the GG-NER complex was found to be the general regulatory factor Autonomously Replicating Sequence (ARS) Binding Factor 1 (Abf1). Abf1 was originally discovered as a DNA replication factor, but has since been identified to have roles in transcription, both as a silencer at the mating type loci, and as an activator or repressor at gene promoters affecting over 100 genes, chromatin remodelling and DNA repair. Non-repair functions of Abf1 are discussed in Chapter 3.1.

It is known that the DNA binding capability of Abf1 is required for efficient GG-NER to occur (Reed et al. 1999). It is also known that this DNA binding function is not required for the Rad16-dependent chromatin remodelling activity of the GG-NER complex (Yu et al. 2004; Yu et al. 2009).

1.5   The Ubiquitin-Proteasome System

The ubiquitin-proteasome system (UPS) has two main cellular functions, a general housekeeping role via targeted degradation of damaged or defective proteins, and a regulatory role by ubiquitination of functional proteins, thus influencing their activity or targeting them for degradation. The action of the UPS is of paramount importance for many aspects of cellular metabolism and maintenance of cellular integrity. Proteasomal and proteasome-like structures have been discovered in prokaryotes, archaea and eukaryotes with varying complexity in their structures.

The basic principle behind the UPS involves tagging damaged proteins, and proteins no longer required with the highly conserved 76-amino acid protein ubiquitin. Covalent attachment of a polyubiquitin chain allows identification of the targeted protein by the proteasome, which subsequently binds to and degrades the protein. The UPS is a major cellular mechanism for targeted degradation of cellular proteins.
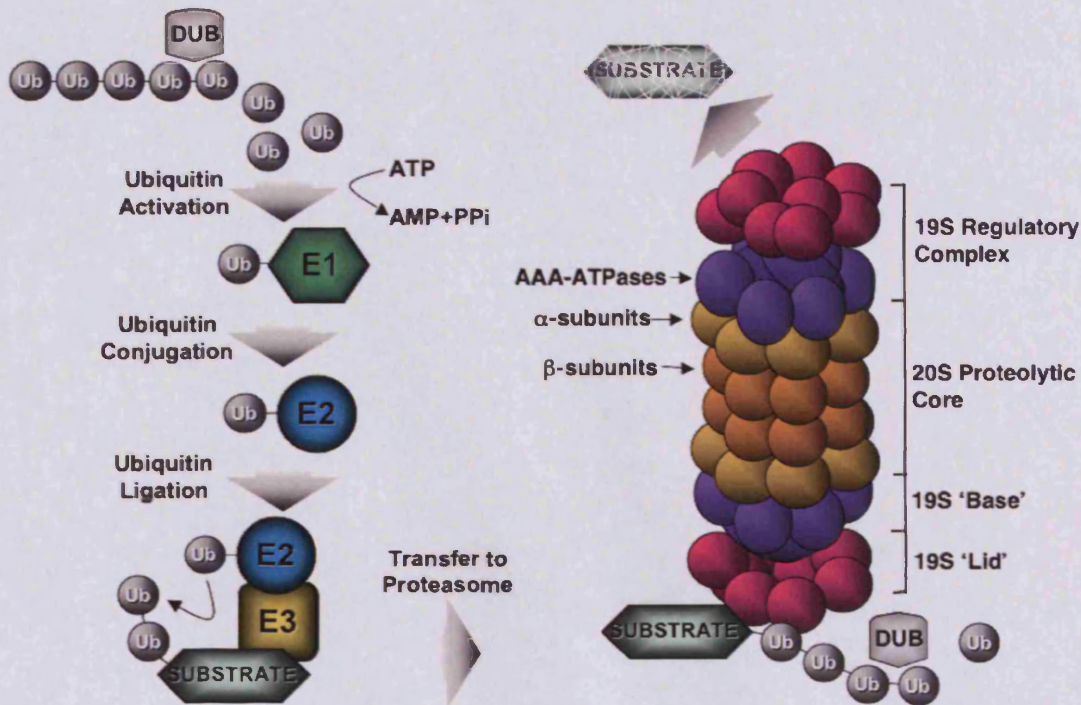
Figure 1.3 - The Ubiquitin Conjugation Pathway and 26S Proteasome Structure Ubiquitin is activated and transferred from E1 to E2 conjugating enzyme, then an E3 ligase facilitates ubiquitin tagging of the required protein, and subsequent ubiquitin chain formation resulting in targeted degradation. The 26S proteasome consists of a 20S proteolytic core flanked by two 19S regulatory complexes. Figure adapted from (Murata et al. 2009).

The ubiquitin gene is translated as a chain of ubiquitin monomers, or an ubiquitin conjugated to ribosomal protein (RB). Free ubiquitin is liberated by the action of deubiquitylating enzymes (DUB), which can be used in the progressive ubiquitin conjugation pathway. Ubiquitin is activated by E1 enzymes, which form a high energy thiol-ester bond between ubiquitin's C-terminus and the E1 cysteine active site, in a reaction that requires ATP hydrolysis. The activated ubiquitin is transferred to an E2 (ubiquitin conjugating enzyme), and subsequently transferred to a specific E3 ubiquitin ligase. E3 ligases exhibit a high level of substrate specificity, and must be able to interact with the target substrate to transfer its ubiquitin. There are two major classes of E3 ligases, RING-type and HECT-type. RING-type E3 ligases bind to the E2 and substrate simultaneously to facilitate ubiquitin transfer, whereas HECT-type E3 ligases form a thiol-ester bond with the E2-bound ubiquitin before transferring it to the target substrate. Covalent

attachment of ubiquitin occurs at lysine residues of the target substrate (Murata et al. 2009).

The eukaryotic 26S proteasome is a dynamic structure, but its most well-characterised and possibly its most common conformation involves a central 20S proteolytic core subcomplex, flanked on each end by a 19S regulatory subcomplex. As a whole this 26S complex is responsible for recognition of ubiquitin tagged proteins followed by unfolding and degradation (Pickart and Cohen 2004) (Figure 1.3).

The 20S proteolytic core is a 700kDa complex comprised of 4 heptameric rings forming a barrel structure. 14 gene products are required for the cylindrical structure of the 20S, α1-7 and β1-7. β1, 2 and 5 are the catalytic subunits, whose Thr protease active sites line the lumen of the barrel. The rings are stacked in an $\alpha\beta\beta\alpha$ formation, which create α-ring 13Å pores at each end providing selective entry into the catalytic chamber (Baumeister et al. 1998) (Figure 1.3).

The 19S regulatory complex can be further separated into 2 subcomplexes, the lid and the base structures. The 19S identifies targeted proteins, has a role in unfolding, and mediates entry into the catalytic chamber. The base structure contains a hexameric ring of AAA-family ATPases, which are involved in ATP-dependent protein unfolding and ubiquitin binding. The hexameric ring sits proximal to the 20S 7α ring (Smith et al. 2006). These 6 ATPases (Rpt1-6 aka Sug proteins) along with 3 non-ATPase subunits (Rpn1, 2 and 13) form the entirety of the base structure. (Figure 1.3)

The remainder of the 19S forms the lid structure, however the function of most lid subunits is currently unknown. Some subunits have exhibited a deubiquitylation activity, which requires the metalloisopeptidase activity of Rpn11. The Rpn10 subunit has a ubiquitin interaction motif (UIM), which can bind polyubiquitin chains (Figure 1.3).

It has been shown more recently that the 26S proteasome does not always adopt the previously described 19S-20S-19S formation, and proteasome composition is in fact extremely dynamic (Demartino and Gillette 2007). Cells can alter proteasome frequency and subunit composition in response to environmental conditions (Glickman and Raveh 2005; Lecker et al. 2006). In some cases, other regulatory complexes than the 19S can bind to the 20S α rings. Although these alternative complexes clearly have a function in proteolysis, many do not have ATPase activity, or ubiquitin-binding capability (Rechsteiner and Hill 2005). It should also be noted that 20S structures have two separate α rings capable of binding regulators, so two different structures can bind to the same 20S. Additional to the main proteasomal subunits, associated proteins also aid efficient proteolysis. Several proteins with polyubiquitin chain binding ability have been identified including Rad23, Dsk2 and Ddi1. These are thought to act as shuttle proteins, which transport polyubiquitinated proteins to the proteasome for degradation without being degraded themselves (Schmidt et al. 2005). These proteins contain UBA domains, to allow interaction with ubiquitin, and an N-terminal UbL domain, to facilitate interaction with the Rpn1, 10, 13 and Rpt5 19S subunits. These subunits can also interact directly with polyubiquitin chains.

Deubiquitination is an important stage of proteasomeal proteolysis. Aside from deubiquitination before degradation, it has also been suggested that the protesome may salvage some proteins by deubiquitinating and not degrading. This implies an active role of the proteasome in determining protein fate (Guterman and Glickman 2004).

1.5.1 Non-Proteolytic Regulatory Activity of the UPS

Aside from its canonical role as a protein degradation machine, the UPS also has non-proteolytic roles in transcription and DNA repair

1.5.2 Discovery and Characterisation of the *SUG* genes and alleles

During an investigation to reveal novel Gal4 transcriptional co-activators, factors found to exhibit a genetic interaction with Gal4 were later discovered to be AAA ATPase subunits of the 19S proteasome base (Swaffield et al. 1992).

The *GAL* system in yeast presents an elegant feedback loop, which allows induction of genes required for galactose metabolism when a suitable alternative carbon source (e.g. glucose) is not available. Gal4 is a *bona fide* transcriptional activator, which is inactivated under non-inducing conditions by interaction with the Gal80 repressor, but still thought to be bound to DNA. Upon induction, which occurs when galactose is the sole available carbon source, the Gal3 inducer facilitates dissociation of Gal4 from Gal80 by sequestering the repressor in the cytoplasm (Peng and Hopper 2002). Gal80 removals triggers binding of the TATA binding protein, and subsequent initiation of transcription of *GAL* genes (Johnston 1987; Traven et al. 2006). *GAL* gene transcription is increased by a thousand fold under inducing conditions (Figure 1.5B). The structure of Gal4 resembles a typical transcriptional activator, as it contains an N-terminal DNA-binding domain and a C-terminal acidic activation domain.

Deletion of 28 amino acid residues from the C-terminus of Gal4 reduced its activity to 3%, which prevents cells from growing on galactose media. This truncated protein, known as *gal4D*, could still bind *GAL* promoters, but had dramatically reduced *GAL* gene transcription, a consequence of the deleted activation domain. Overexpression of the mutant protein can sufficiently increase transcription to allow limited growth on galactose media.

The *SUG1* (SUpressor of Gal phenotype 1, mutant allele *sug1-1*) mutant allele was found to increase Gal4-mediated transcription to 55% of the WT level in the *Gal4D* strain (Figure 1.5D). This suppression was specific to the *gal4D* truncated mutant, which suggested that the identified proteins did not act as typical transcriptional co-activators (Swaffield et al. 1992). Sug1, now more commonly known as Rpt6, is a component of the 19S proteasome base, and more specifically is an AAA ATPase (Swaffield et al. 1995). Members of this group share a conserved 230bp AAA domain (Figure 1.4) which contains Walker A and B nucleotide binding motifs (Walker 1982).

Another 19S base AAA ATPase *SUG2* (mutant allele *sug2-1*) mutant allele restored *GAL* transcription to 70% of the wild-type level in the *Gal4D* strain (Russell et al. 1996). It was also found that Sug2 binds directly to the activation domain of Gal4 (Chang et al. 2001). Sug1 and 2 are not redundant, and both proteins are required for full proteolytic activity of the proteasome (Russell et al. 2001).
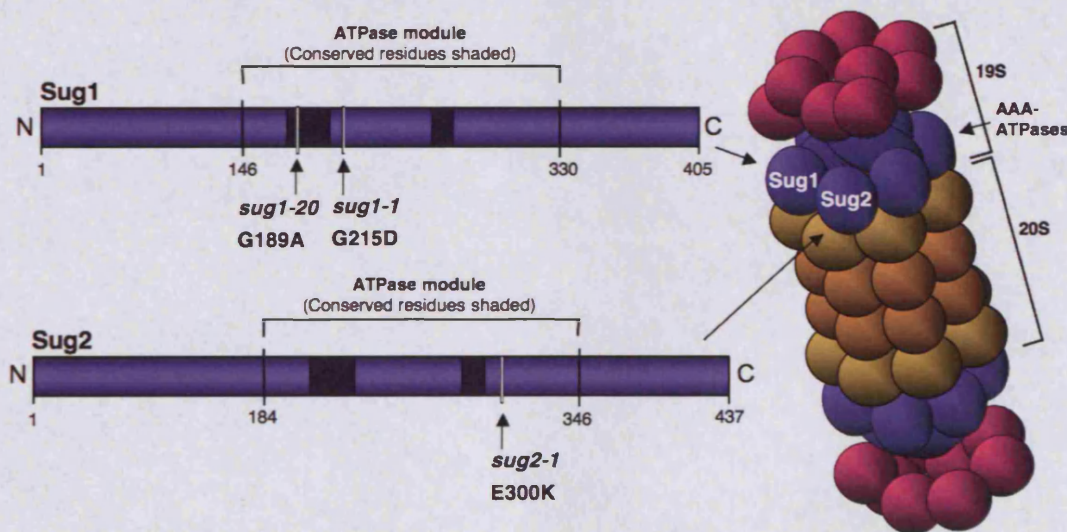
Figure 1.4 – Domain Organisation of Sug1 and Sug2, and their location in the 26S Proteasome

1.5.3 A Non-proteolytic Role of the 19S Proteasome

The association of these ATPases with the proteasome suggested that defective proteolysis due to loss of Sug activity could be the cause of the

suppressed phenotype. Reduced proteolysis leading to accumulation of the less potent Gal4D transcriptional activator, or another protein(s) could be responsible for reinstating transcriptional activation, as overexpression of Gal4D can partly suppress the defective growth on galactose phenotype. However, proteolysis-defective mutants did not suppress the Gal4D phenotype, which clearly indicated that defective proteolysis was not the cause of Gal4D suppression, and the molecular mechanism of transcriptional co-activation has subsequently been deduced (Nalley et al. 2006; Russell and Johnston 2001). The suppressive effect varies between different mutant Sug1/2 alleles with different point mutations, and an elevated level of gal4D protein was found in non-suppressive alleles such as sug1-20. This suggested proteolysis was not responsible for the altered transcriptional regulation of GAL genes.

Specific Sug1 mutant alleles were also found to suppress a temperature sensitive phenotype of a strain containing the cdc68-1 mutation (Xu et al. 1995). WT Cdc68 protein is required for the transcription of many genes and has been found to interact genetically with the transcriptional elongation factors TFIIS and Spt4. (Orphanides et al. 1999) Cdc68 also plays a pivotal role in the G_1/S cell cycle transition in S. cerevisiae. It was found that the sug1-1 allele did not have a suppressive effect on the cdc68-1 mutant phenotype, but another allele, sug1-20, which had a mutation in a more highly conserved residue in the AAA domain, was able to restore transcription of Cdc68-activated genes. This shows another allele-specific effect of the sug mutants. It should also be noted that sug1-1 in an otherwise WT genetic background shows no significant visible phenotype whereas sug1-20 in an otherwise WT background exhibits severe temperature sensitivity, a further example of allele-specificity.

Cdc68 co-immunoprecipitates with the 19S, suggesting a physical interaction (Ferdous et al. 2001). Cdc68 is a known transcriptional elongation factor and it was discovered that the mutant sug alleles had an elongation defect from their sensitivity to 6-azauracil (6-AU), an agent which causes a severe growth defect in elongation-defective strains by reducing intracellular GTP levels. In

vitro studies showed that elongation was inhibited by introduction of a Sug1 antibody or by heat-inactivation of a *sug1-20* mutant allele, but the defect was rescued by addition of purified 19S (Ferdous et al. 2001). This effect did not involve proteolysis, as addition of lactacystin, a potent inhibitor of proteasome-dependent proteolysis, or mutation of subunits of the 20S core did not affect transcription. These discoveries revealed a second non-proteolytic role of the 19S proteasome in transcription, this time regulating elongation instead of transcriptional initiation via Gal4.

1.5.4 Regulation Through Monoubiquitylation

A non-proteolytic function of the proteasome in transcriptional control was investigated. The proteasomal ATPases have a role in recruiting the chromatin-modifying SAGA acetyltransferase complex to promoters during transcription (Lee et al. 2005), and provide a link between histone H2B monoubiquitylation, which recruits the proteasome to the promoter region, and histone H3 methylation, which is abolished by Sug mutation (Baker and Grant 2005; Ezhkova and Tansey 2004). However, none of these functions could explain the suppressive effect of the *sug* mutants, as the mutations are recessive.

The DNA binding dynamics of Gal4 was determined using an artificial GST-Gal4-VP16 transcriptional activator and purified proteasome (26S or 19S). It was found that the 19S was able to rapidly destabilise Gal4-DNA binding in the presence of competitor DNA via a direct interaction with the VP16 activation domain using ATP-hydrolysis (Figure 1.5A). This involved a rapid on-off cycling mechanism, so was only evident in the presence of competitor DNA. This observation resolved the issue of *Gal4D* suppression by 19S mutants, as 19S interaction with Gal4's activation domain is required for Gal4-DNA dissociation and *Gal4D* lacks an activation domain. It remained unclear how Gal4 could maintain stable binding in order to activate transcription when required due to the constant presence of nuclear-localised proteasome (Ferdous et al. 2007).

It is known that for effective proteasomal degradation to occur the protein substrate must be tagged by a K-48 polyubiquitin chain comprising of at least four ubiquitin monomers (Thrower et al. 2000). Monoubiquitination of certain factors has been shown to have a regulatory role, without targeting them for proteasomal degradation. The monoubiquitination event has been shown to increase the potency of some factors, including VP16 (Salghetti et al. 2001), and the human HIV-1 transactivator and CTIIA (Bres et al. 2003; Greer et al. 2003), which shows the mechanism is conserved in higher eukaryotes. This dual function of the UPS in transcriptional control implicates the initial ubiquitination as a licensing event, activating the transcription factor to induce transcription, but also beginning its finite functional lifespan. The single ubiquitin allows ubiquitin chain formation which ultimately triggers proteasomal degradation. This model ensures an appropriate turnover of transcription factors, and controls their duration of function. This duration of function can be further regulated by the action and balance of deubiquitinases and ligases.

Two possible models have been devised for this phenomenon. The 'timer' model assumes monoubiquitination is the licensing event to activate the activator, thus driving transcription until the ubiquitin chain contains at least 4 monomers and the activator is proteasomally degraded. This model was deduced using Gal4 (Gonzalez et al. 2002). The 'black widow' model suggests that activator ubiquitination occurs after transcriptional induction, and is a consequence of the RNA polymerase complex interacting with the activator, which is thought to tag the protein ready for ubiquitin-dependent degradation, based on a study conducted on the Gcn4 transcription factor (Chi et al. 2001). It is possible that different factors use different mechanisms for transcriptional control via ubiquitination.

The model transcriptional activator Gal4-VP16 was incubated with a HeLa nuclear extract and it was found that the DBD of the activator that was stably bound to DNA had been post-translationally modified with a single ubiquitin, in an ATP-dependent manner. This monoubiquitinated form was resistant to 19S-mediated destabilisation. A Gal4 mutant designated Gap71, which has

three point mutations in its DBD; S22D, K23Q and K25F, is unable to be ubiquitinated. It was found that this mutant was hypersensitive to destabilisation from DNA binding *in vitro* and *in vivo* under inducing conditions, where galactose was the sole carbon source (Figure 1.5E). Fusing Ubiquitin to the N-terminal of Gap71 can allow it to stably bind to DNA, which confirmed the conclusion that the presence of a single ubiquitin is required for stable DNA binding (Ferdous et al. 2007).

In the *Gal4D* mutant it was found that the 19S can still bind to the remaining part of the activation domain (Figure 1.5C). The increased sensitivity to destabilisation is due to its inability to be efficiently ubiquitinated both *in vitro* and *in vivo*, but like Gap71, an N-terminal genetic fusion of ubiquitin re-established stable DNA binding. This suggests that a recognition sequence for the E3 ubiquitin ligase was also present in the activation domain, in addition to the 19S-interaction domain (Archer et al. 2008b). It was discovered that the covalently attached ubiquitin on Gal4 DBD interacts directly with the Rpn1 and Rpt1 subunits of the 19S base preventing dissociation from DNA via an allosteric process. The ubiquitin is thought to limit the interaction time between the proteasome and Gal4, therefore preventing a conformational change and activator-promoter dissociation (Archer et al. 2008a);(Kodadek).
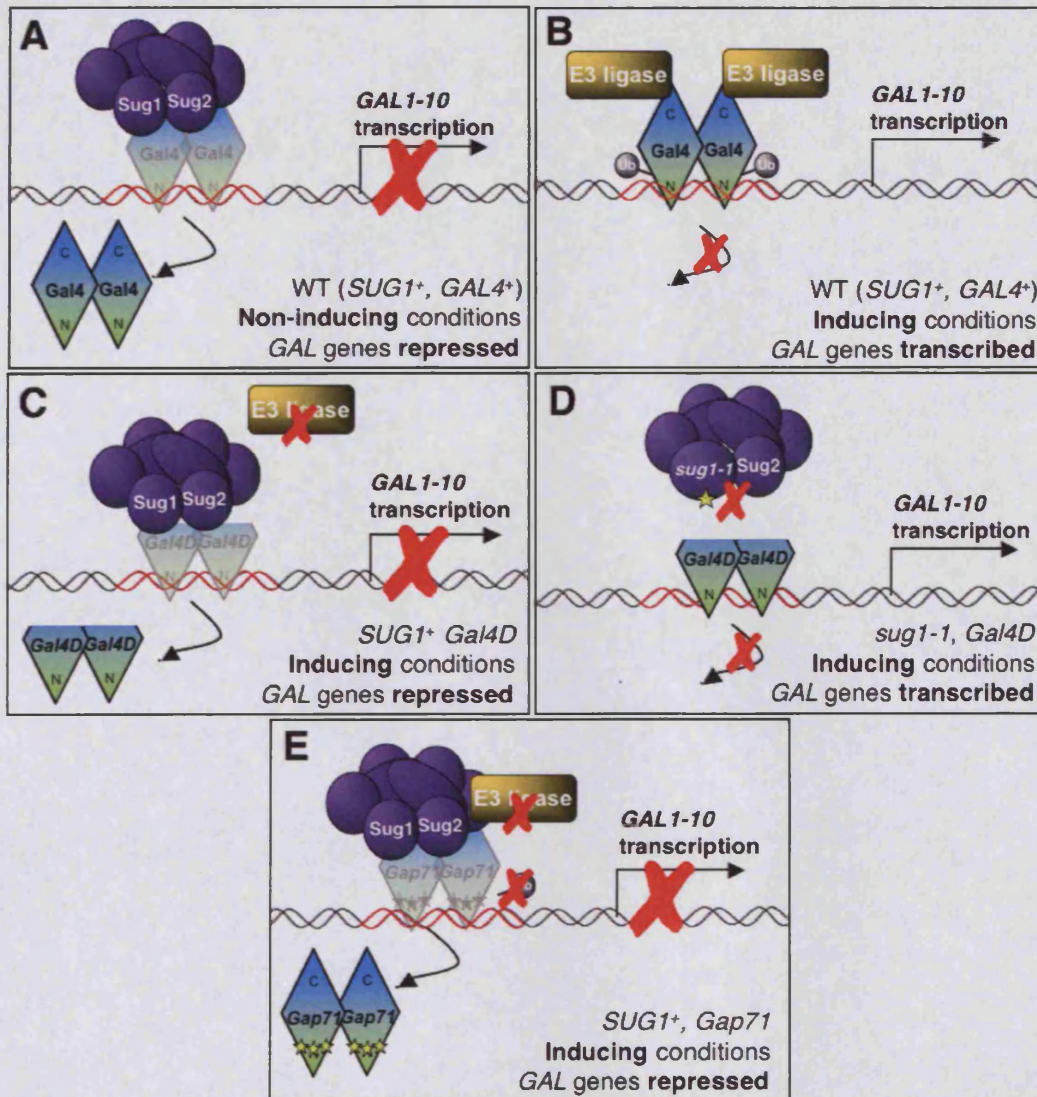
Figure 1.5 - Role of the 19S and Monoubiquitination in Transcriptional Control. A; Under non-inducing conditions (another carbon source other than galactose available) and in a WT strain, Gal4 transiently binds to *GAL* promoters, which is destabilised by the 19S. **B**; Under inducing conditions (galactose as the sole carbon source) and in a WT strain, Gal4's DBD is monoubiquitinated by an unknown E3 ubiquitin ligase, which prevents destabilisation by the 19S, allowing *GAL* transcription to occur. **C**; In the *Gal4D* mutant the bound protein is more susceptible to 19S destabilisation and cannot be ubiquitinated, so *GAL* transcription cannot occur. **D**; In *sug1-1* or *sug2-1* 19S mutant in a *Gal4D* strain, *GAL* transcription is reinstated as the 19S can no longer destabilise Gal4 binding. **E**; The *Gap71* mutant cannot be ubiquitinated, so stable binding cannot occur and *GAL* transcription cannot occur.

1.5.5 NER and the UPS

Many proteins contain domains that can interact with ubiquitin, known as ubiquitin-associated (UBA) domains. Many of these UBA-containing proteins are directly involved in the ubiquitin-proteasome dependent protein degradation pathway, however they have also been found in kinases involved in signal transduction, and in the NER protein Rad23. UBA domains span approximately 40 amino acids and have a conserved sequence from yeast to higher eukaryotes (Bertolaet et al. 2001). Rad23 contains two UBA domains, an internal and a C-terminal UBA domain, which are not required for its interaction with Rad4 and are dispensable for its function in NER (Masutani et al. 1997; Sugasawa et al. 1997). It is thought that these domains allow Rad23 and similar proteins to act as scaffold proteins, to facilitate interaction between the proteasome and proteins targeted for destruction.

Many of these scaffold proteins also contain N-terminal ubiquitin-like domains (UBL) domains, which span approximately 80 amino acids, and although have limited sequence homology to ubiquitin, they adopt a typical ubiquitin fold (Walters et al. 2002). This further facilitates interaction with the proteasome (Schauber et al. 1998). In most cases, these domains can be replaced by the sequence of ubiquitin without affecting the protein's function. The first UBL domain-containing protein discovered in yeast was Rad23. Other examples of UBL domain proteins are Dsk2 and Ddi1, which also harbour ubiquitin-binding domains. It was found that the presence of this domain was required for efficient NER (Hiyama et al. 1999).

Rad23 binds to the Rpn1 subunit of the 19S proteasome base (Saeki et al. 2002), an interaction required for its role in NER. Specific mutations in the 19S base AAA ATPases can suppress the UV-sensitivity of Δrad23 strains. This shows that in WT cells the 19S negatively regulates NER, and this inhibition is prevented by Rad23. When both activities are deleted NER is partly restored. This suppressive effect does not occur in Δrad23 strains with proteasomal mutations causing severe defects in proteolysis, concluding that

the proteasome has a non-proteolytic regulatory activity in NER via Rad23 (Gillette et al. 2001; Russell et al. 1999).

Further interplay between the UPS and NER is evident by the E3 ligase activity of the GG-NER complex. The novel E3 ligase complex comprised of elongin Elc1, cullin Cul3, Rad16 and Rad7, which interacts with the complex via its *SOCS* (suppressor of cytokine signalling) domain (Gillette et al. 2006). One target of this E3 complex is the Rad4 NER factor, which functions in a complex with Rad23 in damage recognition. Contrary to initial reports that Rad4 accumulated in response to DNA damage (Lommel et al. 2002; Ng et al. 2003), it was found that Rad4 was ubiquitinated and subsequently degraded in a proteasome-dependent manner following UV radiation (Gillette et al. 2006).

A *rad7* mutant strain with two point mutations in its *SOCS* domain was unable to facilitate the DNA damage-dependent ubiquitination of Rad4. Surprisingly, this *socs* mutant exhibited no increased UV sensitivity compared to the WT strain, however additionally deleting *RAD23* resulted in a mutant more UV-sensitive than the $\Delta rad23$ $RAD7^+$ strain. These UV sensitivities could be partially suppressed by introducing specific 19S proteasome mutants. It was concluded that the Rad7 E3 ligase-dependent ubiquitination of Rad4 and the Rad23-19S proteasome interaction were functioning in two separate components of the NER response, the latter of which does not require *de novo* protein synthesis for effective CPD removal to occur. It was also shown that Rad4 ubiquitination but not its subsequent degradation was required for its role in the DNA damage response. These observations presented a potential role of NER factors and the UPS in the DNA damage response (Gillette et al. 2006).

1.6 The Budding Yeast Cell Cycle

In order for cells to replicate efficiently a specific progression of events must occur in a meticulously orchestrated order. Evolution has resulted in progressively more elaborate mechanisms for regulating the cell cycle, however the underlying basis of cell growth-DNA replication-cell division remains a well-conserved process. Unlike many organisms, *S. cerevisiae* cells replicate asymmetrically. The process of bud emergence and maturation into a daughter cell facilitates fairly accurate estimation of cell cycle stage through microscopy, which is a powerful tool to investigate the eukaryotic cell cycle.

The eukaryotic cell cycle can be divided into 4 distinct phases; growth gap phase 1 (G_1), DNA synthesis phase (S), growth gap phase 2 (G_2) and mitotic cell division (M). It is imperative that these phases occur only once per replication cycle, and at the correct time in order to replicate the genome once, thus forming a genetically identical daughter cell. Overall cell cycle regulation is governed by the progressive formation and dissociation of specific dimeric complexes involving a cyclin and a catalytic subunit, a cyclin-dependent kinase (CDK). *S. cerevisiae* has 9 cyclins (Cln1-3 and Clb1-6) and 1 CDK (Cdc28) (Hartwell 1991), which heterodimerise at specific stages of the cell cycle. The catalytic activity of Cdc28 is only active when in complex with a cyclin (Evans et al. 1983). Cln1, 2 and 3 are known as the G_1 cyclins, and are involved in progression though late G_1 into S-phase. Deletion of all three G_1 cyclins causes cells to arrest indefinitely in G_1 (Cross 1990). The second class of cyclins are known as B-type cyclins, which refers to Clb1-6, of which Clb1-4 are involved in assembly and maintenance of the mitotic spindle. These cyclins are active during G_2 phase (Richardson et al. 1992). Clb5 and 6 are expressed earlier in the cell cycle, and are involved in S-phase entry and progression (Schwob and Nasmyth 1993). Although the cell cycle appears to be regulated centrally by these few proteins, the full complexity of regulatory pathways remain to be elucidated. Global transcription studies identified a list of 800 genes that have periodically varied transcription during the cell cycle, however this doesn't account for additional factors and helper proteins, which

may be activated by post-translational modification or complex formation (Spellman et al. 1998). Many of these gene promoters contain common elements, which bind transcription factors that are activated by cyclin-CDK complexes.
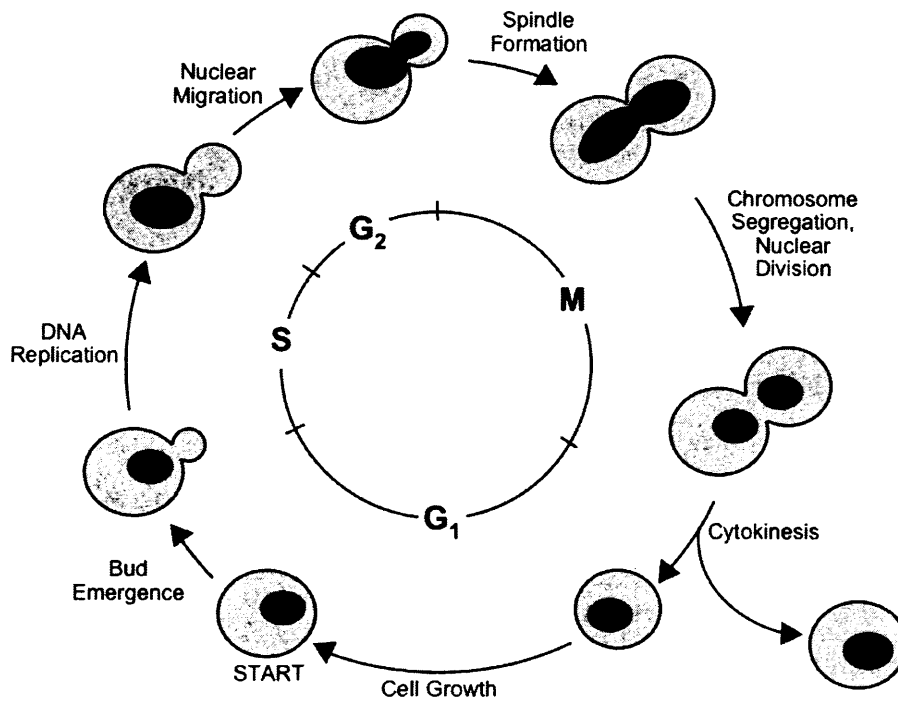
Figure 1.6 - The Budding Yeast Cell Cycle Haploid yeast cells start in G_1, then progress to S phase to begin bud emergence and DNA replication. Bud maturation and nuclear migration occurs in G_2, and spindle formation, nuclear segregation, division and finally cytokinesis occurs during M phase. This produces genetically identical mother and daughter cells. Adapted from (http://mpf.biol.vt.edu/research/budding_yeast_model/pp/).

1.7 The DNA Damage Checkpoint Response

Cells under the threat of DNA damage induce a co-ordinated metabolic response to maintain genetic integrity and continue normal growth. DNA damage must first be identified to trigger the DNA damage response (DDR), which begins a signalling cascade causing checkpoint-mediated cell cycle arrest and DNA repair, or programmed cell death (apoptosis). Only when the damage has been satisfactorily removed or tolerated can the cell resume growth and replication.

1.7.1 The SOS Response in Prokaryotes

Perhaps the most primitive example of a cellular response to DNA damage is *E. coli*'s SOS response system, which allows cells to survive significant amounts of DNA damage without compromising genomic integrity. The SOS response was first described in the mid 1970s by (Radman 1975). Two key proteins were identified, the LexA repressor, which remains bound to the SOS box of genes under non-inducing conditions, and the RecA filament inducer which binds to ssDNA following DNA damage. The SOS gene set includes over forty genes involved in protection, repair, replication, mutagenesis and metabolism of DNA.

Regulatory proteins are required for RecA DNA binding, as ssDNA binding protein prevents RecA binding when damage is not present. The RecFOR proteins are required to load RecA onto ssDNA gaps resulting from damage processing of lesions such as those induced by UV radiation, and RecBC is required for ssDNA created as a result of processed dsb. The LexA repressor is cleaved in response to DNA damage (Figure 1.7).
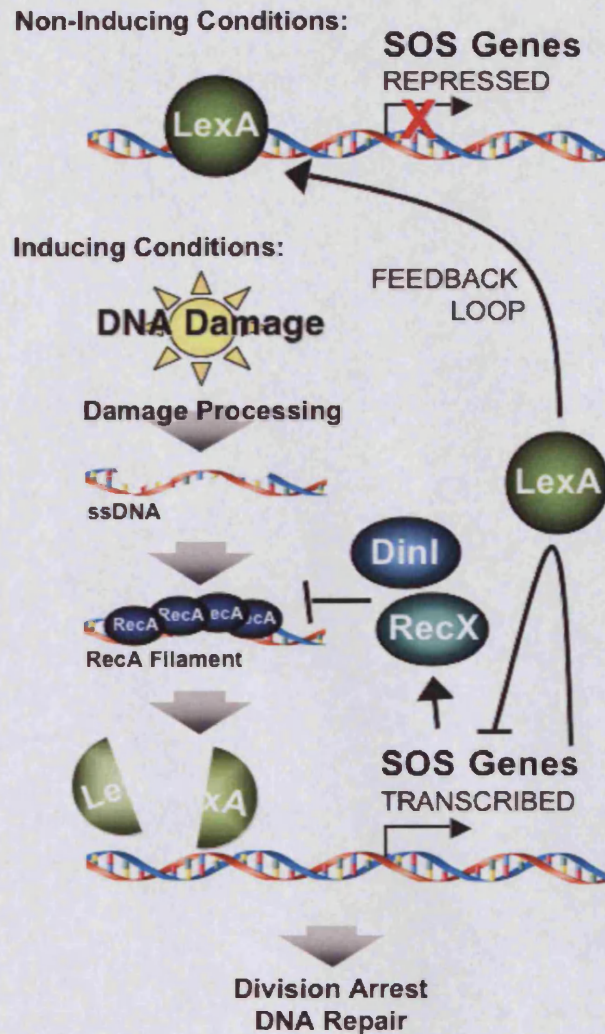
Figure 1.7 - The Bacterial SOS Response The LexA repressor binds at SOS promoters to repress SOS transcription under non-inducing conditions. DNA damage is processed to form stretches of ssDNA, which becomes bound by RecA. RecA binding triggers LexA cleavage and activation of SOS genes, including LexA. Increased LexA transcription functions as a negative feedback loop, as does DinI and RecX, which affect RecA filament stability.   Adapted from (Michel 2005)

SOS gene induction follows a specific order, which begins with the *uvrB, C* and *D* genes, required for bacterial NER, followed more slowly by genes involved in homologous recombination repair. SfiA is also induced, which inhibits cell division, allowing repair to occur sufficiently. If damage persists, the mutagenic DNA repair polymerase Pol V is induced late in the SOS response as a final strategy to maintain the genome and promote survival.

The SOS response is tightly regulated to avoid prolonged delay of cell division, and use of mutagenic error-prone polymerases. LexA is an SOS gene, which provides rapid termination of the response when damage is removed. The transcription of DinI and RecX is also SOS-induced and negatively affects the stability of the RecA filament thus adding another level of SOS regulation (Janion 2008; Michel 2005). This regulation provides an effective feedback loop to reset the system when DNA damage is no longer a threat to cellular integrity.

Although the evolution of far more complex checkpoint responses in eukaryotes has superseded the SOS response, the bacterial system displays the importance of coordinating cell cycle arrest for DNA repair following damage from the simplest to most complex organisms on earth.

1.7.2 The Eukaryotic DNA Damage Checkpoint Response

Sophisticated surveillance mechanisms have evolved in eukaryotic cells to ensure damage to cellular components, particularly genomic DNA, is dealt with effectively. These pathways are also highly conserved between species, and have been well studied in budding and fission yeast, and humans. Unless otherwise stated the pathways described here correspond to the budding yeast *S. cerevisiae* system.

The DNA damage checkpoint response requires the co-ordination of several different metabolic systems within the cell, as many normal biological processes cannot continue in the presence of DNA damage (Weinert and Hartwell 1988). In general, the DNA damage checkpoint response triggers a kinase signalling cascade involving four main factors; sensors, transducers, mediators and effectors. Sensor proteins identify the damage, and convey the signal to transducers and mediators, which localise to the damage site. The signal is then passed along to effector proteins, which activate appropriate pathways that can initiate cell cycle arrest, DNA repair or programmed cell death. This ultimate response depends greatly on the severity and type of damage, and cell cycle stage (Niida and Nakanishi 2006). DNA checkpoints

can also be divided into three stages; activation, maintenance and inactivation. These three stages are required for effective induction of the checkpoint response, allowing sufficient time for the necessary repair/maintenance processes to occur, and promoting re-entry into a proliferative growth cycle when it is 'safe' and viable to do so. This is achieved mostly by cell cycle control. Reviewed in (Harrison and Haber 2006) and summarised in Figure 1.8.

1.7.3 The Mec1-Dependent Checkpoint Response

The eukaryotic DNA damage checkpoint response is coordinated by phosphatidylinositol 3' kinase-like kinases (PIKK). The human PIKK are ATM (Ataxia-Telangiectasia Mutated), which functions primarily as a result of dsb, and ATR (Ataxia-Telangiectasia Mutated and Rad3-related), which responds to lesions producing regions of single-stranded DNA (ssDNA) (Abraham 2001). *S. cerevisiae* also has two checkpoint PIKK. Mec1 (related to ATR) is responsible for the main checkpoint response, and is activated when ssDNA is sensed, a result of most if not all DNA lesions, however in most cases some processing is required to produce ssDNA. The other yeast checkpoint PIKK is Tel1 (related to ATM), which mainly detects blunt-ended or minimally processed dsbs. These PIKK have a conserved C-terminal catalytic domain, which usually preferentially phosphorylates lipids, however no lipid substrates of the PIKK discussed here have been discovered (Toker and Cantley 1997). Although both organisms have two PIKK that have similar functions they have several fundamental differences because human ATR and ATM both appear to have significant roles in the checkpoint response, whereas yeast Mec1 plays a far superior role to Tel1 in the damage response.

1.7.3.1 Generation of ssDNA

ssDNA is an intermediate result of NER, BER, dsb repair and replication fork stalling, which is why it is the main target of Mec1 for checkpoint activation (Carr 2002). ssDNA becomes bound by RPA, the single-strand binding protein complex, which has a role in recruitment of checkpoint factors.

Generation of ssDNA at dsb requires enzymatic processing of dsDNA. This is done via exonucleases or helicase/endonuclease complexes. The yeast MRX complex (comprised of Mre11-Rad50-Xrs2) is responsible for some of this processing, particularly in G_2-synchronised cells (Diede and Gottschling 2001).

1.7.3.2 Damage Sensing and Checkpoint Activation

The most upstream event of checkpoint activation is recruitment of the checkpoint PIKK to DNA, which triggers a signal cascade. When active, Mec1 binds DNA as a heterodimer with Ddc2, and this interaction is required for DNA binding and occurs independently of DNA damage. It is not thought that Mec1 is activated by damaged DNA, but is simply recruited to damage sites by Ddc2 (Paciotti et al. 2000). RPA-bound ssDNA is required for Mec1/Ddc2 recruitment, shown by ChIP using an RPA mutant that cannot interact with Ddc2 (Zou and Elledge 2003). It is unclear however whether the RPA-Ddc2 interaction requires Mec1, but the evidence currently supports a requirement of the heterodimer for binding RPA coated ssDNA (Ball et al. 2005; Melo et al. 2001). Ddc2 can bind directly to DNA via a region of basic residues, which is essential for DNA interaction and checkpoint activation, but not required for Mec1 interaction (Rouse and Jackson 2002). Eventual removal of the Mec1-Ddc2 complex is imperative for release from checkpoint-induced arrest. It has been shown that overexpression of Ddc2 causes a permanant arrest, however overexpression of Mec1 does not produce the same effect (Clerici et al. 2001).

Rad17, Mec3 and Ddc1 form a heterotrimer known as the 9-1-1 complex or checkpoint clamp. The 9-1-1 complex also has a pivotal role in checkpoint activation and cell cycle arrest and is loaded onto the DNA by the checkpoint clamp loader at dsb in an RPA dependent manner. The checkpoint clamp loader is composed of Rad24 with Rfc2-5, a modified PCNA clamp loader complex (Ellison and Stillman 2003). The 9-1-1 complex functions as an alternate damage sensor as it is recruited to damage foci independently of

Mec1, Ddc2, Rad53 or Rad9 (Kondo et al. 2001). The role of the 9-1-1 clamp in checkpoint activation is not yet clear, but it is thought that it recruits substrates for phosphorylation by Mec1 because Rad53 and Rad9 phosphorylation is depleted in 9-1-1 mutants (Emili 1998). It is believed that the Tel1 pathway is less dependent on the 9-1-1 complex, as Tel1 is still able to phosphorylate Rad9 and Rad53 in 9-1-1 defective cells (Giannattasio et al. 2002).

1.7.3.3 The Role of Tel1

Although human ATM has a major role in checkpoint activation in response to dsb, yeast Tel1 has a secondary role in the checkpoint response. It is proposed that inactive Tel1 is sequestered in cells as a multimer, which blocks its kinase domain. Upon DNA damage, autophosphorylation and monomerisation activates Tel1. Tel1 appears to be recruited to blunt or unprocessed ends of dsb independently of RPA. DNA binding is facilitated by the MRX (Mre11-Rad50-Xrs2) complex, which is phosphorylated by Tel1 on the Mre11 and Xrs2 subunits in response to DNA damage (Grenon et al. 2001; Usui et al. 2006). Sae2 also regulates the action of MRX at dsb by stimulating its nuclease activity (Mimitou and Symington 2008). Following Tel1-dependent checkpoint activation, Rad53 becomes phosphorylated and the same downstream pathway is triggered as in Mec1-dependent checkpoint activation.

Although Tel1 appears to respond differently to Mec1, they share some overlapping function, as increasing levels of Tel1 can suppress the sensitivity and lethality of Δmec1 strains (Sanchez et al. 1996).

1.7.3.4 Signal Transduction Following Checkpoint Activation

Following detection of DNA damage, a kinase cascade transduces the checkpoint activation signal to affect the required target proteins. Rad53, a Chk2-family kinase, is the main signal transducer, and becomes phosphorylated in the presence of Mec1 and the adaptor protein Rad9. Rad9

phosphorylation by Mec1 or Tel1 allows it to act as a scaffold protein, thus facilitating the Mec1 or Tel1 interaction with Rad53's phospho-threonine binding FHA domains resulting in Rad53 autophosphorylation (Durocher et al. 2000; Sun et al. 1998). Rad53 phosphorylation sites were identified by progressive mutation of TQ and SQ motifs. TQ and SQ motifs are a structural hallmark of DNA damage responsive proteins and present likely sites for phosphorylation (Traven and Heierhorst 2005). Rad53 contains an N-teminal cluster of TQ sites and a C-terminal cluster of SQ sites. Mutation of both clusters eliminates most phosphorylation by Mec1 *in vitro*. The signalling target Dun1 FHA domain interacts with the TQ cluster, and is not phosphorylated in TQ cluster mutant cells. Rad53 can also bind to its own FHA domain, thus allowing oligomerisation, and facilitating autophosphorylation in response to DNA damage (Lee et al. 2003). Full activation of Rad53 is also dependent upon nuclear import, which it achieves via interaction with the nuclear import factors Srp1 and Kap95. Without this interaction Rad53 accumulation does not occur fully following exposure to the DNA damaging agent methane methylsulphonate (MMS) (Smolka et al. 2005).

Effective function of the adaptor protein Rad9 in the checkpoint response requires homodimer formation via its C-terminal BRCT motifs (Soulier and Lowndes 1999). In addition to facilitating Rad53 phosphorylation, it is also required for Chk1 activation, however Chk1 does not have an FHA domain, so a different function of Rad9 facilitates Chk1 phosphorylation (Blankley and Lydall 2004). Rad53 is also activated in response to replication stress under non-DNA damage conditions. This activation requires Mrc1 instead of Rad9, which becomes hyperphosphorylated in response to replication blocks (Alcasabas et al. 2001).
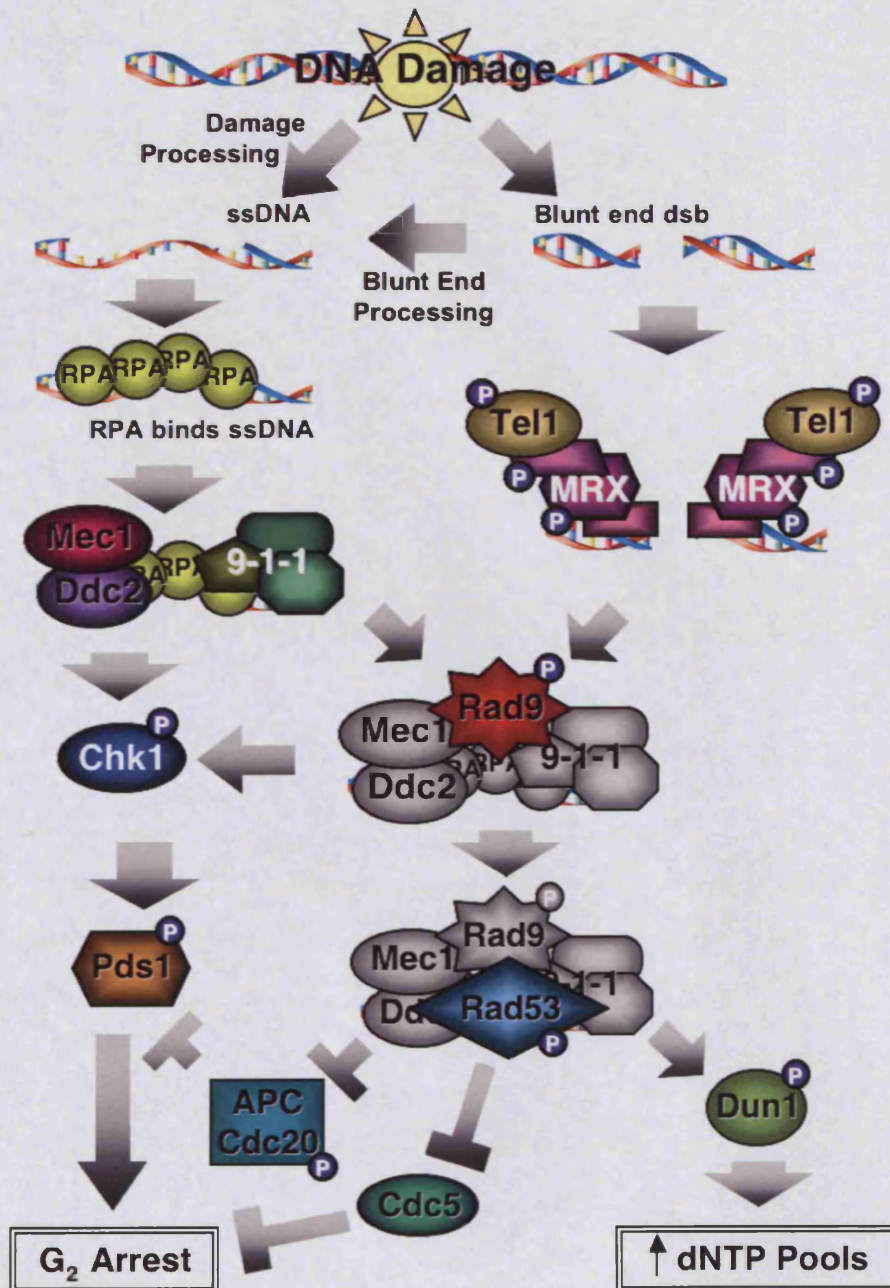
Figure 1.8 - The DNA Damage Checkpoint Response in *S. cerevisiae* ssDNA or dsDNA breaks as a result of DNA damage recruit the Mec1 or Tel1 checkpoint kinases, which begin the DNA damage checkpoint response kinase cascade. The adaptor protein Rad9 becomes phosphorylated, which mediates Rad53 phosphorylation, which affects downstream targets. Dun1 is activated which results in elevated nucleotide pools. Inhibition of Cdc5 and APC/Cdc20 results in cell cycle arrest. Mec1 also activates Chk1, which activates Pds1 and further promotes G_2 arrest. Figure adapted from (Harrison and Haber 2006).

1.7.3.5 Checkpoint-Induced G₂ Arrest

DNA damage checkpoint activation can arrest cell cycle progression in G_2 by activating the anaphase inhibitor Pds1. Pds1 becomes hyperphosphorylated in response to damage, which requires Mec1, Rad9 and Chk1 but not Rad53 (Cohen-Fix and Koshland 1997). During normal proliferative growth Pds1 functions as an inhibitor of anaphase onset during spindle assembly. Progression into anaphase requires ubiquitin-dependent degradation of Pds1 by the anaphase-promoting complex (APC) with Cdc20 specificity factor for mitosis to occur, however it only becomes hyperphosphorylated during the DDR. This Chk1 mediated phosphorylation prevents Pds1 from Cdc20-APC-dependent proteolysis *in vivo*. Δ*chk1* and Δ*pds1* mutants exhibit a checkpoint defect, and display a significant degree of epistasis. Phosphorylation site-defective *pds1* mutants are also strongly checkpoint defective, as Pds1 is not immune to ubiquitin-dependent degradation (Agarwal et al. 2003; Wang et al. 2001). Pds1 stability in vivo is also promoted by Rad53 by blocking the Pds1-Cdc20 interaction possibly by Rad53-dependent or protein kinase A (PKA) Cdc20 phosphorylation (O'Neill et al. 2002; Searle et al. 2004). Regulation of Cdc20 levels is also seen in the yeast S-phase and spindle assembly checkpoint to control cell cycle progression.

Although Rad53 is known to be an upstream regulator of Pds1, genetic evidence suggested that it had other downstream targets too, as the Δ*rad53* mutant had a more severe checkpoint-defective phenotype than Δ*pds1* cells (Gardner et al. 1999). Rad53 is known not only to regulate anaphase entry via Pds1, but also to control mitotic exit, thus having a role in checkpoint maintenance as well as activation. It is thought to maintain CDK activity during the checkpoint response via inhibition of Cdc5, which normally promotes mitotic progression via inhibition of the mitotic exit network (MEN) inhibitor, the Bub2/Bfa1 complex (de Bettignies and Johnston 2003; Geymonat et al. 2003). It is probable, but as yet unknown if Rad53 has other cell cycle-related targets, however the combined Δ*bub2*Δ*pds1* knockout is as checkpoint-defective as Δ*rad53* cells. The null mutant of another known target of Rad53, the Dun1 kinase exhibits a similar checkpoint defective phenotype. This

implies that it is downstream targets of Dun1 rather than other targets of Rad53 that contribute mainly to its faulty checkpoint response (Gardner et al. 1999).

1.7.4 Regulation of Nucleotide Pools

Nucleotide pools become significantly elevated as a downstream effect of the DNA damage checkpoint response. This occurs by regulation of activity of the ribonucleotide reductase (RNR) complex, which catalyses the rate-limiting step of dNTP synthesis, the monomeric precursors of DNA. RNR upregulation is brought about by Dun1, a downstream effector kinase of the Mec1 dependent DNA damage checkpoint pathway. Dun1 facilitates degradation of Sml1, the RNR inhibitor, which activates the RNR complex. Further regulation of the RNR pathway is explored in more detail in Chapter 5 and also see Figure 5.1.

Mec1 dependent Sml1 degradation is an essential process even in the absence of DNA damage, as elevation of nucleotide pools is also essential during normal S-phase for DNA synthesis. This phenomenon is evident in the rescued survival of $\Delta mec1\Delta sml1$ cells, whereas $\Delta mec1$ cells are inviable.

1.7.5 DNA Damage Checkpoint-dependent Chromatin Modification

The DDR also causes Mec1/Tel1 dependent phosphorylation of the histone variant H2AX, termed γ-H2AX when phosphorylated. γ-H2AX is found in the region flanking of dsb, approximately 50-100kb in yeast and up to 1Mb in mammals (Shroff et al. 2004). Yeast cells that cannot synthesise γ-H2AX are sensitive to DNA damage and display a mild G_1/S checkpoint defect (Downs et al. 2000). Its role in the DDR is thought to involve recruitment of the chromatin remodelling complexes Ino80, Rvb1, NuA4 and Swr1 to the dsb, however these do not appear to play a role in the checkpoint response (Paull et al. 2000).

42

1.7.6 The G_1/S Checkpoint

Following DNA damage, human cells can orchestrate a G_1 arrest by activating the tumour suppressor gene p53, which affects many cellular pathways including cell cyle arrest, programmed cell death and general stress response. Yeast do not have a p53 homologue, but *S. cerevisiae* can also arrest the cell cycle in G_1 in response to DNA damage. In order to trigger a G_1/S checkpoint and delay S-phase onset a threshold dose of ~30Jm^{-2} UV is required. S-phase delay can be reduced by exposing the UV-irradiated cells to visible light, thus allowing photoreactivation to occur, which suggests that the presence of CPDs have a role in G_1/S checkpoint maintenance (Goodin et al. 1971). It was suggested that NER intermediates were required for G_1/S checkpoint activation, however due to the fairly large UV dose required to invoke the G_1/S checkpoint, the NER process is considered insufficient to be solely responsible for checkpoint activation (Neecke et al. 1999). It is most likely that the G_1/S checkpoint is also triggered by dsb or UV-induced DNA gaps rather than common UV-induced lesions. This was supported by the discovery of mutants that have a defective G_1/S checkpoint but are UV-resistant (Paciotti et al. 2001). The G_1/S checkpoint fails to be activated in a $\Delta rad14$ NER-defective strain so cells arrest during S-phase due to accumulation of replication/recombination intermediates (Neecke et al. 1999). It is thought that the G_1/S checkpoint is activated by Rad53-dependent inhibition of *CLN1/2* transcription via Swi6 phosphorylation, thus delaying S-phase onset (Sidorova and Breeden 1997).

1.7.7 Cellular Responses to UV – The Postreplication Checkpoint

Contrary to past belief, which considered the yeast checkpoint response as a cell cycle arrest between G_1/S or G_2/M phases, it was discovered that this was only a response to relatively high doses of UV (>20Jm^{-2}) that induced cell cycle arrest. It was found that a lower dose of UV (~5Jm^{-2}) instigated a different response, termed a postreplication checkpoint (Callegari and Kelly 2006). It was proposed that this level of UV was more representative of environmental solar radiation. Although virtually all solar UV that penetrates the earth's atmosphere is >290nm and laboratory UV lamps emit 254nm

radiation it was found that the same DNA damage was induced (Cadet et al. 2005), and the same genes are required to survive the different wavelengths (Harm 1979).

Following a sunlight-comparable dose of UV, instead of arresting before S-phase, cells carried the damage through bulk DNA replication, then delayed cell cycle progression. The length of the second cell cycle was also found to be highly dependent on cell cycle phase at the point of irradiation. The first cell cycle after irradiation appeared to progress normally, but the second and third cell cycles were dramatically extended. This was also found to be the case in budding yeast, which did not exhibit delayed bud emergence, but bud emergence during the next cell cycle was delayed (Callegari and Kelly 2006).

During the postreplication checkpoint, the concept of damage bypass or damage tolerance is pivotal for cell cycle progression (Friedberg 2005a). This adaptation is also known as translesion synthesis (TLS), and involves switching between different DNA polymerases to cope with damaged DNA. These polymerases, among other TLS genes belong to the *RAD6* epistasis group of DNA damage-responsive genes. Rad6 is an E2 ubiquitin-conjugating enzyme (Jentsch et al. 1987), which forms a complex with Rad18, an E3 ubiquitin ligase (Bailly et al. 1997). This complex targets PCNA for monoubiquitination at Lys164, a modification that allows an alternate polymerase to be loaded onto the DNA, allowing damage bypass (Hoege et al. 2002). PCNA can also be polyubiquitinated by the Rad6-Rad18 complex in order to function in error-free TLS. The Ubc13-Mms2-Rad5 complex is also required for PCNA polyubiquitination to activate the error-free TLS pathway. This complex also contains E2 ubiquitin-conjugating (Ubc13-Mms2), and E3 ubiquitin-ligase (Rad5) activities, which target Lys63 of ubiquitin instead of Lys48. Rad5 can also interact with Rad18, which choreographs contacts between the two ubiquitin-conjugating complexes (Brusky et al. 2000). The Ubc13-Mms2-Rad5 dependent TLS pathway is error-free, and *RAD30* encodes a polymerase, which has a central role in the alternate error free TLS pathway. A third pathway also exists, which involves the *REV1*, *REV3* and

REV7 genes, but this pathway is error-prone and therefore mutagenic (Prakash et al. 2005).

1.8   The Current Study

The aim of the current study is to further uncover the complex interplay between factors involved in NER and the UPS. The main focus of this has been regarding the role of DNA damage-dependent ubiquitylation of the NER factor Rad4, resulting in its subsequent degradation. This follows on from work conducted by Gillette et al., which identified Rad7's *SOCS* domain, and its role as an E3 ubiquitin ligase, and partially characterised the mutant phenotype of the *psocs* strain, which cannot ubiquitinate Rad4. This study has striven to further characterise the *psocs* strain, with regard to UV sensitivity and cell cycle progression, and to identify the role of the Rad4-Rad23 complex in DNA damage-dependent global transcription.

Following identification of potential transcriptional targets of the Rad4-Rad23 complex involved in the DNA damage checkpoint response, particularly the RNR branch of the pathway, the next objective of the study was to create mutants of these factors and use these genetic tools to further characterise the role of Rad7's E3 ligase, thus uncovering its role in the DNA damage response.

The initial aim of the project focussed on another GG-NER factor, Abf1. It was speculated that interaction between Abf1 and specific subunits of the 19S proteasome had a regulatory role in DNA replication and DNA repair, dependent on Abf1's DNA binding domain. This was conducted using various mutant alleles to identify phenotypic variations on the mutant strains.

2 Materials and Methods

2.1 Storage and Growth Conditions

All equipment and growth media was sterilised appropriately by autoclaving, and all manipulations were conducted under aseptic conditions.

Yeast strains were grown, when required, in appropriate liquid medium at 30°C or 25°C, and were stored for short periods on solid media at 4°C or RT. Yeast strain genotype and source are described in each corresponding results chapter.

Large amounts of cell culture were produced by growing a single colony from a plate in a 5ml preculture overnight to stationary phase, diluting this to $O.D_{600}$ of 0.1 in 50ml media and allowing it to grow for several population doublings but not reach stationary phase, then diluting appropriately into the required volume. The dilution was calculated empirically to achieve the required cell density for the following day.

For long-term storage, cells were grown in media to exponential phase, then frozen in 30% glycerol using liquid nitrogen and stored at -70°C. Prior to use, frozen cultures were streaked onto solid media, and allowed to grow to stationary phase.

2.2 Yeast Transformation

Yeast strains were transformed using the lithium acetate (LiAc)/single-stranded carrier DNA/polyeythylene glycol (PEG) method (Gietz and Woods 2002).

50 ml yeast culture was grown in YPD to mid/late log phase ($O.D_{600}\sim0.6$), and cells were harvested by centrifugation at 4 000 rpm for 3 minutes and washed in 50ml sterile water. Cells were resuspended in 15ml 0.1M LiAc and 1 x TE (0.1M Tris-HCl, 0.01M EDTA), and incubated for 1 hour at RT on a Roller

Mixer (Stuart). Cells were pelleted and suspended in a suitable volume of H_2O (100μl per 0.1 OD_{600}). 100μl cells were added to the transformation mixture containing 0.1M LiAc, 1 x TE, 50% PEG 3350, 15μl denatured salmon sperm carrier DNA, and a suitable amount of DNA, and incubated for 30 minutes at RT on a Mini LabRoller (Labnet). The mixture was heat-shocked at 42°C for 15 minutes, and then cooled on ice for 3 minutes. 1ml sterile water was added before centrifugation at 4 000 rpm for 3 minutes, then the pellet was resuspended in 500μl sterile water. 200μl of the cell suspension was spread onto suitable dropout media plates, which were incubated at an appropriate temperature for 2-3 days to allow colonies to form.

2.3 Rapid Preparation of Yeast Genomic DNA

Rapid preparation of yeast genomic DNA was employed to check the state of transformed cells during strain construction. Cells were grown from a single colony overnight in 5ml of appropriate media. Cells were then harvested by centrifugation for 2 minutes at 4 000 rpm in a benchtop centrifuge. The pellet was vortexed vigorously for 6 minutes with 300μl DNA lysis buffer, (4M Urea, 0.2M NaCl, 0.01M EDTA, 0.05%SDS, 0.1M Tris-HCl) 200μl glass beads and 200μl 1:1 phenol:chloroform. The mixture was then centrifuged for 10 minutes at 13 000 rpm, and the upper aqueous layer was retained. To precipitate the DNA, 1ml 100% ethanol was added, and incubated at -20°C for at least an hour. The precipitate was spun for 10 minutes at 13 000 rpm and the supernatant discarded. The pellet was washed with 70% ethanol and dried at RT for 30 minutes. DNA was resuspended in 100μl water or TE.

2.4 DNA Manipulation

2.4.1 Yeast Colony PCR

Colony PCR was used to screen potential correct transformant colonies. A small cell sample was picked from a single colony using a 10μl pipette tip and suspended in 12.5μl water. Then, in sealed 0.2ml tubes, cells were vortexed, microwaved on full power for 2 minutes, then vortexed again. The boiled cell suspension was used to make a 25μl PCR reaction mix (1x

ReddyMix (Thermo) 0.16µM forward and reverse primer, to 25µl with ddH$_2$O).
The PCR reaction was run and analysed using agarose gel electrophoresis.

2.4.2 PCR Conditions

Two PCR programs were used during this study, depending upon the
predicted size of PCR product. For products <1.5kb, an initial denaturation
step of 4 minutes at 95°C was employed, followed by 30 cycles of 40 seconds
denaturation at 94°C, 50 seconds annealing at a temperature suitable for the
primers used and 30 seconds elongation at 72°C, adding 3 seconds per
cycle. The program was finished with a final elongation step at 72°C for 10
minutes, then the temperature was reduced to 4°C to store the product.

In the program used for products <1.5kb, an initial denaturation step of 4
minutes at 95°C was employed, followed by 5 cycles of 20 seconds
denaturation at 94°C, 30 seconds annealing at 45°C and 40 seconds
elongation at 68°C, adding 5 seconds per cycle. This was followed by 25
cycles of 15 seconds denaturation at 94°C, 30 seconds annealing at a
temperature suitable for the primers used and 60 seconds elongation at 72°C,
adding 5 seconds per cycle. The program was finished with a final elongation
step at 68°C for 8 minutes, then the temperature was reduced to 4°C to store
the product. <1.5kb PCRs were conducted using the Expand High Fidelity
PCR System (Roche).

2.4.3 DNA Electrophoresis

Agarose gel electrophoresis was employed on numerous occasions
throughout the study to check the size, quality and quantity of DNA. A 1.2%
agarose gel was mostly used, dissolved in TAE buffer with 1µl 10mg/ml EtBr
per 100ml buffer. DNA samples were run with loading buffer (Fermentas) at
10V/cm with an appropriate DNA marker. DNA bands were visualised using a
UV transilluminator.

2.5 Yeast Total RNA Extraction

The hot phenol method (Schmitt et al. 1990) was employed to extract RNA from yeast cells. 10ml yeast culture was grown to mid/late log phase ($O.D_{600} \sim 0.6$) and cells were harvested by centrifugation at 3 000 rpm for 5 minutes at 4°C, and resuspended in 500μl RNA lysis buffer (10mM Tris-base, 10mM EDTA, 0.5% SDS). 500μl equilibriated phenol (pH 4.3) was added, and incubated for 1 hour at 65°C with regular vigorous vortexing. The lysate was then chilled on ice for 10 minutes, then 100μl 3M NaAc (pH 5.2) was added, then the samples were centrifuged at 10 000 rpm for 10 minutes at 4°C. The top (aqueous) phase was then collected. 2 phenol extractions were carried out, by adding 500μl 1:1 phenol:chloroform, mixing, then centrifugation for 10 minutes at 10 000 rpm at 4°C, then removing the top aqueous layer and repeating the process. Another extraction was performed using chloroform/isoamyl alcohol, and the final extract was added to 1ml 100% ethanol, and precipitated overnight at -20°C. RNA pellets were collected, washed and redissolved in 80μl ddH$_2$O with 20μl 5x RNA loading buffer (0.16% saturated aqueous bromophenol blue, 4mM EDTA, 2.664% formaldehyde, 30% formamide, in 4x FA gel buffer (200mM 3-[N-morpholino]propanesulphonic acid (MOPS), 50mM NaAc, 10mM EDTA, pH 7.0)). RNA was stored at -80°C.

2.6 Formaldehyde-Agarose (FA) Gel Electrophoresis and Northern Blotting

The gel was prepared by melting 1.5% agarose in 1x FA gel buffer, and allowed to cool to 65°C, which was followed by addition of 1.8ml formaldehyde and 1μl 10mg/ml ethidium bromide (per 100ml buffer). The gel was then poured and allowed to set, then 1x FA gel buffer was added, and left to equilibrate for 30 minutes. 20μl of each sample was loaded, and the gel was run for 2 hours at 70V, then briefly visualised using a UV transilluminator to ensure proper running and equal loading.

Prior to transfer, a nylon based membrane (Genescreen Plus, PerkinElmer Life Sciences Inc) was soaked in water, then the gel, filter paper wick, 2 sheets of filter paper and the membrane were soaked in 20x SSC (3M NaCl, 0.3M Na Citrate 2H$_2$O, pH 7.0) The transfer was assembled according to Figure 2.1, and RNA was transferred overnight. The RNA side of the membrane was irradiated with 254nm UV for 2 minutes to allow cross-linking to the membrane. The membrane was then rinsed with ddH$_2$O, and rolled in a glass tube with hybridisation buffer (0.5M phosphate buffer, 7% SDS, 1% BSA, 1mM EDTA) at 65°C for 1 hour.
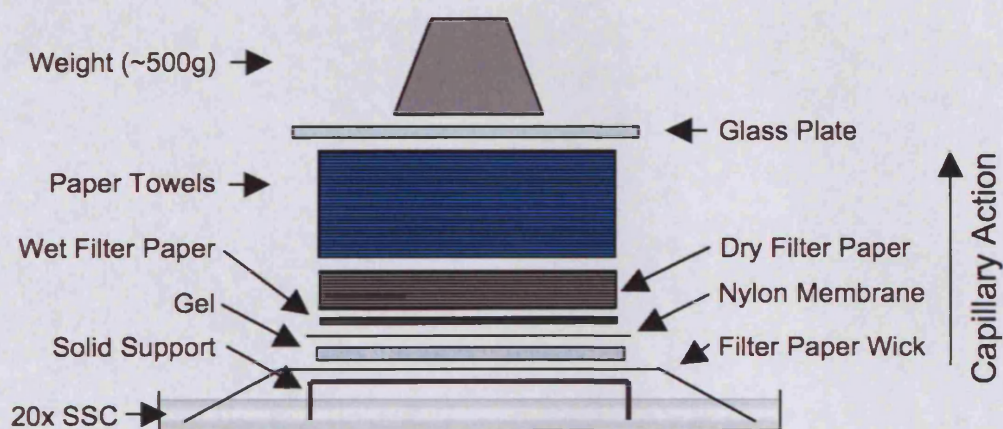
Figure 2.1 – Setup of Equipment for Northern Blotting

2.6.1 Probe Preparation

A 50µl PCR reaction (1x ReddyMix (Thermo) 0.16µM forward and reverse primers) was conducted to amplify a 200-500bp fragment from the ORF of the required gene. A 5' biotin-label was applied to the primer homologous to he non-transcribed strand. PCR reactions were checked for size and quality using agarose gel electrophoresis. 10µl of the PCR mix was added to 20µl streptavidin-coated Dynabeads (Invitrogen) in 2x BW (binding and washing buffer – 2M NaCl, 10mM Tris-HCl ph 8.0, 1mM EDTA), mixed by pipette and incubated at RT for 15 minutes, with occasional mixing. A magnetic particle collector (MPC) was used to extract the Dynabeads and discard the supernatant. The beads were washed twice with 60µl ddH$_2$O and resuspended in 30µl 0.1M NaOH to denature the dsDNA. After 10 minutes

incubation at RT, the MPC was used to discard the supernatant and the beads were washed twice with ddH$_2$O, then resuspended in 10μl 1x BW. 2μl of non-biotinylated primer (10μM) was added, and the mix was heated to 65°C for 2 minutes, then allowed to cool slowly to RT. Bound matter was retrieved and the supernatant discarded, followed by 2 washes with ddH$_2$O. The beads were finally resuspended in 17.2μl ddH$_2$O and the following were added for radioactive labelling of the probe: 8μl 8x Sequenase reaction buffer (Amersham), 4μl dATP buffer (0.1mM dTTP, dGTP and dCTP), 2.8μl 0.1M DTT, 2μl α-[^{32}P]dATP (6000 Ci/mmol, Amersham) and 6μl Sequenase mixture (1μl Sequenase in 5μl Sequenase dilution buffer, Amersham). This was mixed thoroughly and incubated for 10 minutes at 37°C. The beads were then collected using the MPC, and following 2 washes with ddH$_2$O the beads were resuspended in 20μl 0.1M NaOH and incubated at RT for 10 minutes. The supernatant, containing the radiolabelled probe was then transferred to a new tube and checked for radioactivity.

2.6.2 Membrane Probing, Washing and Detection

The membrane buffer was removed, and replaced with 10ml fresh hybridisation buffer. The probe (in 20μl NaOH) was added to the buffer, and incubated in a rolling oven at 65°C overnight. The buffer was then discarded, replaced with washing buffer, (2x SSC, 1% SDS) and incubated for 30 minutes. Washing buffer was then removed, replaced and incubated for a further 30 minutes. The membrane was then placed against a phosphorimager screen (Molecular Dynamics) and exposed overnight. The screen was scanned (Typhoon 9410, Molecular Dynamics) and visualised using ImageQuant software version 5.0 (Molecular Dynamics).

2.7 Yeast Whole Cell Extract (WCE) Preparation

100ml yeast culture was grown to mid/late log phase (O.D$_{600}$ ~ 0.6) and cells were harvested by centrifugation at 4 000 rpm for 5 minutes, and resuspended in 500μl cold yeast dialysis buffer (YDB – 20mM Hepes-KOH,

0.01M EDTA, 0.01M MgSO₄, 10% Glycerol, 5mM DTT, 1x proteinase

inhibitors) with 500µl glass beads, and vortexed vigorously for 8 minutes at

4°C (1 minute break for every 2 minutes vortexing to prevent tube heating up).

The supernatant was collected, and protein content was quantified using the

Bradford assay. (BioRad) WCEs were stored at -80°C.

2.8 SDS-PAGE and Western Blotting

Gel plates were assembled according to manufacturers instructions (BioRad)

and gels were prepared. 10ml resolving gel (8% acrylamide, 0.375M Tris,

0.1% SDS, 0.1% ammonium persulphate (APS), 0.06% N,N,N',N'-

tetramethylethylenediamine (TEMED)) was prepared per gel. Resolving gel

was poured, and allowed to set completely. 2.5ml stacking gel (8%

acrylamide, 0.375M Tris, 0.1% SDS, 0.1% APS, 0.06% TEMED) was

prepared per gel, then was poured, a comb was inserted and the gel was

allowed to set. The gel running tank was set up, and filled with SDS running

buffer (25mM Tris-Base, 0.2M Glycine, 0.1% SDS). The comb was removed,

the wells were rinsed and the samples were loaded. (20µg WCE, variable for

IP samples) The gel was run at 100V for a suitable period of time, dependent

on the size of the required protein.

A PVDF (Polyvinylidene Fluoride) membrane (BioRad) was prepared by

submerging in methanol then water, and transfer apparatus was arranged

with sponge supports, filter paper, membrane and gel in correct orientation

(Figure 2.1). The transfer tank was assembled with a magnetic stirrer and ice

pack, and filled with cold (4°C) western transfer buffer (25mM Tris-Base,

15mM Glycine, 0.015% SDS, 20% Methanol). Transfer was run for 45

minutes at 100V, then the membrane, with transferred proteins, was allowed

to dry completely at RT in a sterile hood.
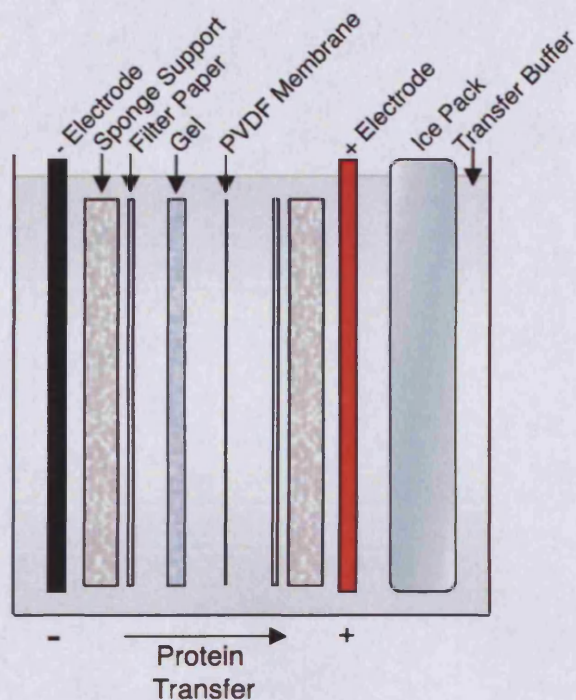
Figure 2.2 - Setup of Equipment for Western Blotting Electrophoretic Transfer to Membrane

Before blocking, the membrane was returned to a hydrophillic state by submerging in methanol, then rinsing in water. Blocking was conducted overnight at 4°C in blocking solution (1x TBST (10mM Tris-Base, 150mM NaCl, 0.05% Tween) with 3% blocking agent (GE Healthcare)). The membrane was then rinsed briefly in 1x TBST, and then incubated for 1 hour at RT in blocking solution supplemented with primary antibody. This incubation was followed by 3x 10 minute washes in 1x TBST. The membrane was then incubated for another hour at RT in blocking solution supplemented with secondary antibody, then washed 3 times as before. The secondary antibody was designed to have an affinity for the primary antibody, and the ability to catalyse a luminescent chemical reaction via a Horseradish Peroxidase (HRP) domain. Detection was carried out using the ECL Plus western blotting kit (Amersham-GE), and the blot was visualised by chemilluminescence using autoradiography.

2.9 Yeast Growth Curve

Growth curves were conducted on yeast strains to determine the rate and manner in which the culture grows. 5ml yeast cultures were grown from a colony overnight to reach early stationary phase. The cultures were then diluted to OD_{600} 0.1, and exact OD_{600} value recorded. OD_{600} values were recorded at hourly intervals for at least 12 hours using a spectrophotometer. When cultures reached OD_{600} 1 they were diluted 10-fold in the same media, prior to measurement of optical density, and the dilution factor was accounted for when plotting timepoints.

2.10 Yeast Growth Analysis via Serial Dilution

Yeast growth analysis was also performed using a serially diluted culture spotted onto solid growth media. This was employed to reveal differences in sensitivity to various environmental stimuli between yeast strains.

5ml yeast cultures were grown from a colony overnight to reach early stationary phase. Cells were counted, and cultures were diluted to 10^6 cells/ml. A serial dilution was then conducted, using a dilution factor of 3, to create 9 suspensions of decreasing cell content. Using a template, 10μl spots of each dilution were transferred to plates. The cell counts were: 10 000, 3 333, 1 111, 370, 123, 41, 14, 4.5, 1.5. Cells were allowed 2 days to grow, then photographed.

2.11 UV Survival Analysis

Cells were grown to late log-phase in appropriate media, then counted and diluted to 10^7 cells/ml. Further serial dilution then occurred in media to provide 2 000 cells/ml. 100μl of cell suspension (200 cells) was plated on 2% agar plates containing appropriate media. Plates were then irradiated with a range of UV doses, including an untreated control. All UV doses were conducted in triplicate. Following UV irradiation, plates were kept in darkness and allowed to form colonies for 48 hours. Colonies were counted, and % surviving cells were calculated using the untreated average as 100%.

3 Investigating the Role of a Possible Interaction Between the 19S Proteasome and Abf1 in DNA Replication and NER

The subtle interplay between different and diverse cellular pathways allows complex and coordinated regulation of metabolic processes required for survival and integrity of living organisms. A connection between the UPS and NER is well established, as is the relationship between the UPS and transcriptional control. The aim of this chapter is to investigate a possible regulatory function of the 19S proteasome in DNA replication involving the global regulator Abf1, a DNA binding factor that participates in multiple cellular processes including NER, DNA replication and transcription.

3.1 Introduction

The UPS primarily provides a highly efficient and specialised system for degradation of damaged cellular proteins and removal of regulatory protein factors to influence their regulatory activity. Aside from its canonical role in ubiquitin-dependent proteolysis, the 19S proteasome base subcomplex, more specifically the AAA ATPase subunits (Chapter 1.5, Figure 1.3), have been found to have a non-proteolytic regulatory role in transcription, both in activation and elongation, (Swaffield et al. 1992; Xu et al. 1995) and DNA repair (Gillette et al. 2001).

Another factor involved in a variety of cellular processes is Abf1, a 'global regulator'. Abf1 was discussed previously as a GG-NER factor (Chapter 1.4.6), in a complex with Rad7 and Rad16, however the scope of Abf1 function extends beyond DNA repair. Originally identified as a DNA replication factor, Abf1 has since been implicated in such diverse processes as gene silencing (Wiltshire et al. 1997), transcriptional control of numerous genes involved in a diverse set of cellular processes such as meiosis (Gailus-Durner et al. 1996), sporulation (Ozsarac et al. 1997) and nutrient metabolism (Park et al. 1999), and Abf1 functions in NER as discussed previously (Chapter 1.4.6) (Reed et al. 1999).

3.1.1 Abf1 – A DNA Replication Factor

Abf1 was originally discovered as a DNA-binding protein that interacts with the B3 DNA element of Autonomously Replicating Sequences (ARS), and has a regulatory effect on DNA replication at certain sites in the genome (Diffley and Stillman 1988).

3.1.1.1 Autonomously Replicating Sequences (ARS)

The *S. cerevisiae* genome contains numerous defined cis-acting sequences dispersed throughout the genome that function as DNA replication origins, known as ARS (Clyne and Kelly 1997). ARS were first discovered as sequences that improved the efficiency of DNA transformation into yeast cells. They were found to allow a plasmid to replicate in a stable manner without integrating into the genome (Stinchcomb et al. 1979). It was then found that these ARS correspond to origins of DNA replication, and were spaced at a frequency of 32-40kb across the genome.

The structure of ARS are modular and variable, however they all have a high A/T content, and all contain the essential 11bp ARS consensus sequence (ACS), which provides a binding site for the 6-subunit origin recognition complex (ORC). ARS also contain additional near-matches to the ACS that are dispensable for ARS function, but mutation of sequences flanking the ACS can affect ARS function. The ACS along with its immediate flanking sequence is known as the A-element. Although the ACS-containing element is essential for origin function it is not sufficient, and requires the action of additional ARS elements known as B-domains (Figure 3.1). The variable structure of ARS allows staggered initiation of DNA replication during S-phase to ensure efficient replication of the entire genome (Marahrens and Stillman 1992).

The B-domain is composed of several short elements (B1-B4) that share very little sequence homology and are highly variable between ARS. The B1 element functions with the A-element to bind the ORC, and the B3 element provides a binding site for ARS Binding Factor 1 (Abf1). Abf1 binding is

required for specific ARS function, but not all ARS contain a B3 element or require Abf1 binding (Theis and Newlon 1997). There are numerous other proteins that bind to ARS, which have various regulatory roles in initiation of DNA replication. The precise function of the B2 and B4 elements is not known, however the B2 elements of ARS1 and ARS307 can substitute for each other. The B4 element of ARS305 cannot be substituted by any of the ARS1 B elements (Figure 3.1) (Yang et al. 1999).
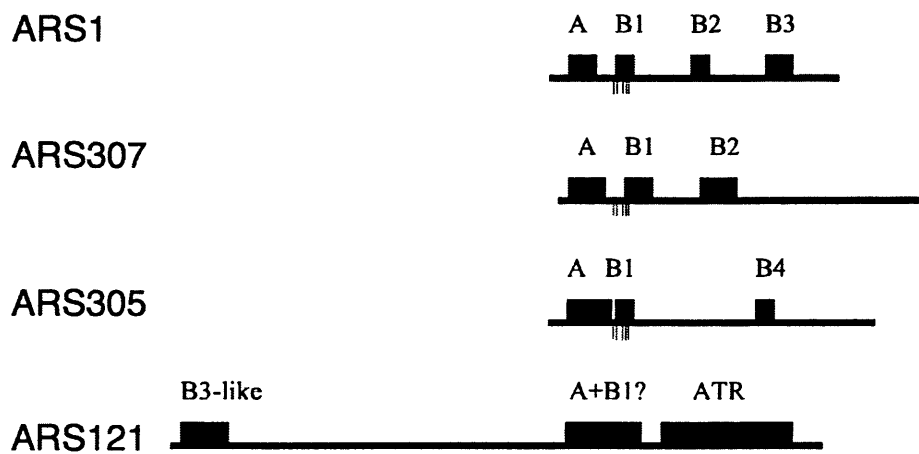
Figure 3.1 – The Variable Modular Structure of ARS. Four different genomic ARS are displayed here, revealing their varied modular structure and aligned according to the essential ACS sequence (tick marks below line). The A and B elements are shown, and ATR is the AT rich region present in some ARS. Figure adapted from (Theis and Newlon 1997).

3.1.2 Abf1 – Transcriptional Regulator

Following its discovery as an ARS binding factor, it was soon evident that Abf1 was more than just a DNA replication factor. It is a site-specific DNA binding protein, and following extensive editing and redefinition since its original sequence was published, the currently accepted DNA binding motif of Abf1 is $^{5'}$TnnCGTnnnnnnTGAT$^{3'}$, deduced by *in vitro* selection (Beinoraviciute-Kellner et al. 2005). In addition to ARS, Abf1 binding sites are found at numerous other specific loci throughout the genome, including the mating type loci where it is required for transcriptional silencing, at telomere X-regions and in the promoter regions of many genes (Miyake et al. 2004).

The function of Abf1 in transcription and DNA replication was characterised by the Campbell lab in 1992 (Rhode et al. 1992), which identified a variety of single-nucleotide mutant alleles in the N-terminal DNA binding domain. The most severe viable mutant allele (abf1-1) was found to have compromised DNA binding at the semi-permissive temperature (32°C) and DNA binding was completely abolished at 37°C resulting in cell death. Microscopic observation of these cells showed they were enlarged with small elongated buds, a phenotype resembling cells overproducing STE12, a transcription factor involved in pheromone response (Dolan and Fields 1990). The mutant alleles also exhibited reduced ARS function, DNA and RNA synthesis, and reduced plasmid stability in plasmids containing an Abf1-dependent ARS.

The transcription of over 100 genes is regulated by Abf1 binding, thus impacting upon a variety of metabolic processes including carbon source regulation (Chambers et al. 1990), nitrogen utilisation (Park et al. 1999), sporulation (Ozsarac et al. 1997), meiosis (Gailus-Durner et al. 1996) and ribosomal function (Planta 1997), and also regulates its own expression (Miyake et al. 2004). Abf1 binding is only required for transcriptional initiation, and ongoing transcription can occur after Abf1 dissociation (Yarragudi et al. 2007). Silencing at the HMR-E mating type locus is also mediated by Abf1 binding, which occurs via nucleosome positioning (Zou et al. 2006). Abf1 is also reported to affect chromatin structure in ARS, acting as a boundary element to prevent nucleosome invasion of the A-element, allowing ORC binding and DNA replication to occur (Venditti et al. 1994).

3.1.3 Abf1 Structure and Function

The structure of Abf1 is that of a typical site-specific transcription factor, due to its N-terminal DNA-binding domains and C-terminal protein interaction/activation domains (Figure 3.2). The N-terminal domain has two essential binding regions, amino acids 40-91, which resembles a zinc finger metal binding domain, and residues 323-496, a basic region. Both domains are required for specific DNA-binding (Cho et al. 1995).

The C-terminal portion has also been mapped extensively, and contains two essential regions: CS1 occurs between residues 624-628 and CS2 at residues 639-662. These were deduced via construction of various C-terminal truncation and alanine substitution mutants, some of which were found to have similar sensitivities to the N-terminal mutants described previously. It was also found that CS1 is required for transcriptional silencing and gene repression whereas CS2 is involved in transcriptional silencing and gene activation, stimulation of DNA replication and chromatin remodelling (Miyake et al. 2002).
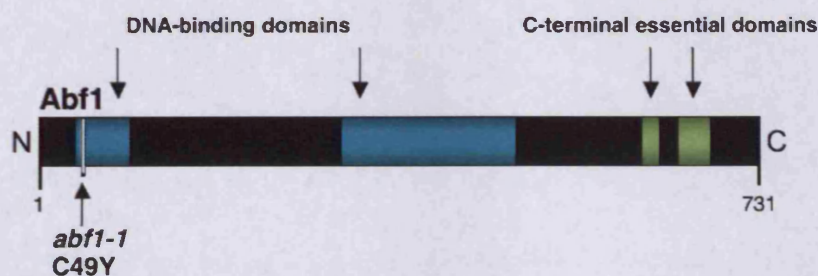
Figure 3.2 - Domain Structure of Abf1, Showing Location of *abf1-1* Point Mutation

3.1.4 Abf1 – A Promiscuous General Regulatory Factor

The high cellular abundance of Abf1, far greater than most other site-specific transcription factors, has placed the protein in a group known as general regulatory factors, of which three have been identified in *S. cerevisae*: Rap1, Reb1 and Abf1. These factors bind frequently throughout the genome, including at several gene promoters, and affect a multitude of cellular activities (Fourel et al. 2002).

In addition to its global DNA binding capacity, Abf1 is a promiscuous protein-binder, and its presence in a number of distinct protein complexes suggests Abf1 is a 'hub protein' (Luscombe et al. 2004). This indicates that the main function of Abf1 is to facilitate the formation of a variety of protein and nucleoprotein complexes. Abf1 has been found to co-precipitate with complexes involved in chromatin assembly and remodelling, notably the histone proteins Hta2 and Htb1, and the chromatin modifiers Rvb1, Rvb2 and Isw2. It has also been found in complexes with factors for transcriptional

59

regulation (Mot1, Sth1 and Taf5), activity of RNA Polymerase I (Hmo1 and Rpc40) and III (Rpc34, Rpc53 and Rpo31) and mRNA nuclear export (Yra1)(Luscombe et al. 2004; Schlecht et al. 2008).

Another distinct Abf1-containing protein complex is the Rad7-Rad16 GG-NER complex, which has revealed the role of Abf1 in NER of non-transcribed DNA. This was initially shown *in vitro* by defective NER in a strain with depleted Abf1 levels, and the UV-sensitive phenotype of the DNA binding-compromised *abf1-1* allele, which also implies that the DNA binding function of Abf1 is required for its role in NER (Reed et al. 1999).

3.1.5 Non-Proteolytic Regulatory Function of the 19S Proteasome

The 19S proteasome affects the DNA binding dynamics of the Gal4 transcriptional activator, which regulates its ability to drive *GAL* transcription. This is discussed in detail in Chapter 1.4. It is known that components of the 19S proteasome interact physically with Gal4's activation domain, which is thought to promote destabilisation of Gal4 DNA binding thus preventing unregulated transcriptional activation (Ferdous et al. 2002; Ferdous et al. 2007). This proteasome-mediated destabilisation of Gal4 from DNA was found to be inhibited by monoubiquitination of Gal4, allowing transcription initiation to proceed from *GAL* promoters for cells to utilise galactose as a carbon source (Archer et al. 2008b).

The regulatory activity of the 19S proteasome is not unique to Gal4, and like Abf1, the 19S has multiple interacting partners, with which it performs a variety of regulatory functions in cellular processes such as transcription (via Gal4 and Cdc68) (Chapter 1.5.3) (Swaffield et al. 1992; Xu et al. 1995) and NER (via Rad23) (Chapter 1.5.5) (Gillette et al. 2001). These overlapping functions could suggest interplay between the two factors. Gal4 and Abf1 share the common structure of a typical transcription factor, featuring an N-terminal DNA binding domain and a C-terminal activation domain. They are both sequence-specific DNA binding factors and have a role in transcriptional

control. The similarities between Abf1 and Gal4 structure suggest that the 19S proteasome could act upon them in a similar manner, by destabilising their DNA binding activity.

The following chapter aims to investigate a possible interaction between Abf1 and the 19S proteasome. Firstly, a physical interaction between Abf1 and Sug1 was investigated by conducting a co-immunoprecipitation (Co-IP) assay in a WT strain. In order to investigate whether the physical interaction was a functional, genetic interaction or not, strains with *abf1-1* and *sug2-1* mutant alleles were constructed. Growth analysis of the *abf1-1 sug2-1* mutant strain was performed to determine the effect on regulation of DNA replication. This was performed by serial dilution growth analysis on solid YPD plates and monitoring logarithmic growth of the mutant strains in liquid media. A UV survival assay was also performed to determine whether the Abf1-19S genetic interaction could affect Abf1's role in NER.

3.2 Materials and Methods

3.2.1 Yeast Strains Used

Strain	Genotype	Source
W303-1A	MATa ade2-1 trp1-1 leu2-3, 112 his3-11, 15 ura3-1 can1-100	(Russell et al. 1999)
WT	W303-1A S10-SUG1	(Russell et al. 1999)
sug1-20	W303-1A S10-sug1-20	(Russell et al. 1999)
sug2-1	W303-1A sug2-1	(Russell et al. 2001)
abf1-1 (JCA31)	MATa trp1Δ his3Δ200 ura3-52 lys2-801 ade2-1 gal abf1-1 HIS3[a]	(Rhode et al. 1992)
abf1-1	W303-1A S10-SUG1 abf1-1 URA3	This study
abf1-1 sug2-1	W303-1A sug2-1 abf1-1 URA3	This study

Yeast Strains were used and stored as described previously, except the *sug* mutants, which were grown at 25°C, stored at RT and re-plated frequently. This was due to severe genetic instability resulting in an increased tendency to revert to WT when grown at 30°C or stored at 4°C.

3.2.2 Construction of *abf1-1* and *abf1-1 sug2-1* Strains

The *abf1-1, sug2-1* and *abf1-1 SUG2* strains were constructed using a two-step linear DNA transformation process, similar to (Toulmay and Schneiter 2006), which exploits *S. cerevisiae's* homologous recombination system (Figure 3.3).

3.2.2.1 Insertion of *URA3* at the 3' End of *ABF1* ORF in *abf1-1* Strain

A *URA3* marker gene was inserted at the 3' end of the genomic *ABF1* sequence in the original *abf1-1 (JCA31)* strain. Insertion was targeted to 300bp downstream of the terminal codon to minimise defects caused by loss of downstream regulatory sequences. A 1.5kb fragment was amplified from the *pRS306* plasmid (Sikorski and Hieter 1989), using primers with 20bp homology to the plasmid flanking the *URA3* gene, and 50 bp overhang with homology to the sequence downstream of *ABF1* ORF. This was transformed

into the *abf1-1 (JCA31)* strain and transformants were grown on minimal media lacking uracil. Insertion was screened by colony PCR then confirmed by PCR amplification of genomic DNA from the newly constructed strain. One correct transformant was selected and a 500µl PCR was conducted to amplify the whole *ABF1* gene with the downstream *URA3* marker, using genomic DNA as a template. This provided a 4.2kb product, which was purified and concentrated into 30µl H$_2$O using the QIAquick PCR Purification Kit (Qiagen). The DNA was sequenced before proceeding to the transformation stage to ensure the presence of the *abf1-1* (G146A) mutation.
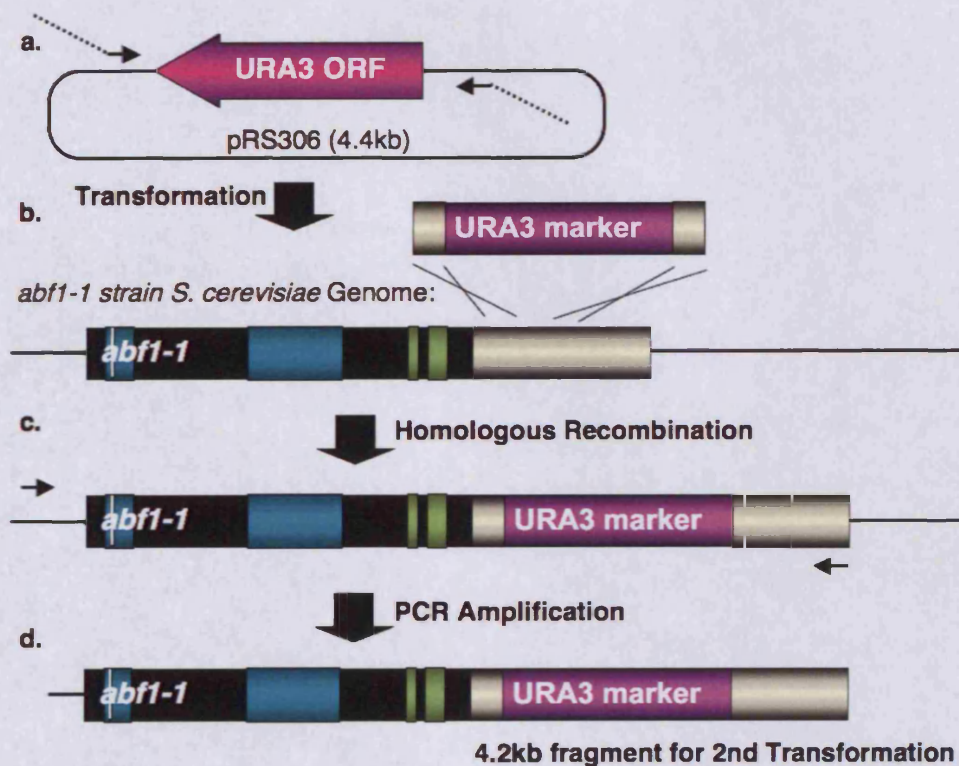
Figure 3.3 - Two-Step Transformation Procedure – Adapted From (Toulmay and Schneiter 2006). a: A *URA3* marker was amplified from the plasmid *pRS306*, using primers with 50bp homology to *ABF1* 3' UTR. **b**: The resulting *URA3* fragment was transformed into an *abf1-1* strain, which was inserted 3' of *ABF1* via homologous recombination. **c**: Genomic DNA was purified from the transformed strain and a 4.2kb region was amplified (**d**) and was transformed into *sug2-1 and sug1-20* mutant strains. The abf1-1 mutation and URA3 marker were then incorporated into the genome via homologous recombination.

3.2.2.2 Construction of *abf1-1 URA*⁺ Mutant Strains

This 4.2kb product was used to transform the *sug2-1* and corresponding WT strain, and transformants were once again grown on media lacking uracil. Insertion was checked by colony PCR and prospective mutant colonies were replated onto new plates lacking uracil. Although the *URA3* insertion may have been successful in the transformants, it was imperative that the resulting colonies harboured the *abf1-1* mutation. Rather than sequencing every colony a higher throughput method was developed using the restriction endonuclease *Mae*III, (Roche) which recognises and cuts at $^{5'}$GTNAC$^{3'}$ sequences. The *abf1-1* mutation creates a *Mae*III restriction site, not present in the WT sequence (Figure 3.4).

Figure 3.4 - Formation of *Mae*III digestion site in *abf1-1* mutant, and result of *Mae*III digestion on 388bp fragment in *abf1-1*

Colonies were screened by extracting genomic DNA, then amplifying a 388bp sequence incorporating the *abf1-1* mutation site. The fragment was digested using *Mae*III, then run on an agarose gel, which was photographed using UV light and the visible bands were analysed. Two bands (147 and 241bp) confirmed the presence of *abf1-1* whereas a single band (388bp) represented the WT sequence. Transformants displaying two DNA bands following digestion were sequenced.

3.2.3 Co-Immunoprecipitation (Co-IP) Assay

2μl anti-Abf1 (Santa Cruz) was added to 400μg WCE in 500μl YDB, which was incubated on a Mini Labroller (Labnet) at 4°C for 1 hour. 100μl 10% Protein A-coated Sepharose beads (Amersham) were added and incubated for a further 2 hours. The suspension was centrifuged for 10 minutes at 13 000 rpm, and the supernatant was discarded. Beads were then washed 3 times with YDB, and then proteins were incubated at RT for 1 hour in 30μl 1x SDS loading buffer containing 6M urea to denature protein complexes. Beads were then removed by centrifugation, and the supernatant was incubated at 95°C for 10 minutes then used for SDS-PAGE and western blotting.

3.3 Results

3.3.1 Identification of a Physical Interaction Between Abf1 and Sug1

Prior to undertaking experiments to examine a possible functional interaction between Abf1 and the 19S proteasome, a Co-IP assay was employed to determine whether a physical interaction between the two factors existed. The presence of Sug1, a 19S proteasomal AAA ATPase, in an IP assay conducted using an Abf1 antibody was used to test the existence of a physical interaction. A whole-cell protein extract (WCE) was obtained from a WT strain, and protein complexes with affinity for an Abf1 antibody (Santa Cruz) were isolated using immunoprecipitation. Complexes were denatured by boiling in SDS loading buffer, and denatured proteins were separated by polyacrylamide gel electrophoresis. The proteins were transferred to a PVDF membrane, and the presence of Abf1 and Sug1 in the IP sample were detected by Western Blotting (Figure 3.5).
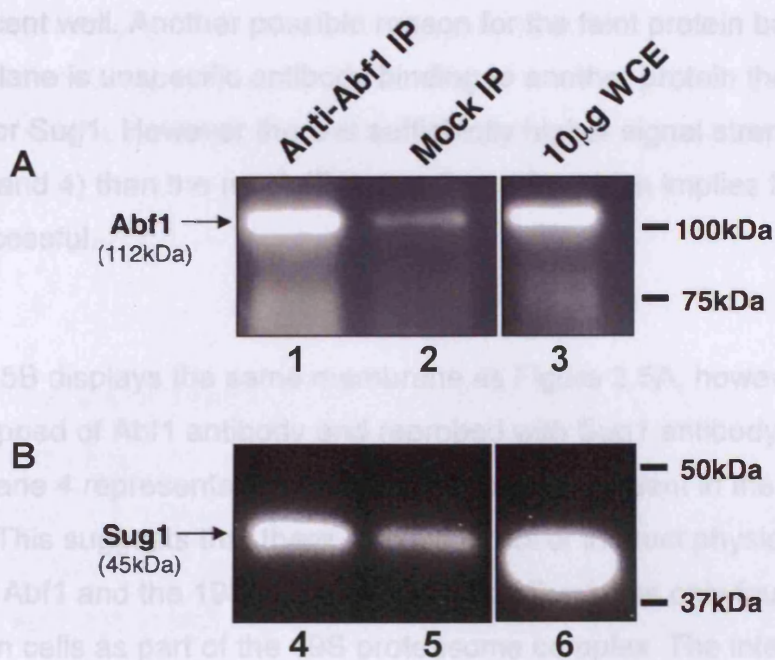
Figure 3.5 – Western Blot of anti-Abf1 Immunoprecipitation Probed with A: anti-Abf1 and B: anti-Sug1. An immunoprecipitation (IP) was performed by incubating WT WCE with anti-Abf1 and Protein A beads. Co-immunoprecipitated proteins were run on a polyacrylamide gel and used to conduct a western blot. The blot was probed with anti-Abf1(A), then stripped and probed with anti-Sug1 (B). The lanes represent proteins precipitated from the anti-Abf1 IP (1 and 4), a Mock IP using no anti-Abf1 (2 and 5), and 10µg non-immunoprecipitated WCE (3 and 6).

Figure 3.5A displays the Western Blot conducted using the anti-Abf1 IP sample, probed with the same Abf1 antibody for western blotting. This blot was conducted as a control experiment to ensure the Abf1 IP was successful. The intense band in lane 1 representing the 112kDa Abf1 protein confirms that the Abf1 IP was successful. The WCE sample in Lane 3 displays a band of an identical size to lane 1, which indicates the presence of Abf1.

The mock IP (Figure 3.5A and B, lanes 2 and 5) was conducted as a negative control. The IP conditions were the same for the mock as the actual IP but an equivalent volume of pre-immune serum was added instead of Abf1 antibody. Limited signal for both Abf1 and Sug1 is detected in their corresponding mock IP lanes (Figure 3.5A and B, lanes 2 and 5). This is most likely due to loading of the polyacrylamide gel, whereby some of the IP sample may have entered

the adjacent well. Another possible reason for the faint protein band in the mock IP lane is unspecific antibody binding to another protein the same size as Abf1 or Sug1. However there is sufficiently higher signal strength in the IP (lanes 1 and 4) than the mock IP (lanes 2 and 5), which implies that the Co-IP was successful.

Figure 3.5B displays the same membrane as Figure 3.5A, however it has been stripped of Abf1 antibody and reprobed with Sug1 antibody. The intense band in lane 4 represents the 45kDa Sug1 protein present in the anti-Abf1 IP sample. This suggests that there exists a direct or indirect physical interaction between Abf1 and the 19S proteasome, since Sug1 has only found to be present in cells as part of the 19S proteasome complex. The intense band in lane 6 displays the presence of Sug1 in the WCE sample, at the same size as lane 4. These results provide evidence that Abf1 physically interacts with the 19S proteasome.

3.3.2 Investigating a Functional Genetic Interaction between Abf1 and the 19S Proteasome via Phenotypic Analysis of Mutant Strains

The outcome of the Co-IP provided preliminary supporting evidence that Abf1 physically interacts with the 19S proteasome. The study proceeded to investigate the function of this possible interaction by examining cellular phenotypes, thus determining whether a genetic interaction is occurring or not. *ABF1* and the *SUG* genes are essential for cell viability, so in order to deduce the significance of their interaction a double mutant strain was constructed, using the *abf1-1* and *sug2-1* alleles characterised previously (Rhode et al. 1992; Russell et al. 2001). The *abf1-1* mutant allele has defective DNA binding, and the 19S proteasome is known to disrupt stable DNA binding of factors such as Gal4. Introduction of the *sug2-1* point mutation into the 19S proteasome was found to prevent Gal4-DNA destabilisation and thus promote stable Gal4 DNA binding (Figure 1.5). It was therefore speculated that the 19S proteasome may have a role in destabilising Abf1 DNA binding, an effect that may be accentuated in the DNA binding-defective

abf1-1 mutant allele. It was therefore hypothesised that introduction of both of *sug2-1* and *abf1-1* mutations in one strain could stabilise Abf1 DNA binding and suppress the cellular phenotypes associated with the *abf1-1* strain such as temperature sensitivity, slow growth and UV sensitivity (Rhode et al. 1992) (Reed et al. 1999).

3.3.2.1 Analysis of Temperature Sensitivity in *abf1-1 sug2-1* Strains

Temperature sensitivity of the newly constructed mutant strains was observed to characterise the possible functional genetic interaction between Abf1 and the 19S proteasome. The temperature sensitivity of the *abf1-1* mutant strain has been well documented previously. It results in a significant growth defect, visible at 30°C but more apparent at higher temperatures due to defective Abf1 DNA binding (Rhode et al. 1992). The *sug2-1* mutant allele does not have a significant defective growth phenotype compared to the WT strain under normal conditions (25°C or 30°C) or increased temperature (37°C). Failed DNA binding in the *abf1-1* mutant allele causes temperature sensitivity, so if the temperature sensitivity was reduced in the *abf1-1 sug2-1* double mutant it would suggest that the 19S defect was improving the binding stability of *abf1-1* to DNA and indicate a genetic interaction between Abf1 and the 19S proteasome.

In order to analyse temperature sensitivity, a serial dilution growth analysis assay was performed. *abf1-1* and *sug2-1* mutant strains were serially diluted in liquid YPD and spotted onto YPD plates, then allowed to grow for 2 days at a range of temperatures. The plates were photographed after 48 hours growth (Figure 3.6).
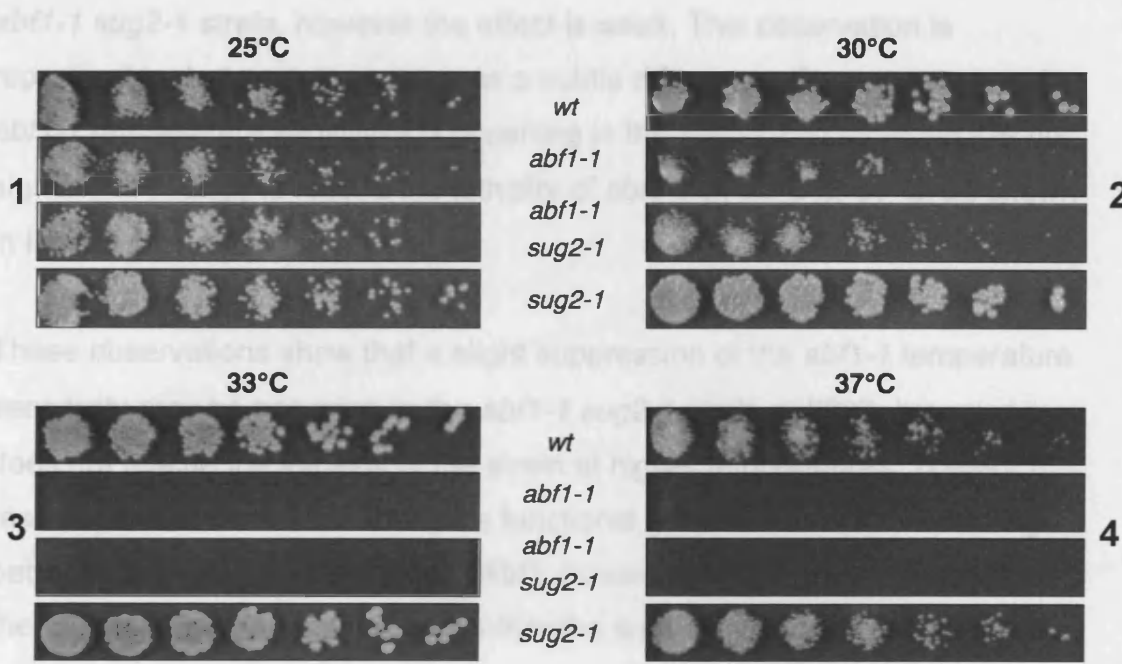
Figure 3.6 – Serial Dilution Growth Analysis of *abf1-1* and *sug2-1* Mutants. *abf1-1* and *sug2-1* mutant cells were serially diluted in liquid YPD, then 10µl cell suspensions were spotted and grown on YPD plates at the stated temperatures (Panels 1-4). The plates were photographed after 48 hours growth.

Figure 3.6, Panel 1 displays all four strains growing at the same rate at 25°C, which suggests that *abf1-1* binds DNA normally at this temperature. This also confirms the consistent accuracy of cell counts and concentrations across the strains, which greatly aids comparative analysis between the strains.

Panel 2 exhibits growth rate variations between the strains, displaying the severe temperature sensitivity of the *abf1-1* strain. This phenotype shows the same sensitivity as the original strain *(abf1-1 (JCA31))*, which helps confirm that introduction of the *abf1-1* mutation has been performed successfully. This is also the case in Panel 3 and 4, which are lethal temperatures for the *abf1-1 (JCA31)* strain, and the lethality is displayed clearly here for the *abf1-1* strain. The *sug2-1* strain exhibits no temperature sensitivity at any temperature investigated, which can be seen by comparing the *sug2-1* strain to the WT strain in Panels 1-4. It appears that a slight suppression of the *abf1-1* temperature sensitivity may be occurring in the *abf1-1 sug2-1* strain at 30°C, as seen in Panel 2. This could represent improved Abf1 DNA binding in the

abf1-1 sug2-1 strain, however the effect is weak. This observation is reproducible, but always appears as a subtle difference. If a suppression of *abf1-1* temperature sensitivity is occurring in the *abf1-1 sug2-1* strain it is not significant enough to rescue the lethality of *abf1-1* at 33°C or 37°C, as shown in Panels 3 and 4.

These observations show that a slight suppression of the *abf1-1* temperature sensitivity may be occurring in the *abf1-1 sug2-1* strain at 30°C, however it does not rescue the lethality of the strain at higher temperatures. These results provide some indication of a functional genetic interaction occurring between the 19S proteasome and Abf1, however further growth analysis of the mutant strains is required to confirm the subtle effect seen in Figure 3.6, panel 2.

3.3.2.2 Growth Analysis of *abf1-1 sug2-1* Mutant Strains

The *abf1-1 sug2-1* strain exhibited slightly reduced temperature sensitivity than the abf1-1 strain, which could indicate a functional genetic interaction was occurring. In order to examine the interaction further, growth curves were performed on the strains to observe their rate and manner of growth. Strains were grown in YPD, and cell concentration was measured at hourly intervals (Figure 3.7). Numerical OD_{600} reading are displayed in Appendix V.

1 Growth at 25°C

Legend: wt, abf1-1, sug2-1, abf1-1 sug2-1

OD_{600} vs Time (hours)

2 Growth at 30°C

Legend: wt, abf1-1, sug2-1, abf1-1 sug2-1

OD_{600} vs Time (hours)

3 Growth at 37°C

Legend: wt, abf1-1, sug2-1, abf1-1 sug2-1

OD_{600} vs Time (hours)
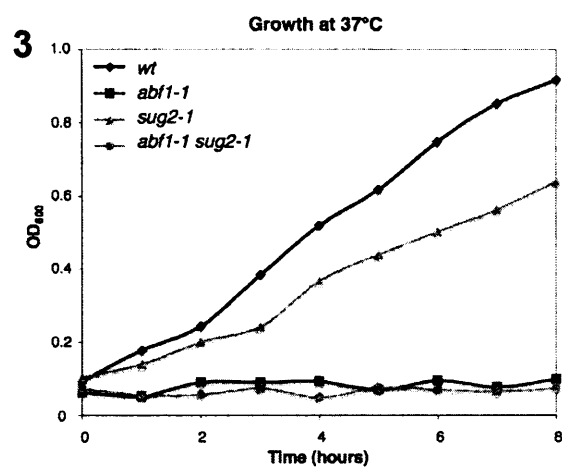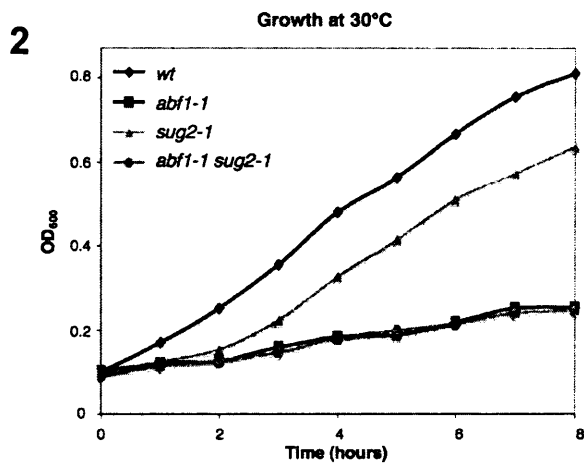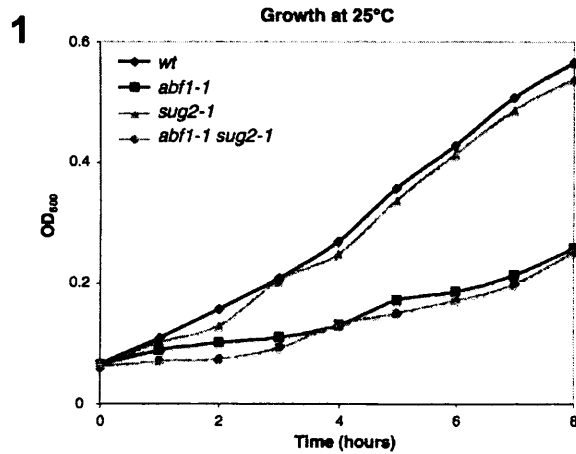
Figure 3.7 - Growth Curve of *abf1-1* and *sug2-1* Mutant Strains. WT, *abf1-1*, *abf1-1 sug2-1*, and *sug2-1* strains were diluted to OD_{600} 0.1 then grown in YPD for 8 hours at the stated temperatures (graphs 1-3). Cell concentration was observed at hourly intervals by measuring OD_{600} using a visible light spectrophotometer.

Graph 1 in Figure 3.7 shows growth of all strains at 25°C, which unlike the temperature sensitivity analysis shows that the *abf1-1* strains have a slower growth phenotype. This phenotype suggests that Abf1 binding appears to be less efficient at 25°C and not just at higher temperatures, although this does not appear to affect cell viability at 25°C, as shown in Figure 3.6, Panel 1.

The main interest of Figure 3.7 is Graph 2, which was intended to characterise further the suppression of the *abf1-1* temperature sensitivity in the *abf1-1 sug2-1* strain observed in Figure 3.6, Panel 2. The growth curves of Figure 3.7, Graph 2 show the *sug2-1* strain exhibiting a slightly slower growth phenotype than the WT strain, but the *abf1-1* and *abf1-1 sug2-1*

71

strains appear to have precisely the same growth rate at 30°C. This suggests that the slight suppression of temperature sensitivity observed in Figure 3.6, Panel 2 by the *sug2-1* mutation in the *abf1-1* strain is not due to improved DNA replication, otherwise it would be expected that the cell cycle time, i.e. growth rate would be increased to a rate closer to the WT rate.

Figure 3.7, Graph 3 also fails to show suppression of the lethality of the *abf1-1* allele at 37°C in the *abf1-1 sug2-1* strain, and also shows the slower growth phenotype of the *sug2-1* strain. The *abf1-1* and *abf1-1 sug2-1* strains are unable to grow at 37°C.

From the results displayed in Figure 3.7, it can be concluded that the slight suppression of temperature sensitivity observed in Figure 3.6, panel 2 is not due to increased growth rate in the *abf1-1 sug2-1* strain compared to the *abf1-1* strain. This suggests that the genetic interaction between Abf1 and the 19S proteasome does not affect the DNA replication defect caused by the *abf1-1* mutation, so therefore may affect another specific function of Abf1 or the 19S.

3.3.3 UV Survival Analysis of *abf1-1* and *sug2-1* Mutant Strains

Abf1 and the 19S proteasome both have roles in NER (Reed et al. 1999; Russell et al. 1999). In order to investigate further the genetic interaction between Abf1 and the 19S proteasome a UV survival assay was conducted using the WT, *abf1-1* and *abf1-1 sug2-1* strains. This analysis was performed to deduce whether the Abf1-19S interaction has a functional role in NER, and thus characterising a genetic interaction between the factors. It is proposed that the functional interaction could involve the 19S proteasome affecting Abf1 DNA binding stability. This hypothesis predicts that introduction of the *sug2-1* mutation in the *abf1-1* strain could suppress the DNA binding defect of *abf1-1*, thus allowing it to bind DNA more stably thus improving NER efficency in the *abf1-1 sug2-1* mutant strain. Logarithmically growing cells were exposed to a range of UV doses and allowed to form colonies for 48 hours. Colonies were counted and are displayed in Figure 3.8.
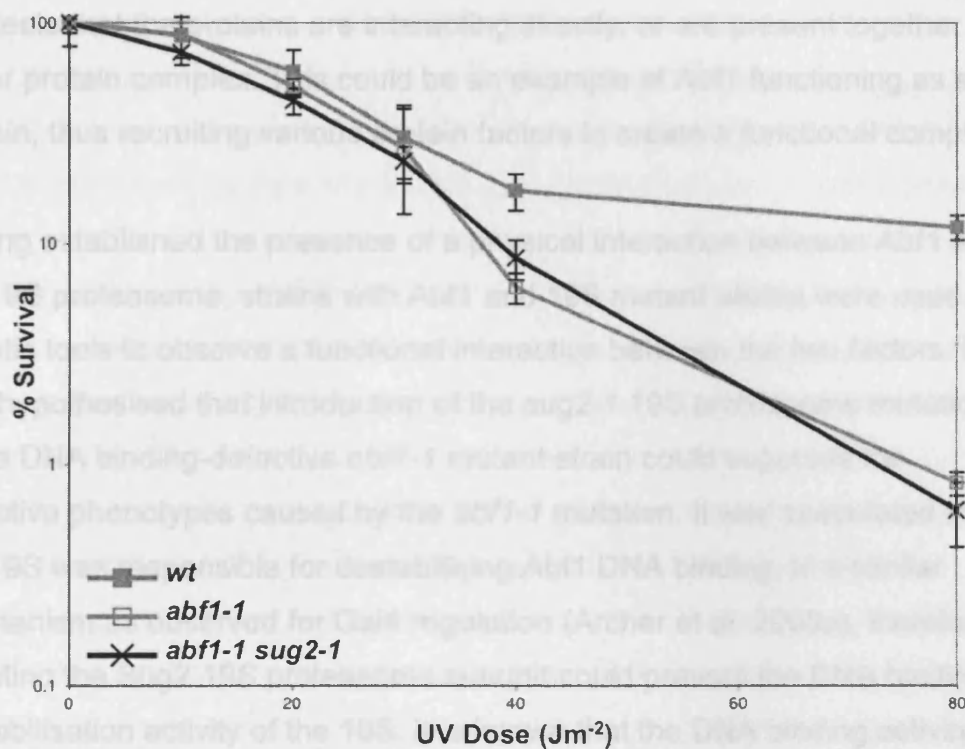
Figure 3.8 - UV Survival of *abf1-1* and *abf1-1 sug2-1* Strains Cells were spread onto agar plates and irradiated with the stated doses of UV. Following 2 days growth surviving colonies were counted and % survival calculated. Raw data values are presented in Appendix II.

It has been characterised previously that the *abf1-1* allele causes significantly increased sensitivity to UV irradiation, which was one of the first indications that Abf1 was involved in NER (Reed et al. 1999). Figure 3.8 shows that the *abf1-1 sug2-1* strain exhibits no altered UV sensitivity compared to the *abf1-1* strain. This suggests that the functional interaction between Abf1 and the 19S proteasome does not affect Abf1's role in NER.

3.4 Discussion and Further Work

The aim of this chapter was to deduce a possible functional interaction between the 19S proteasome and Abf1, thus revealing a novel role of the 19S proteasome in DNA replication, and further characterising Abf1 and the 19S proteasome's role in NER. The Co-IP (Figure 3.5) provided evidence of a

physical interaction between Abf1 and the 19S proteasome, which either suggests that the proteins are interacting directly, or are present together in a larger protein complex. This could be an example of Abf1 functioning as a hub protein, thus recruiting various protein factors to create a functional complex.

Having established the presence of a physical interaction between Abf1 and the 19S proteasome, strains with Abf1 and 19S mutant alleles were used as genetic tools to observe a functional interaction between the two factors. It was hypothesised that introduction of the *sug2-1* 19S proteasome mutation into a DNA binding-defective *abf1-1* mutant strain could suppress the defective phenotypes caused by the *abf1-1* mutation. It was speculated that the 19S was responsible for destabilising Abf1 DNA binding, in a similar mechanism as observed for Gal4 regulation (Archer et al. 2008a), therefore mutating the Sug2 19S proteasome subunit could prevent the DNA binding destabilisation activity of the 19S. It is known that the DNA binding activity of Abf1 is required for its role in DNA replication and NER, so the mutant strain was analysed phenotypically for growth rate and UV resistance to investigate a suppression of the *abf1-1* defects in the *abf1-1 sug2-1* strain.

It was found that combining the *sug2-1* mutation in a strain containing the *abf1-1* allele had a slight suppressive effect of the temperature sensitivity of the *abf1-1* mutant strain at 30°C (Figure 3.6 panel 2), but was unable to suppress the lethality of the *abf1-1* allele at higher temperatures (Figure 3.6 panels 3 and 4). The suppressive effect at 30°C was experimentally reproducible, but always appeared as a subtle effect. This suggests that the Abf1-19S proteasome interaction can slightly enhance cell viability at the permissive temperature, possibly by improving Abf1 DNA binding stability. The suppression of temperature sensitivity showed a possible functional interaction, but did not reveal what aspect of Abf1 or 19S proteasome activity was being enhanced. Analysis of logarithmic growth in the mutant strains was performed to reveal improved DNA replication, as defects in DNA replication cause delayed cell cycle progression resulting in slow growth. The growth curves of the *abf1-1 sug2-1* strain showed no difference in growth rate to the

abf1-1 strain (Figure 3.7), which would suggest that the Abf1-19S proteasome interaction does not have a role in DNA replication.

The UV survival analysis of the mutant strains was performed to identify whether the functional role of the Abf1-19S genetic interaction was involved in NER or not. Figure 3.8 shows no suppression of UV sensitivity caused by the *abf1-1* mutation in the *abf1-1 sug2-1* strain. This suggests that the functional interaction between Abf1 and the 19S proteasome does not have a role in NER. An alternative explanation of the results observed in Figure 3.7 and Figure 3.8 could be the loss of the *sug2-1* mutation, as the *sug* alleles are known to be prone to reversion to WT. The starter colonies used for the growth analysis and UV survival assay had genomic DNA extracted and sequenced at the *abf1-1* and *sug2-1* mutation sites. The sequencing results showed that the *abf1-1* and *sug2-1* mutations were present in all samples, so reversion of the mutations is not the cause of the same growth pattern and same UV survival curve of the *abf1-1* and *abf1-1 sug2-1* strains. It has therefore been concluded that the Abf1-19S proteasome interaction does not have a significant function in NER or DNA replication.

The *sug2-1* mutation was used in this study because it is known to prevent the 19S from destabilising Gal4 DNA binding, the mechanism that was proposed to be occurring for Abf1 too, however, alternative *sug* mutant alleles are known to behave differently. Certain *sug* mutant alleles can suppress phenotypes that others cannot, and vice versa. The *sug1-20* mutant allele is known to suppress the transcriptional elongation defect of the *cdc68-1* mutant (Xu et al. 1995), but does not affect Gal4 DNA binding stability like *sug2-1* or *sug1-1*. Construction of an *abf1-1 sug1-20* double mutant was attempted by introducing *abf1-1* into a *sug1-20* background. The mutagenesis was undertaken using the same method as used for the *sug2-1* strain, however all prospective URA^+ mutants lacked the *abf1-1* and/or *sug1-20* mutations. This could be due to the high reversion rate of *sug1-20*, or that the combined effect of the mutations is lethal. Whatever the cause, a stable double mutant could not be constructed, so allele specificity could not be investigated.

Abf1 also has several functional mutant alleles, such as the C-terminal mutants characterised by (Miyake et al. 2002) These mutants can still bind to DNA, but have similar temperature sensitivity to *abf1-1* due to defective C-terminal activation function. This could be a more suitable representation of the Gal4-Sug system mentioned previously, which also used C-terminal mutants (Swaffield et al. 1992). The DNA binding dynamics of the Abf1 C-terminal mutants have not been characterised previously, but this could be conducted using chromatin immunoprecipitation (ChIP) at various Abf1 binding sites such as ARS and gene promoters.

An effect of the Abf1-19S proteasome interaction on DNA replication could not be identified by growth analysis, but it may be of interest to investigate Abf1 occupancy at ARS using ChIP in the mutant strains. This would provide a more direct insight into Abf1 DNA binding stability, and could be performed at a local level on specific ARS or for a more comprehensive overview of global Abf1 binding, ChIP-chip analysis could be performed using *abf1* and *sug* mutant strains.

The aim of this chapter was to identify and characterise a functional interaction between Abf1 and the 19S proteasome. A physical interaction between the two factors was observed via protein Co-IP (Figure 3.5), so phenotypic analysis of an *abf1-1 sug2-1* mutant strain was conducted. A slight suppression of temperature sensitivity was observed in the *abf1-1 sug2-1* strain (Figure 3.6), however a suppression of the *abf1-1* DNA replication defect via growth analysis (Figure 3.7), or the *abf1-1* NER defect via UV survival (Figure 3.8), was not visible. Therefore, it appears that a functional interaction may exist between Abf1 and the 19S proteasome, which provides scope for further investigation in this area, however the functional interaction could not be characterised using the techniques employed in this chapter. Consequently, the study will now proceed to focus on another aspect of the function of GG-NER factors in the DNA damage response, thus terminating this specific area of research at this stage of the study.

4 The Role of the Rad4-Rad23 Complex in Regulating DNA Damage-Responsive Gene Transcription

4.1 Introduction

Exposure of eukaryotic cells to DNA damaging agents instigates a variety of cellular responses, including a significant transcriptional response involving altered expression of a variety of genes throughout the genome. The intricate induction of stress responsive and DNA-damage responsive pathways at the transcriptional level is of paramount importance to maintain cell integrity and promote cell survival when faced with the insult of DNA damage.

4.1.1 The Rad4-Rad23 NER Complex and the DNA Damage Response

The Rad4-Rad23 complex is known to be an integral component of the NER pathway in *Saccharomyces cerevisae* and is thought to function in the DNA damage-recognition step of NER (Min and Pavletich 2007). Recently an important insight into the regulation of these early stages of NER was revealed, involving a novel function of the UPS (Gillette et al. 2006).

It was shown that UV irradiation triggered the UPS-dependent ubiquitination and proteolysis of Rad4, contrary to previous reports that UV-induced damage caused accumulation of Rad4 and its human homologue XPC, resulting in enhanced NER (Lommel et al. 2002; Ng et al. 2003). It has also been shown that the lower steady state levels of the Rad4 protein was not due to increased Rad4 proteolysis in the Δrad23 strain because lower levels of *RAD4* mRNA were observed. This could suggest that reduced *RAD4* transcription was the cause of lower Rad4 protein levels in the Δrad23 strain rather than increased protein turnover, however this remained speculative as many confounding factors could also have an influence (Gillette et al. 2006). The ubiquitin ligase responsible for ubiquitinating Rad4 was discovered to be an E3 ubiquitin ligase containing the Rad7 and Rad16 GG-NER factors with the Elc1 and Cul3 proteins, a function proposed in (Ramsey et al. 2004). Rad7

contains a *SOCS* domain, which classifies the ligase complex as a cullin-based Elongin-cullin-*SOCS* box (ECS)-type E3 ligase. Rad7's *SOCS* domain is essential for post-UV ubiquitination of Rad4.

A mutant strain was created that contained two point mutations in the *SOCS* domain of *RAD7* (L168A and C172A), which specifically prevented UV-dependent Rad4 ubiquitination. This E3 ligase-defective mutant was denoted the *psocs* strain, as it contains the mutant *RAD7* gene on a plasmid. The *psocs* strain was found to have no additional UV sensitivity compared to a WT strain, which initially suggested that post UV ubiquitination of Rad4 did not have a role in promoting UV survival, however, Rad23, which functions in NER in a complex with Rad4, contains an ubiquitin-like (UBL) domain, which is essential for its role in NER. It was investigated whether the presence of an ubiquitin-like sequence in the Rad4-Rad23 complex could affect its role in the DNA damage response by compensating for the lack of ubiquitinated Rad4. It was observed that the *psocs* mutant with *RAD23* deleted, or the *RAD23*'s UBL domain deleted strain resulted in increased UV sensitivity in these strains, significantly more so than the intermediate UV sensitivity of the Δ*rad23* or *rad23*Δ*ubl* strains (Gillette et al. 2006).

4.1.2 Two Distinct Components Regulate NER

Rad23 is thought to function in NER by mediating an interaction with the 19S proteasome via its UBL domain, and antagonising the 19S proteasome's inhibitory effect on NER. This has been shown by suppression of the Δ*rad23* strain's UV sensitivity by introduction of the *sug2-1* proteasome mutation (Gillette et al. 2001). It has been documented previously that two distinct components function in the NER pathway, one that requires *de novo* synthesis of protein factors and one that doesn't (Al-Moghrabi et al. 2003; Waters et al. 1993). Using the protein synthesis inhibitor cycloheximide, it was deduced that the Rad23 and 19S proteasome's activity in NER does not require *de novo* protein synthesis, whereas the other regulatory pathway, involving the Rad7-containing E3 ligase complex-mediated Rad4 ubiquitination does require *de novo* protein synthesis (Gillette et al. 2006).

This observation, along with the finding that *RAD4* is expressed at a lower level in the Δ*rad23* strain prompted the possibility that the Rad7-containing E3 ligase complex-mediated Rad4 ubiquitination could play a role in DNA damage-responsive gene transcription, thus having a role in regulating NER via the pathway that requires *de novo* protein synthesis.

4.1.3 The Rad4-Rad23 Complex as a Transcriptional Regulator

The ability of the Rad4-Rad23 DNA damage recognition complex to bind damaged DNA has been reported, and it is known that the complex can also bind to non-damaged DNA. Recent evidence from our laboratory has suggested a role of this complex in transcriptional control. It has been revealed by our laboratory that the Rad4-Rad23 complex binds to the promoters of certain genes by ChIP analysis (Z. Zhou, unpublished data).

Furthermore, a recent study has suggested a more global role of Rad23 in transcription, however this somewhat dismissed the involvement of Rad4, concluding that Rad23 was not acting with Rad4. This role of Rad23 in transcriptional regulation was observed in untreated and UV-irradiated cells, and it was suggested that Rad23, in conjunction with the 19S proteasome influences numerous downstream effectors to control the transcriptional response to UV. The mechanism also involved the DNA binding transcription factor Mig3. Rad23 was implicated in both activation and repression of genes affected by the transcriptional response to DNA damage (Wade et al. 2009).

This chapter will investigate further the role of the Rad23-Rad4 complex in transcription, with particular attention to the role of Rad7-dependent Rad4 ubiquitination in transcriptional control of the DNA damage response. It will also further investigate the role of Rad23 as a global regulator of transcription, as proposed by (Wade et al. 2009).

4.1.4 Transcriptional Responses to DNA Damage in S. cerevisiae

Early experiments using high throughput screening methods to identify transcriptionally altered genes in response to DNA damage discovered several genes including the Damage INducible genes (*DIN1-6*) and the DNA Damage Responsive genes (*DDR1-4*) (Ruby and Szostak 1985). These global screens paved the way for more powerful microarray technologies, which continue to reveal that a significant proportion of the genome is differentially expressed in response to DNA damage.

It is thought that most, if not all DNA damage-responsive genes are activated as a downstream effect of the Mec1-Rad53-Dun1 kinase cascade. Three main transcriptional targets of this cascade have been identified (Fu et al. 2008). Activation of the RNR pathway via phosphorylation of the Crt1 repressor by the Dun1 kinase results in elevation of cellular dNTP pools, a requirement for effective DNA synthesis. Regulation of the RNR pathway is discussed in more detail in Chapter 5.

DNA damage also induces transcription of *PHR1*, a photolyase that exclusively repairs UV-induced CPDs, however *PHR1* transcription is induced by a wide range of DNA lesions. The promoter of *PHR1* contains three regulatory elements, an upstream activating sequence (UAS) an upstream repression sequence (URS) and an upstream essential sequence (UES) (Sancar et al. 1995). Ume6, a transcriptional regulator involved in various metabolic pathways binds to the UAS and positively regulates *PHR1* transcription (Sweet et al. 1997). *PHR1* transcription is negatively regulated by Rph1 and Gis1, which bind to the URS. Rph1 becomes phosphorylated by the DNA damage response signal transduction pathway, which causes upregulation of *PHR1*. *PHR1* induction is dependent on Rad9, Rad17, Mec1 and Rad53, but not Dun1, which suggests that the Mec1-Rad53 kinase cascade is responsible for Rph1 phosphorylation, but via an upstream or separate branch of the pathway to Dun1. Rad53 does not interact with Rph1, so an alternative kinase is most likely involved (Kim et al. 2002).

The *MAG1* base excision repair factor is also transcriptionally induced by a wide variety of DNA damages, however is only required for repair of a small subset of lesions. Another damage-inducible gene, *DDI1* was found immediately upstream of *MAG1*. The expression of these genes is jointly regulated. The *MAG1* promoter contains an URS and an UAS, which surprisingly lies within the *DDI1* coding sequence. Another UAS regulates the expression of both genes (Liu and Xiao 1997). The transcriptional activator Pdr3 was found to bind to this UAS and induce *MAG1* and *DDI1* transcription (Zhu and Xiao 2004). The transcriptional activator, Rpn4, has also been shown to regulate *MAG1* and *DDI1* transcription, but it does not appear to bind the *MAG1-DDI1* UAS. Rpn4 deletion does not affect *MAG1/DDI1* expression in *pdr3* mutant cells, which suggests it functions upstream of Pdr3 (Zhu and Xiao 2004).

4.1.5 The Current Study

The aim of this chapter was to investigate the role of the Rad4-Rad23 complex in DNA damage-responsive global gene transcription following on from (Gillette et al. 2006), which presented evidence that suggested a possible role for the Rad4-Rad23 complex in transcriptional control. Global gene expression studies were performed in various mutant strains to identify genes with altered transcription both in untreated strains and strains exposed to UV radiation. The *psocs* strains were used to investigate the role of Rad4 in DNA damage-responsive transcription, because the *psocs* mutant specifically prevents post-UV Rad4 ubiquitination from occurring, and does not display the severe UV sensitivity of the Δ*rad4* strain. Two sets of microarrays were performed in this study. The first set observed transcriptional alterations in Δ*rad4*, Δ*rad23* and Δ*rad4*Δ*rad23* strains in the absence of UV. These 12 arrays are referred to as *rad4/rad23* arrays throughout this study. The second set of arrays looked at the transcriptional response to UV using the *psocs/rad23* mutant strains constructed in this chapter. These 30 arrays are referred to as the *psocs/rad23* arrays throughout this study. All microarrays performed in this study are available for public use on the Gene Expression

82

Omnibus (GEO) Database, the *rad4/rad23* arrays at:

http://www.ncbi.nlm.nih.gov/geo/query/acc.cgi?acc=GSE11871

and the *psocs/rad23* arrays at:

http://www.ncbi.nlm.nih.gov/geo/query/acc.cgi?acc=GSE23204

.CEL files are also included on the electronic Appendix IV CD.

4.2 Materials and Methods

Prior to investigation of global transcription, strains were constructed and checked for quality by observing UV sensitivity, which was required to confirm the sensitivity observed in (Gillette et al. 2006). The method of cell preparation and irradiation was also optimised prior to conducting microarrays to enhance the quality and accuracy of expression data acquired. For most analyses of DNA repair, it is common practice to UV-irradiate yeast cells in cold PBS. For the purposes of analysing global transcription, exposure to cold PBS would trigger a transcriptional response of its own, not related to the UV response. For this reason, a method of irradiating cells in minimal media was devised, and a UV survival assay was conducted to compare UV penetration in PBS versus minimal media.

4.2.1 Yeast Strains Used

Strain	Genotype	Source
Δrad4	*BY4742: MATα his3Δ1 leu2Δ0 ura3Δ0 YER162C::KanMx4*	EUROSCARF
Δrad23	*BY4742: MATα his3Δ1 leu2Δ0 ura3Δ0 YEL037C::KanMx4*	EUROSCARF
Δrad4 Δrad23	*BY4742: MATα his3Δ1 leu2Δ0 ura3Δ0 YEL037C::KanMx4 YER162C::HIS3*	EUROSCARF
Δrad7	*BY4742: MATα his3Δ1 leu2Δ0 ura3Δ0 YJR052W::KanMx4*	EUROSCARF
pRS314-pRAD7	*W303-1A S10-SUG1 Δrad7::LEU2 pRS314-RAD7*	(Gillette et al. 2001)
pRS314-psocs	*W303-1A S10-SUG1 Δrad7::LEU2 pRS314-RAD7*	(Gillette et al. 2001)
pRAD7 sug2-1	*W303-1A sug2-1 rad23::HIS3 pRS314-RAD7*	(Gillette et al. 2001)
psocs sug2-1	*W303-1A sug2-1 rad23::HIS3 pRS314-socs*	(Gillette et al. 2001)
pRAD7	*BY4742 pRS313-RAD7*	This Study
psocs	*BY4742 pRS313-socs*	This Study
pRAD7 Δrad23	*BY4742 rad23::URA3 pRS313-RAD7*	This Study
psocs Δrad23	*BY4742 rad23::URA3 pRS313-socs*	This Study

4.2.2 UV Sensitivity Streak Test

Yeast cell cultures were grown from a single colony overnight in 5ml of the appropriate liquid media. They were then diluted to OD_{600} = 0.1 in of 1ml media, and a streak of this cell suspension was drawn across an agar plate using a sterile cotton swab. The plate was then covered, and exposed to UV (254nm, $10Jm^{-2}s^{-1}$). The cover was progressively removed over a 10 second period, so the streak of cells received an increasing dose of UV ($0-100Jm^{-2}$). Then the cover was replaced and cells were allowed to grow at 30°C for 48 hours and photographed after this period. This method was used for colony screening to get an initial indication of UV sensitivity. For more accurate

analysis of UV sensitivity, a UV survival assay was employed, involving plating irradiated cells and counting surviving colonies, performed in triplicate.

4.2.3 Analysis of Gene Expression Using qPCR

Total mRNA was extracted using the hot phenol method (Chapter 2.5), then reverse-transcribed into cDNA (Bio-Rad iScript cDNA Synthesis kit). This cDNA was then used for 20μl qPCR reactions, using SYBR green labelling buffer (Bio-Rad), and was run and analysed using the iCycler iQ qPCR Detection System (Bio-Rad). Each sample was conducted in triplicate, and a standard curve was prepared for each 96 well plate. qPCR data is displayed in Appendix VII.

4.2.4 Methods Pertaining to Microarray Preparation, RNA Submission and Analysis

4.2.4.1 Preparation of Cells and RNA Extraction

Cells were grown in YPD to late log phase (OD_{600} ~ 0.6), then total RNA was isolated using the hot phenol method (Schmitt et al. 1990) then run on agarose gel to visualise quality. mRNA was isolated from total RNA using Qiagen's Oligotex mRNA kit, and a single round of poly(A)$^+$ mRNA selection was performed to obtain optimal yield and purity of mRNA.

4.2.4.2 RNA Quality Controls

To check RNA quality, absorbance was measured at 260 and 280nm using a spectrophotometer (DU 800 UV/Visible Spectrophotometer, Beckman Coulter, Fullerton, CA) using the convention that 1 absorbance unit at 269nm equals 40μg RNA per ml. The A_{260}/A_{280} ratio should be within 1.9 and 2.1 in order to be of acceptable quality and purity. If the ratio fell within this range they were submitted for microarray expression analysis to the Affymetrix GeneChip expression profiling service (CBS, School of Medicine, Cardiff University).

4.2.4.3 Data Acquisition

Further RNA processing and microarray data acquisition was carried out by Affymetrix GeneChip expression profiling, performed at CBS (Cardiff), and described in Figure 4.1. The cDNA was hybridised to the Yeast Genome S98 chip, which represents all known yeast ORFs. Following scanning, microarray data was received as Affymetrix cell intensity (.CEL) files, which were then processed to obtain a representation of gene expression.
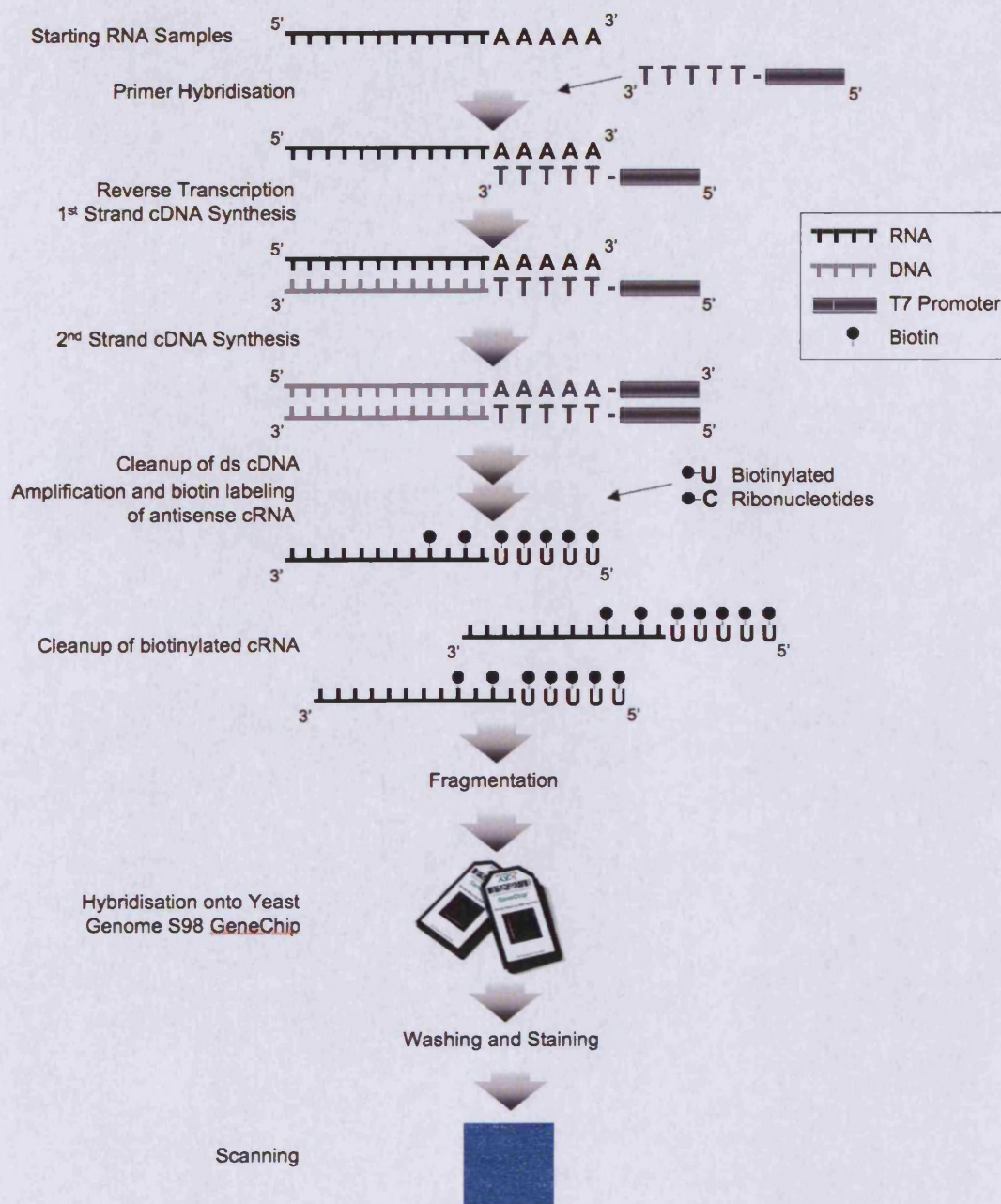
Figure 4.1 - RNA and Microarray Processing Adapted from Affymetrix GeneChip Expression Analysis Technical Manual.

4.2.4.4 Arrays Quality Assessment

Array quality was assessed using the Bioconductor *simpleaffy* package within R (Team 2010). A quality control (QC) plot was constructed to visualise RNA quality. Figure 4.2 shows the QC plot for the *psocs/rad23* arrays. In the QC plot each array is represented by a horizontal line. The central solid black line represents 0 fold-change (fc), and the two dotted black lines depict 3 fold up and down regulation. The blue bar shows the region that all arrays have scale factors within, over a default 3-fold range. The lines representing the arrays begin at the central 0 fc, and end with a dot, which corresponds to their scale factor. In Figure 4.2 all lines terminate in the blue region, which confirms their scale factors are compatible. The lines are coloured red if they are not compatible and blue if they are (all lines are blue).

The circular and triangular points represent the RNA pol III and Actin 3/5 ratios respectively. The values show the % of genes present (blue), and average background (red). It is preferable that the values are similar, which constitutes <10% variation in gene presence, and <20 units variation in background intensity. Figure 4.2 shows some variation in background intensity. This is most probably because the overall signal from the array is greater due to different amounts of cRNA present in the hybridisation cocktails or because of variations in hybridisation efficiency, thus incorporating different amounts of label and altering brightness of the chip (Wilson). The background intensity variation forms two groups with limited variation within each group. The groups coincide with the two different array sets *(pRAD7/psocs* (orange) and Δ*rad23 pRAD7/psocs* (green)) so variation within array sets is not significant (Figure 4.2).
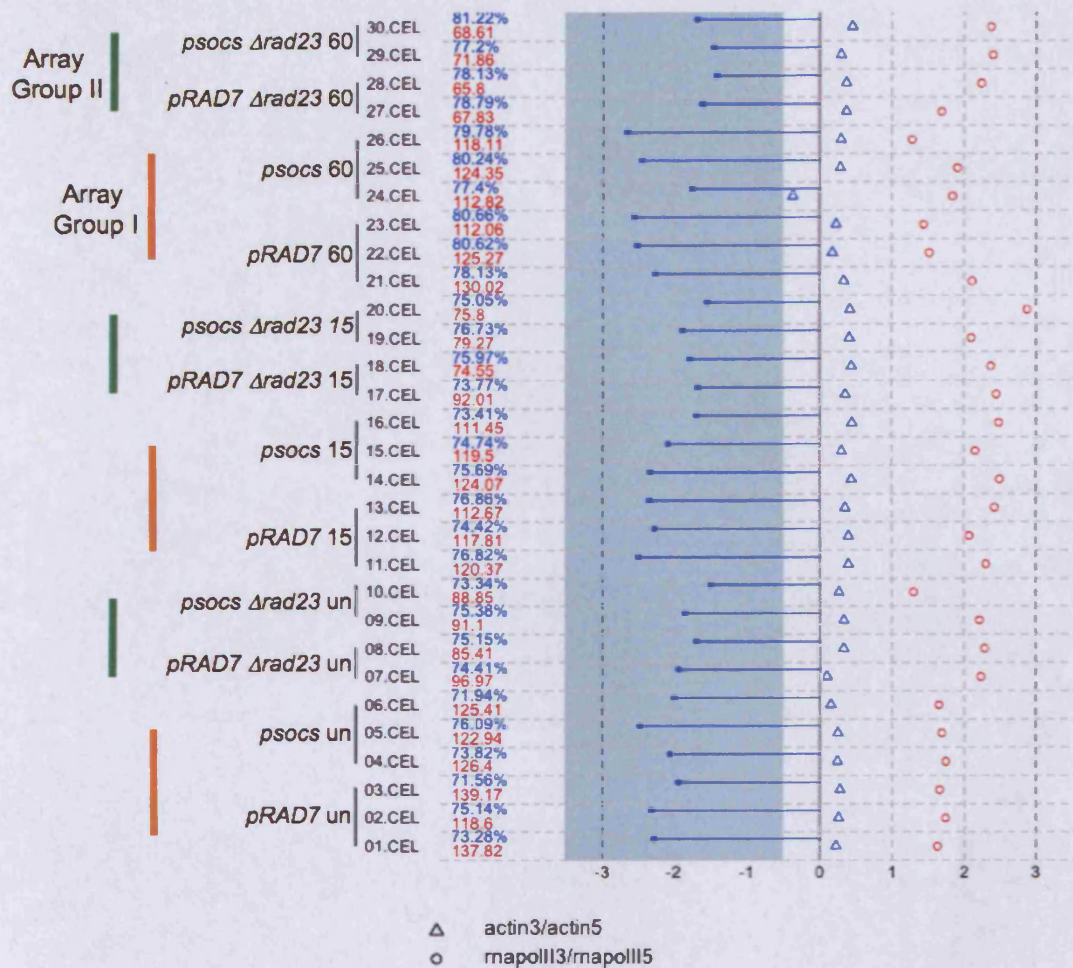
Figure 4.2 - QC Plot of *psocs/rad23* Microarray Data Quality of the 30 *psocs/rad23* microarrays was visualised using the Bioconductor R *simpleaffy* package.

4.2.4.5 Quantile Normalisation of Raw Data

Normalisation was also performed in R as part of the *gcrma* package.
Quantile normalisation was applied to all data sets, which is visualised by boxplots in Figure 4.3. The boxplots show the range of the data (dotted lines), interquartile range (box) and the median value (central line through box). Quantile normalisation transforms the data to equalise the range, interquartile range and median value in order to compare differential expression between arrays.
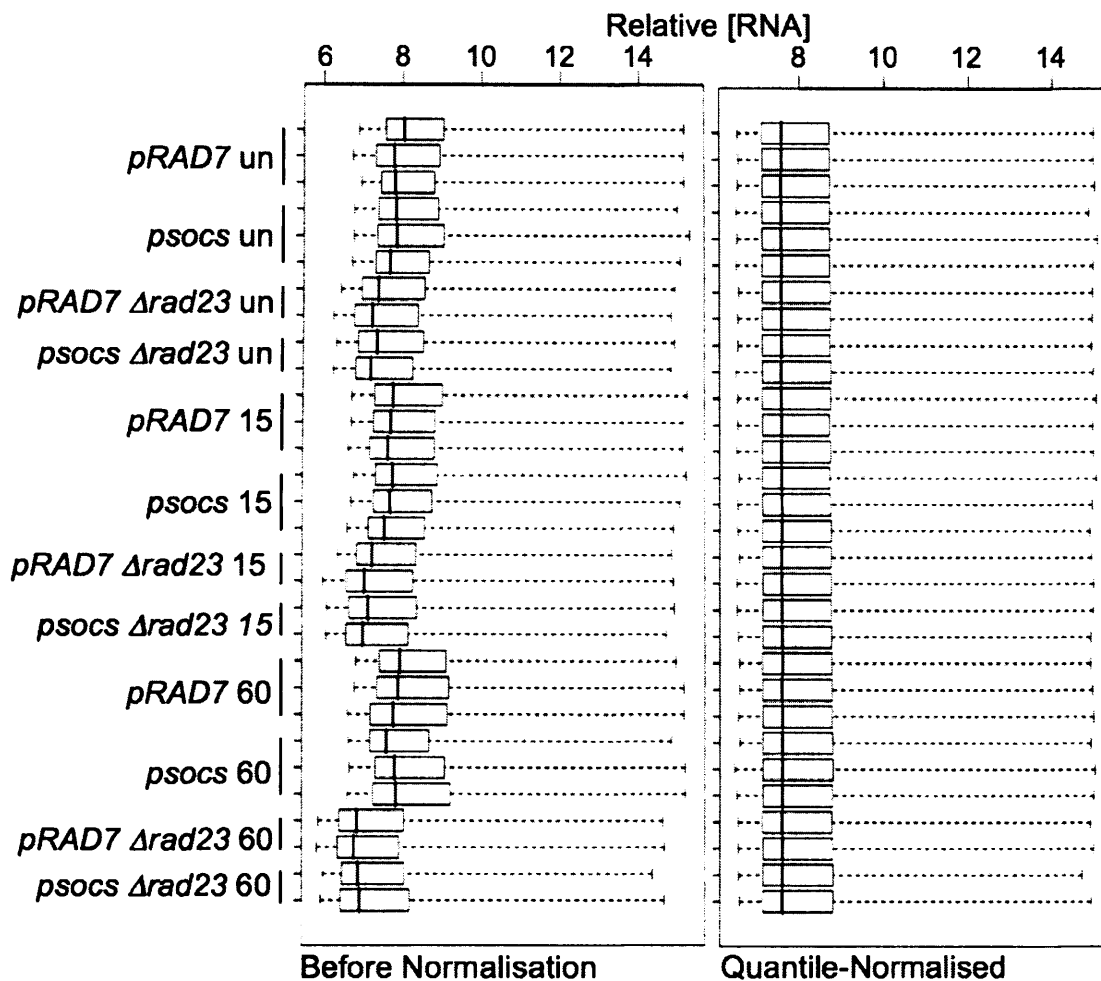
Figure 4.3 - Quantile Normalisation of *psocs/rad23* Microarray Data
Quantile normalisation of the 30 *psocs/rad23* microarrays was conducted and visualised using the R *gcrma* package.

4.2.4.6 Quantification of Differential Expression

Relative expression values were obtained using the R Bioconductor *gcrma* package, which produced $\log_2$ expression values. Significance testing including t-test and FDR correction was performed using GeneSpring software, version 7.3 (Agilent Technologies, Stockport, UK). Gene Lists were transferred to a Microsoft Excel spreadsheet where further analysis was conducted. Mean values of duplicate and triplicate data sets were calculated. Fold-change (fc) values were also calculated where appropriate by obtaining log ratios, by subtracting WT or untreated values from mutant or UV-treated values ($\log a - \log b = \log(a/b)$).

To identify genes that were significantly differentially expressed a t-test was applied to the data filtering p=0.05, to test for genes with a significant difference in mean value between WT and mutant or untreated and UV-treated strains. A false-discovery rate (FDR) correction was also applied to control for multiple testing issues. A fc cut off was also employed to find significantly differentially expressed genes. In order to produce gene lists of a manageable size, a 1.5 fc cut off was employed when investigating variance between untreated mutants, and a 2 fc cut off was used to define UV-responsive genes.

4.2.4.7 Functional Analysis – GO Analysis and Clustering

Gene lists were analysed for commonalities and differences using the online Venn diagram generator (http://www.pangloss.com/seidel/Protocols/venn.cgi). Cluster analysis was performed using Genesis software (Sturn et al. 2002), which was also used for visualisation of gene expression using heat-maps. All other graphical and statistical analysis was performed in Microsoft Excel. Gene Ontology (GO) analysis was performed using the online GO Slim Mapper (http://www.yeastgenome.org/cgi-bin/GO/goSlimMapper.pl). This was used to identify common pathways and gene functions from a statistically obtained gene list. GO and other functional analyses were also performed online using the Database for Annotation, Visualisation and Integrated Discovery (DAVID), which also proved useful for converting Affymetrix Probe IDs to gene symbols and vice versa (Dennis et al. 2003; Huang da et al. 2009).

4.3 Results

The experiments described in this chapter investigate a role for the Rad4-Rad23 complex in DNA damage-responsive gene transcription, with particular attention to the role of the Rad7 E3 ligase-dependent Post-UV ubiquitination of Rad4. Prior to conducting microarrays, suitable mutant strains were constructed and characterised and the process of UV irradiation of cells was optimised.

4.3.1 Construction of *pRS313-RAD7* and *pRS313-socs* Strains

Strain background can have a significant impact on experimental accuracy and reproducibility. For this reason, mutant strains with EUROSCARF genetic background were created, which allowed comparison to previously investigated strains. The *psocs* mutant strains were constructed using plasmids based on those described in (Gillette et al. 2006), which were based on the *pRS314* plasmid (Sikorski and Hieter 1989), containing a *TRP1* marker gene and the full genomic *RAD7* sequence with promoter region. For the purposes of this study, the *RAD7* and *RAD7-socs* sequences were inserted into the *pRS313* vector (Sikorski and Hieter 1989) to allow selection via histidine instead of tryptophan, as EUROSCARF strains are TRP⁺.

The original *pRS314*-based *RAD7* and *RAD7-socs* plasmids (Gillette et al. 2006) were digested with *ClaI/SacII*, which specifically removed the *RAD7* sequences. The *pRS314-RAD7*, *pRS314-socs* and *pRS313* plasmids were digested for 90 minutes at 37°C, using 2µl *ClaI*, 2µl *SacII*, 5µl buffer 4 (NEB) with 0.5µl 10mg/ml BSA in 50µl reaction volume. The required DNA fragments were recovered from the gel (Qiagen QIAquick Gel Extraction Kit) and then ligated to form *pRS313-RAD7* and *pRS313-socs* constructs. Correct ligation was confirmed by DNA sequencing, and the various mutations were found to be present and correct.

The newly constructed plasmids were transformed into Δ*rad7* EUROSCARF cells (*BY4742*) and transformants were grown on HIS⁻ media. Successful

transformation was phenotypically checked by examining UV sensitivity using a streak test. As expected, the transformed strains had a less severe UV sensitivity than the parental *BY4742* strain, due to the reinstated *RAD7* gene (Figure 4.4).
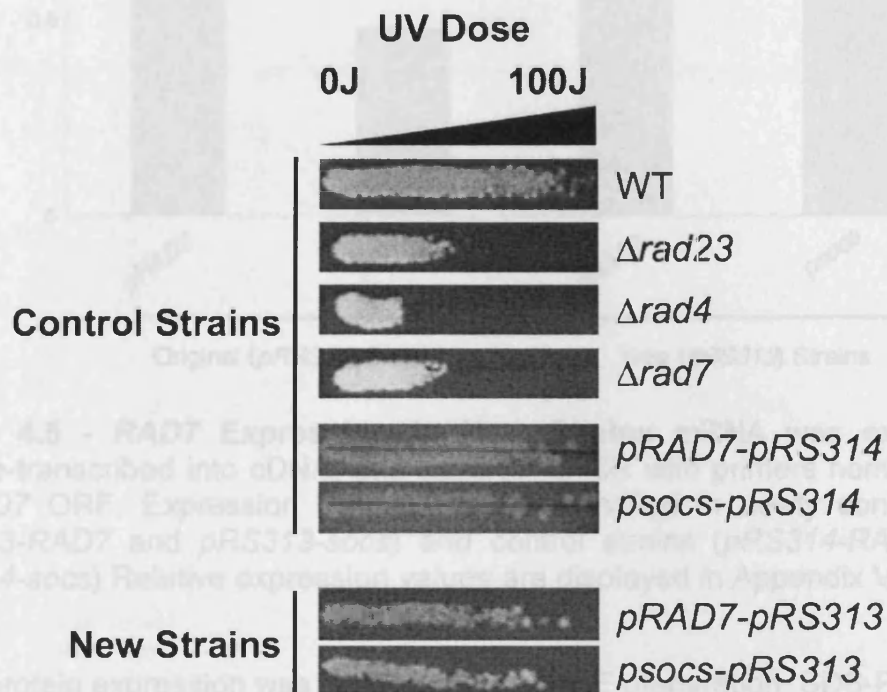
Figure 4.4 - UV Sensitivity Streak Test of New Strains Yeast cell cultures were streaked across solid media, then irradiated with 0-100Jm^{-2} UV. As can be seen, the strains harbouring plasmids containing *RAD7* have increased UV resistance compared to the *Δrad7* strain. The control strains show the WT strain with normal UV sensitivity, the severely UV-sensitive *Δrad4* strain, and the moderately UV-sensitive *Δrad23* and *Δrad7* strains.

In order to assess the transformants, expression of *RAD7* transcript and protein level was observed by qPCR and Western Blotting. qPCR was performed to check *RAD7* gene expression levels by detecting mRNA concentration (Figure 4.5). Quantification of relative gene expression revealed that both *pRAD7* and *psocs* mRNAs were expressed at approximately the same level but *psocs* expression appears to occur at a lower level, however this does not affect the UV sensitivity of the strain (Figure 4.7) so will not be considered as reason for concern for future experiments.
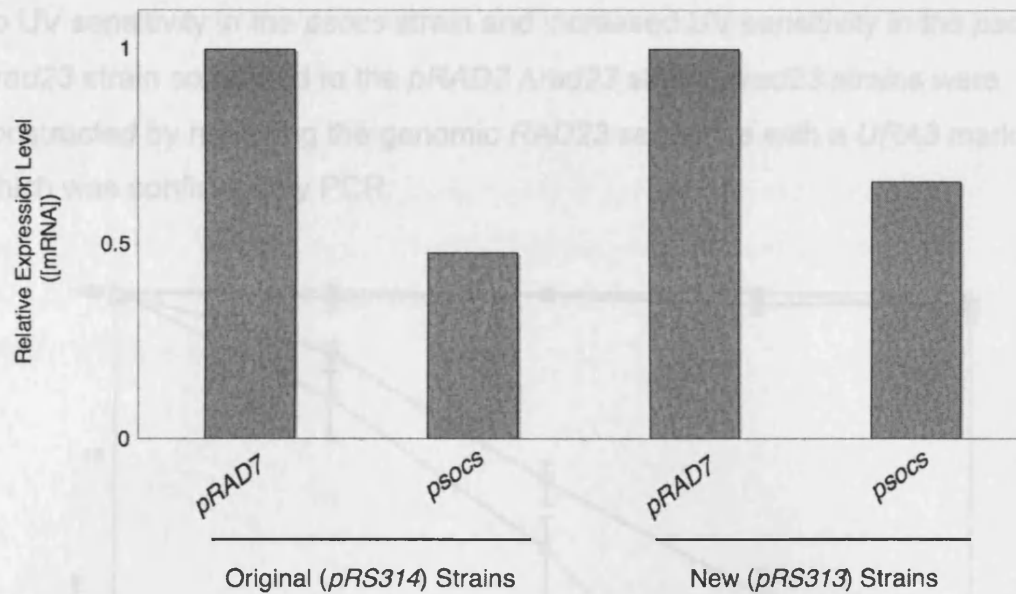
Figure 4.5 - *RAD7* Expression in New Strains mRNA was extracted, reverse-transcribed into cDNA, and used for qPCR with primers homologous to *RAD7* ORF. Expression of *RAD7* was quantified in newly constructed *pRS313-RAD7* and *pRS313-socs*) and control strains (*pRS314-RAD7* and *pRS314-socs*) Relative expression values are displayed in Appendix VII.

Rad7 protein expression was deduced using WCE preparation, SDS-PAGE and western blotting. The blot was probed using an anti-Rad7 polyclonal antibody (Figure 4.6), and revealed Rad7 expression in all strains except Δ*rad7*, which shows Rad7 is being successfully expressed from the plasmid.
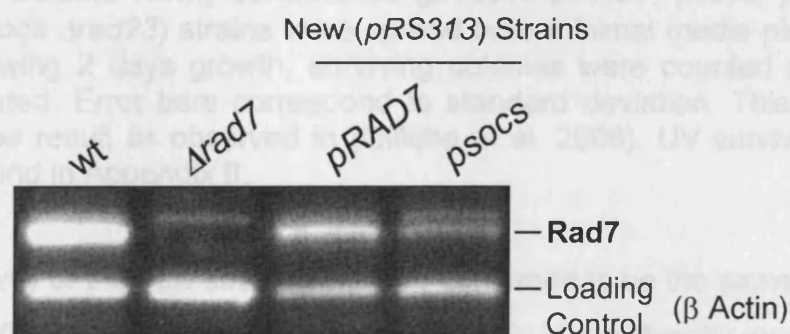
Figure 4.6 - Rad7 Protein Levels in New Strains SDS-PAGE and western blotting was performed on WCEs from new strains (*pRAD7* and *psocs*) and control strains (WT and Δ*rad7*). The western membrane was probed with Rad7 antibody to monitor protein levels in newly synthesised strains.

The newly constructed strains were also characterised by comparing their UV survival phenotype to those observed in (Gillette et al. 2006), thus displaying

no UV sensitivity in the *psocs* strain and increased UV sensitivity in the *psocs* Δ*rad23* strain compared to the *pRAD7* Δ*rad23* strain. Δ*rad23* strains were constructed by replacing the genomic *RAD23* sequence with a *URA3* marker, which was confirmed by PCR.
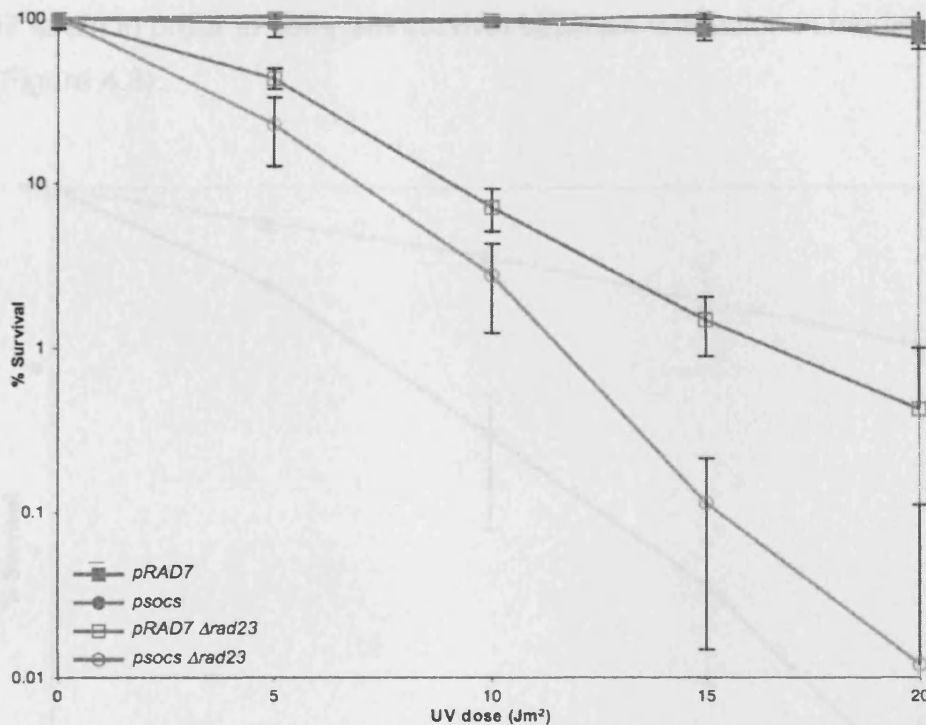
Figure 4.7 - UV Survival of *pRS313 pRAD7, psocs, pRAD7* Δ*rad23* and *psocs* Δ*rad23* Strains Newly constructed (*pRS313 pRAD7, psocs, pRAD7* Δ*rad23* and *psocs* Δ*rad23*) strains were spread onto minimal media plates in triplicate. Following 2 days growth, surviving colonies were counted and % survival calculated. Error bars correspond to standard deviation. This figure shows the same result as observed in (Gillette et al. 2006). UV survival raw data can be found in Appendix II.

The UV sensitivity of the new strains was also confirmed to be the same as (Gillette et al. 2006) whereby the *psocs* Δ*rad23* strain is significantly more UV-sensitive than the Δ*rad23* strain, and the strain which only has the *psocs* mutation shows no UV sensitivity (Figure 4.7). These observations confirmed that the new strains had the same phenotype as those used previously, so future experiments could be compared to the results obtained in (Gillette et al. 2006).

4.3.2 Determination of UV-Irradiation Conditions for *psocs*/*rad23* Arrays

pRAD7 Cells were grown to 10^7 cells/ml in HIS⁻ minimal media. 50ml cell
culture was centrifuged for 3 minutes at 4 000 rpm, and cells were diluted in
50ml cold PBS. Another 50ml portion of cell culture was also irradiated
without dilution in PBS. An UV survival assay was conducted using the
pRAD7 strain in order to compare survival between irradiation in media and
PBS (Figure 4.8).
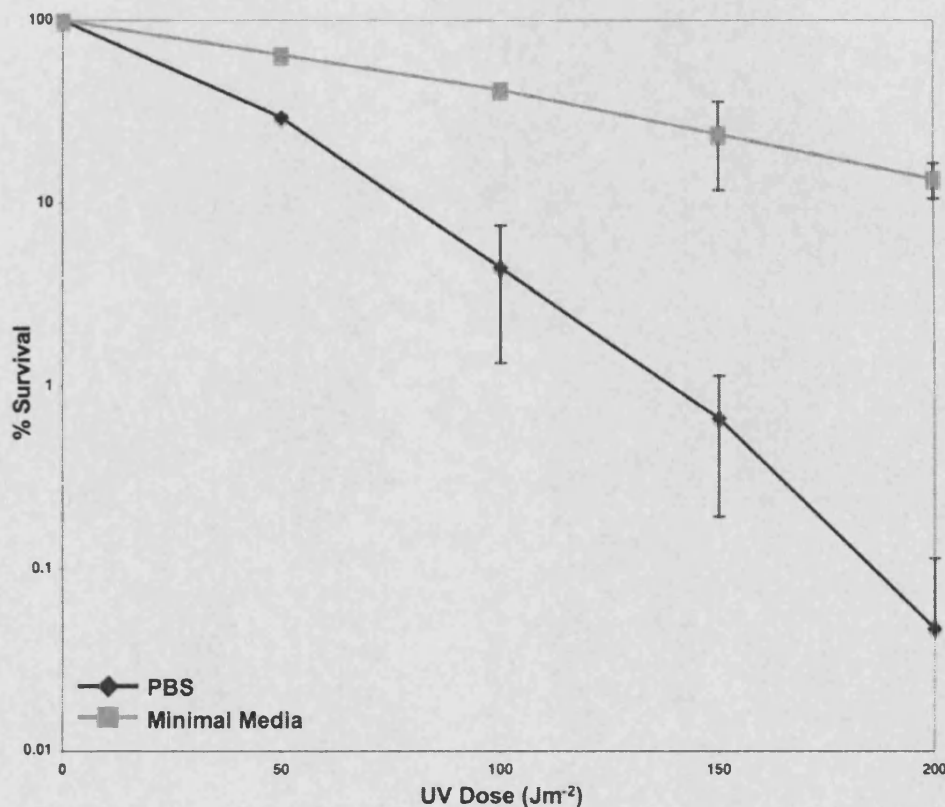
**Figure 4.8 - UV Survival of *pRAD7* Strain Irradiated in PBS or Minimal
Media** *pRAD7* cells were exposed to UV in PBS or minimal media, then 200
cells were spread onto minimal media plates in triplicate. Following 2 days
growth, surviving colonies were counted and % survival calculated. Error bars
correspond to standard deviation.

As displayed in Figure 4.8, UV radiation was found to penetrate PBS more
effectively thus killing more cells at a lower dose. It is important for the
purposes of global transcriptional analysis to induce a UV-dependent
transcriptional response, without causing an unnecessarily high cell death
rate, which would induce transcription of genes involved in extreme survival or
programmed cell death and make it more difficult to identify UV-inducible

96

genes. It was decided a survival rate of approximately 50% was appropriate to invoke a suitable UV response. This equates to a dose of $40Jm^{-2}$ in PBS, or $100Jm^{-2}$ in minimal media. A dose of $100Jm^{-2}$ in minimal media was applied to cells prior to mRNA extraction for use in microarrays.

Two sets of arrays were analysed in order to deduce the role of the Rad4-Rad23 complex in DNA damage-responsive global transcription. Firstly, the *rad4/rad23* used Δ*rad4*, Δ*rad23* and Δ*rad4*Δ*rad23* strains without UV irradiation to identify altered global gene expression in untreated cells. The *psocs/rad23* microarray set was then conducted, which used the strains constructed in this chapter – the *pRAD7*, *psocs*, *pRAD7* Δ*rad23* and *psocs* Δ*rad23* mutant strains. These strains were irradiated with UV to identify genes regulated by the Rad4-Rad23 complex in response to DNA damage, particularly the Rad7 E3 ligase-dependent ubiquitination of Rad4. The *psocs* strain was used instead of a Δ*rad4* strain to deduce the role of the Rad4-Rad23 complex in UV-responsive transcription as the Δ*rad4* strain is highly UV-sensitive and transcriptional responses caused by the high rate of cell death may mask the UV-induced transcriptional response.

4.3.3 Initial Analysis of *rad4/rad23* Arrays

The *rad4/rad23* arrays were conducted to identify transcriptional targets of the Rad4-Rad23 damage recognition complex, which may contribute to its role in the DNA damage response. Due to the severe UV sensitivity of the Δ*rad4* mutant these arrays were conducted in the absence of UV or DNA damaging agents. The *rad4/rad23* arrays were conducted using a WT strain and strains with Δ*rad4*, Δ*rad23*, or Δ*rad4*Δ*rad23* mutations, with three biological repeats conducted for each strain. RNA preparation, submission, microarray processing and initial data handling including QC and normalisation was conducted by Dr J. Smirnova and will not be included in this report. Genes with significantly differential expression in the mutant strains compared to WT were identified, using a FDR corrected t-test ($p<0.05$) and a 1.5 fc cut-off. To initially assess the transcriptional disruption in the strains, scatter plots were

created. Figure 4.9 shows mutant gene expression compared to WT, with genes identified as expressed at a significantly lower level in the mutant highlighted green, and genes identified as expressed at a significantly higher level in the mutant highlighted red. Genes that were not significantly differentially expressed are shown in grey. Genes which lie on the black y=x line exhibit no transcriptional change in the mutant strains.
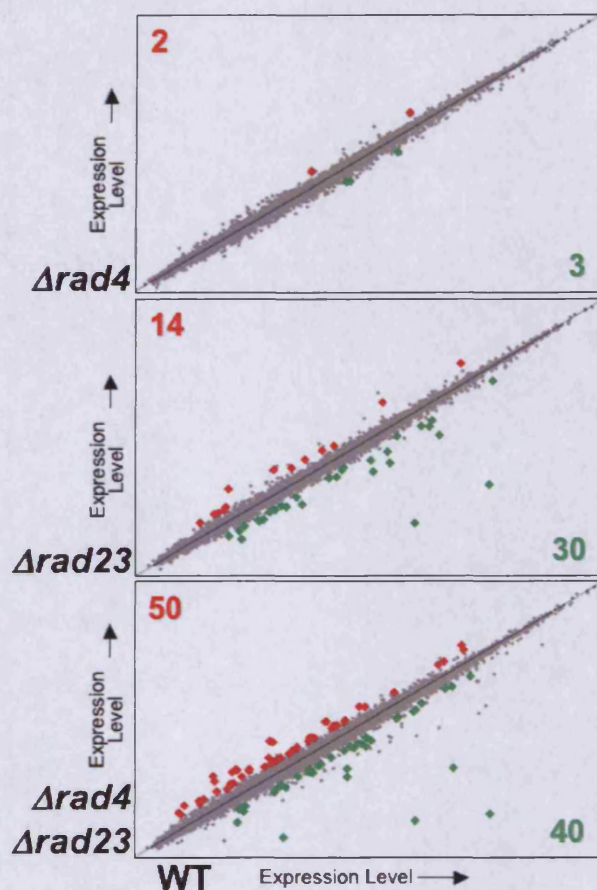
Figure 4.9 - Scatter Plots of *rad4/rad23* Microarrays Expression values were plotted for mutant against WT strains, and significantly differentially expressed genes were identified. The scatter plots show genes expressed at a significantly lower level in the mutant strain in green and genes expressed at a significantly higher level in the mutant strain in red. The numbers correspond to the number of significantly up- and downregulated genes in the stated strains.

The Δ*rad4* strain has only 5 significantly altered genes compared to the WT, and the Δ*rad23* strain also shows a fairly mild phenotype of 44 genes significantly altered. A more substantial alteration in gene expression is displayed in the double Δ*rad4*Δ*rad23* strain, which has 90 significantly differentially expressed genes. This initial observation from the data could

suggest a genetic redundancy for the two genes, whereby the Rad4-Rad23 complex can still function as a transcription factor if one gene is absent for a subset of genes.
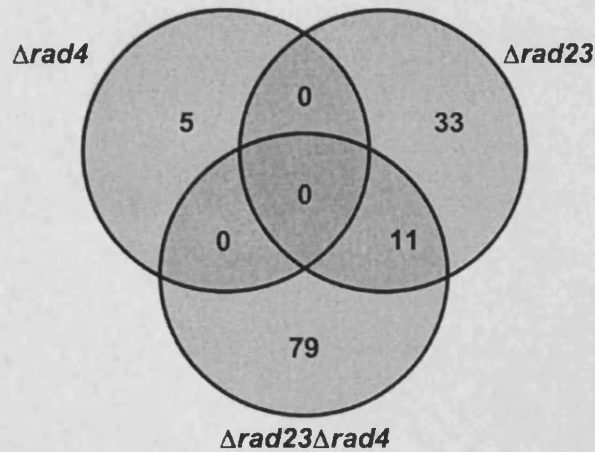
Figure 4.10 - Venn Diagram to Show Overlap Between Different Gene Lists Commonly misregulated genes are represented here in the *rad4/rad23* mutant strains using the aforementioned significant gene lists.

The gene lists were also organised into a Venn diagram (Figure 4.10). The slight altered transcription of the Δ*rad4* phenotype could be caused by the action of the recently characterised Rad4 homologue, Rad34. It has been reported that Rad34 can fulfil the role of Rad4 in repair of ribosomal DNA and interacts with Rad23. This compensatory function of Rad34 could explain the Venn diagram data shown in Figure 4.10 (den Dulk et al. 2005; den Dulk et al. 2006; Tremblay et al. 2008).

4.3.4 Cluster Analysis of *rad4/rad23* Arrays

In order to obtain manageable gene lists, the conditions were relaxed to omit the t-test and just include genes which exhibited a >1.5 fc. This provided a list of 205 genes, which was then clustered using average linkage hierarchical clustering in order to find similarly expressed genes. Four main clusters were found and they are visualised in Figure 4.12. The clusters (from top to bottom) represent 1). Genes that are unaffected in single mutants and downregulated in the double mutant, 2). Genes that are downregulated in single mutants and upregulated in the double mutant, 3). Genes that are downregulated in all mutants and 4). Genes that are upregulated in all mutants. In order to assess the relevance of these gene lists in response to DNA damage, a list of UV-responsive genes in the *pRAD7* (WT) strain was compiled.

4.3.5 Compilation of a UV-Responsive Gene List

The threat of DNA damage invokes a vast transcriptional response to stimulate DNA repair, stress response and checkpoint pathways, and promoting cell cycle arrest. As part of the *psocs/rad23* arrays a microarray to deduce which genes were significantly up or down regulated in response to UV in the *pRAD7* WT strain was conducted. Cells were exposed to $100Jm^{-2}$ UV and mRNA was extracted after 15 minutes and 1 hour. Microarrays were conducted and expression values were obtained. The $\log_2$ untreated values were subtracted from $\log_2$ UV-treated values, and a FDR corrected t-test ($p<0.05$) was applied to the untreated and UV-treated values to obtain significantly differentially expressed genes. A 2 fc cut off was applied to identify genes significantly regulated in response to UV. Amalgamating genes significantly differentially expressed 15 or 60 minutes after UV produced a list of 1360 UV-responsive genes (Figure 4.11). The UV-responsive gene list is displayed in the electronic Appendix IV, list 2.
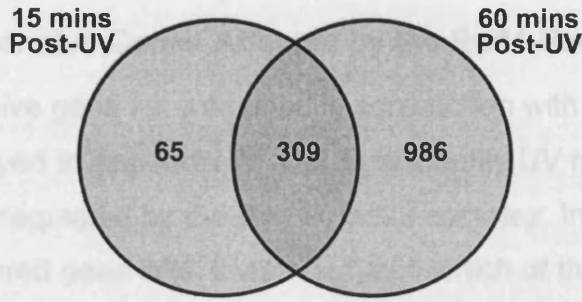
Figure 4.11 - Venn Diagram to Show Genes Significantly Differentially Expressed in Response to UV in the *pRAD7* Strain The three gene lists shown here were combined to form a list of 1360 UV-responsive genes. This gene list is displayed in the electronic Appendix IV, List 2.

4.3.6   UV-Responsive Genes Affected by the Rad4-Rad23 Complex

The UV-responsive gene list was used in conjunction with the *Δrad4/Δrad23* gene list (Displayed in Appendix IV, List 1) to identify UV responsive genes transcriptionally regulated by the Rad4-Rad23 complex. In the context of the previously clustered gene lists, it was deduced which of those genes were UV-responsive.
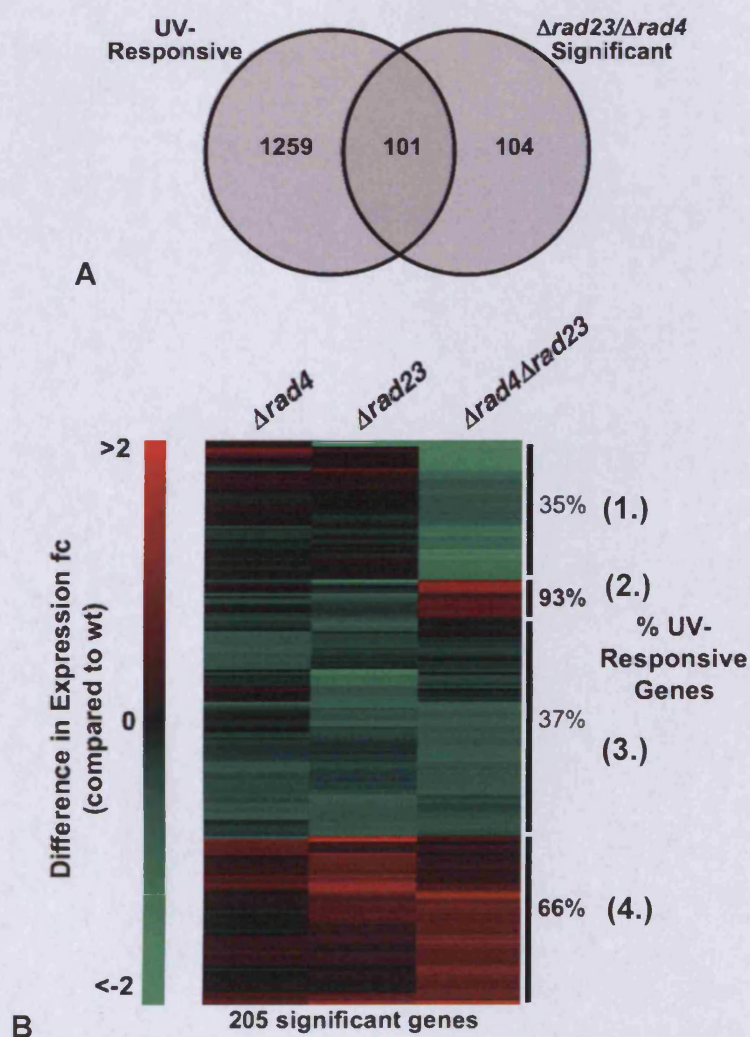
Figure 4.12 – Analysis of *Δrad4/Δrad23* Significantly Differentially Expressed Gene Lists A: Venn diagram to show proportion of UV-responsive genes that are also significantly misregulated in *Δrad4/Δrad23* strains. B: heatmap of *Δrad4/Δrad23* significantly differentially expressed genes hierarchically clustered. Genes were divided into 4 distinct clusters, and % values refer to the proportion of UV-responsive genes in each cluster. This gene list is displayed in Appendix IV, List 1.

Figure 4.12A shows that approximately half of the genes significantly differentially expressed in *Δrad4Δrad23* mutants are UV responsive in the *pRAD7* strain. This suggests that the Rad4-Rad23 complex has an important role in the transcriptional response to UV. In order to further analyse the UV-responsive genes under transcriptional control of Rad4-Rad23, UV-responsive genes in individual clusters were investigated. % values in Figure 4.12 show the UV-responsive proportion of each cluster. The 101 UV responsive genes were extracted, and are displayed in the same cluster order in Figure 4.13.
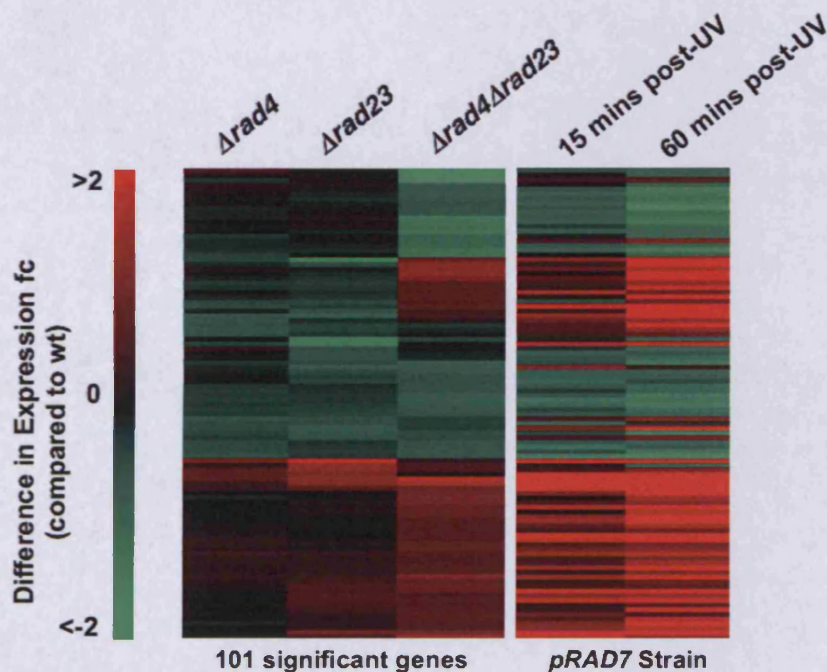
Figure 4.13 - Heatmap of UV-Responsive *Δrad4/Δrad23* Significantly Differentially Expressed Genes Untreated mutant strains are shown in the first three columns, and the UV-treated *pRAD7* strain is shown in the final two columns

Comparing the untreated and UV-treated columns in Figure 4.13, an interesting observation is how the UV response appears to mimic the transcriptional pattern seen in the *Δrad4Δrad23* double mutant. This may suggest that removal of the Rad4-Rad23 complex from gene promoters is required for UV-responsive transcription.

The cluster with the largest proportion of UV-responsive genes is the second, which will be analysed in further detail. 13/17 genes were found to be UV responsive in this cluster and are displayed in Figure 4.14. These genes were subjected to analysis to deduce common regulatory pathways. It was found that 5 of these genes contain 5' *STRE* sequences, and expression of 2 of the genes is controlled by the Crt1 transcription factor. *STRE* sequences are found in several gene promoters and become bound by the Msn2/4 transcription factors in response to different stresses to induce transcription of stress responsive genes. The Crt1 protein was initially discovered as a repressor of the RNR pathway, which functions to regulate nucleotide pools in the cell. It has been found to affect the transcription of several other genes involved in stress response (Zaim et al. 2005). The UV-responsive, Rad4-Rad23 regulated genes (Figure 4.13) are mostly misregulated in the same direction (up- or down-regulated), but with a smaller magnitude, as the WT UV response. This could suggest that the removal, inactivation or destruction of the Rad4-Rad23 complex is important for transcription of these UV responsive genes.
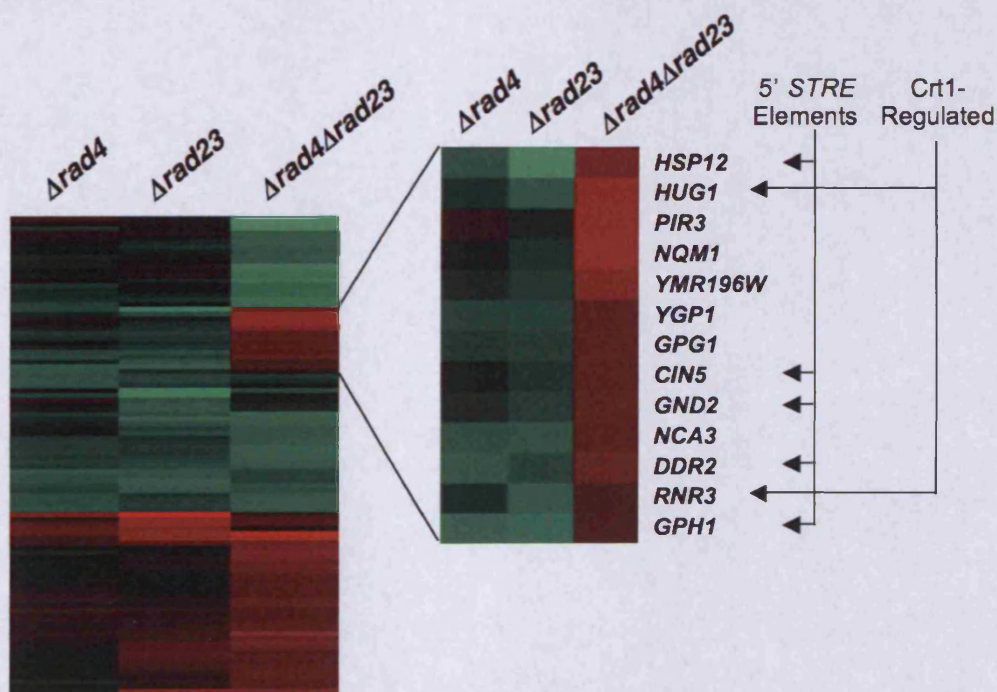
Figure 4.14 - Genes of Cluster Two – the genes of cluster two are shown with common regulatory elements.

In order to analyse further the role of the Rad4-Rad23 complex in transcription, specifically focussing on the role of post-UV Rad4 ubiquitination, the untreated *psocs/rad23* arrays were analysed.

4.3.7 Initial Analysis of Untreated *psocs/rad23* Arrays

The untreated arrays were initially analysed in the same way as the *rad4/rad23* arrays. Genes with significantly differential expression in the mutant strains compared to the *pRAD7* strain were identified using a FDR corrected t-test ($p<0.05$) and a 1.5 fc cut-off. To initially assess the transcriptional disruption in the strains, scatter plots were created. Figure 4.15 shows mutant gene expression compared to the *pRAD7* strain, with genes identified as expressed at a significantly lower level in the mutant highlighted green, and genes identified as expressed at a significantly higher level in the mutant highlighted red. Genes that were not significantly differentially expressed are shown in grey. Genes which lie on the black y=x line exhibit no transcriptional change in the mutant strains.
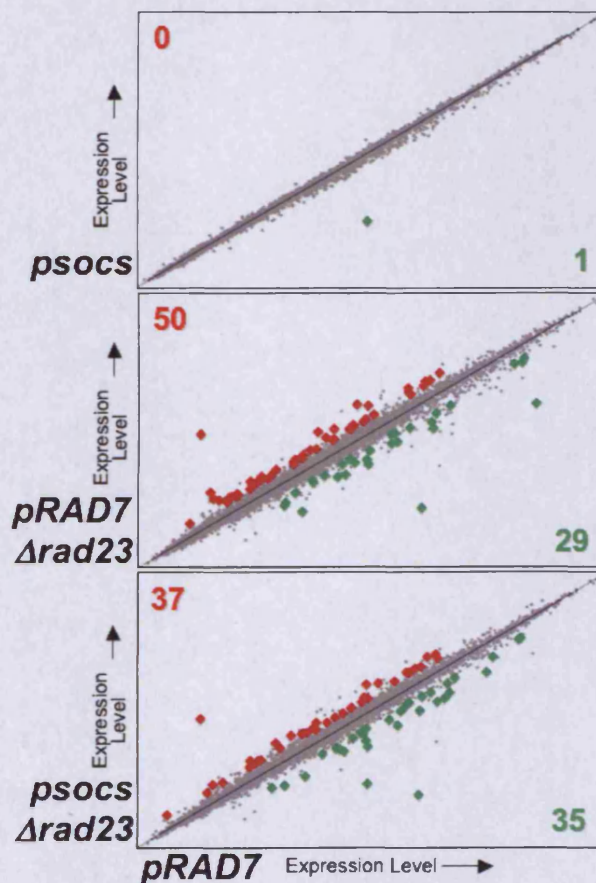
Figure 4.15 - Scatter Plots of *psocs/rad23* Microarrays fc values were calculated from the *psocs/rad23* expression value microarray data, and significantly differentially expressed genes between the mutant and *pRAD7* strains were identified. The scatter plots show genes expressed at a significantly lower level in the mutant strain in green and genes expressed at a significantly higher level in the mutant strain in red. The numbers correspond to the number of significantly up- and downregulated genes in the stated strains.

The *psocs* strain has only 1 significantly altered gene compared to *pRAD7*, which was the *RAD7* gene itself. For the purpose of this study, this result will be ignored as the plasmids have been sequenced, and *RAD7* expression has been addressed previously (Section 4.3.1).

The *pRAD7* and *psocs Δrad23* strains exhibit a similar magnitude of transcriptional disruption but they exhibit a far greater difference than the *pRAD7* and *psocs RAD23⁺* strains. This transcriptional variation will be considered when progressing to investigate variations in transcriptional response to UV.

Commonly misregulated genes in the different strains were determined by constructing a Venn diagram (Figure 4.16). This shows that *RAD7* was significantly misregulated in all strains (the central 1 gene). The *Δrad23* strains show an unexpected crossover based on their UV survival phenotype. It would be predicted that the genes that are misregulated in the *pRAD7* *Δrad23* strain would be a subset of the genes misegulated in the *psocs* *Δrad23* strain. Like the data seen in the *rad4/rad23* arrays, there is relatively little overlap of gene lists. This suggests that Rad4, and its ubiquitination has a complex role in global transcription.
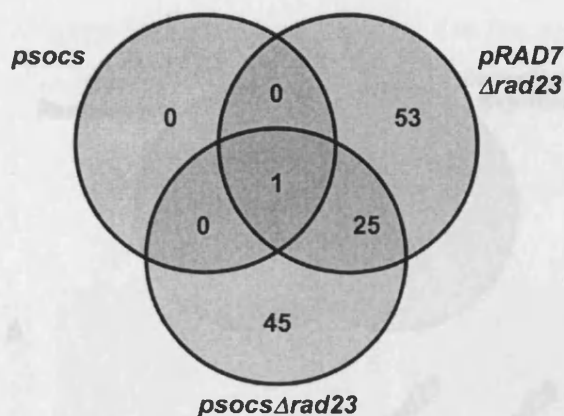
Figure 4.16 - Venn Diagram to Show Overlap Between Different Gene Lists Commonly misregulated genes are represented here in the *psocs/Δrad23* mutant strains using the aforementioned significant gene lists.

4.3.8 Cluster Analysis of *psocs/Δrad23* Untreated Arrays

In order to obtain manageable gene lists, the conditions were relaxed to omit the t-test and just include genes which exhibited a >1.5 fc. This provided a list of 306 significant genes that were compiled into a list and hierarchically clustered, then UV-responsive genes were identified (Figure 4.17). The gene list is displayed in Appendix IV, List 3. Hierarchical clustering revealed three main clusters. Cluster 1 represents genes that were downregulated in the *pRAD7 Δrad23* and *psocs Δrad23* strains, Cluster 2 represents genes downregulated in the *psocs* and *pRAD7 Δrad23* strains, and Cluster 3 represents genes upregulated in the *pRAD7 Δrad23* and *psocs Δrad23* strains. This shows that in most significantly regulated gene sets the two *Δrad23* strains appear to behave similarly, and the *psocs* strain behaves as the *pRAD7* strain. It is therefore of great importance to extract and identify the small minority of genes that are differentially expressed between the *psocs* and *pRAD7* strains in the presence or absence of Rad23.

Figure 4.17 – Analysis of *psocs/Δrad23* Significantly Differentially Expressed Gene Lists A: Venn diagram to show proportion of UV-responsive genes that are also significantly misregulated in *psocs/Δrad23* strains. B: heatmap of *psocs/Δrad23* significantly differentially expressed genes Hierarchically clustered. Genes were divided into three distinct clusters, and % values refer to the proportion of UV-responsive genes in each cluster. The gene list is displayed in Appendix IV, List 3.

It appears in Figure 4.17 that genes that are upregulated in the mutants are mostly UV-responsive. The *rad4/rad23* and *psocs/rad23* untreated arrays had similar numbers of significantly altered genes (205 and 306), and of these genes, approximately half of each are common to the UV-responsive gene list. Despite these commonalities, only 43 genes are common to both sets.

The UV-responsive genes were extracted from the *psocs/rad23* significant gene list and are displayed in Figure 4.18.
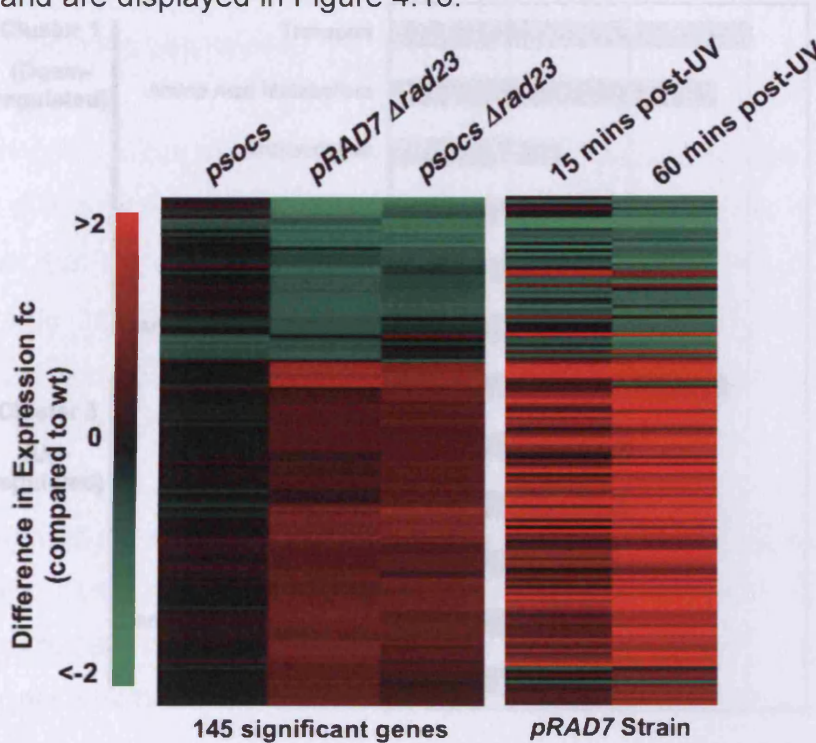
Figure 4.18 – Heatmap of UV-Responsive *psocs/Δrad23* Significantly Differentially Expressed Genes Untreated mutant strains are shown in the first three columns, and the UV-treated *pRAD7* strain is shown in the final two columns.

Figure 4.18 shows that some of the untreated mutant strains also mimic the UV response without UV treatment compared to the WT, which is most evident in the *Δrad23* strains. GO analysis was performed on the three clusters in Figure 4.17. The top 6 GO terms for Clusters 1 and 3 were extracted, and are shown in Figure 4.19.

Figure 4.19 - GO Analysis of *psocs/rad23* Significant Genes. GO analysis was performed on the genes from the named clusters in Figure 4.17

The top 6 GO terms selected in Figure 4.19 support the idea that the transcriptional misregulation in $\Delta rad23$ mutants without UV treatment mimics the WT transcriptional response to UV, as stress response, cell cycle and DNA metabolism genes are upregulated, and genes for more general housekeeping tasks such as amino acid, lipid and RNA metabolism are downregulated.

Further analysis of the upregulated gene lists reveal key genes involved in the DNA damage response in the Cluster 3 stress response GO list. These include *RAD53*, the checkpoint kinase, and 2 subunits of RPA (*RFA1* and *RFA2*) the ssDNA binding protein involved in the checkpoint response. Another checkpoint protein, *DDC2* is present in Cluster 2. *CLB5* and *CLB6* the G_1 cyclins are present in the cell cycle category from Cluster 3, which promote entry into S-phase. Another G_1 cyclin, *CLB3* is present in Cluster 2 (not shown in figure). These observations suggest disruption of the transcriptional

response to UV in the mutant strains but further analysis must be conducted to determine which genes are affected in which mutant, and how these could produce the phenotypes shown.

It was seen in the initial analyses of the arrays that the transcription of a large proportion of the genome is altered in response to UV in WT cells. It has also been shown that the untreated *Δrad4Δrad23, pRAD7 Δrad23* and *psocs Δrad23* strains display a similar transcriptional pattern to UV-irradiated cells, however the expression changes in untreated mutant cells occur at a lower magnitude than the WT UV response.

Having identified misregulated genes in the mutant strains in the absence of DNA damage, the study then progressed to identify differentially regulated genes in the mutant strains in response to UV radiation in order to identify candidate genes whose altered transcription could cause the increased UV-sensitivity in the *psocs Δrad23* strain compared to the *pRAD7 Δrad23* and *pRAD7* strains, observed by (Gillette et al. 2006).

4.3.9 Differentially Expressed Genes in Response to UV

The purpose of this investigation was to identify genes and pathways responsible for the additional UV sensitivity of the *psocs Δrad23* strain compared to the *Δrad23* strain, and therefore revealing the role of the Rad4-Rad23 complex in global transcription. It is not appropriate to compare different UV-treated strains directly, so fc between untreated and UV treated arrays for each strain was calculated, and fc difference was compared as a measure of differential expression between different mutant strains. A Venn diagram displaying differentially expressed genes between the *pRAD7 Δrad23* and *psocs Δrad23* strains is shown in Figure 4.20. A threshold value of 1.5 fc difference was employed between the two strains, a suitable cut-off to produce manageable gene-lists.
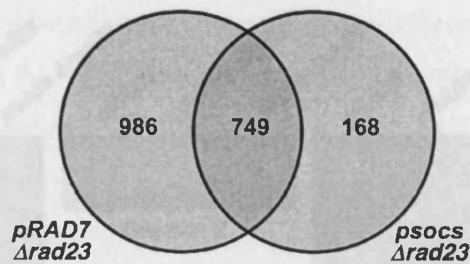
Figure 4.20 - Venn Diagram to Show Commonly Misregulated Genes in the *pRAD7* Δ*rad23* and *psocs* Δ*rad23* Strains Either 15 or 60 Minutes Post-UV. Gene lists shown here exhibit >1.5 fc difference between the *pRAD7* and the *pRAD7* Δ*rad23* strains or the *pRAD7* and the *psocs* Δ*rad23* strains fc in response to UV.

The most likely candidates responsible for the increased UV sensitivity in the *psocs* Δ*rad23* strain are genes that are significantly misregulated in the *psocs* Δ*rad23* strain but not the *pRAD7* Δ*rad23* strain. For this reason the 168 gene list from Figure 4.20 was extracted, and clustered using a K-Means technique to identify genes with a similar expression pattern in response to UV. This gene list is displayed in Appendix IV, List 4. Three significant clusters were found (Figure 4.21). Cluster 1 had reduced gene activation in the *psocs* Δ*rad23* mutant compared to the *pRAD7*Δ*rad23* and *pRAD7* strain. Cluster 2 had reduced gene downregulation in the *psocs* Δ*rad23* strain, and Cluster 3 had increased gene downregulation in the *psocs* Δ*rad23* strain, not evident in the *pRAD7* Δ*rad23* strain or *pRAD7* strain (Figure 4.21).
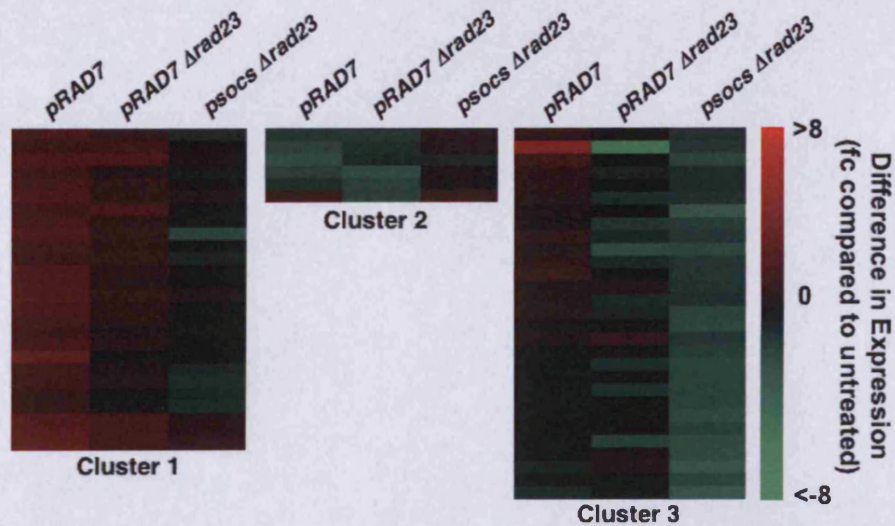
Figure 4.21 - K-means Clusters from 168 Gene List. Genes with significantly differential expression in response to UV between the *pRAD7 Δrad23/psocs Δrad23*, and *pRAD7* strain were extracted (Figure 4.20), and 168 genes were identified as significantly differentially regulated in the *psocs Δrad23* but not the *pRAD7 Δrad23* strain. These were subjected to K-Means clustering. The 3 clusters that showed the most striking differential expression are shown here. The heatmaps show expression values 1 hour after UV in the 3 strains.

Genes identified in clusters shown in Figure 4.21 include proteasomal subunits, *RAD7* itself and the *RTT109* histone acetyltransferase, which is involved in histone modification in response to DNA damage.

Although these clusters revealed a few candidate genes, most genes were not significantly differentially expressed in the *psocs Δrad23* strain compared to the *pRAD7 Δrad23* strain and *pRAD7* strain. This occurred because most genes were expressed close to the threshold value so did not actually show a significant difference between the *pRAD7 Δrad23* strain and the *psocs Δrad23* strain. A more appropriate method was derived whereby the difference in expression between the *pRAD7*, *pRAD7 Δrad23* and the *psocs Δrad23* in response to UV was taken into account.

This alternative method of identifying misregulated genes was to compare the fc difference between the *pRAD7 Δrad23* and *psocs Δrad23* strains, and extract genes that exhibited a difference in fc of at least 0.2. This produced a

list of 110 genes, which was also hierarchically clustered. The gene list is displayed in Appendix IV, List 5. In order to extract the required genes, clusters were obtained which showed more extreme or different misregulation in the *psocs* Δ*rad23* strain than the *pRAD7* Δ*rad23* strain. This was intended to identify likely candidates responsible for the additional UV sensitivity of the *psocs* Δ*rad23* strain, and thus possible targets of transcriptional regulation by the Rad4-Rad23 complex.

The clusters selected in Figure 4.22 display a variety of gene misregulation in the *psocs* Δ*rad23* strain compared to other strains. The identified clusters were extracted and are displayed as individual genes in Figure 4.23. The clusters show genes that are upregulated in *pRAD7* and downregulated in *psocs* Δ*rad23* (Cluster 1), not changed in *pRAD7* but downregulated in *psocs* Δ*rad23* (Cluster 2), further downregulated in *psocs* Δ*rad23* than *pRAD7* (Cluster 3) and upregulated in *pRAD7* but no change in *psocs* Δ*rad23* (Cluster 4). All clustering was performed with regard to expression change 1 hour after UV treatment.
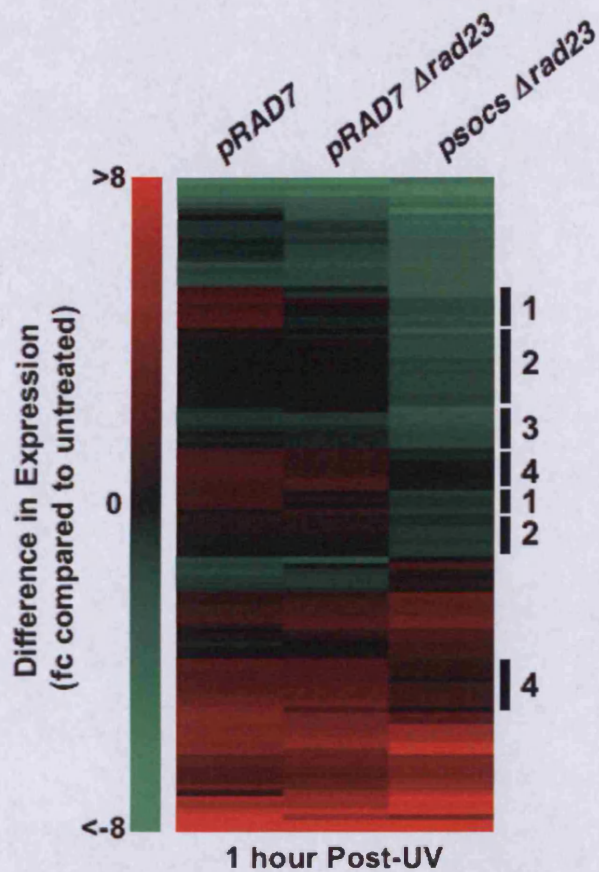
Figure 4.22 - Genes Significantly Differentially Regulated in Response to UV in *psocs Δrad23* Strain. A list of 110 genes that were significantly misregulated in response to UV in the *psocs Δrad23* strain, and >0.2 fc different to the *pRAD7 Δrad23* strain. These 110 genes were hierarchically clustered and four biologically interesting clusters have been labelled. Some clusters have been merged to amalgamate similarly expressed genes, which are shown by the same cluster number. The gene list is displayed in Appendix IV, List 5.
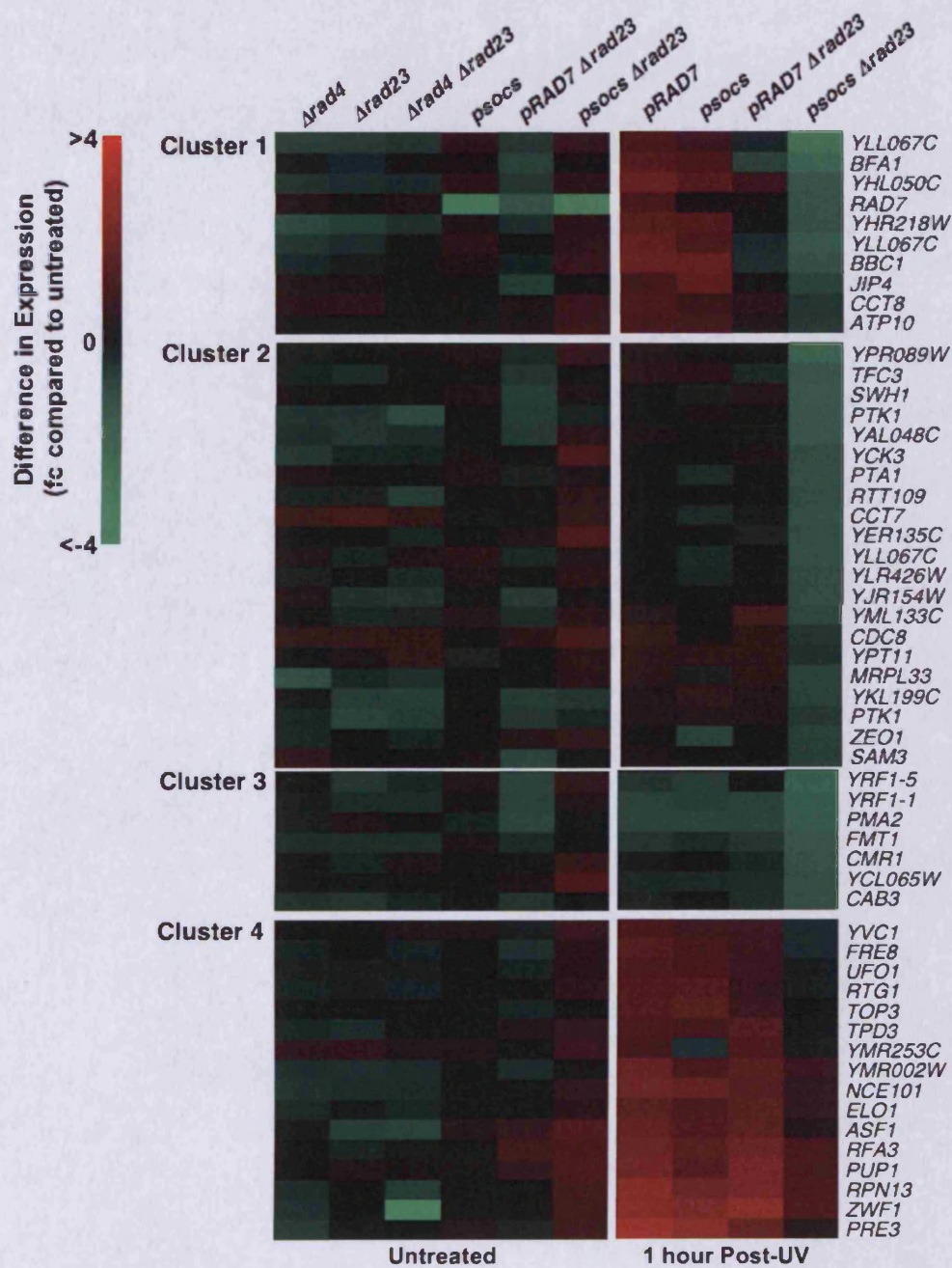
Figure 4.23 - Gene Clusters from Figure 4.22. Gene names are shown for the four clusters identified in Figure 4.22. Heatmap values are shown for untreated samples in all mutants compared to the WT or *pRAD7* strain value and expression values 1 hour after UV treatment are compared to the corresponding untreated value.

Further analysis of individual genes from the clusters displayed in Figure 4.23, using SGD (www.yeastgenome.org), was conducted in order to reveal genes from common pathways or with similar functions. Cluster 1 contains several subtelomeric elements (*YLL067C*, *YHL050C* and *YHR218W*) downregulated in the *psocs Δrad23* strain, which although are not well classified ORFs, all have similarity to helicases, and are all situated in the telomeric Y' element. They are thought to have a role in chromosome segregation and stability (Louis 1995), so downregulation of these elements in the *psocs Δrad23* mutant could affect the UV survival. Cluster 1 also contains *BFA1*, a checkpoint gene, which functions as part of the mitotic exit network (MEN) inhibitor complex and functions to prevent anaphase onset (de Bettignies and Johnston 2003; Geymonat et al. 2003).

Cluster 2 also contains subtelomeric Y'-element helicase-like ORFs (*YLL067C* and *YML133C*), which are also downregulated in the *psocs Δrad23* strain. It should be noted that the subtelomeric ORFs represented here are located across a variety of chromosomes, so it appears to be a genome-wide effect and not just localised to one telomere. Cluster 2 also contains the histone acetyltransferase *RTT109*, which acetylates histone H3 during S-phase and in response to DNA damage (Han et al. 2007). *CDC8* is also in Cluster 2, and is a gene involved in dTTP synthesis, an important step in DNA synthesis downstream of the RNR pathway. Although *CDC8* regulation is not as well understood as RNR regulation, downregulating *CDC8* may upset nucleotide levels, which would affect DNA replication and repair. Reduction of *CDC8* levels is also known to affect telomere length (Toussaint et al. 2005).

Subtelomeric helicases are also found in Cluster 3. *YRF1-1* and *YRF1-5* are highly expressed in cells which lack functional telomerase, however are not usually induced in WT cells (Yamada et al. 1998). Misregulation of these telomeric elements could affect genome stability and therefore possibly pose a threat to cellular integrity and survival.

Cluster 4 features genes that exhibit failed upregulation in the *psocs* Δ*rad23* mutant in response to UV. The most striking feature is the presence of several proteasomal subunits (*PRE3*, *PUP1* and *RPN13*), whose expression is controlled by the Rpn4 transcription factor. The proteasome is known to have a varied function in the DNA damage response with both proteolytic and non-proteolytic regulatory roles. *RFA3* is a subunit of RPA, the ssDNA binding complex which has a pivotal role in the DNA damage checkpoint response. Regulation of transcription of RPA subunits may have an important role in DNA damage sensitivity, however there is no evidence of previous research in this area. But the identification of other RPA subunits in Section 4.3.8 may suggest they are of interest, and a possible regulatory target of the Rad4-Rad23 complex. Other genes in Cluster 4 that may affect DNA damage sensitivity are *ASF1*, a nucleosome assembly factor and possible downstream target of Rad53, and *TOP3*, which affects telomere stability.

The Rpn4 transcriptional activator controls transcription of most proteasomal subunits and several other genes, most of which are known to be proteasome-associated. Due to the apparent over-representation of Rpn4-regulated genes in Cluster 4 (*PUP1*, *RPN13* and *PRE3*), all proteasome subunits and several other Rpn4-regulated genes were extracted and are displayed in Figure 4.24. It can be seen that the expression levels of most proteasome subunits in the Δ*rad23* strains show a uniform lower induction than the $RAD23^+$ strains, which does not appear to be a *psocs*-dependent expression change for most genes. *RPN4* transcription is not siginificantly affected by the mutations, so it may be affected post-transcriptionally by Rad23. This may also demonstrate the Rad23 regulatory mechanism proposed by (Wade et al. 2009), whereby Rad23 regulates transcription independently of Rad4. Although many of the proteasome subunits are less upregulated in the Δ*rad23* mutants, the role of proteasomal transcriptional upregulation in response to DNA damage is not well studied so it is unknown whether DNA damage sensitivity is affected by reduced induction of transcription of proteasome subunits.
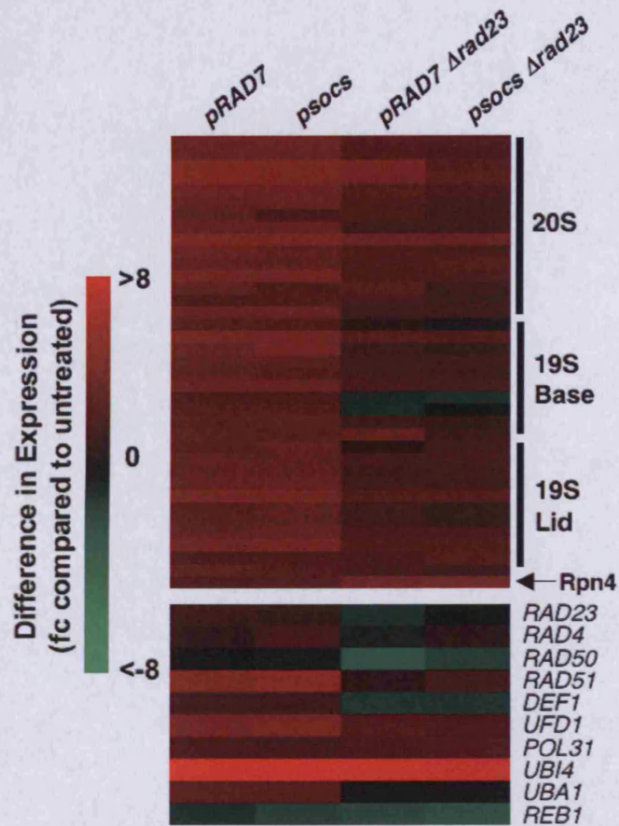
Figure 4.24 - Rpn4-Regulated Genes Including All Proteasome Subunits
Rpn4 is a transcription factor that activates transcription of most proteasome subunits and other genes shown here, many of which are proteasome-related. Expression values represent 1 hour after UV treatment in the different strains.

Another well-represented pathway, identified in several analyses so far is the Mec1-Rad53 dependent DNA damage checkpoint pathway. Genes involved in this pathway were extracted from the arrays and are displayed in Figure 4.25 to reveal any common transcriptional misregulation in the mutant strains. Genes from pathways commonly induced in response to DNA damage (discussed in Section 4.1.4), are also displayed in Figure 4.25 in order to view disruption of the well-characterised transcriptional response to UV in the mutant strains.
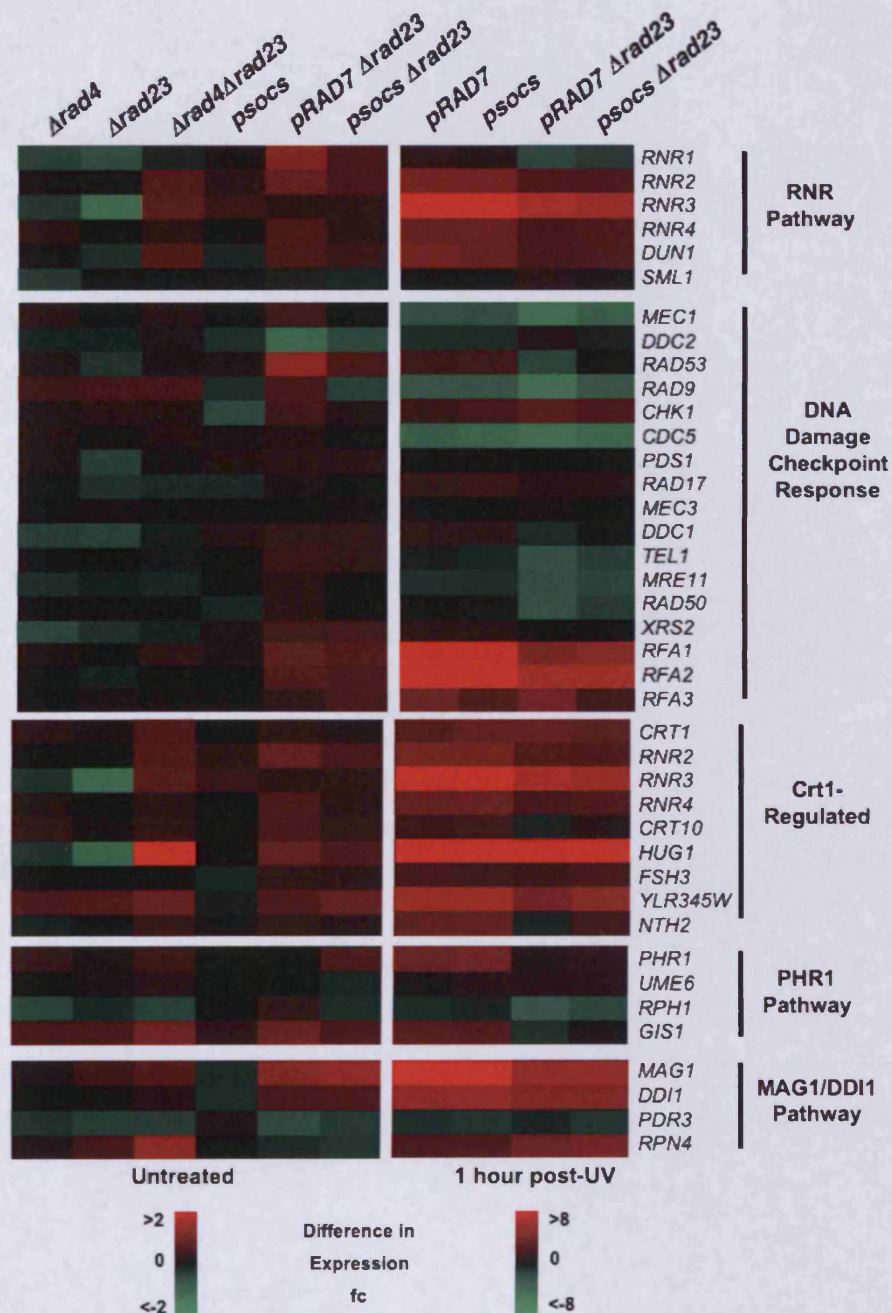
Figure 4.25 - Genes Involved in the DNA Damage Checkpoint Pathway, and Genes Commonly Induced In Response to DNA Damage. Genes were extracted from *rad4/rad23* and *psocs/rad23* microarrays, and expression values are displayed as fc values.

Transcription of the RNR pathway shows strong evidence of being regulated by the Rad4-Rad23 complex. Basal transcriptional levels are altered in the *rad4/rad23* mutants for most RNR subunits, and there is reduced expression of *RNR1-4* in *pRAD7 Δrad23* and *psocs Δrad23* strains following UV. This reduction in RNR transcription could cause reduced RNR activity, which may

result in reduced dNTP pools and inefficient repair. *DUN1*, the RNR activator exhibits reduced transcription in the *pRAD7* Δ*rad23* and *psocs* Δ*rad23* mutants, which could contribute to or cause the reduced RNR transcription. RNR transcriptional induction is regulated by the Crt1 repressor. In order to test if defective Crt1 activity was responsible for reduced RNR induction, all other known Crt1-regulated genes were extracted. Figure 4.25 illustrates that most other Crt1-regulated genes also exhibit reduced expression in the *pRAD7* Δ*rad23* and *psocs* Δ*rad23* strains, which could explain the reduced expression of RNR.

The DNA damage checkpoint pathway genes also exhibit altered transcription in response to UV in the mutant strains. The most striking transcriptional alteration appears in *RFA3*, a subunit of RPA the ssDNA binding factor, which appears to lose upregulation in a *psocs*-dependent manner. *RAD53* also exhibits altered expression in response to UV in the mutants, which could affect coordination of the DNA damage checkpoint response, as Rad53 is a central key player in the pathway. The *TEL1* pathway shows some Rad23-dependent transcriptional misregulation, which would implicate Rad23 in affecting the response to more than just NER-repairable lesions as Tel1 responds exclusively to dsb.

The other two pathways mentioned previously to be upregulated in response to DNA damage are the *PHR1* and *MAG1-DDI1* pathways. Figure 4.25 suggests that UV-induced transcription of the *PHR1* photolyase is highly dependent on Rad23, but does not show any *psocs*-dependent variation. Every effort was made to keep strains in the dark following UV irradiation, however the contribution of photolyase activity to UV sensitivity is not known, and reduced *PHR1* induction could be a contributor to the Δ*rad23* strains' damage sensitivity. The *MAG1/DDI1* pathway shows no significant variation in UV-induced transcription between the mutants shown.

4.4 Discussion

The aim of this chapter was to investigate and identify the role of the Rad4-Rad23 complex and particularly the Rad7-dependent ubiquitination of Rad4 in DNA damage-responsive global transcriptional control. This was investigated based on observations seen by (Gillette et al. 2006) that the Rad7-dependent ubiquitination of Rad4 is involved in a component of the NER pathway that requires *de novo* protein synthesis. This provoked the theory that the Rad4-Rad23 complex has a role in global transcriptional control in response to DNA damage.

Rad23 has been reported previously to have a role in global gene transcription, by (Wade et al. 2009). They suggested that Rad23 had a regulatory role in global gene transcription, affecting a third of the genome dependent on its interaction with the 19S proteasome. They also concluded that Rad23's function in transcriptional regulation did not involve Rad4. The analyses undertaken in this chapter aimed to reveal the role of Rad4-Rad23 as a complex in UV-responsive transcription, and more specifically the function of Rad4 post-UV ubiquitination. This may present a role for Rad23 in transcription separate to the function observed by (Wade et al. 2009), possibly revealing a DNA-damage specific regulatory role of Rad23 in transcription, involving Rad4 ubiquitination. Whether the role of Rad23 in transcription affects a vast proportion of the genome as suggested in (Wade et al. 2009), or affects a smaller range of genes as revealed in this study, it was concluded that this represents a separate function of Rad23 in transcriptional control than the Rad4-Rad23 complex-dependent UV-responsive transcriptional control observed here.

The original *rad4/rad23* microarrays identified genes misregulated in untreated strains with Δ*rad4*, Δ*rad23* or Δ*rad4*Δ*rad23* mutations. Genes of interest from these arrays included downstream elements of the checkpoint pathway including *RNR3* and *HUG1*, and genes with STRE elements in their promoter (*HSP12, CIN5, GND2, DDR2* and *GPH1*). STRE elements bind the Msn2-Msn4 transcription factors in order to activate a vast array of genes in

response to a variety of stresses (Martinez-Pastor et al. 1996). Analysis of the *rad4/rad23* microarrays suggested a significant role for the Rad4-Rad23 complex in global transcription, particularly in stress-responsive gene expression.

4.4.1 Transcriptional Misregulation of the RNR Pathway and Other Factors Involved in dNTP Synthesis

The DNA damage checkpoint pathway presents a highly specialised response to DNA damage, featuring the culmination of several effectors with one common goal, to protect genomic integrity. Two of the main effects of the DNA damage checkpoint response are altered cell cycle control and upregulation of dNTP synthesis. The *psocs Δrad23* mutant strain studied here exhibited reduced transcription of genes required for regulation of dNTP levels in response to DNA damage (Figure 4.23), including significantly reduced induction of *RNR3*, and increased downregulation of *CDC8*. *RNR3* is a subunit of the ribonucleotide reductase (RNR) complex, which catalyses the rate limiting step of dNTP synthesis, an essential precursor of DNA synthesis (See Chapter 5.1.1). The RNR complex is most active during S-phase and following DNA damage, when DNA synthesis is required. There are four RNR genes, which encode interchangeable subunits of the RNR complex, but *RNR3* is the most DNA damage-inducible subunit. RNR subunit composition is specific to activity during S-phase or during DNA repair. The reduced induction of *RNR3* observed here may present a novel regulatory mechanism of the DNA damage-dependent RNR subunit specificity.

Whereas the regulation of RNR is fairly well understood, a lot less is known about regulation of the second dNTP level-regulatory gene identified by the arrays, *CDC8*. *CDC8* is an essential gene in *S. cerevisiae*, and is a thymidylate (and uridylate) kinase required for the conversion of dTMP to dTDP (and dUMP to dUDP), an important step in dTTP synthesis (Chien et al. 2009). A specific balance between the four nucleotides levels in cells is essential for accurate DNA synthesis, so impaired synthesis of any dNTP could jeopardise genomic integrity and cellular survival. Reduced expression

of *CDC8* in the *psocs Δrad23* strain could cause reduced dTTP synthesis and thus infringe upon genomic integrity.

4.4.2 Altered Expression of Genes Involved in Telomere Maintenance

It has been shown that reduced cellular dNTP levels can cause telomeric shortening. This has been displayed in *mec1* and *rad53* checkpoint mutants, which exhibit slightly shortened telomeres, a phenotype enhanced by the absence of Sir proteins. The phenotype can be suppressed by deletion of *SML1* the RNR inhibitor, or RNR overexpression, which suggests that shortened telomeres is an effect of inadequate dNTP supply (Longhese et al. 2000). A shortened telomere phenotype is also evident in cells harbouring a temperature sensitive, reduced function mutant *cdc8* gene (Adams and Holm 1996; Flurin et al. 2005). This implies that effective maintenance of cellular dTTP level is required for cell survival, and failure to regulate dTTP synthesis can impact upon genomic integrity by reducing telomere length. Figure 4.23 displays increased transcriptional downregulation of *CDC8* in the *psocs Δrad23* strain in response to DNA damage, which could reduce Cdc8 levels thus decreasing dTTP synthesis, which could cause the shortened telomere phenotype observed in the *cdc8* mutant strain discussed previously. This could result in reduced genome stability, thus contributing to the increased UV sensitivity phenotype of the *psocs Δrad23* strain.

In support of the theory that the *psocs Δrad23* strain may exhibit shortened telomeres, another group of genes involved in telomere maintenance were also revealed in the analysis. The organisation of the ends of *S. cerevisiae* chromosomes comprise of ~350bp telomeric DNA, containing a simple repetitive sequence of $(TG_{1-3})_n$. These regions of DNA are elongated by telomerase to prevent gradual telomeric shortening caused by DNA replication. Telomere maintenance is essential for maintaining genomic integrity of immortal cells. Proximal to the telomeric sequence exist multiple copies of a more complex subtelomeric repeat, known as the Y' element (Zakian 1996). Y' elements occur in two forms, Y'-L (~6.7 kb) and Y'-S (~5.3 kb), and are involved in telomere maintenance by homologous recombination

in telomerase-negative strains. Both varieties of element contain a helicase-like ORF, known as the *YRF1* gene, encoding Y'-Help1 (Yamada et al. 1998). The mechanism of telomerase-independent telomere maintenance is thought to involve reverse transcription of Y' mRNA, then using Y' cDNA to extend telomeres. Significant transcriptional induction of *YRF1* has been observed in telomerase-negative strains, but has also been observed following exposure to the DNA damaging agent enediyne (Watanabe et al. 2002). The microarrays performed and analysed here show reduced expression of Y' element transcripts (*YRF1-1*, *YRF1-5*, *YLL067C*, *YHL050C*, *YHR218W* and *YML133C*) in the *psocs Δrad23* strain in response to DNA damage. Y' element transcription has only been studied as being induced as a backup system for telomere maintenance in the absence of telomerase. This is not relevant to the arrays performed here as the strains are assumed to have an active telomerase. The increased downregulation of Y' element transcription in the *psocs Δrad23* strain represents lower levels of transcript following DNA damage, which could impact on telomere stability, thus affecting genome stability and therefore cause or contribute to the increased UV sensitivity observed in the *psocs Δrad23* strain. The altered regulation of Y' elements may be a result of genome instability or may represent a potential regulatory target for the Rad4-Rad23 complex.

4.4.3 Transcriptional Changes in Genes That Affect Chromatin Structure

Another group of functionally related genes that displayed significantly altered transcriptional control in the *psocs Δrad23* strain is genes involved in chromatin modification, particularly the histone acetyltransferase (HAT) *RTT109*, and the nucleosome assembly factor *ASF1* (Anti-Silencing Factor 1). In order for factors to access DNA to conduct processes such as DNA replication, repair and transcription, chromatin modification is required, which involves the controlled disassembly of nucleosomes, and the subsequent reassembly following the DNA metabolic process. Asf1 is a H3/H4 histone chaperone (Tyler et al. 1999), which facilitates nucleosome reassembly, observed *in vitro* using human extracts, following NER (Mello et al. 2002).

Asf1 facilitates nucleosome assembly via interaction with the chromatin assembly factor CAF-1 and promotes heterochromatin formation via interaction with Hir1 (Green et al. 2005; Sharp et al. 2001). Genetic studies in yeast have deduced that *ASF1* is required for *RTT109*-dependent acetylation of Lysine 56 on histone H3 (Recht et al. 2006). Deletion of *ASF1* results in cells with increased sensitivity to DNA damage (including UV) (Le et al. 1997), and increased genomic instability. Asf1 is also known to dynamically interact with Rad53 (Emili et al. 2001), which implies that Asf1 has a role in the DNA damage response. If reduced *ASF1* expression causes reduced Asf1 protein levels, it could disrupt DNA damage-dependent chromatin modification, thus compromise cellular integrity and could contribute to the increased UV sensitivity of the *psocs Δrad23* strain. These observations suggest that *ASF1* or *RTT109* could be a regulatory target of the Rad4-Rad23 complex, dependent on Rad7-dependent Rad4 ubiquitination in a *Δrad23* strain.

Mobilisation of Y' elements in telomerase-negative strains is mediated by the Ty1 retrotransposon. Ty1 facilitates reverse transcription of the subtelomeric Y' element, and promotes cDNA insertion (Maxwell et al. 2004). It has been shown that histone modification involving Asf1 and Rtt109 can function to protect the genome from Ty1 mediated insertional mutagenesis (Nyswaner et al. 2008). These observations could provide a regulatory link to the subtelomeric and chromatin modificatory transcripts revealed in this analysis. Further work in this area could include observing H3 K56 acetylation levels in the *psocs Δrad23* strain following UV irradiation to assess Asf1 and Rtt109 activity. Telomere length assays could also be performed to observe the effects of reduced expression of Y' elements or reduced expression of dNTP level-maintenance genes (RNR and *CDC8*) in the *psocs Δrad23* strain. If shortened telomeres or altered H3 K56 acetylation levels were observed in the *psocs Δrad23* strain this could suggest a cause of genomic instability in the strain.

4.4.4 Altered Expression of Proteasomal and Proteasome-Associated Genes

Multiple proteasomal genes were also shown to be significantly downregulated in the *psocs Δrad23* strain (*PUP1*, *RPN13* and *PRE3*). The proteasome has many complex and essential roles in various cellular metabolic processes, therefore it is likely that transcriptional regulation of proteasomal subunits is important for cell survival and metabolism. Transcription of almost all proteasomal subunits is governed by the transcriptional activator protein Rpn4. Rpn4 activity represents an elegant negative feedback loop whereby Rpn4 promotes transcription of proteasomal subunits, and Rpn4 is subsequently degraded by the proteasome which decreases its transcription when sufficient proteasome has been synthesised. Rpn4 is not an essential gene, but *Δrpn4* cells are hypersensitive to a variety of stresses including DNA damage, however this stress hypersensitivity may not be due to lack of proteasomal upregulation as Rpn4 regulates transcription of several other genes, many of which are proteasome-associated, including Rad23 (Jelinsky et al. 2000; Ju et al. 2008). These genes are displayed in Figure 4.24, which shows a uniform lack of upregulation of proteasomal subunits, but also in several other Rpn4-dependent genes in *pRAD7 Δrad23* and *psocs Δrad23* strains. Rpn4 is activated by numerous stress-responsive factors including Hsf1, Pdr1, Pdr3 and Yap1 (Ju et al. 2008), so it is possible that the other factors such as the Rad4-Rad23 complex could transcriptionally activate Rpn4 or Rpn4-regulatory factors in response to DNA damage stress.

4.4.5 Identification of Potential Transcriptional Regulatory Targets of the Rad4-Rad23 Complex in the DNA Damage Response

The main goal of this chapter was to explore and identify misregulated genes and pathways that could cause or contribute to the UV sensitivity phenotype of the *psocs* Δ*rad23* strain in order to reveal potential transcriptional regulatory targets of the Rad4-Rad23 complex in the DNA damage response. Four main pathways have been revealed in the final analysis; maintenance of dNTP levels (RNR and *CDC8*), control of proteasomal genes (Rpn4 target genes), genome stability-related chromatin modification (*RTT109* and *ASF1*) and telomere maintenance (Y' element transcripts). Links between these functional gene groups were also observed, for example the role of Asf1 and Rtt109 in preventing insertional mutagenesis involving the Ty1 retrotransposon, the pathway by which Y' elements are replicated, and the role of dTTP and dNTP levels in telomere maintenance. All genes investigated from Figure 4.23 exhibit reduced expression in the *psocs* Δrad23 *strain*. Reduced expression of genes that are known to promote genome stability and cellular integrity could reduce an organism's tolerance to cellular threats such as DNA damaging agents, which could cause an effect such as the phenotype displayed by the *psocs* Δ*rad23* strain in response to UV irradiation, and thus present likely regulatory targets of the Rad4-Rad23 complex, with regulation dependent of Rad4 ubiquitination.

The study will now progress to investigate the role of the Rad7 E3 Ligase in regulation of the RNR pathway. A recurring theme in these analyses has been inappropriate downregulation of genes involved in the maintenance of dNTP levels following DNA damage. The RNR pathway is a well-defined pathway for regulating dNTP levels. The inappropriate downregulation of genes involved in dNTP synthesis in the *psocs* Δ*rad23* strain could be assumed to cause reduced dNTP levels. If dNTP levels were artificially elevated in the *psocs* Δ*rad23* strain by constitutive expression/activation of RNR, and a suppressive effect was observed from UV survival data, it would suggest that the increased UV sensitive phenotype of the *psocs* Δ*rad23* strain is caused (wholly or partly) by insufficient cellular dNTP supply.

5 The Rad7 E3 Ligase Regulates the DNA Damage Response via the RNR Pathway

The previous chapter employed analysis of global gene expression to identify misregulated genes and pathways in the *psocs Δrad23* strain, in order to reveal the function of Rad4 ubiquitination by the Rad7-containing E3 ubiquitin ligase in DNA damage-responsive transcription. This followed on from work conducted by (Gillette et al. 2006), which identified Rad4 ubiquitination as having a possible role in the DNA damage response, particularly in the absence of Rad23. One pathway that exhibited significantly altered transcription in response to DNA damage in the *psocs Δrad23* strain was the Ribonucleotide Reductase (RNR) pathway, a downstream sub-pathway of the Mec1-Rad53 checkpoint response. The RNR pathway modulates cellular dNTP levels at specific stages of the cell cycle and in response to DNA damage. Genetic analysis will be employed in this chapter to attempt to characterise the possible regulatory function of the Rad4-Rad23 complex and if and how it regulates the RNR pathway.

5.1 Introduction

Regulation of cellular dNTP pools is of paramount importance for survival and genomic stability. During periods of DNA synthesis, during replication and repair, nucleotide pools are elevated and balanced between the four nucleotide varieties to facilitate efficient DNA synthesis and minimise mutagenesis. Although yeast can tolerate variations in dNTP level and still maintain cell viability, hyper-recombination but a decreased spontaneous point mutation rate have been associated with lower dNTP levels in a *dun1* strain (Datta et al. 2000; Fasullo et al. 1999), and higher than normal dNTP levels can result in an increase in spontaneous or DNA damage-associated mutagenesis due to encouraged damage bypass by replicative polymerases (Sabouri et al. 2008).

The RNR pathway is the main target for regulation of nucleotide levels, as it is responsible for the rate-limiting step of nucleotide synthesis, and thus DNA synthesis. dNTP concentration is increased by 6-8 fold in response to DNA damage (Chabes et al. 2003).

5.1.1 The RNR Pathway

The rate-limiting step of DNA synthesis is production of deoxyribonucleotides (dNTPs) by reduction of ribonucleotides catalysed by the RNR complex. This creates increased cellular pools of dNTPs, which are used by the DNA polymerase enzyme complex to synthesise DNA. RNR is an $\alpha_2\beta_2$ holoenzyme complex, consisting of 2 large (α) and 2 small (β) subunits. There are 4 RNR genes (*RNR1-4*) of which the highly homologous *RNR1* and *RNR3* encode the α subunits, however only *RNR1* is essential for cell viability. *RNR1* transcription fluctuates between 15 and 30 fold during the unperturbed cell cycle, with a peak in mRNA concentration during S-phase. It is slightly induced by DNA damage by 3-5 fold, whereas *RNR3* is minimally expressed during the normal cell cycle but is highly induced in response to DNA damage by over 100 fold. This DNA damage dependent transcriptional induction of *RNR3* does not contribute much to the DNA damage response and ribonucleotide reduction. Although overexpression of *RNR3* can rescue the lethality of the *mr1* mutant, deletion of *RNR3* does not result in increased damage sensitivity (Elledge and Davis 1990). *RNR2* and *4* encode the β subunits and are both essential and DNA damage inducible, however some yeast strains appear to be able to survive without *RNR4* (Wang et al. 1997a). The β_2 subcomplex consists of an Rnr2-Rnr4 heterodimer. Only Rnr2 is capable of forming the (Fe)2-Y* cofactor, however Rnr4 is required for Rnr2-dependent radical formation although it cannot bind iron itself (Perlstein et al. 2005).

Regulation of RNR activity occurs at several distinct levels. Firstly, the transcription of DNA damage-inducible RNR genes is governed by the Crt1 transcription factor. The RNR complex itself is regulated by allosteric control, altered subcellular localisation and by inhibition by the Sml1 peptide.

131

Allosteric control of RNR occurs via dATP feedback inhibition. As the level of dATP rises by the action of RNR, dATP binds to an allosteric site on the RNR α subunit. The α subunit contains two allosteric sites: the activity site that monitors dNTP pools based on the dATP:ATP ratio, and the specificity site that regulates the balance between the dNTP varieties and can bind ATP, dATP, dCTP and dGTP (Reichard et al. 2000). A recent study by (Symington et al. 1996) has elegantly revealed the importance of the balance between levels of each dNTP. A series of *mr1* mutant alleles were constructed, containing various point mutations in the allosteric specificity site. It was found that specific *mr1* point mutations resulted in differentially balanced levels of dNTP varieties, which appeared to follow a purine/pyrimidine trend. The *mr1* *Y285F* and *Y285A* mutants exhibited dramatically increased pyrimidine dNTP (dCTP/dTTP) levels, and the *mr1* *Q288A* mutant exhibited increased purine dNTP (dATP/dGTP) levels and reduced pyrimidine dNTP levels. Mutants with reduced pyrimidine dNTP levels were also observed to have a prolonged S-phase causing slower growth, due to pyrimidines limiting DNA synthesis. The reduced dNTP level was also found to activate the S-phase checkpoint, detected by increased expression of the *RNR2*, *3* and *4* subunits, however these mutants do not exhibit an increased mutation rate. These observations show that excessively high levels of specific dNTPs can increase mutation rate but do not affect cell cycle progression, however decreased levels of specific dNTPs can limit DNA synthesis and therefore delay cell cycle progression (Symington et al. 1996). Despite the conserved allosteric site between yeast and mammalian Rnr1, yeast Rnr1 can tolerate far higher levels of dATP *in vitro* before feedback inhibition occurs (Domkin et al. 2002).

5.1.2 Regulation of RNR transcription by the Crt1 repressor

The product of the *CRT1* gene regulates the RNR pathway by binding at the promoter of various genes. It is known to bind to *RNR2*, *RNR3* and *RNR4* promoters (Huang et al. 1998), and repress transcription under non-inducing conditions, when elevation of nucleotide pools is not required. Crt1 becomes

phosphorylated by active Dun1 kinase and vacates the promoters in response to DNA damage to allow RNR transcription and subsequent elevation of nucleotide pools (Hao et al. 2009; Huang et al. 1998).

Crt1 has other genetic targets aside from *RNR2*, *3* and *4*. It also binds to its own promoter and several other genes, only some of which are known to be involved in the DNA damage response. Crt1 recognises a 13bp cis-regulatory nucleotide sequence, which shares significant homology with the mammalian X-box motif. This motif becomes bound by RFX transcription factors, which have a role in regulation of major histocompatability complex genes (Huang et al. 1998). Crt1-regulated genes contain variations of the Crt1 binding motif in their promoters. Different strong and weak binding sequences have been discovered, and variable combinations of the different motifs is thought to provide a graded transcriptional response for different genes, as Crt1 dissociates from weak binding sites before strong when active Crt1 levels become progressively depleted (Huang et al. 1998).

Whilst bound to gene promoters, Crt1 interacts with the Tup1-Ssn6 global corepressor complex, which negatively regulates many DNA damage-inducible genes. Crt1 has 2 repression domains, at residues 1-130 (N-terminal repression domain) and 709-811 (C-terminal repression domain). Crt1 N-terminal repression domain is required for Tup1-Ssn6 recruitment to X-box-containing promoters. The Crt1-Tup1-Ssn6 repressor complex orchestrates a precise nucleosomal array across the promoter that blocks access to the TATA box by the transcriptional machinery. DNA damage-induced Dun1 dependent Crt1 phosphorylation results in loss of Tup1-Ssn6 recruitment, chromatin remodelling and derepression of damage-inducible genes. Repression by Tup1-Ssn6 is known, at other loci, to occur by HDAC recruitment. This could be the case at Crt1-repressed genes, however the action of HDACs at these promoters is not well understood (Zhang and Reese 2005).

The N-terminal repression domain of Crt1 is also known to interact with the SWI/SNF and TFIID complexes, which both act as co-activators of damage-

inducible genes by chromatin remodelling. It has been proposed that Crt1 can act as a repressor or activator of transcription depending on the DNA damage status (Zhang and Reese 2005).

A novel regulator of Crt1 has been discovered recently. Crt10 was found to positively regulate Crt1 transcription. Crt10 was also found to be epistatic to Dun1, and induced by Dun1. It is most probable that Crt10 functions in checkpoint recovery to reinstate Crt1 levels and repression of damage-inducible genes (Fu and Xiao 2006). Another factor thought to influence the levels of Crt1 is the mRNA deadenylase Ccr4. It is thought that Ccr4 affects Crt1 mRNA stability thus adding an extra level of Crt1 regulation (Woolstencroft et al. 2006).

The *HUG1* gene, although its function is unknown, is also repressed by Crt1, and is transcriptionally induced in response to DNA damage. Several other genes have been computationally identified as possible targets of Crt1 repression, from which three genes have been experimentally confirmed as Crt1-regulated. These genes, *FSH3*, *NTH2* and *YLR345W* have been implicated in regulation of central metabolism in response to stress. This suggests Crt1 has a more general role in stress response signalling as a downstream effector of the Mec1-Rad53 checkpoint pathway, however the abundance of Crt1 binding sites in RNR gene promoters suggest that the RNR pathway is the main target of Crt1(Zaim et al. 2005).

5.1.3 Further Transcriptional Regulation of RNR

Transcription of *RNR3*, the main damage-inducible RNR gene has been studied further to reveal additional factors involved in its regulation. The transcriptional modulator proteins Wtm1 and Wtm2 also influence *RNR3* transcription. It has been shown that Wtm2 interacts with *RNR3*'s promoter, and is required for *RNR3* expression (Tringe et al. 2006). Wtm1 interacts with the Rnr2-Rnr4 complex to anchor it to the nucleus under normal conditions.

This interaction is disrupted following DNA damage, which causes export of active Rnr2-Rnr4 to the cytoplasm (Lee and Elledge 2006).

Damage-induced *RNR3* transcription also requires histone modification by the histone deacetylases (HDAC) Rpd3 and Hos2. Rpd3 has been shown to bind to the *RNR3* promoter independently of Crt1 or Tup1. The action of both HDAC is required for effective RNA polymerase recruitment and *RNR3* transcription (Sharma et al. 2007).

5.1.4 RNR Inhibition by Sml1

Sml1 acts post-translationally upon the RNR tetramer by binding via its C-terminal region to the RNR α subunits and inhibiting RNR enzyme action. *SML1* expression fluctuates throughout the normal cell cycle. During S-phase, when dNTPs are in high demand, removal of active Sml1 is essential for cell viability. The checkpoint kinase Dun1 is responsible for Sml1 phosphorylation, which triggers its subsequent degradation both during S-phase and following DNA damage (Zhao and Rothstein 2002). This Dun1-dependent degradation is a downstream event of the Mec1-Rad53 pathway, as Mec1 and Rad53 proteins are required to alter Sml1 protein levels. Further evidence of the involvement of Dun1 in Sml1 protein levels is a prolonged S-phase in $\Delta dun1$ cells, which can be suppressed by Sml1 deletion. The $\Delta dun1$ cells do not exhibit a slow-growth phenotype as G_2/M phase is suitably adjusted so the overall cell cycle time remains the same. This prolonged S-phase suggests defective DNA repair when Sml1 levels are too high. Deletion of *SML1* has been shown to increase cell viability compared to WT cells in response to DNA damaging agents in some cases. This would suggest that the dNTP level that cells normally operate at is not set to allow maximal survival in response to damaging agents, but probably to maintain genetic integrity and an optimum rate of DNA synthesis. $\Delta sml1$ cells exhibit 2.5x elevated pools of all dNTPs in asynchronous untreated cells (Zhao et al. 1998).
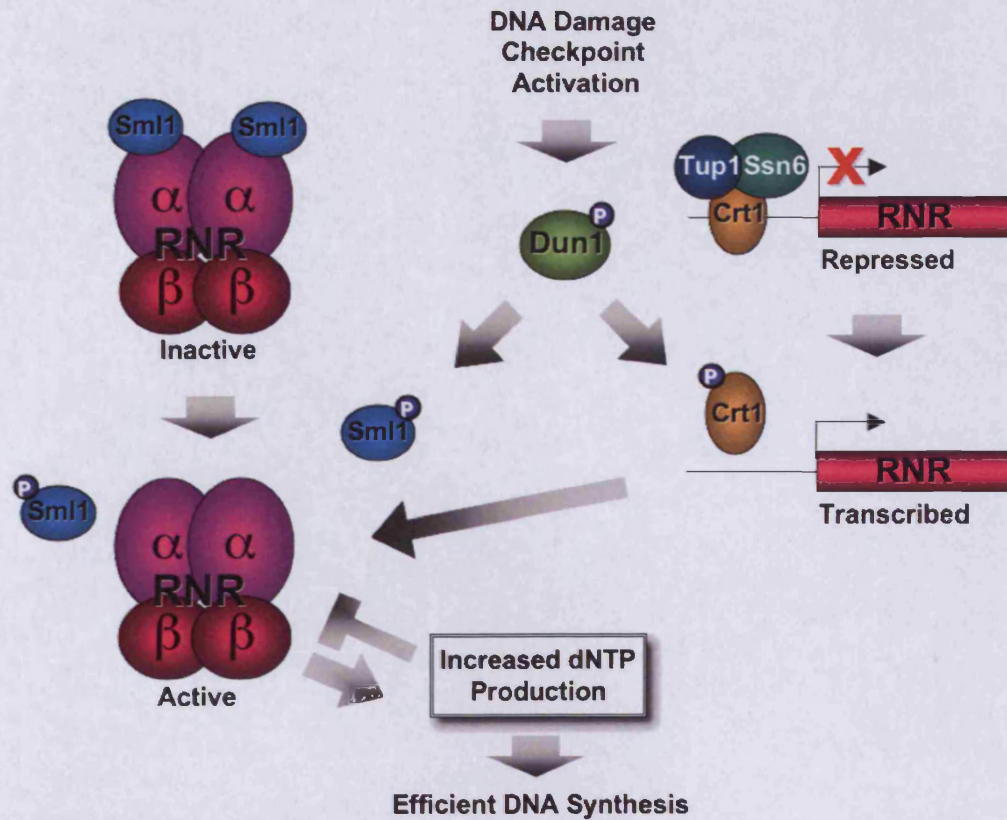
Figure 5.1 - Regulation of the RNR Pathway The RNR pathway is regulated at many different levels. At the transcriptional level the Crt1 repressor vacates RNR gene promoters in response to checkpoint activation by phosphorylation of Crt1 by activated Dun1 kinase. This also triggers Crt1 transcription which provides a feedback loop to rapidly suppress RNR genes when no longer required. The Dun1 kinase also phosphorylates the Sml1 RNR inhibitor, which activates the RNR complex. The active RNR complex catalyses dNTP synthesis thus increasing dNTP levels and DNA synthesis. RNR activity is also inhibited by increased nucleotide levels thus providing a further negative feedback loop. The upstream factors in the DNA damage checkpoint response are displayed in Figure 1.7. This figure was created from multiple sources cited in this chapter.

5.2 Materials and Methods

5.2.1 Yeast Strains Used

Strain	Genotype	Source
Δrad7	BY4742: MATα his3Δ1 leu2Δ0 ura3Δ0 YJR052W::KanMx4	EUROSCARF
Δrad7 Δrad23	BY4742 Δrad7 Δrad23::URA3	This Study
pRAD7 Δrad23 Δsml1	BY4742 Δrad7 Δrad23::URA3 Δsml1::LEU2 pRS313-RAD7	This Study
psocs Δrad23 Δsml1	BY4742 Δrad7 Δrad23::URA3 Δsml1::LEU2 pRS313-socs	This Study
pRAD7 Δrad23 Δcrt1	BY4742 Δrad7 Δrad23::URA3 Δcrt1::LEU2 pRS313-RAD7	This Study
psocs Δrad23 Δcrt1	BY4742 Δrad7 Δrad23::URA3 Δcrt1::LEU2 pRS313-socs	This Study

5.2.2 Chromatin Immunoprecipitation (ChIP)

5.2.2.1 Preparation of Chromatin

Cells were grown to mid/late log phase (O.D$_{600}$ ~ 1), and 2.8ml of 37% formaldehyde was added to 100ml of the culture medium (containing at least 2×10^9 cells). The mixture was incubated at room temperature for 20 mins with occasional mixing to allow efficient DNA and protein cross-linking. The cross-linking reaction was stopped by adding 5.5ml of 2.5M glycine to a final concentration of 0.125M. Cells were collected by centrifugation and then washed with ice-cold TBS buffer and ChIP lysis buffer (50mM HEPES-KOH pH 7.5, 140mM NaCl, 1mM EDTA, 1% Triton X-100, 0.1% Na-deoxycholate 1mM PMSF, 1mM Benzamidine, 10μg/ml Aprotinin, 1μg/ml Leupeptin, 1μg/ml Pepstatin). Cells were resuspended in 500μl of ChIP lysis buffer supplemented with 12.5μl of 20% SDS and 12μl of 100× protease inhibitors. After 0.5ml glass beads were added to this solution, the mixture was vortex (at the highest speed on a turboMix) at 4°C for 10-15 mins. The cell lysate was carefully collected by centrifugation. The cell lysate was sonicated by a

Diagenode sonication system at the high output rate for 3 mins (6 × 0.5 min on/0.5 min off cycle). The sonicated cell lysate was centrifuged at 13 200 rpm for 15 mins at 4°C. Supernatant (chromatin extract) was transferred to a clean tube and stored at -80°C until further use.

5.2.2.2 Chromatin Immunoprecipitation

Protein A beads were washed twice with ChIP lysis buffer and then equilibrated with ChIP lysis buffer supplemented with 0.1% BSA and 40μg/ml single strand salmon sperm DNA for 3 hours at 4°C. 50μl of chromatin extracts were added to 500μl of ChIP binding buffer (ChIP lysis buffer supplemented with 0.25% SDS and 1× protease inhibitors) and then the solution was cleaned with the equilibrated Protein A beads. After removal of the Protein A beads by centrifugation, the chromatin immunoprecipitation was carried out by adding 1-5μl antibody to this solution at 4°C overnight. 20-30μl of Protein A beads slurry were washed twice with ChIP lysis buffer, then added to the solution and incubated for 2-3 hours at 4°C. The Protein A beads were quickly spun down and washed successively with ChIP lysis buffer, ChIP lysis buffer with an increased salt concentration (500mM NaCl), LiCl solution and TE buffer. The Protein A beads were incubated for 15 minutes at 65°C in 100μl pronase buffer, supplemented with 5μl pronase to reverse-crosslink and elute proteins. This was then centrifugated for 2 mins at 13 000 rpm, then supernatent was incubated overnight at 65°C to ensure reverse-crosslinking. 1μl RNAse was added and incubated at 37°C for 30 mins. DNA was then isolated using the QIAquick PCR Purification Kit (Qiagen). The DNA suspension was stored at -20°C and used for qPCR, described in Section 4.2.3.

5.2.3 Strain Construction

In order to activate RNR activity constitutively throughout the cell cycle and following DNA damage, two new strains were constructed. Deletion of the Crt1 repressor results in constitutive expression of RNR, and deletion of the Sml1 inhibitor results in loss of RNR complex inhibition, thus causing constitutive RNR activation.

Using the Δ*rad7* Δ*rad23* strain, the *SML1* or *CRT1* gene was deleted by replacement with a *LEU2* marker gene. Marker gene insertion was detected by colony PCR and confirmed by DNA sequencing. The *pRS313-RAD7* and *pRS313-socs* plasmids were transformed into the Δ*sml1* and Δ*crt1* strains to produce the last four strains displayed in the above Table.

5.2.4 Northern Expression Analysis

Northern Blotting was performed to ensure *SML1* and *CRT1* were not being expressed in the knockout strains. Total RNA was extracted by the hot phenol method, and quality-checked by briefly running an agarose gel. The RNA was then used for Northern Blotting, and hybridisation of radiolabelled probe was detected.
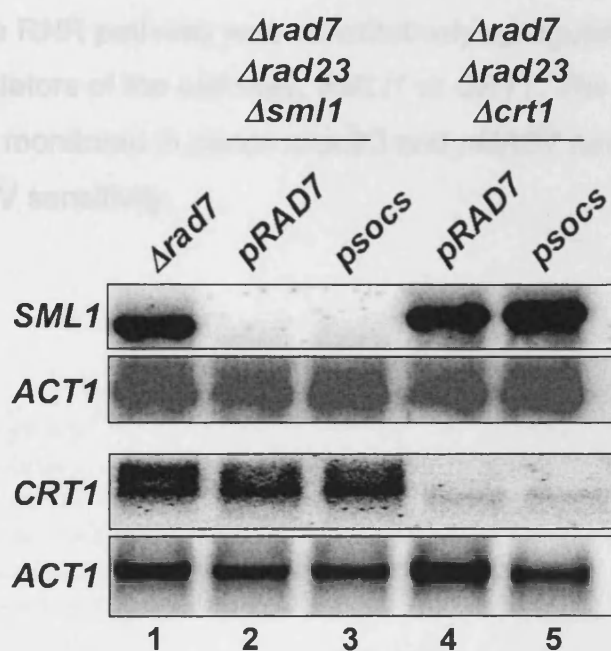
Figure 5.2 - Northern Expression Analysis of *CRT1* and *SML1* in *Δrad7* and New Strains RNA was extracted from *pRAD7Δrad23Δsml1* (lane 2), *psocsΔrad23Δsml1* (lane 3), *pRAD7Δrad23Δcrt1* (lane 4) *psocsΔrad23Δcrt1* (lane 5) and *Δrad7* (lane 1)(*CRT1*⁺, *SML1*⁺) strains and used for northern analysis. The hybridised radiolabelled probe was detected as shown here to visualise *SML1*, *CRT1* and *ACT1* RNA as a loading control.

The northern blots (Figure 5.2) display clearly that *SML1* and *CRT1* are not being expressed in their respective deletion strains. Lane 1 shows expression of both *SML1* and *CRT1* in the control *Δrad7* strain. Lanes 2 and 3 show expression of *CRT1* but not *SML1* in the *Δsml1* strains and lanes 4 and 5 show expression of *SML1* but not *CRT1* in the *Δcrt1* strains. This confirms that strain construction was successful.

5.3 Results

It was observed previously that components of the RNR pathway exhibit decreased upregulation in response to UV in the *psocs Δrad23* strain (Chapter 4), a strain unable to facilitate Rad4 ubiquitination following UV (Gillette et al. 2006). This suggested that ubiquitination of Rad4 has a regulatory role in activation of the RNR pathway. In order to investigate the role of Rad4 ubiquitination in regulation of the RNR pathway in response to DNA damage, the RNR pathway was constitutively upregulated by deletion of the negative regulators of the pathway, *SMLI1* or *CRT1*. The effect of RNR upregulation was monitored in *psocs Δrad23* and *pRAD7 Δrad23* strains with respect to their UV sensitivity.

5.3.1 Constitutive RNR Activation Suppresses the UV Sensitivity of the psocs Δrad23 Strain

The RNR complex was constitutively activated by deleting the RNR inhibitor Sml1. A UV survival assay was conducted in the psocs Δrad23 Δsml1 strain, with pRAD7 Δrad23 and psocs Δrad23 strains as controls (Figure 5.3).
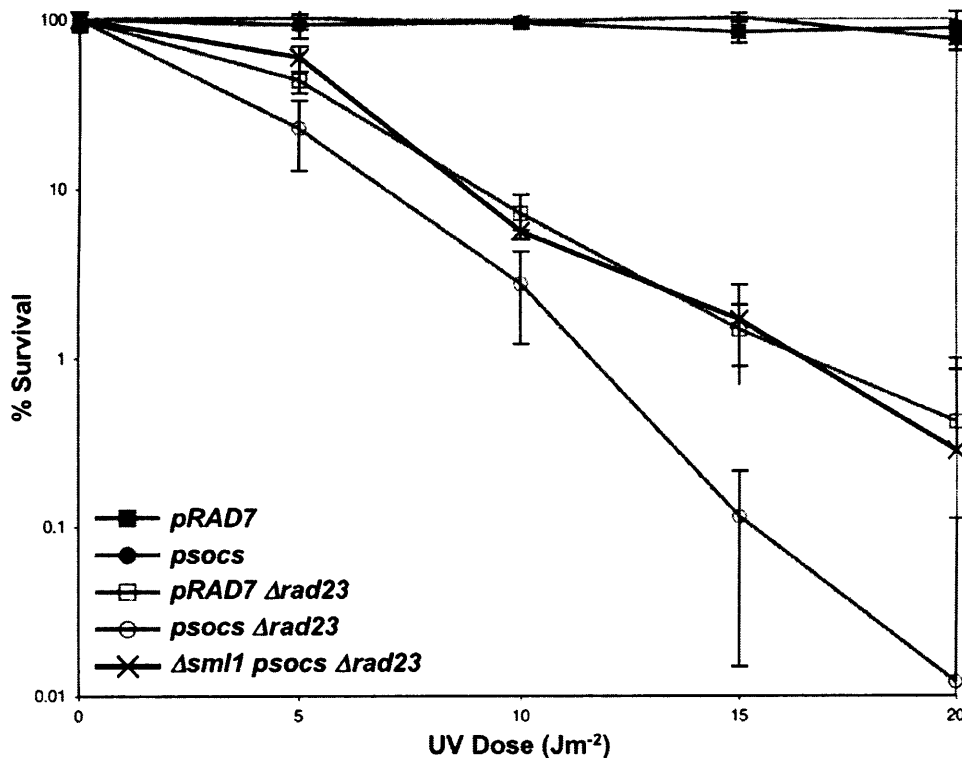
Figure 5.3 - UV Survival of Δsml1 psocs Δrad23 strain. The psocs Δrad23 Δsml1 strain, with the pRAD7, psocs, pRAD7 Δrad23 and psocs Δrad23 strains were spread onto minimal media plates in triplicate. Following 2 days growth, surviving colonies were counted and % survival calculated. Error bars correspond to standard deviation. UV survival raw data can be found in Appendix II.

Figure 5.3 shows that constitutive activation of RNR suppressed the additional UV sensitivity of the psocs Δrad23 strain compared to the pRAD7 Δrad23 strain. The UV resistance appears to be elevated to the pRAD7 Δrad23 level, which suggests that deletion of SML1, which is reliably assumed to cause elevated dNTP pools, can completely suppress the UV sensitivity caused by failed Rad4 ubiquitination when RAD23 is deleted.

5.3.2 Constitutive RNR Activation Does Not Significantly Affect UV

Sensitivity of the *pRAD7 Δrad23* Strain

To examine further the suppressive effect of *SML1* deletion, a UV survival assay was conducted in the *pRAD7 Δrad23 Δsml1* strain. If *SML1* deletion does only suppress the UV sensitivity caused by the *psocs* mutation as suggested previously, then the UV survival curve should not be affected in the *pRAD7 Δrad23 Δsml1* strain compared to the *pRAD7 Δrad23 SML1*^{+} strain.
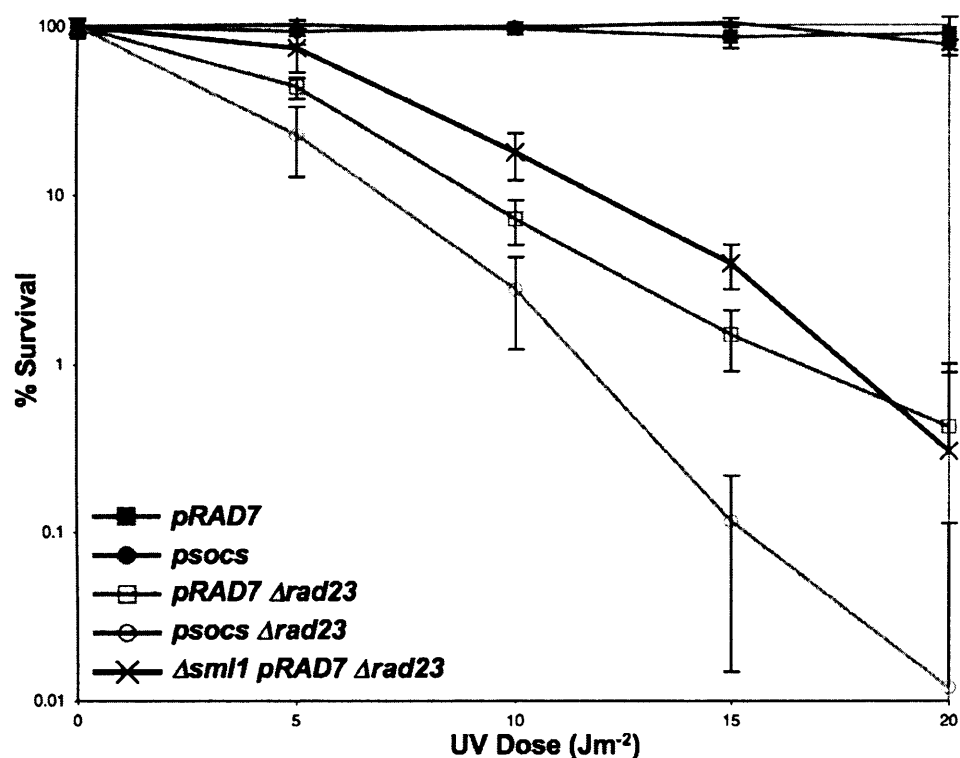
Figure 5.4 - UV Survival of *Δsml1 pRAD7 Δrad23* Strain The *pRAD7 Δrad23 Δsml1* strain, with the *pRAD7, psocs, pRAD7 Δrad23* and *psocs Δrad23* strains were spread onto minimal media plates in triplicate. Following 2 days growth, surviving colonies were counted and % survival calculated. Error bars correspond to standard deviation. UV survival raw data can be found in Appendix II

Figure 5.4 shows that deletion of *SML1* in the *pRAD7 Δrad23* strain does not significantly suppress its UV sensitivity. Although there appears to be slight suppression at lower UV doses, the strains are equally sensitive at $20Jm^{-2}$, which suggests that an overall suppressive effect is not occurring. This

suggests that the intermediate UV sensitivity caused by *RAD23* deletion is not due to insufficient elevation of nucleotide pools following DNA damage-induced checkpoint activation. An alternative concusion could be that the dNTP levels are insufficiently elevated in the Δ*sml1* strains to allow complete suppression of UV sensitivity, as Δ*sml1* strains are known to elevate dNTP levels 2-3 fold, whereas a 6-8 fold increase occurs in a typical WT strain in response to DNA damage. This is explored further in the discussion section.

5.3.3 Constitutive RNR Expression Suppresses the UV Sensitivity of the pRAD7 and psocs Δrad23 Strain

The Crt1 repressor was deleted in order to constitutively express RNR throughout the cell cycle and in response to DNA damage. A UV survival assay was conducted in the *psocs Δrad23 Δcrt1* strain, with *pRAD7 Δrad23* and *psocs Δrad23* strains as controls (

Figure 5.5).
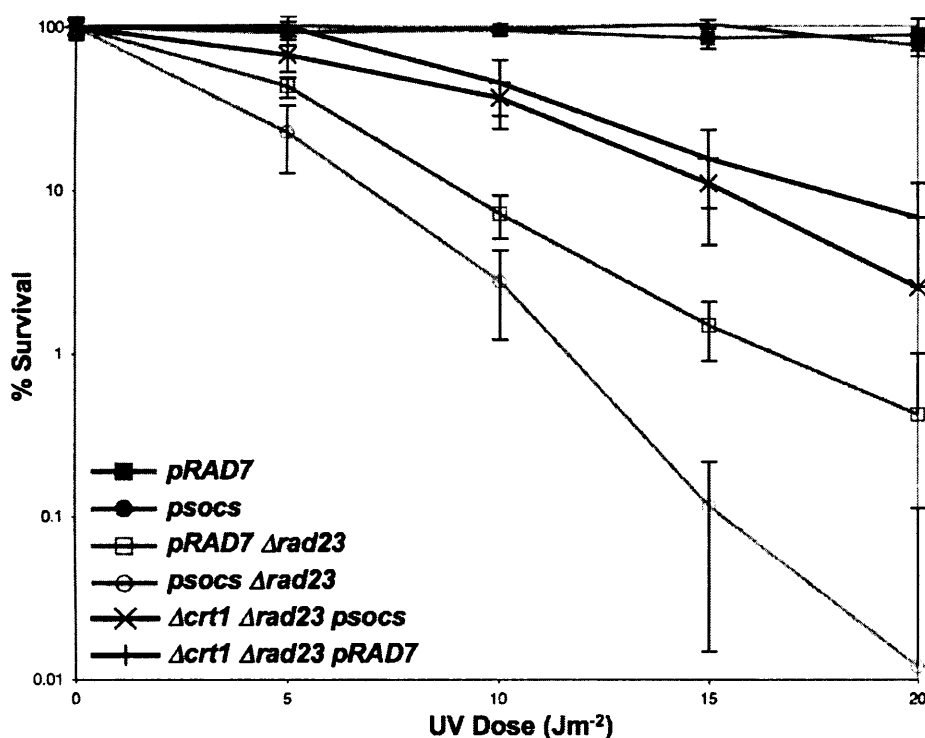
Figure 5.5 - UV Survival of Δcrt1 pRAD7 Δrad23 and Δcrt1 psocs Δrad23 Strains The *pRAD7 Δrad23 Δcrt1* and *psocs Δrad23 Δcrt1* strains, with the *pRAD7, psocs, pRAD7 Δrad23* and *psocs Δrad23* strains were spread onto minimal media plates in triplicate. Following 2 days growth, surviving colonies were counted and % survival calculated. Error bars correspond to standard deviation. UV survival raw data can be found in Appendix II

Figure **5.5** displays a dramatic increase in UV resistance in strains with *CRT1* deleted. This implies that constitutive upregulation of RNR transcription suppresses the UV sensitivity of *Δrad23 pRAD7* and *psocs* strains. This exhibits a similar effect to the *Δsml1* strains, however whereas in the *Δsml1*

strains it was only the additional sensitivity of the *psocs* mutant in the Δ*rad23* strain that was suppressed,

Figure 5.5 displays further suppression of the UV sensitivity caused by deletion of *RAD23*. This suggests that RNR activation is able to suppress the additional UV sensitivity of the *psocs* Δ*rad23* strain (as shown in Figure 5.3) whereas deletion of *CRT1* appears to suppress the additional UV sensitivity of the *psocs* Δ*rad23* strain by RNR activation, but can also partly suppress UV sensitivity caused by *RAD23* deletion, possibly by a function of Crt1 not involving RNR.

5.3.4 The Rad4-Rad23 Complex Binds at the *DUN1* Promoter

The suppression of UV sensitivity in Δ*sml1* and Δ*crt1* strains provide phenotypic evidence to suggest that the Rad7 E3 ligase has a role in regulation of cellular dNTP levels. In order to characterise this role further the regulatory mechanism must be revealed. Following DNA damage, the Dun1 kinase activates the RNR pathway by inactivating the Sml1 inhibitor and the Crt1 repressor (Huang et al. 1998; Zhao and Rothstein 2002). The microarray data from Chapter 4 indicated that several RNR pathway genes exhibited reduced upregulation in response to DNA damage in the *psocs* Δ*rad23* strain. This may indicate that the Rad4-Rad23 complex is acting on a regulator of the RNR pathway, rather than the RNR genes themselves, which presents Dun1 as a likely candidate to be Rad4-Rad23-regulated. Dun1 also exhibited a degree of reduced upregulation in response to UV from the microarray data, which was confirmed by northern blot (Z. Zhou, Unpublished Data). In order to begin to elucidate the mechanism by which the Rad4-Rad23 complex regulates the RNR pathway, ChIP analysis was performed at the *DUN1* promoter to examine Rad4-Rad23 occupancy.

A double-ChIP assay was performed using the *pRAD7* and Δ*rad4*Δ*rad23* strains, by first conducting an immunoprecipitation using a Rad23 antibody, then immunoprecipitating Rad23-associated chromatin using a Rad4

antibody. qPCR was then performed on the resulting precipitated chromatin. The result of this ChIP assay is displayed in Figure 5.6.
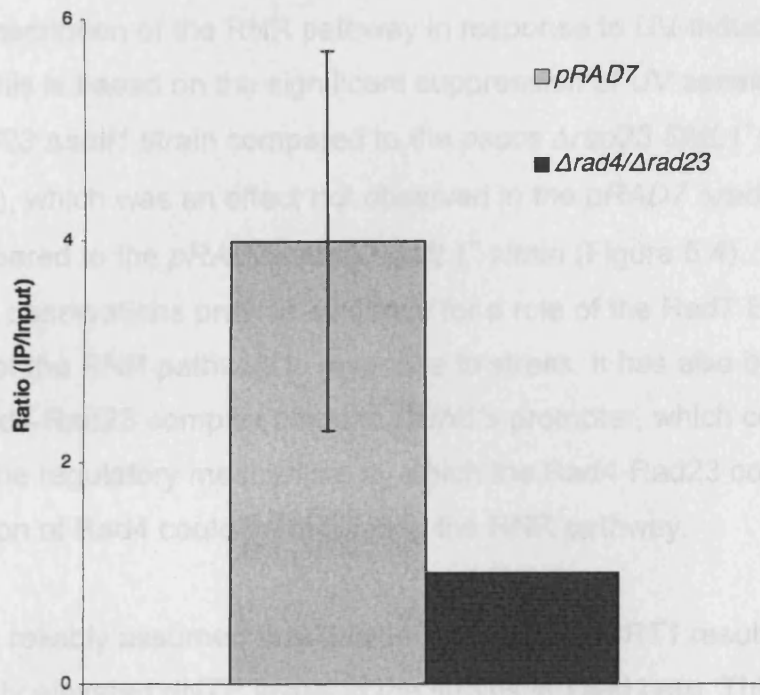
Figure 5.6 - ChIP Assay Detecting Occupancy of the Rad4-Rad23 Complex at the *DUN1* Promoter. Chromatin was extracted from the *pRAD7* and *Δrad4Δrad23* strains, and used to perform a Double IP assay, using a Rad23 antibody followed by a Rad4 antibody. Rad4-Rad23 binding at the *DUN1* promoter was then quantified by qPCR. qPCR data is displayed in Appendix VIII.

Figure 5.6 displays the presence of the Rad4-Rad23 complex at *DUN1*'s promoter region in untreated cells in a WT (*pRAD7*) strain. This can be seen from the increased IP/Input ratio in the *pRAD7* strain compared to the *Δrad4Δrad23* strain. This suggests that the Rad4-Rad23 complex affects *DUN1* transcription, and due to the fact that *DUN1* is not significantly expressed during the normal cell cycle it could be assumed that the Rad4-Rad23 complex acts as a negative regulator of transcription. This result demonstrates the potential of this study, and provides further evidence to suggest that the Rad4-Rad23 complex acts as a transcriptional regulator.

147

5.4 Discussion

The results obtained in this chapter suggest that UV-dependent ubiquitination of Rad4 by Rad7's E3 ligase has a role in regulating cellular dNTP levels via altering transcription of the RNR pathway in response to UV-induced DNA damage. This is based on the significant suppression of UV sensitivity in the psocs Δrad23 Δsml1 strain compared to the psocs Δrad23 SML1⁺strain (Figure 5.3), which was an effect not observed in the pRAD7 Δrad23 Δsml1 strain compared to the pRAD7 Δrad23 SML1⁺ strain (Figure 5.4). These phenotypic observations provide evidence for a role of the Rad7 E3 ligase in regulation of the RNR pathway in response to stress. It has also been shown that the Rad4-Rad23 complex binds to DUN1's promoter, which could represent the regulatory mechanism by which the Rad4-Rad23 complex by ubiquitination of Rad4 could be regulating the RNR pathway.

It has been reliably assumed that deletion of SML1 or CRT1 results in constitutively elevated dNTP levels in the strains studied here. This prompted the theory that the increased UV sensitivity of the psocs Δrad23 strain is due to improper regulation of dNTP levels via the RNR pathway. Studies to determine the dNTP level in logarithmically growing cells have revealed previously that dNTPs are elevated by ~2 fold in Δsml1 cells and ~3-4 fold in Δcrt1 cells (Tang et al. 2009). Although these mutants have increased cellular dNTP levels, dNTP levels are generally increased 6-8 fold in response to DNA damage (Chabes et al. 2003). It is plausible that the UV survival curves for the various mutants could portray incomplete suppression of the psocs Δrad23 strain's UV sensitivity because dNTP levels are being raised insufficiently. This raises the possibility that the actual level of dNTPs could relate to UV survival in this case, which would also explain the higher level of suppression in the Δcrt1 strain, assuming that deletion of CRT1 results in higher dNTP levels than deletion of SML1. It is not being proposed that dNTP levels are completely depleted in the psocs Δrad23 strain, but that the dNTP levels are lowered sufficiently to affect DNA synthesis in response to DNA damage. In order to test this theory, direct detection of dNTP levels could be performed using an HPLC technique, as employed by (Chabes et al. 2003). This would

reveal whether cellular dNTP levels are misregulated and therefore lowered in the *psocs Δrad23* strain. This could be conducted following UV treatment to reveal whether the *psocs Δrad23* strain exhibits altered dNTP levels following DNA damage. dNTP levels could also be raised higher than the levels expected in the *Δsml1* and *Δcrt1* strains using overexpression of the *mr1 D57N* mutant strain, a strain that exhibits significantly higher dNTP levels due to the Rnr1 protein being insensitive to dATP allosteric feedback inhibition (Chabes et al. 2003). This mutant strain could demonstrate further suppression of the UV sensitivity in the *psocs Δrad23* strain if insufficient dNTP levels are the cause of the UV sensitivity of *psocs Δrad23 Δsml1/Δcrt1* strains. Higher dNTP levels could also be achieved using an *Δsml1 Δcrt1* double mutant, however the use and viability of this mutant has not been reported previously, so it can only be assumed that deleting *SML1* and *CRT1* could increase dNTP levels further than the single mutants.

The microarray data in Chapter 4 displayed transcriptional downregulation of components of the RNR pathway in the *psocs Δrad23* strain in response to UV, thus presenting potential transcriptional regulatory targets of the Rad4-Rad23 complex, and the regulatory function of Rad4 ubiquitination. It was proposed that downregulation of the RNR pathway in this strain caused decreased elevation of cellular dNTP levels and thus affected DNA synthesis following DNA damage. The data obtained in this chapter support the notion that dNTP levels are less elevated in the *psocs Δrad23* strain following DNA damage, as constitutive activation or expression of RNR, reliably assumed to increase dNTP levels has specifically suppressed the additional UV sensitivity of the *psocs Δrad23* strain compared to the *pRAD7 Δrad23* strain. The most straightforward method to test this theory would be to investigate actual dNTP levels in the cell using an HPLC technique, as performed by (Chabes et al. 2003). This would also provide information regarding the balance of different dNTPs, as *CDC8*, an essential gene involved solely in dTTP synthesis, was also identified as a downregulated gene in the *psocs Δrad23* strain, which could upset the cellular dNTP balance.

dNTP levels must also be increased periodically in an RNR-dependent manner for DNA replication during S-phase of the unperturbed cell cycle. Both S-phase and DNA-damage dependent RNR activation is dependent upon the Mec1-Rad53 checkpoint pathway however it is not fully understood how the pathway differentiates between the S-phase and DNA damage response. It is possible that the Rad4-Rad23 complex is either affected by the Mec1-Rad53 checkpoint pathway, or an alternative DNA damage-specific RNR regulatory pathway such as those discussed in Section 5.1.3. The regulatory mechanism could be probed further using genetic analysis by deleting or using functionally defective mutant alleles of the checkpoint response pathway.

The role of the Rad4-Rad23 complex in DNA damage-responsive transcription has been investigated further by measuring DNA occupancy of the Rad4-Rad23 complex at the *DUN1* promoter, which upregulates the RNR pathway in response to DNA damage. Figure 5.6 shows that the Rad4-Rad23 complex binds at the *DUN1* promoter, thus suggesting it plays a regulatory role in *DUN1* transcription. This also supports the theory that the Rad4-Rad23 complex regulates a subset of DNA damage-inducible genes, and provides investigative potential to identify other Rad4-Rad23-regulated genes. Other potential Rad4-Rad23 target genes and pathways could be those suggested in Chapter 4, such as *DDR2*, *CDC8*, *ASF1* and *RTT109*. This could be investigated in the absence of DNA damage, and then at specific timepoints following UV survival in the *pRAD7 Δrad23* and *psocs Δrad23* strains. Rad4-Rad23 occupancy could be deduced using ChIP analysis and qPCR. This would reveal binding dynamics of Rad4-Rad23 following DNA damage, and would thus provide indications of genes being transcriptionally affected by post-UV Rad4 ubiquitination. In order to get a more global perpective, ChIP-chip analysis could be perfomed to identify all Rad4-Rad23 target genes, using untreated and UV-irradiated strains.

When examining the suppression of UV sensitivity, the effect of *SML1* or *CRT1* deletion in a WT strain must also be considered, to ensure a general decrease in UV sensitivity is not observed in all strains where *SML1* or *CRT1* are deleted. The Δ*sml1* data provide an internal control for this, as the *pRAD7*

Δ*rad23* strain does not exhibit significant suppression of UV sensitivity. The majority of previous reports assessing DNA damage resistance using Δ*sml1* or Δ*crt1* strains conclude that the mutations do not cause a generic increase in UV resistance, particularly with the relatively low doses of UV used in this study (Tang et al. 2009).

The data presented here suggests that the Rad7 E3 ligase functions in regulation of the DNA damage checkpoint via the RNR pathway. It remains to be speculated which level of regulation the ligase acts upon. The role of the Rad4-Rad23 complex in gene transcription has been presented in Chapter 4, so it is possible that Rad7-dependent ubiquitination of Rad4 affects Rad4-Rad23-mediated transcription, thus regulating the RNR pathway.

6 The Rad7 E3 Ligase Regulates DNA Damage and Stress Responsive Cell Cycle Progression Involving the RNR Pathway

6.1 Introduction

Precise regulation of cell cycle progression is essential for successful and accurate replication of eukaryotic organisms. Defects in cell cycle regulation can result in genomic instability, inappropriate cell division and cell death. Upon encountering environmental stresses such as DNA damaging agents, the cell cycle must respond by arresting until it is suitable to continue, to avoid replication of damaged cellular components. These arrests occur at certain cell cycle stages known as checkpoints. Checkpoints are conserved throughout evolution from prokaryotes to higher eukaryotes, and they provide a successful mechanism to maintain cellular and genomic integrity.

6.1.1 Activation of the DNA Damage Checkpoint Response

DNA damage triggers a complex response involving a kinase cascade signalling pathway, resulting in numerous effects such as cell cycle arrest and DNA repair. It is thought that the Mec1-Ddc2 complex is able to sense RPA-coated ssDNA, resulting from sites of DNA damage processed by DNA repair machinery, however the exact mechanism is not clear. This triggers a signalling cascade involving the kinases Rad53, Rad9, Chk1 and many other downstream effectors. This cascade is able to halt cell cycle progression by phosphorylation of the anaphase inhibitor Pds1, which prevents cells from progressing through anaphase with damaged DNA, thus creating a G_2 cell cycle arrest (Harrison and Haber 2006).

DNA damage checkpoint-induced cell cycle arrest can also occur at the G_1/S cell cycle phase. This occurs by Rad53-dependent phosphorylation of Swi6, which inhibits *CLN1/2* transcription, thus delaying S-phase onset. The DNA

damage checkpoint is discussed in detail in Chapter 1.7, and reviewed in (Harrison and Haber 2006).

6.1.2 Cell Cycle-Dependent Regulation of dNTP Levels

The Mec1-Rad53 DNA damage checkpoint pathway also activates the Dun1 kinase, which triggers activation of the RNR pathway, thus upregulating cellular dNTP production. This pathway is also required to upregulate dNTP production during DNA replication in S-phase. Deletion of members of the Mec1-Rad53 pathway render cells inviable, however deletion of the RNR inhibitor Sml1 can suppress the lethal phenotype, thus restoring cell viability. This observation illustrates the essential nature of elevation of dNTP levels during S-phase (Discussed in Chapter 5.1.1 and (Zhao and Rothstein 2002).

6.1.3 The Ubiquitin Proteasome System and Cell Cycle Control

Cell cycle progression relies upon the progressive activation and deactivation or removal of regulatory complexes. Proteolysis, largely facilitated by the ubiquitin proteasome system (UPS) is required at specific stages to promote correct cell cycle progression. The UPS is also responsible for degradation of negative regulators of cell cycle progression, therefore it must be tightly regulated to balance promotion and inhibition of cell cycle progression (Glotzer et al. 1991; Nakayama and Nakayama 2006).

6.1.4 The Current Study

It was proposed in the previous chapters that the Rad7 E3 ligase-dependent ubiquitination of Rad4 had a regulatory role in maintenance of cellular dNTP levels. dNTP levels are tightly regulated in synchrony with the cell cycle to facilitate efficient DNA replication and repair. Altered regulation has been shown to cause defective cell cycle progression, as displayed by the *dun1* mutant strain, which exhibited an extended S-phase, a phenotype that could be suppressed by deletion of *SML1* (Zhao and Rothstein 2002). This observation prompted the possibility that the Rad7 E3 ligase-defective *psocs*

strains could exhibit altered cell cycle progression. The aim of this chapter was to investigate cell cycle progression in the *psocs* strains in response to DNA damage and characterise the observed defects.

6.2 Materials and Methods

6.2.1 Cell Cycle Synchronisation by Centrifugal Elutriation

The process of centrifugal elutriation allows separation of particles according to their sedimentation rate, which in the case of most cells is directly related to their size. Size-mediated separation is useful in cell cycle studies as the smallest cells in an asynchronously growing *S. cerevisiae* culture are G_1 cells. Isolation of these cells from the rest of the population provides an effective method of cell cycle synchronisation without resorting to more disruptive methods such as α-factor pheromone treatment.

The main principle of elutriation uses two opposing forces to create a gradient of particles with varying sedimentation rates. Cells are pumped into a chamber within a centrifuge rotor at a constant flow rate. The increasing width of the chamber causes a decrease in the fluid velocity of the cells as they enter, while the centrifugal force acts against the pump and promotes the decrease in velocity. Each cell migrates to a position in the chamber relating to its sedimentation rate. When constructing the gradient, the pump flow rate and centrifuge speed are adjusted so the smallest required cells are retained just before the widest part of the chamber (known as the elutriation boundary). When cells cross this boundary, which is achieved by increasing the pump flow rate or decreasing the centrifugal speed, they leave the chamber and proceed to a collecting vessel. Using controlled incremental increases in pump flow rate, cell fractions of increasing size can be collected.

6.2.2 Elutriation

Elutriation was conducted using the Beckman JE-5.0 Elutriation System (Beckman 1989). 1L of each required culture was grown to late log-phase in

appropriate media. Cells were harvested by centrifugation at 4 000 rpm for 10 minutes, and resuspended in 50ml of the same media. The rest of the media was retained for use in the elutriator, and will be referred to as "clarified media." Reusing this media minimises cell stress during the procedure.

The elutriation apparatus was assembled as shown in (Beckman 1989) using a Masterflex pump (model 900-292) with a Beckman J6-MC centrifuge, with a JE-5.0 rotor. The centrifuge temperature was set at RT (23°C), and the system was filled with the clarified media using the pump at a setting of 1.30 (~25ml/min flow rate) until all air had been expelled from the tubes and chamber. The tubes were arranged to recycle the clarified media by placing the exit tube in the same bottle as the entry tube. The centrifuge was turned on at 3 000 rpm, and once the top speed was reached the viewing window was adjusted to allow visualisation of the chamber via the synchronised firing of the strobe light. The cells were introduced by briefly turning the pump off to change from media to cells to prevent introduction of air bubbles. Once almost all the cells had entered the system, the tubes were switched back to recycling the clarified media (still at pump setting 1.30). The sedimentation gradient was allowed to form in the chamber for 5 minutes, with frequent visual checks (Figure 6.1B).

The pump was then increased incrementally by no more than 0.10 units/min until the gradient moved to the elutriation boundary and the smallest cells began to exit the chamber (Figure 6.1C). At this point the exit tube was placed into a clean flask and a 100ml fraction was taken. Cell count and budding index was conducted and the pump was adjusted accordingly. At this stage the pump speed was increased very gradually, as an excessive increase would cause significant amounts of budded cells to exit the chamber. In this case, the procedure must be abandoned, the cells flushed out of the system and re-harvested, however this could stress the cells and may affect the result. G_1 cells are unbudded, so the budding index (% budded cells in a population) should ideally be as low as possible. The cell count is not as crucial, but a count of more than 10^6 cells/ml is preferential. 5 fractions were

collected and counted, and suitable fractions were centrifuged at 4 000 rpm for 5 minutes to make a resuspension of 10^7 cells/ml in 50ml minimal media.
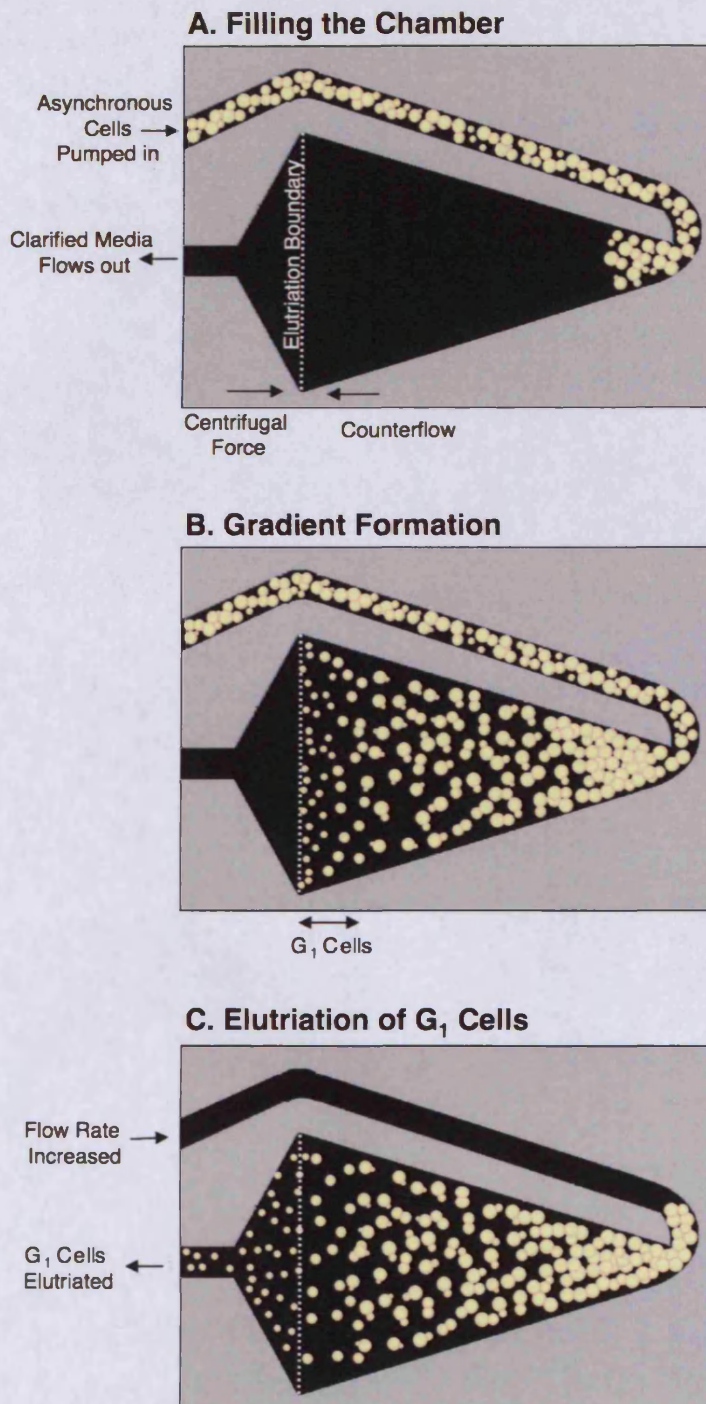
Figure 6.1 - Principles of Elutriation. A: Cells were pumped into the elutriation chamber, which arrange themselves in a gradient with the smallest cells at the elutriation boundary and largest cells at the chamber entrance (**B**). **C**: Increasing the flow rate causes smallest (G_1) cells to exit the chamber for collection. Figure adapted from (Beckman 1989).

6.2.3 UV Irradiation, G_1 Release and Cell Fixation

The elutriated culture was irradiated with $100Jm^{-2}$ or 20 Jm^{-2} UV (254nm bulb, delivered at 10 $Jm^{-2}s^{-1}$) in 25ml portions of minimal media, then centrifuged at 4 000 rpm for 3 minutes and resuspended in 50ml YPD. The cultures were then incubated at 30°C to allow recovery and G_1 release. To observe G_1 release without UV cells were immediately incubated at 30°C for observation of cell cycle progression.

In order to monitor cell cycle progression across a time-course, 1ml portions of cell culture were removed at suitable times and centrifuged at 10 000 rpm for 2 minutes. $700\mu l$ of supernatant was removed, and the pellet was resuspended in the remaining media. $700\mu l$ of 100% ethanol was added while vortexing to fix the cells, and cells were stored at 4°C until required.

Timepoints were chosen at appropriate times to observe the G_1-S-G_2 transition most effectively, which occurred at 20 minute intervals in untreated samples for up to 3-4 hours, and 30-60 minute intervals in UV-treated samples for up to 12 hours in some strains. Timepoints were continued until the budding index value settled on a constant value, usually ~70%.

6.2.4 Plasmid Stability Assay

Cells were prepared for G_1 synchronisation by growth in 1L HIS⁻ media, then elutriated and allowed to continue growth in 50ml YPD. When timepoints were taken to fix cells for cell cycle analysis, 200 cells were also suspended in water and spread onto HIS⁻ and YPD plates in triplicate. Plasmid stability was represented as % cells able to grow on HIS⁻ media, using the number of cells growing on YPD as 100%, as only cells containing the *pRS313* plasmid could grow on HIS⁻ media. This was conducted 0h and 4h.

6.2.5 Budding Index Measurement

At each timepoint the cell culture was analysed to measure the proportion of budded cells in the culture and thus monitor cell cycle progression. $10\mu l$ of cell

culture was vortexed vigorously to help separate cells, and placed on a haemacytometer. Cells were counted, and the percentage of budded cells was calculated. At least 200 cells were counted at each time point to obtain sufficiently accurate percentage values. Budded cells were defined as cells that exhibited a defined bud of any size, but not just an undefined protrusion from the cell, known as a schmoo, which would represent an unbudded early S-phase cell.

6.2.6 Cell Staining and Flow Cytometry

The cell cycle stage of individual cells in a population was identified using flow cytometry. All genomic DNA is replicated once per cell cycle so by quantifying cellular DNA using fluorescent staining a 1N state (G_1 phase), a 2N state (G_2 phase), or somewhere between (S phase) can be determined.

Fixed cells were centrifuged at 10 000 rpm for 2 minutes, and resuspended in 200μl Sodium Citrate Buffer (50mM, pH 7.0) then sonicated on low power for 40 seconds to reduce clumping (Diagenode Bioruptor). 800μl buffer was added and cell count and budding index was performed. Cells were then diluted to 1.5 x 10^6 in 1ml buffer, and treated with 0.25mg/ml RNase A overnight at 37°C. Cells were centrifuged at 10 000 rpm for 2 minutes, washed once in 1ml buffer, then resuspended in 200μl buffer and re-sonicated on low power for 40 seconds. Cells were stained by adding 8μg/ml Propidium Iodide (Invitrogen), and incubating for 30 mins at RT prior to flow cytometric analysis.

20 000 cells for each timepoint were analysed for DNA content using the BD FACScalibur (Becton-Dickinson Immunocytometry Systems, San Jose, CA, USA) flow cytometer. Parameters were collected using CellQuest software (Becton-Dickinson Immunocytometry Systems, San Jose, CA, USA). Data analyses were also performed using CellQuest software, and data were gated using forward and 90° light scatter were analysed to exclude cell debris.

6.3 Results

The results obtained in previous chapters have revealed a possible role of the Rad7 E3 ligase in the DNA damage response via regulation of the RNR pathway. Alterations in dNTP levels can affect cell cycle progression, so this chapter will focus on regulation of cell cycle progression in the mutant strains constructed in Chapter 4 to identify a possible regulatory role of the Rad7-containing E3 ligase in cell cycle control. Cell cycle progression was monitored initially by growth analysis, then more specifically by G_1 synchronisation and flow cytometry. The microarray data from Chapter 4 was then examined to attempt to identify genes whose altered transcription could cause the observed altered cell cycle progression in the untreated *psocs* strain. The Δ*sml1* and Δ*crt1* strains from Chapter 5 were then analysed for cell cycle progression.

6.3.1 Growth Defect of *psocs* Mutant

In order to analyse cell cycle progression in the *psocs* and *psocs* Δ*rad23* strain initially, a standard growth curve was conducted. Growth of *pRAD7* and *psocs* strains in HIS⁻ media was monitored over 14 hours, using a visible light spectrophotometer to detect cell concentration by optical density (OD_{600}). OD_{600} was plotted against time to display growth rate (Figure 6.2). It was discovered that the *psocs* strain exhibited a slower growth phenotype, as displayed in Figure 6.2. This suggested that the Rad7's E3 ligase function affects cell cycle progression. Without this E3 ubiquitin ligase function (*psocs* strain), the cell cycle appears to have a longer overall duration. However, further analysis of the growth curve shows that the *psocs* strain actually has the same population doubling time during logarithmic growth as the *pRAD7* strain of approximately 104 minutes. The average cell doubling time was calculated during initial growth (0-8 hours) and during logarithmic growth (9-12 hours) as a representation of the time taken for cells to complete 1 complete cell cycle, assuming that cell concentration correlates to OD_{600} in a linear fashion between 0.1 and 1 (Table 6.1). It was found that the cause of the apparent slow growth phenotype occurred during the initial growth phase

between 0-8 hours. During this period, the *psocs* strain had an 8.2% shorter doubling time than the *pRAD7* strain. This suggests that the E3 ligase function of Rad7 has a role in cell cycle progression in initial growth phase, so further growth observation and analysis of cell cycle progression was performed.
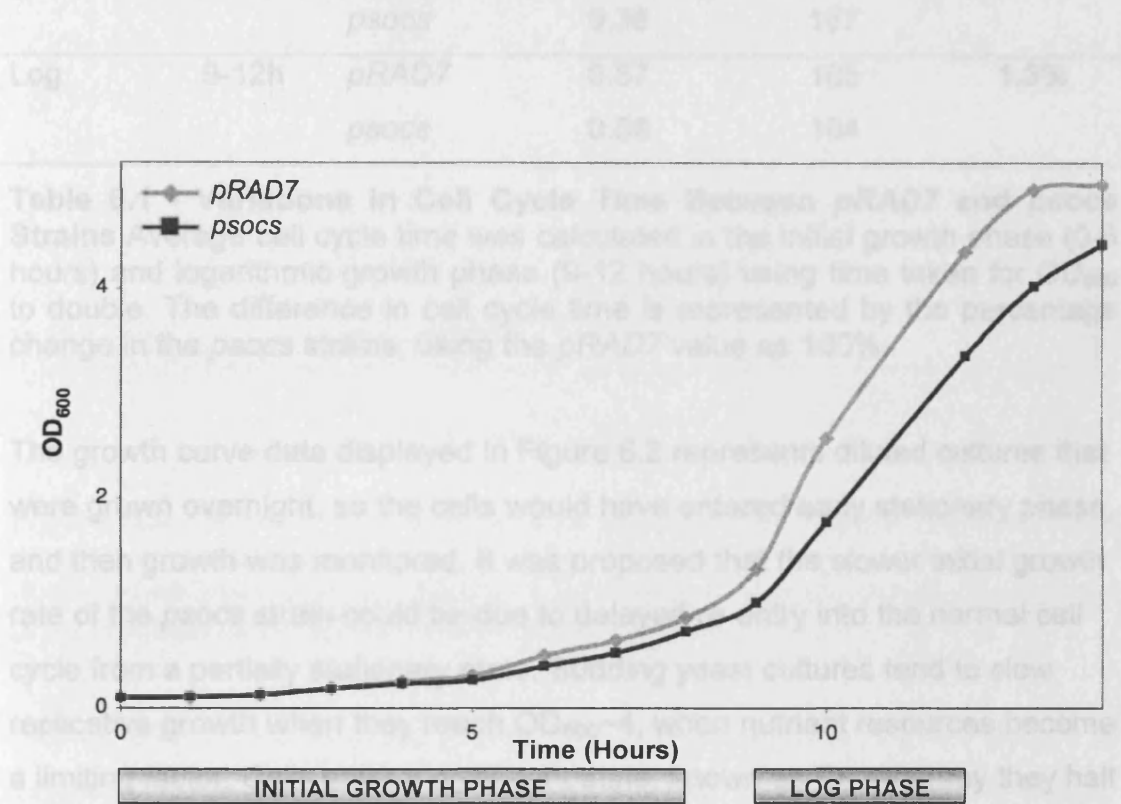
Figure 6.2 - Growth Curve of *pRAD7* and *psocs* Strains Early stationary phase cultures were diluted to OD_{600}=0.1 and grown in HIS⁻ media, with hourly measurement of cell density. It can be seen that the *psocs* strain has a growth defect compared to the *pRAD7* strain.

Growth Phase	Time	Strain	Cell Cycles per hour	Cell Cycle Time (mins)	% Difference
Initial	0-8h	*pRAD7*	0.39	154	**8.2%**
		psocs	0.36	167	
Log	9-12h	*pRAD7*	0.57	105	**1.3%**
		psocs	0.58	104	

Table 6.1 - Variations in Cell Cycle Time Between *pRAD7* and *psocs* Strains Average cell cycle time was calculated in the initial growth phase (0-8 hours) and logarithmic growth phase (9-12 hours) using time taken for OD_{600} to double. The difference in cell cycle time is represented by the percentage change in the *psocs* strains, using the *pRAD7* value as 100%.

The growth curve data displayed in Figure 6.2 represents diluted cultures that were grown overnight, so the cells would have entered early stationary phase, and then growth was monitored. It was proposed that the slower initial growth rate of the *psocs* strain could be due to delayed re-entry into the normal cell cycle from a partially stationary state. Budding yeast cultures tend to slow replicative growth when they reach $OD_{600}{\sim}4$, when nutrient resources become a limiting factor. Cells enter a quiescent state, known as G_0, whereby they halt growth until nutrient availability changes. Cells undergo several physical changes as they enter stationary phase, including shutting off biochemical pathways required for growth and replication, and as they progress to later stages of stationary phase the cell wall structure becomes altered, transcription decreases, cells become more thermotolerant and storage carbohydrates accumulate (Werner-Washburne et al. 1993; Werner-Washburne et al. 1996). To eliminate the influence of stationary phase recovery from the growth curve, strains were diluted once from early stationary phase to $OD_{600}=0.1$, then allowed to grow to $OD_{600}{\sim}0.5{-}0.8$, then rediluted to $OD_{600}=0.1$ and growth monitored as before. The results of this growth curve are displayed in Figure 6.3.
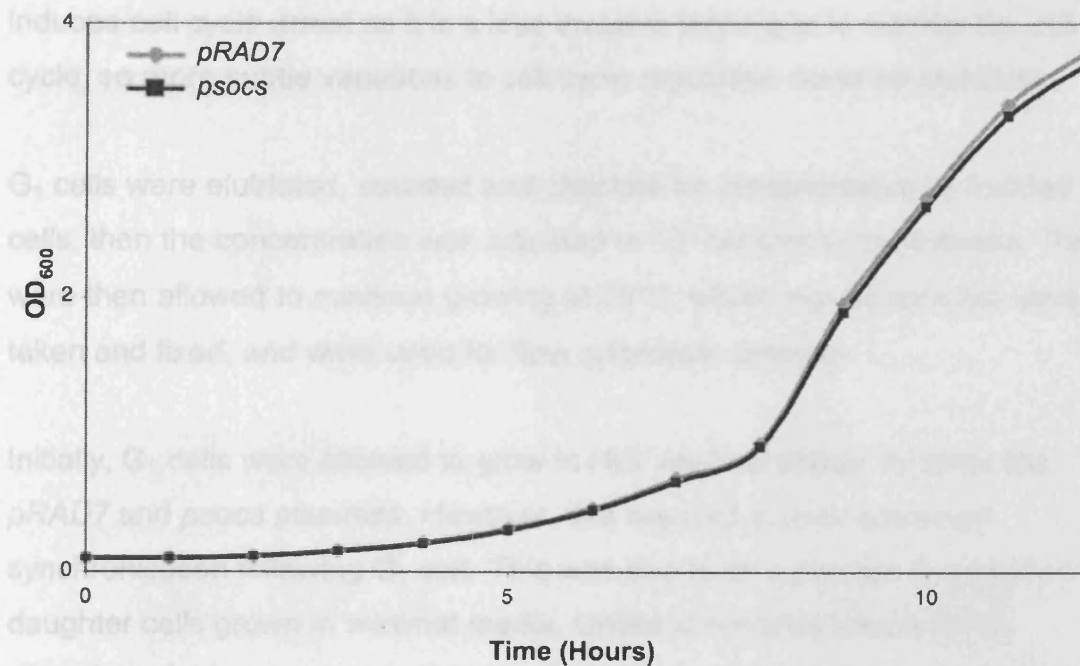
Figure 6.3 - Growth Curve of *pRAD7* and *psocs* Strains Logarithmically growing cultures were diluted to $OD_{600}=0.1$ and grown in *HIS⁻* media, with hourly measurement of cell density. It can be seen that the *psocs* strain grows at an identical rate compared to the *pRAD7* strain.

The identical *pRAD7* and *psocs* strains' growth curves observed in Figure 6.3 suggest that the *psocs* strain does exhibit delayed exit from stationary phase, but does not exhibit altered regulation of the unperturbed cell cycle during logarithmic growth phase.

Although the *psocs* strain does not appear to exhibit alterations in cell cycle time compared to the *pRAD7* (WT) strain, it may still display a phenotype similar to the *dun1* mutant strain reported by (Zhao and Rothstein 2002), which exhibited a delayed S-phase but the same overall cell cycle length. In order to characterise cell cycle progression in the *psocs* strain further, G_1 synchronisation and flow cytometry was employed.

6.3.2 Altered Cell Cycle Progression in *psocs* Strain

Logarithmically growing cells were synchronised in G_1 phase using centrifugal elutriation, which separates cells on the basis of size, a reliable marker of cell cycle stage. Cell cycle synchronisation was employed instead of pheromone-

induced cell cycle arrest as it is a less invasive technique to monitor the cell cycle, so more subtle variations in cell cycle regulation could be identified.

G_1 cells were elutriated, counted and checked for contamination by budded cells, then the concentration was adjusted to 10^7 cells/ml in fresh media. They were then allowed to continue growing at 30°C, whilst regular samples were taken and fixed, and were used for flow cytometric analysis.

Initially, G_1 cells were allowed to grow in HIS⁻ minimal media, to retain the *pRAD7* and *psocs* plasmids. However, this resulted in poor sustained synchronisation following G_1 exit. This was due to an extended G_1 phase in daughter cells grown in minimal media. Unlike in complex media (YPD) whereby cytokinesis occurs when mother and daughter cells are similarly sized, and successive cell cycles can occur in approximate synchrony, in minimal media cell division occurs when daughter cells are significantly smaller than mother cells in order for the mother cell to conserve energy (Carter and Jagadish 1978) (Figure 6.4). This results in highly asymmetric division, caused mainly by an extended G_1 phase in daughter cells, as they must reach critical size before budding can occur, whereas the mother can begin budding again almost immediately after division. This produces mother-daughter asynchrony, thus creating confusion in cell cycle experiments involving a synchronised cell population. This is visualised in Figure 6.4 and Figure 6.5 as an increased G_1 population.
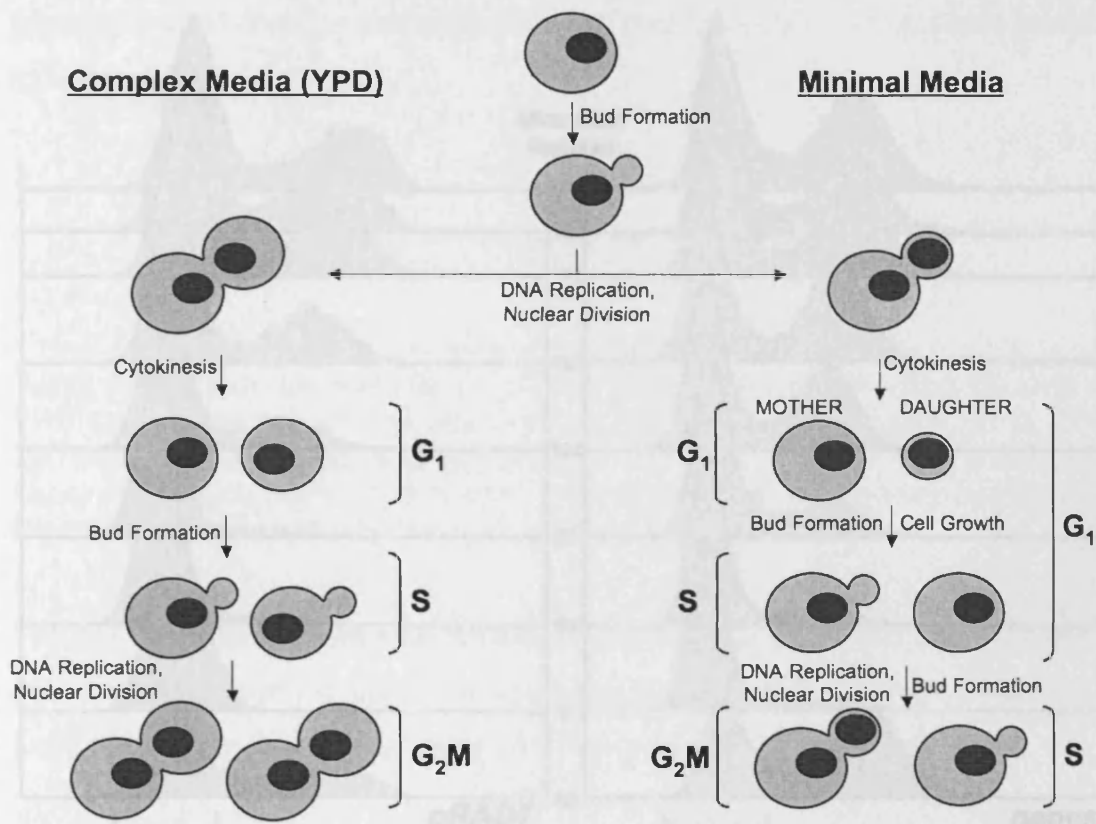
Figure 6.4 - Growth in Complex Media vs Minimal Media Cell division in minimal media occurs more asymmetrically than in complex media, due to the elongated G_1 phase in daughter cells grown in minimal media.

164

Mins After
Release

180
160
140
120
100
80
60
0
AS

pRAD7   psocs

Disproportionately High G₁ Population

Figure 6.5 - Cells Grown, Elutriated, then Continued to Grow in Minimal Media Exhibiting a Disproportionately High G₁ Population Following G₁ exit, cells should remain synchronised for the next cell cycle, however in minimal media daughter cells remain in G₁ significantly longer than mother cells, thus resulting in a higher overall G₁ population.

An alternative strategy was devised which produced more interpretable results. Cells were grown and elutriated in minimal media, then, following adjustment of cell concentration, resuspension and cell growth was performed in complex medium (YPD). Initial growth in minimal media allows more efficient elutriation of small, unbudded G₁ cells as they are more common, which is advantageous for isolation of G₁ cells. To assess plasmid loss during growth in complex media, a plasmid stability assay was employed. This showed that there was not significant plasmid loss after 4 hours, to represent the time course being monitored because the 0h and 4h timepoints only show ~20% variation in HIS⁺ colonies (Table 6.2). The plasmid stability was concluded to be acceptable after 4h growth, so the method was adopted of

growing and elutriating cells in HIS⁻ media, then allowing synchronised growth to occur in YPD.

	0h	4h
pRAD7	86.3%	59.3%
psocs	80.9%	67.4%

Table 6.2 - Plasmid Stability of *pRS313-RAD7/socs* Following Growth in YPD Cells were grown and elutriated in HIS⁻ media, then switched to YPD. 200 cells were removed and spread onto triplicate HIS⁻ and YPD plates at 0 hours and after 4 hours, and % HIS⁺ cells were deduced, and are displayed in the table. Plasmid Stability data is displayed in Appendix VI.

The elutriation procedure was repeated with cells grown in HIS⁻ media, then counted and allowed to grow synchronously in YPD. Cell samples were then fixed and cell cycle stage analysed by flow cytometry (Figure 6.6).

The flow cytometry data shows phenotypic variation between the *pRAD7* and *psocs* strain. The *psocs* strain exits G_1 synchrony approximately 20 minutes earlier than the WT (*pRAD7*) strain. This observation is rather unexpected, as the growth curve data shows a slower growth phenotype in the *psocs* strain, in the initial growth period, however this may suggest delayed progression of a later cell cycle phase. Both strains exhibit an elongated G_1 phase following synchronisation, which differs from many similar flow cytometric experiments in the literature, which exhibit complete passage to G_2 within 60 minutes of growth. This is most probably due to growing the pre-elutriated culture in minimal media. G_1 cells in minimal media range from small daughter cells which have just undergone cytokinesis to much larger mother and daughter cells which have undergone cell growth, reached critical mass and are soon to begin budding (Carter and Jagadish 1978). The process of elutriation will first isolate the smallest daughter cells, then proceeding fractions will contain the larger G_1 cells, however the vast majority would be smaller cells. The extended G_1 phase is most likely due to cell growth of the more immature daughter cells. It should also be noted that growth in YPD reduced the initial G_1 phase compared to minimal media in Figure 6.5.
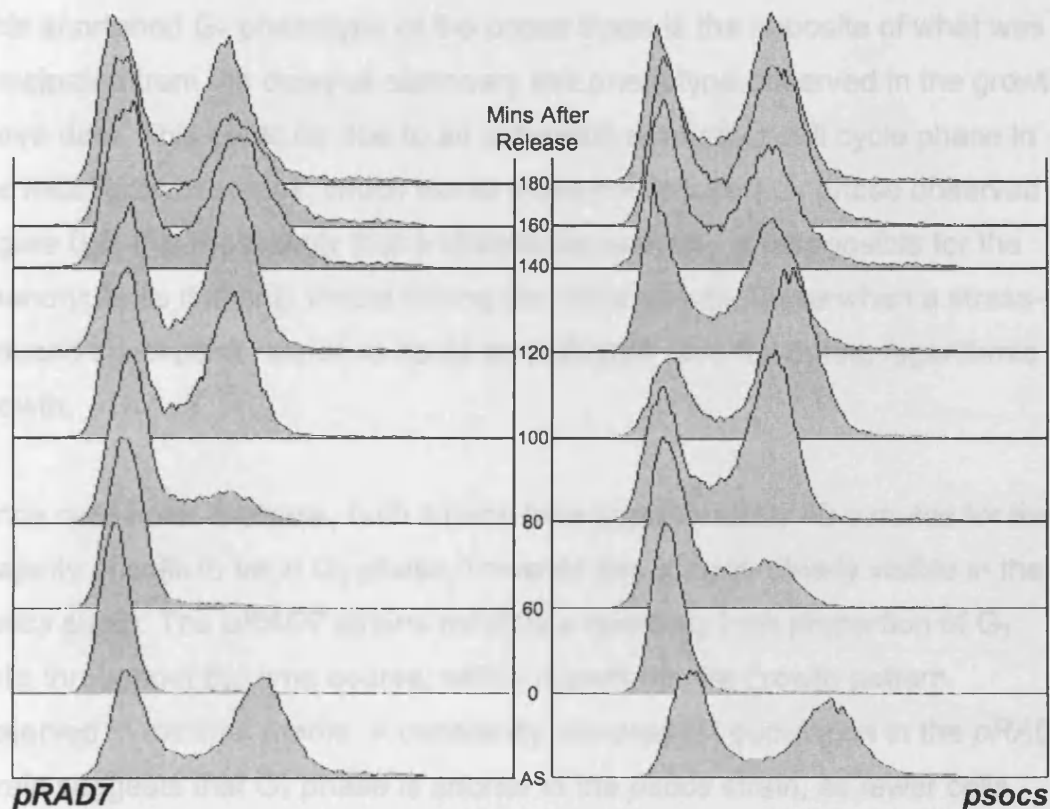
Figure 6.6 - G₁ Exit and Cell Cycle Progression of *pRAD7* and *psocs* Strains *pRAD7* and *psocs* strains were G_1-synchronised by elutriation, then allowed to continue growth in YPD. Cell samples were taken at the stated timepoints and analysed by flow cytometry. Budding index data for this progression is displayed in Appendix III (A3.1).

To account for the extended G_1 phase observed here it is possible that the *psocs* strain can increase cell mass faster than the *pRAD7*, thus reaching critical mass sooner and allowing earlier S-phase entry. Another possibility is that the *psocs* strain begins S-phase at a smaller critical mass, or that cell division occurs when daughter cells are larger. These explanations would require less increase in cell mass from cytokinesis to onset of S-phase, and would therefore require a shorter G_1 growth phase. It could also be speculated that an intra-G_1 or G_1/S checkpoint response becomes activated during the elutriation process, thus instigating a cell cycle arrest cascade, which is switched off with variable efficiency in the different strains when normal growth conditions are reinstated.

This shortened G_1 phenotype of the *psocs* strain is the opposite of what was anticipated from the delayed stationary exit phenotype observed in the growth curve data. This could be due to an extension of another cell cycle phase in the initial growth stages, which would mask the reduced G_1 phase observed in Figure 6.6. It is most likely that a checkpoint pathway is responsible for the phenotype, as it is only visible during the initial growth phase when a stress-induced checkpoint response could be activated, and not during logarithmic growth.

Once cells enter S-phase, both strains take approximately 40 minutes for the majority of cells to be in G_2 phase, however this is more clearly visible in the *psocs* strain. The *pRAD7* strains exhibits a relatively high proportion of G_1 cells throughout the time course, which resembles the growth pattern observed in minimal media. A constantly elevated G_1 population in the *pRAD7* strain suggests that G_1 phase is shorter in the *psocs* strain, as fewer cells remain in G_1, and cell synchrony is maintained for a full cell cycle.

The premature G_1 exit of the *psocs* strain is a subtle phenotypic difference compared to G_1 exit in the *pRAD7* strain. Previous work has identified that the Rad7 E3 ligase functions in one of two separate components of the NER pathway. It was found that deletion of *RAD23* in a *psocs* strain results in increased UV sensitivity, compared to the *pRAD7* Δ*rad23* strain (Gillette et al. 2006). In the case of UV sensitivity, removing the Rad23-dependent component of the NER pathway exposed the phenotype caused by the *psocs* mutation. If the premature G_1 exit phenotype observed here is caused by the same defect that causes increased UV sensitivity, then it was hypthesised that deletion of *RAD23* could characterise the G_1 exit phenotype further. *pRAD7* Δ*rad23* and *psocs* Δ*rad23* cells were grown, elutriated and allowed to exit G_1 as performed previously (Figure 6.7). It has been shown previously that deletion of Rad23 does not affect G_1 exit in pheromone-arrested G_1 cells, so any visible phenotypic difference between *pRAD7* Δ*rad23* and *psocs* Δ*rad23* cells would most likely be an effect of the defective E3 ligase (Wade et al. 2009).
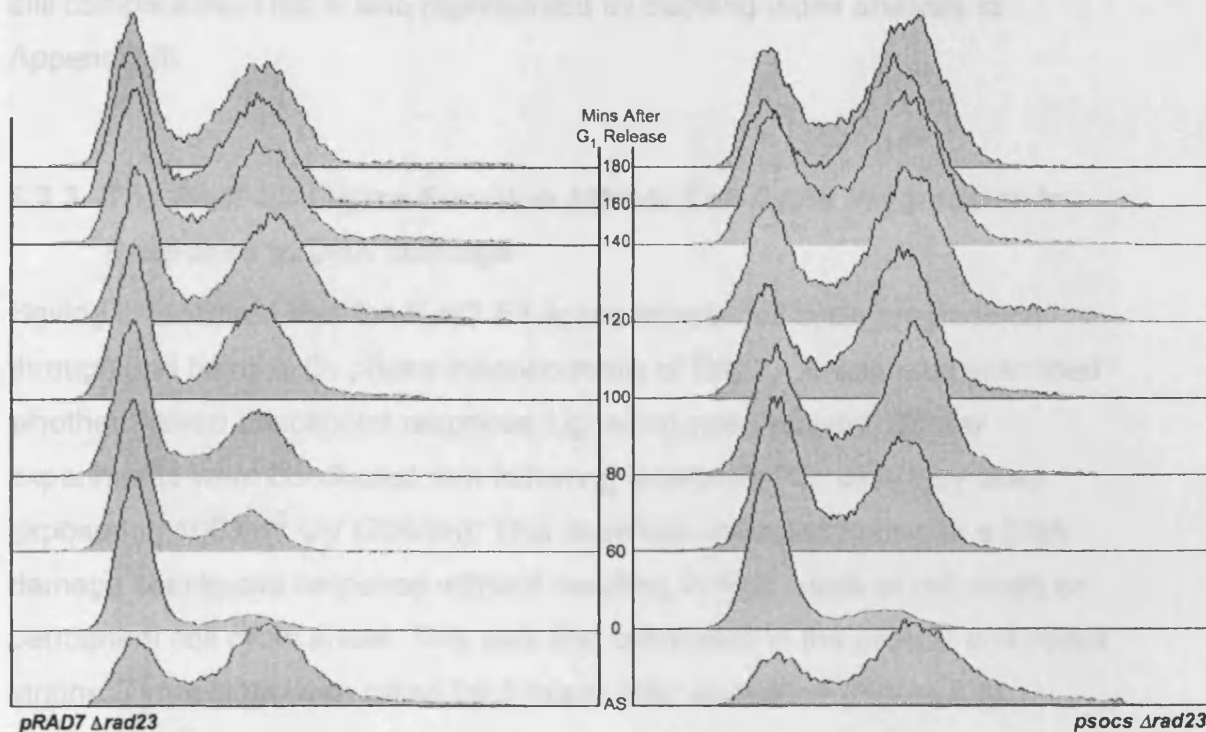
Figure 6.7 - G₁ Exit and Cell Cycle Progression of *pRAD7 Δrad23* and *psocs Δrad23* Strains *pRAD7 Δrad23* and *psocs Δrad23* strains were G₁-synchronised by elutriation, then allowed to continue growth in YPD. Cell samples were taken at the stated timepoints and analysed by flow cytometry. Budding index data is displayed in Appendix III (A3.2).

Figure 6.7 shows that in the absence of Rad23 the *psocs* strain still exits G₁ sooner than the *pRAD7* strain. There is also a reduced population of cells in G₁ in the *psocs* strain, which suggests that the strain still exhibits the shorter G₁ phenotype. This implies that the Rad7 E3 ligase function in cell cycle regulation occurs independently of Rad23, however this will be discussed later.

A further observation of the *Δrad23* elutriation was that it was far more difficult to isolate G₁ cells in *Δrad23* cells without elutriating budded cells. This would either suggest that there were fewer G₁ cells in *Δrad23* populations, or that G₁ cells were unusually large, so were therefore difficult to distinguish from budded cells. Although the elutriation was not completely effective in this case, samples were obtained with the same levels of G₂ cell contamination (visible G₂ peaks at time = 0, Figure 6.7) so it is assumed the two strains are

169

still comparable. This is also represented by budding index analysis in Appendix III.

6.3.3 The Rad7 E3 Ligase Function Affects Cell Cycle Progression in Response to DNA Damage

Having established that the Rad7 E3 ligase affects cell cycle progression through and beyond G_1 phase independently of Rad23, it was next examined whether altered checkpoint response signalling was involved. Similar experiments were conducted, but following isolation of G_1 cells they were exposed to $100Jm^{-2}$ UV (254nm). This dose was intended to invoke a DNA damage checkpoint response without resulting in high levels of cell death or permanent cell cycle arrest. This was first conducted in the *pRAD7* and *psocs* strains. Timepoints were taken for 8 hours after elutriation (Figure 6.8).
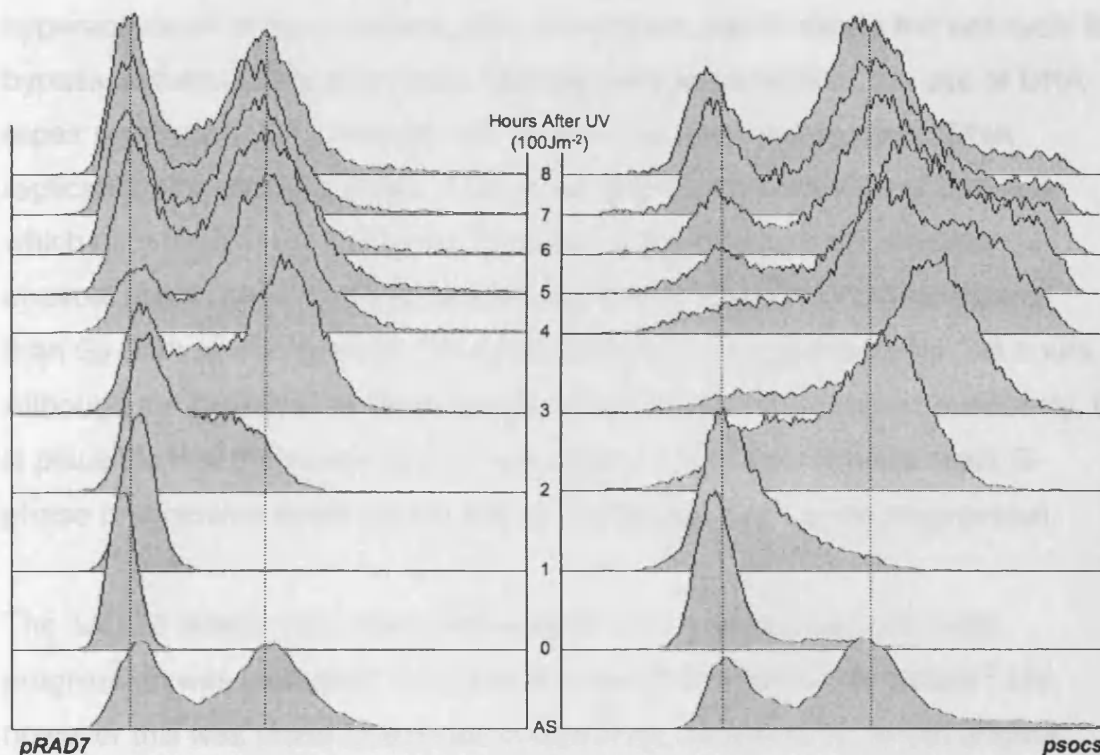
Figure 6.8 - G₁ Exit and Cell Cycle Progression Following UV Irradiation of *pRAD7* and *psocs* Strains *pRAD7* and *psocs* strains were G_1-synchronised by elutriation, irradiated in clarified media with $100Jm^{-2}$ UV, then allowed to continue growth in YPD. Cell samples were taken at the stated timepoints and analysed by flow cytometry. Budding index data is displayed in Appendix III (A3.3).

Following irradiation the G_1/S checkpoint response would be triggered to maintain genomic integrity prior to DNA replication. Figure 6.8 shows a UV-induced G_1 arrest lasting for 1-2 hours in the *pRAD7* strain, and a further 2 hours pass before the majority of cells are in G_2 phase (4 hour timepoint). The G_1 arrest period has a similar duration to the untreated sample, which arrests for 60-80 minutes. However the untreated sample reaches a G_2 majority at 2 hours, whereas the UV-irradiated sample requires an additional 2 hours in S-phase to contend with the damage.

The *psocs* strain behaves in a similar manner to the untreated sample in regard to G_1 release and initial cell cycle progression. Cells begin to enter S-phase after 1 hour, and a G_2 majority is reached at the 2 hour timepoint. It then appears that the cells arrest in G_2, and unlike *pRAD7*, the G_1 population

is almost completely diminished. The shortened S-phase could suggest hyperactivation of the postreplication checkpoint, which allows the cell cycle to bypass damage using alternative DNA polymerases, without the use of DNA repair processes. This process can cause increased mutagenenic DNA replication (Friedberg 2005a). This could lead to accumulation of damage, which may explain the extended G_2 arrest in the *psocs* strain. Another unusual observation from the *psocs* data is the presence of peaks greater than G_2 DNA levels between 3-6 hours, which is not apparent after 7-8 hours. Although the presence of these peaks has not been documented previously, it is plausible that the suspected accumulation of damage from the rapid S-phase progression could cause further disruption to cell cycle progression.

The *Δrad23* strains were also subjected to UV radiation, and cell cycle progression was analysed. The strains were also treated with $100Jm^{-2}$ UV, however this was found to activate a seemingly indefinite G_1 arrest (Figure 6.9).
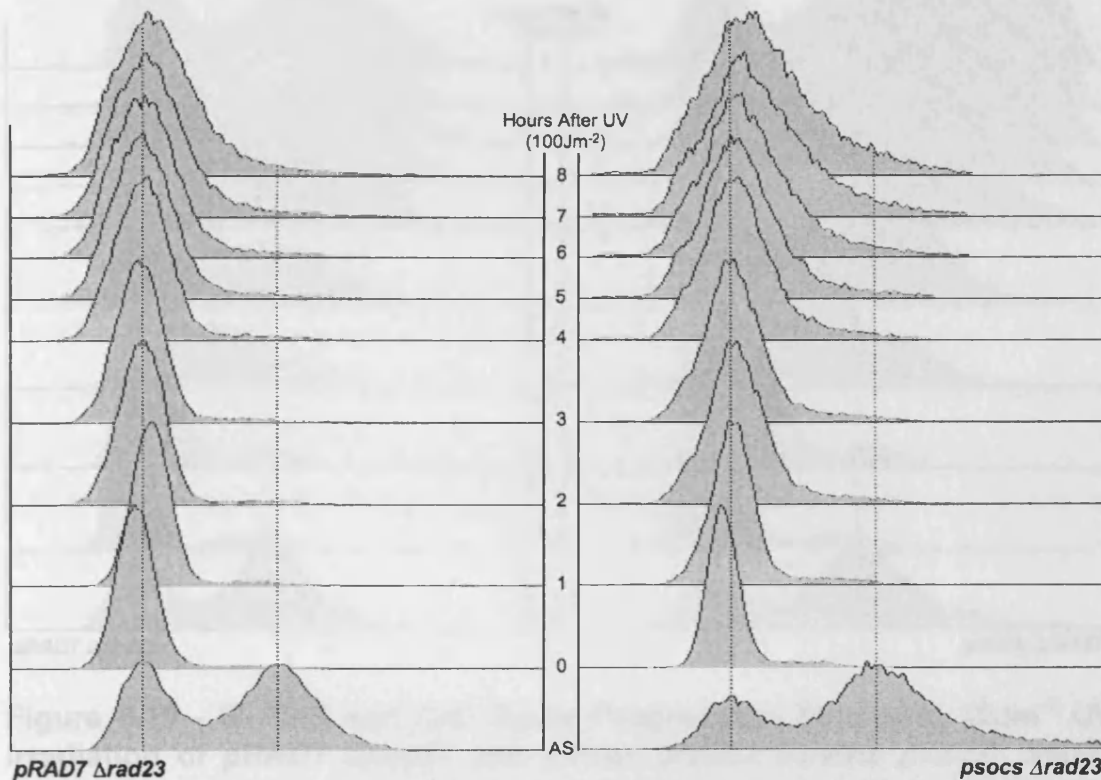
Figure 6.9 - G₁ Exit and Cell Cycle Progression Following 100Jm⁻² UV Irradiation of *pRAD7* Δ*rad23* and *psocs* Δ*rad23* Strains *pRAD7* Δ*rad23* and *psocs* Δ*rad23* strains were G₁-synchronised by elutriation, irradiated in clarified media with 100Jm⁻² UV, then allowed to continue growth in YPD. Cell samples were taken at the stated timepoints and analysed by flow cytometry.

This experiment was repeated using a lower dose of UV to provide a situation whereby a temporary arrest was invoked, and G₁ exit could be analysed. This was achieved using a dose of 20Jm⁻² (Figure 6.10), which appeared to induce the postreplicative checkpoint rather than a G₁/S arrest from which the Δ*rad23* strains cannot recover.
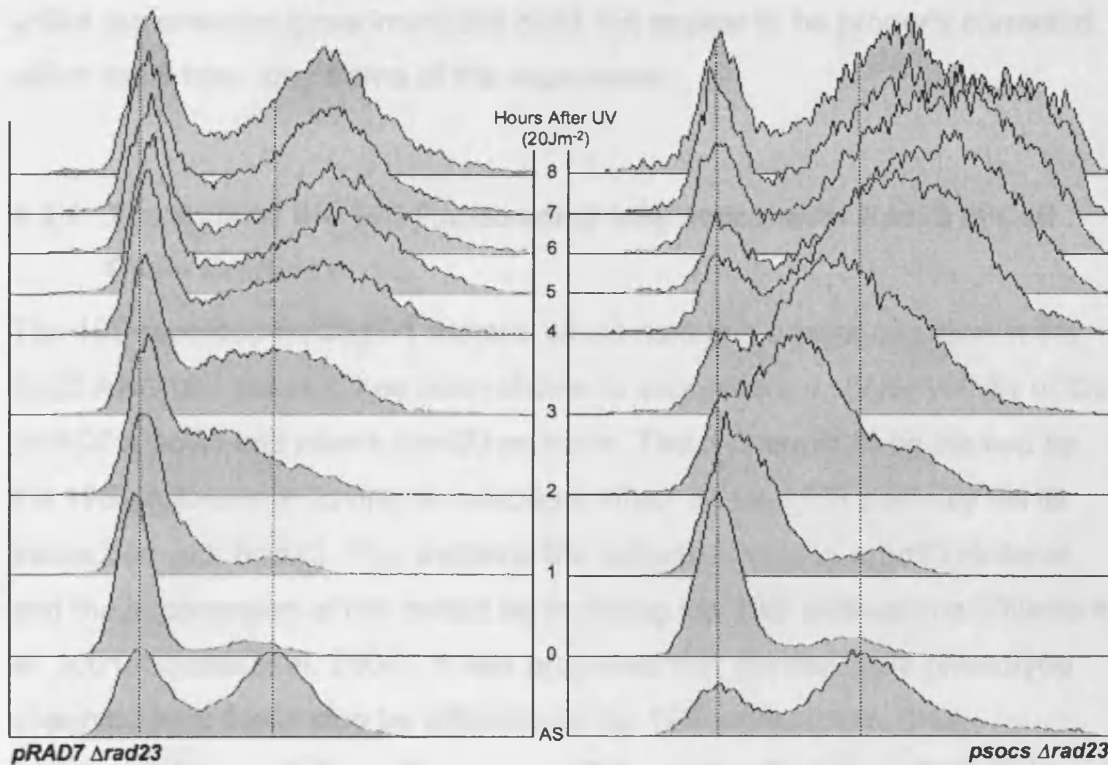
Figure 6.10 - G$_1$ Exit and Cell Cycle Progression Following 20Jm^{-2} UV Irradiation of *pRAD7 Δrad23* and *psocs Δrad23* Strains *pRAD7 Δrad23* and *psocs Δrad23* strains were G$_1$-synchronised by elutriation, irradiated in clarified media with 20Jm^{-2} UV, then allowed to continue growth in YPD. Cell samples were taken at the stated timepoints and analysed by flow cytometry. Budding index data is in Appendix III (A3.4).

This lower dose of UV induces a response similar to Figure 6.8, whereby G$_1$ arrest is shorter, and therefore S-phase entry is sooner in the *psocs* strain, however it appears that a degree of indefinite G$_1$ arrest is occurring in the *pRAD7* strain. This suggests Δ*rad23* cells can reach a damage threshold before indefinitely arresting in G$_1$, so some cells in the population can progress through S-phase and some remain arrested in G$_1$. This either does not occur, or occurs to a much lesser extent in the *psocs* strain, thus supporting a role for the Rad7 E3 ligase in G$_1$ progression or exit. This suggests a defective G$_1$/S checkpoint response in Δ*rad23* cells that is suppressed in *psocs* Δ*rad23* cells. The *psocs* Δ*rad23* cells appear to exhibit a postreplicative checkpoint response. It also appears that a significant proportion of cells have more DNA than G$_2$ cells in both strains. However,

unlike the previous experiment this does not appear to be properly corrected within the 8 hour time frame of the experiment.

6.3.4 The Role of the 19S Proteasome Interaction with Rad23 in Cell Cycle Control

The 19S proteasome *sug2-1* mutant, which contains a point mutation in the Sug2 AAA 19S subunit, has been shown to suppress the UV-sensitivity of the *pRAD7 Δrad23* and *psocs Δrad23* mutants. This is thought to be caused by the 19S proteasome having an inhibitory effect on the NER pathway via its interaction with Rad23. This explains the defective NER in *Δrad23* mutants, and the suppression of this defect by mutating the 19S proteasome (Gillette et al. 2001; Gillette et al. 2006). It was proposed that the cell cycle phenotype observed here could also be affected by the 19S proteasome, thus introducing the *sug2-1* mutation could influence the phenotype. Cell cycle synchronisation and G_1 release were conducted with the *pRAD7 Δrad23 sug2-1* and *psocs Δrad23 sug2-1* strains using untreated cells (Figure 6.11).

Mins After
G$_1$ Release

180
160
140
120
100
80
60
0
AS

pRAD7 Δrad23 sug2-1   *psocs Δrad23 sug2-1*
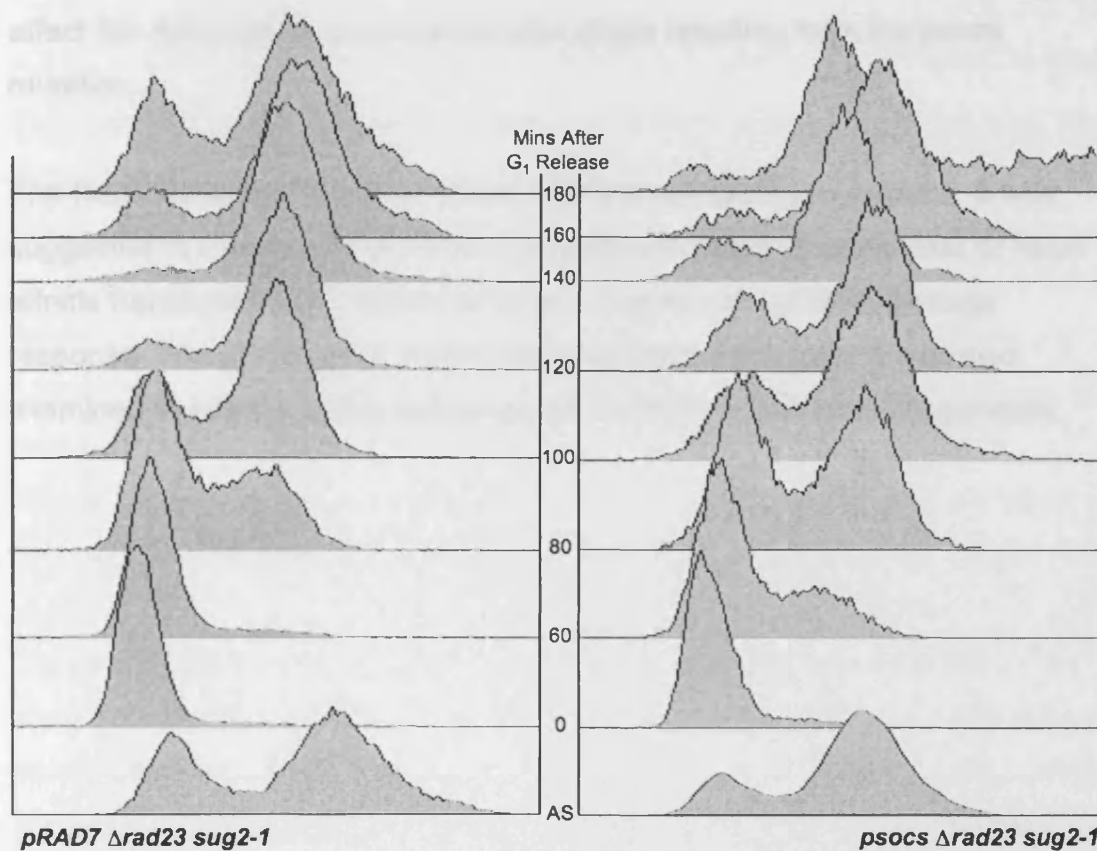
Figure 6.11 - G$_1$ Exit and Cell Cycle Progression of *pRAD7 Δrad23 sug2-1* and *psocs Δrad23 sug2-1* Strains *pRAD7 Δrad23 sug2-1* and *psocs Δrad23 sug2-1* strains were G$_1$-synchronised by elutriation, then allowed to continue growth in YPD. Cell samples were taken at the stated timepoints and analysed by flow cytometry.

The *psocs Δrad23 sug2-1* strain in Figure 6.11 shows no suppression of the *psocs*-related phenotype of faster G$_1$ release, however the *sug2-1* mutation appears to alleviate the disproportionately large G$_1$ population, a trait present in most previous samples. This could be due to more symmetrical growth caused by a shorter daughter G$_1$ phase, possibly a result of differences in strain background. The *sug2-1* strains were those used in (Gillette et al. 2006), which were not EUROSCARF-based so may show phenotypic variance not related to the *sug2-1* mutation. It does however appear that G$_2$ phase is extended, as cells delay returning to G$_1$ in the *pRAD7* strain, and do not significantly return to G$_1$ over the 3 hour timecourse in the *psocs* strain. This G$_1$ depletion is also evident in the asynchronous (AS) cell sample. This result suggests that neither Rad23 nor interaction with the 19S proteasome

176

affect the defective G_1 progression phenotype resulting from the psocs mutation.

The Rad7 E3 ligase has been found to affect cell cycle progression. It was suggested in Chapter 4 that Rad7 E3 ligase-mediated ubiquitination of Rad4 affects transcription of a subset of genes involved in the DNA damage response. The global gene expression data used in Chapter 4 was also examined to identify misregulated genes involved in cell cycle progression.

6.3.5 A Transcriptional Role of the Rad7 E3 Ligase in Cell Cycle Control

The Rad7 E3 ligase has been discovered to affect cell cycle progression. The *psocs/rad23* microarrays used in Chapter 4 were utilised to detect misregulation of genes known to be involved in cell cycle control, or known to be transcribed periodically throughout the cell cycle in order to reveal potential target of the Rad4-Rad23 complex. The *pRAD7* strain was compared to the *psocs* strain, as the defective cell cycle progression phenotype was observed between these two strains. Genes were identified using SGD GO Slim Mapper (www.yeastgenome.org) for cell cycle-related genes, and the list of 800 cell cycle-differentially expressed genes from (Spellman et al. 1998).

The observed *psocs* premature G_1 exit phenotype can be seen in the *psocs* strain compared to the *pRAD7* strain independently of Rad23. For this reason transcriptional changes between the *pRAD7* and *psocs RAD23$^+$* strains will be compared. Using significance testing (FDR corrected t-test ($p<0.05$) and a 1.5 fc cut-off), no genes could be identified as differentially expressed between the *pRAD7* and *psocs* strains. It should also be noted that genes involved in cell cycle may be more up or down regulated at a particular cell cycle stage than is visible in the data due to the use of asynchronous cells. Instead of lowering the stringency for significance testing, the top 100 differentially expressed genes were extracted, and were subjected to hierarchical clustering to find similarly expressed genes (This gene list is displayed in Appendix IV, List 6). GO analysis of these 100 genes showed that 6 out of 100 genes were involved in cell cycle progression (Figure 6.12). It was also suggested that the premature G_1 exit seen in the *psocs* strain was due to a checkpoint response to stress caused by centrifugation. GO analysis also identified 7 genes involved in stress response, which may contribute to the *psocs* G_1 phenotype.
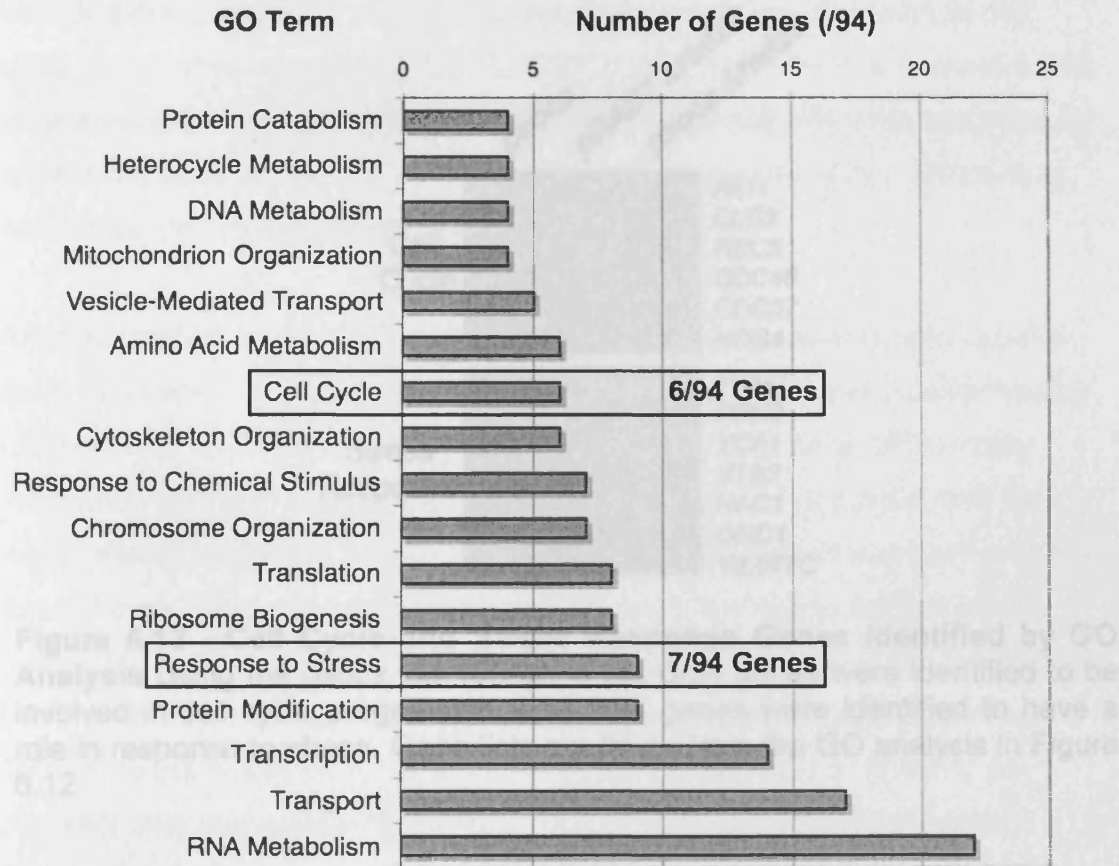
Figure 6.12 - GO Analysis of Top 100 *psocs* vs *pRAD7* Differentially Expressed Genes The top 100 *psocs* gene list was input into the GO Slim Mapper, which identified 94 known ORFs. Genes were allocated to functional pathways, and the top 17 GO terms are displayed here. Genes involved in cell cycle progression account for 6/94 genes, and genes involved in stress response account for 7/94 genes. The gene list is displayed in Appendix VI, List 6.

179
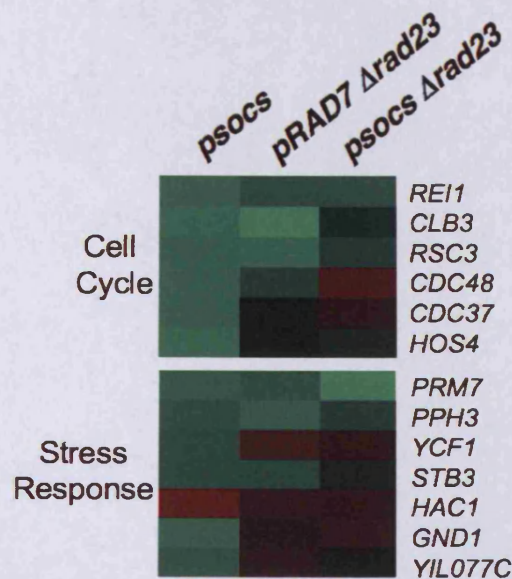
Figure 6.13 - Cell Cycle and Stress Response Genes Identified by GO Analysis Using the *psocs* top 100 gene list, 6/94 genes were identified to be involved in cell cycle progression, and 7/94 genes were identified to have a role in response to stress. Gene lists are taken from the GO analysis in Figure 6.12.

The gene lists obtained from GO analysis represent the most likely candidates from known ORFs, which could contribute to the premature G_1 exit phenotype seen in the *psocs* strain, assuming the phenotype is due to altered transcription (Figure 6.13). The *pRAD7 Δrad23* strain does not exhibit the same premature G_1 exit phenotype as the *psocs* or *psocs Δrad23* strains. For this reason, the expected expression pattern of the responsible genes would be an elevated or decreased expression level in the *psocs* and *psocs Δrad23* strains, and WT expression level in the *pRAD7 Δrad23* strain. This would indicate that the expression is only dependent on the *psocs* mutation. The only gene that fits these criteria from Figure 6.13 is *PRM7*, which is a poorly characterised pheromone-responsive membrane protein, possibly controlled by the Gcn4 transcription factor. Gcn4 is thought to bind to 1% of all gene promoters, and stimulates transcription of genes involved in amino acid and nucleotide metabolism. Other genes from the list that show suitable downregulation in the *psocs* strain, but inappropriate expression levels for the observed phenotype are *RSC3*, a chromatin remodelling factor that can cause cell cycle arrest when repressed, *CDC48*, which is involved in shuttling

ubiquitinated proteins to the proteasome for degradation and exhibits cell cycle arrest when repressed, and *CDC37*, a co-chaperone that is essential for progression through cell cycle START. All these genes affect the cell cycle by arresting it when repressed and are downregulated in the array, which does not correspond to the *psocs* G_1 phenotype.

Another method of identifying cell cycle regulated target genes is to use the gene list devised in (Spellman et al. 1998). Global studies were performed by (Spellman et al. 1998) to identify genes that were temporally differentially expressed during the cell cycle. A list of 800 genes was compiled, and they were ordered according to their chronological order of peak expression during the cell cycle. Five cell cycle phase groups were devised to categorise the genes: M/G_1, G_1, S, S/G_2 and G_2/M. For the purpose of this study, this list will be referred to as the Spellman 800 list. Although all genes in the Spellman 800 list do not necessarily have a role in cell cycle control, and many are probably only upregulated to perform cell cycle phase-specific activities. These genes may have an indirect function in cell cycle progression. The Spellman 800 list was extracted from the *psocs/rad23* untreated microarrays and is displayed in Figure 6.14.
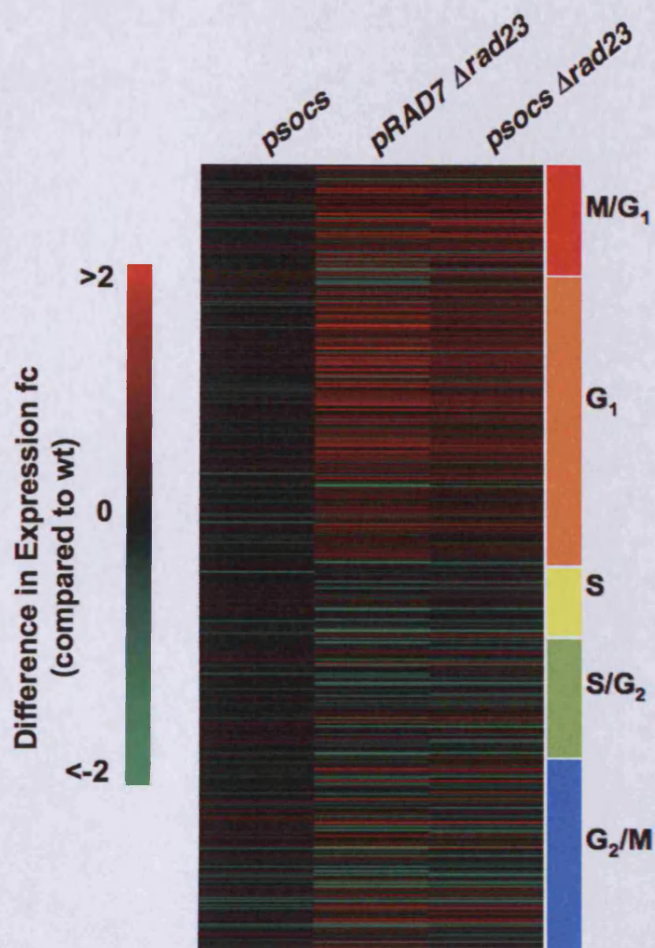
Figure 6.14 - The Spellman 800 Gene List – Genes from the Spellman 800 list (Spellman et al. 1998) were extracted from the *psocs/rad23* microarrays, and arranged into chronological order of expression.

The entire Spellman 800 gene list (Figure 6.14) shows some variation in expression, however differences may have been more evident if synchronised cells were used. Genes that were most misregulated in the *psocs* strain were identified from the Spellman 800 list (The gene list is displayed in Appendix IV, List 7), which was then edited further to reveal genes which showed a difference in *psocs* vs *pRAD7* expression, and also showed a difference in *pRAD7 Δrad23* and *psocs Δrad23* expression. This formed a list of 8 genes (Figure 6.15).
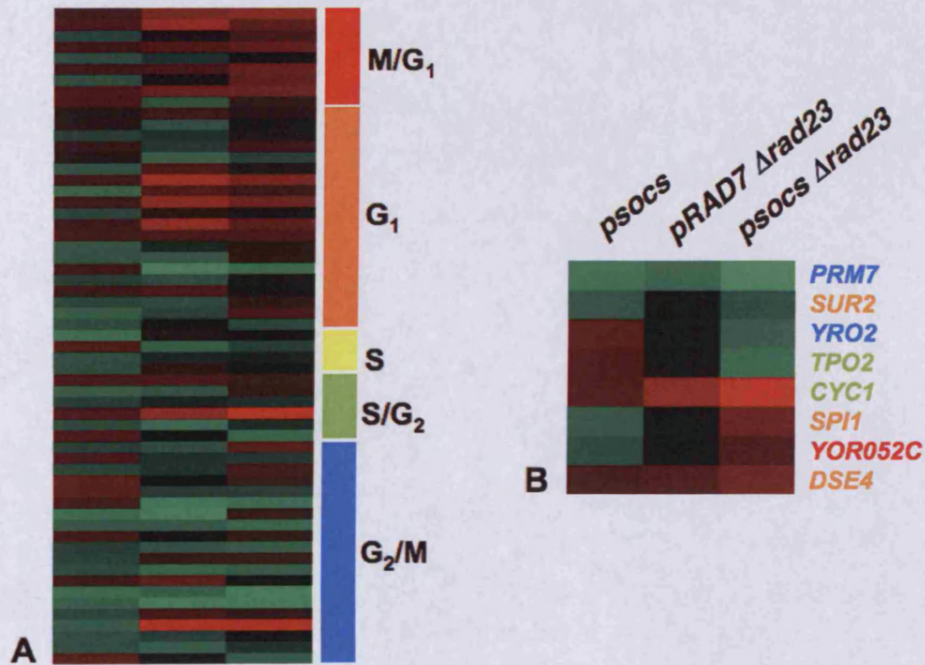
Figure 6.15 - *psocs* Differentially Expressed Genes from Spellman 800 List A. Genes extracted from Figure 6.14 that were differentially expressed in the *psocs* strain compared to the *pRAD7* strain. This gene list is displayed in Appendix IV, List 7. **B**. Genes extracted from (A) that showed an expression pattern that could explain the *psocs* G$_1$ phenotype.

The gene list in Figure 6.15B displays genes temporally transcriptionally regulated in a cell cycle dependent manner, which are misregulated in the *psocs* mutant. None of these 8 genes have been previously implicated in cell cycle control, however some genes (*SPI1* and *YOR052C*) have been found to be stress induced. *SPI1* is regulated by Msn2/4, which bind to STRE elements to induced genes in response to a variety of stresses. STRE-responsive genes were also identified as significantly misregulated in the *rad4/rad23* mutants (4.3.6), so it is possible that STRE-responsive genes are regulated by the Rad4-Rad23 complex in order to alter cell cycle progression.

6.3.6 The Role of the Rad7-Containing E3 Ligase in Cell Cycle Progression via the RNR Pathway

It has been identified previously in this study that the Rad7-containing E3 ligase has a role in regulating genes involved in dNTP synthesis, including the RNR pathway. Although analysis of microarray data did not identify any suitable targets known to be involved in cell cycle progression (Chapter 6.3.5), it is possible that misregulated dNTP levels could also be the cause of the defective cell cycle progression observed in psocs strains. If this is the case, then elevation of dNTP levels by constitutive activation or expression of the RNR pathway could affect the defective cell cycle progression observed in *psocs* strains. The Δ*sml1* and Δ*crt1* strains constructed in Chapter 5 were used for cell cycle analysis, regarding stationary phase recovery, and cell cycle progression following G_1 synchronisation.

6.3.6.1 Constitutive Activation of RNR Restores Normal Exit from Early Stationary Phase in *psocs* Strain

A growth defect of the *psocs* strain was observed previously when cells were re-introduced to logarithmic growth following early stationary phase entry. The *psocs* strain exhibited slower re-entry to logarithmic growth from early stationary phase. This phenotype was alleviated by diluting logarithmically growing strains into fresh media (Section 6.3.1). It was proposed that defective regulation of cellular dNTP levels could delay cellular recovery and re-entry into logarithmic growth. A growth curve was conducted for the *pRAD7* and *psocs* Δ*rad23* Δ*sml1* and Δ*crt1* strains to monitor recovery from early stationary phase (Figure 6.16).

184
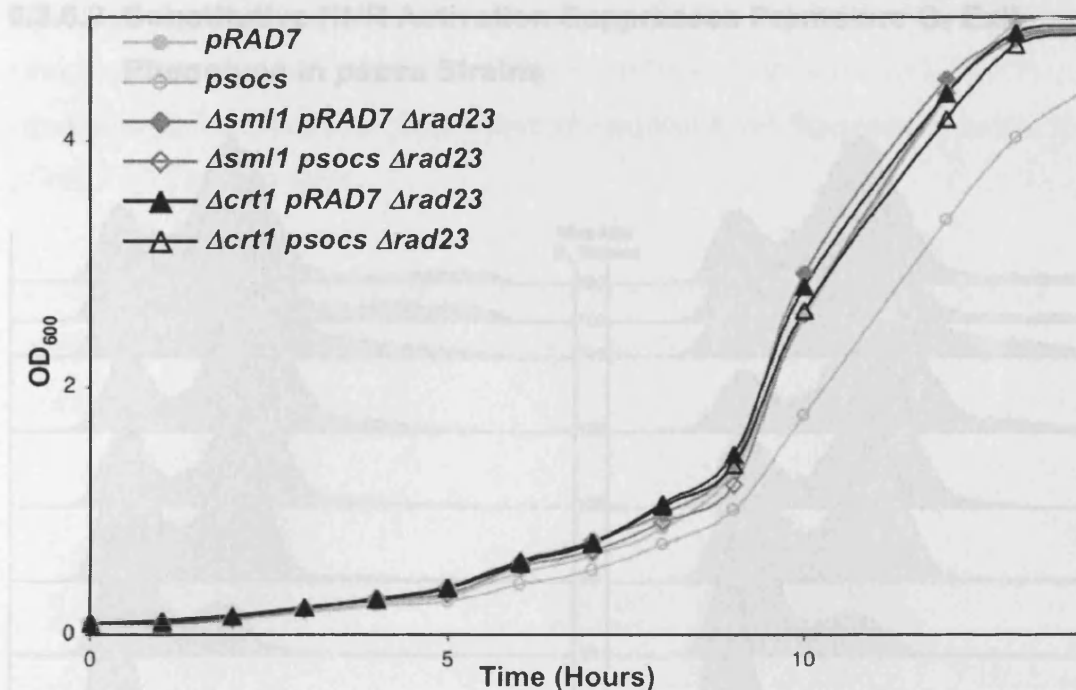
Figure 6.16 - Growth Curve of RNR-Activated Strains Early stationary phase cultures were diluted to OD_{600}=0.1 and grown in HIS⁻ media, with hourly measurement of cell density. OD_{600} values are displayed in Appendix V.

The growth curve in Figure 6.16 demonstrates suppression of the *psocs* delayed exit from early stationary phase phenotype. It appears that constitutive activation of RNR causes the *psocs* strain to exit early stationary phase at the same rate as the *pRAD7* strain. This occurs to same extent in $\Delta sml1$ and $\Delta crt1$ strains, which could provide evidence that insufficient dNTP levels are the cause of the defect in the *psocs* strains. This observation suggests that the Rad7 E3 ligase has a role in elevating dNTP levels following early stationary phase entry caused by a period of nutrient starvation.

6.3.6.2 Constitutive RNR Activation Suppresses Premature G₁ Exit Phenotype in *psocs* Strains

pRad7 *Δrad23 Δsml1*   *psocs Δrad23 Δsml1*
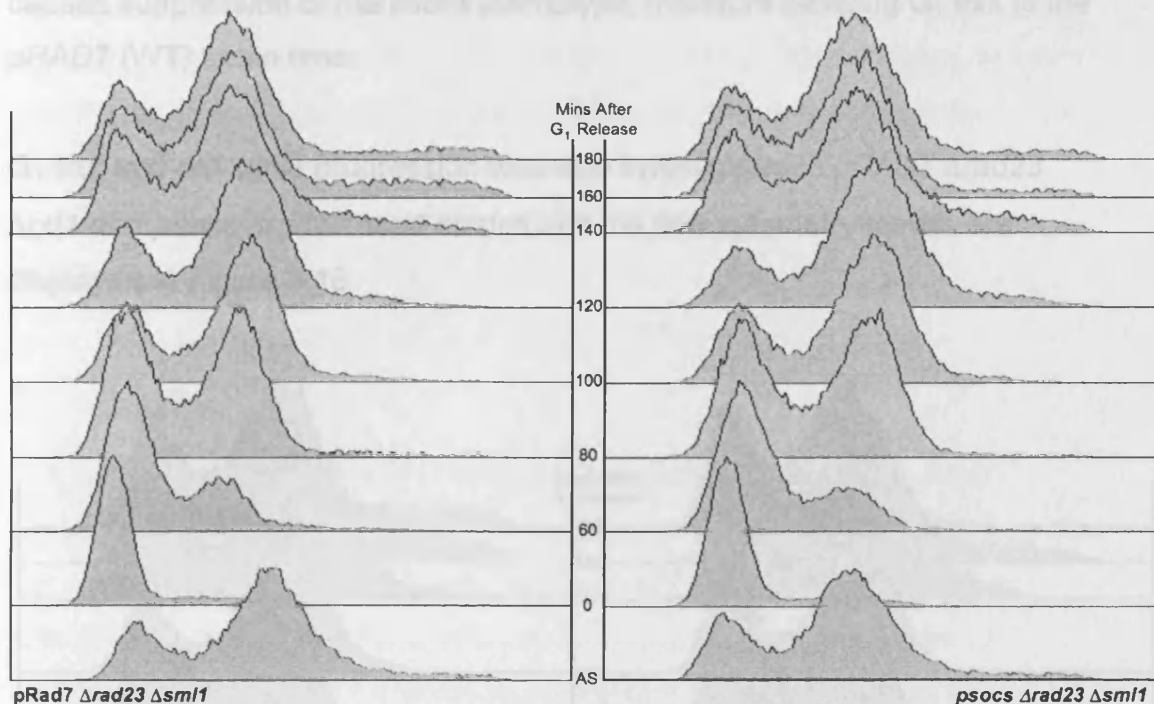
Figure 6.17 - G₁ Exit and Cell Cycle progression of *Δsml1 Δrad23 pRAD7* and *psocs* Strains Strains were G₁-synchronised by elutriation, then allowed to continue growth in YPD. Cell samples were taken at the stated timepoints and analysed by flow cytometry. Budding index data is displayed in Appendix III (A3.5).

G₁ exit and cell cycle progression appear identical in the two strains displayed in Figure 6.17. The strains both appear to exit G₁ at the 60 minute timepoint, and reach a G₂ majority at 100 minutes. A G₁ exit after 60 minutes was observed previously for the *psocs* strain, however the elutriation was more successful in the *psocs* strain, which would affect apparent cell cycle progression as there was a lower proportion of non-G₁ cells in the 0 timepoint. Evidence of this effect can be seen in the *pRAD7* and *psocs Δrad23* strains (Figure 6.7), which proved difficult to isolate purely G₁ cells from and therefore exhibited an apparent accelerated G₁ exit. Taking this into account, the *Δsml1* strains in Figure 6.17 display a cell cycle progression that reflects the *psocs* strain but could also reflect progression of the *pRAD7 Δrad23* strain if quality of elutriation is considered.

The most significant observation from Figure 6.17 is that both strains exhibit identical cell cycle progression and it is most likely that deletion of *SML1* causes suppression of the *psocs* phenotype, therefore delaying G_1 exit to the *pRAD7* (WT) strain time.

G_1 exit and cell cycle progression was also investigated in *pRAD7 Δrad23 Δcrt1* and *psocs Δrad23 Δcrt1* strains and the flow cytometry results are displayed in Figure 6.18.
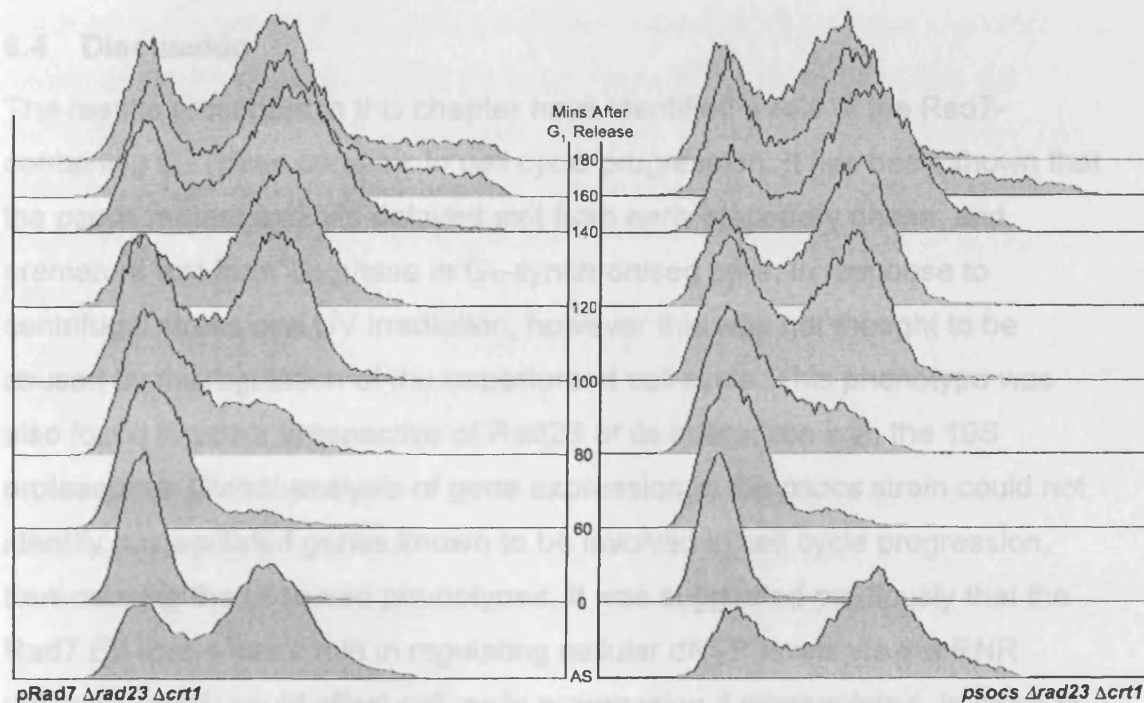
Figure 6.18 - G_1 Exit and Cell Cycle progression of *Δcrt1 Δrad23 pRAD7* and *psocs* Strains Strains were G_1-synchronised by elutriation, then allowed to continue growth in YPD. Cell samples were taken at the stated timepoints and analysed by flow cytometry. Budding index data is displayed in Appendix III (A3.6).

The *Δcrt1* strains in Figure 6.18 show the same pattern of G_1 exit and cell cycle progression as the *Δsml1* strains in Figure 6.17. This suggests that elevating dNTP levels abolishes the premature G_1 exit phenotype of the *psocs* strain as both strains exit G_1 at the same (80 minutes) timepoint, and progress to a G_2-majority at 120 minutes. This pattern of cell cycle progression suggests that the *psocs* G_1 exit phenotype is being suppressed to the *pRAD7* G_1 exit time.

It has been identified that the Rad7 E3 ligase affects cell cycle progression in two ways, by promoting exit from stationary phase and by preventing premature progression to S phase following stress- or DNA damage-induced checkpoint arrest. The complete suppression of these phenotypes by increasing cellular dNTP levels suggests that the defective cell cycle progression is due to misregulation of dNTP levels in the *psocs* mutant strains.

6.4 Discussion

The results presented in this chapter have identified a role of the Rad7-containing E3 ligase complex in cell cycle progression. It has been shown that the *psocs* mutant exhibits delayed exit from early stationary phase, and premature exit from G_1 phase in G_1-synchronised cells, in response to centrifugal stress and UV irradiation, however this was not thought to be caused by misregulation of the unperturbed cell cycle. This phenotype was also found to occur irrespective of Rad23 or its interaction with the 19S proteasome. Global analysis of gene expression in the *psocs* strain could not identify misregulated genes known to be involved in cell cycle progression, thus causing the observed phenotypes. It was suggested previously that the Rad7 E3 ligase has a role in regulating cellular dNTP levels via the RNR pathway, which could affect cell cycle progression if misregulated. In order to examine the effect of elevating dNTP levels in the *psocs* strain, the *Δcrt1* and *Δsml1* mutants were analysed with regard to cell cycle progression. Both *Δsml1* and *Δcrt1* strains were found to suppress both delayed stationary phase exit and premature G_1 exit phenotypes of the *psocs* strain. This suggests the effect on cell cycle progression of the *psocs* mutation is a result of misregulated dNTP levels.

6.4.1 The *psocs* Strain Exhibits a Delayed Stationary Phase Exit Phenotype

It has been shown that the *psocs* strain exhibits slower recovery from early stationary phase than the *pRAD7* strain (Figure 6.2). This suggests that the Rad7-containing E3 ligase functions to promote cell cycle progression following a period of nutrient starvation. It has been observed that the *psocs* strain does not exhibit an elongated overall cell cycle time during logarithmic growth. This implies that the Rad7-containing E3 ligase functions in stress responsive regulation, and not in a general cell cycle regulatory role. The work conducted in Chapter 4 suggested that the Rad4-Rad23 complex regulated transcription of a subset of DNA damage-responsive genes, and that the Rad7-dependent Rad4 ubiquitination has a role in this regulatory activity. The observed *psocs* delayed stationary phase phenotype may suggest that the ubiquitination of Rad4 may have a more general role in response to stress, and not just DNA damage.

6.4.2 The Rad7 E3 Ligase Affects G_1/S Phase Progression

It has also been shown that the Rad7-containing E3 ligase defective *psocs* mutant displays altered cell cycle regulation from a population of G_1-synchronised cells. The *psocs* cell population appears to progress out of G_1 sooner than the *pRAD7* cell population. It is most likely that this a defect in stress response, and not misregulation of the unperturbed cell cycle because the effect is only visible following the initial G_1 exit of the synchronised cells, following which the *psocs* strain appears to continue the cell cycle at the same rate as the *pRAD7* strain. The *psocs* strain does not appear to exhibit a generally shorter G_1 phase, only in the initial G_1 phase following synchrony. The process of elutriation is thought to evoke a checkpoint mediated stress response due to centrifugation and changing media. A centrifugation-induced stress response has been well documented in the fission yeast *S. pombe*, which identify activation of Spc1 following centrifugation which triggers a MAPK stress response pathway (Petersen and Hagan 2005; Shiozaki et al. 1998; Soto et al. 2007). The *S. cerevisiae* homologue of Spc1 is Hog1, which is activated in response to a variety of stresses. Defective activation of stress

189

response pathways could be responsible for the *psocs* premature exit from G_1 synchrony. These genes could also provide potential regulatory targets of the Rad4-Rad23 complex if it is involved in general stress-responsive transcription and not just DNA damage-responsive transcription.

The Rad7 E3 ligase functions in one of two separate components of the NER pathway. It was found that deletion of *RAD23* in a *psocs* strain results in increased UV sensitivity, compared to the *pRAD7 Δrad23* strain (Gillette et al. 2006). A UV-sensitive phenotype of the *psocs* strain is only apparent when *RAD23* is deleted and the UV-sensitive phenotype is suppressed by mutation of the 19S proteasome, a negative regulator of NER (Gillette et al. 2006). Deletion of *RAD23* in *pRAD7* and *psocs* strains appears to have no effect on the previously observed cell cycle phenotype. The *psocs* strain still exhibits a premature exit from G_1 phase to the same extent as observed in $RAD23^+$ strains. This is also the case in *pRAD7* and *psocs Δrad23 sug2-1* strains. This shows that neither Rad23 nor its interaction with the 19S proteasome affect the Rad7-containing E3 ligase role in cell cycle progression, which therefore may suggest that the defective E3 ligase is affecting cell cycle progression by a different mechanism to the mechanism promoting UV survival, as the *psocs* strain is not significantly UV sensitive. An alternative conclusion is that the disrupted cell cycle progression in *psocs* strains is a result of the same misregulated pathway(s) as for the UV survival, however the UV sensitivity may be cell cycle phase-specific. If G_1 cells are affected more severely by UV, then the cell cycle defect observed in *psocs* strains could affect their UV survival. This could be investigated by performing a UV survival assay on G_1 synchronised *psocs* cells and comparing it to the UV survival curve of asynchronous *psocs* cells. If G_1 cells are more sensitive to UV it could suggest that the cell cycle defect does affect UV sensitivity. This could be due to increased activation of pathways such as damage bypass or translesion synthesis (TLS) in *psocs* strains, thus avoiding repair pathways, which could lead to potentially harmful mutagenesis. However this effect could be masked in asynchronous *psocs* cell populations, thus explaining the lack of UV sensitivity of the *psocs* strain.

In order to analyse further the *psocs* G_1-exit phenotype, and its potential role in maintenance of stress-induced cell cycle arrest, cells were treated with UV to evoke a more significant stress-induced arrest, and to observe how the mutant strains respond to DNA damage. The *psocs* strain compared to the *pRAD7* strain exhibited the same phenotype as observed in untreated strains, with the *psocs* strain exhibiting a premature G_1 exit, however the *pRAD7* and *psocs* strains exhibited a greater difference in S-phase progression. Whereas the *pRAD7* strain exhibited delayed progression through S-phase then normal cell cycle progression, the *psocs* strain appeared to progress through S-phase much faster and accumulate in G_2, then a significant amount of particles with a >2N DNA content were visible. This could suggest genome instability in the *psocs* strain. It is possible that the faster progression through S-phase in the *psocs* strain is due to increased dependency and activation of the TLS pathway, which could bypass damage without activation of repair pathways. This process may be mutagenic and cause accumulation of DNA damage, which would explain the extended arrest in G_2. The pattern of cell cycle progression also suggests that G_1 *psocs* cells may be more vulnerable to DNA damage than other cell cycle phases, due to the rapid progression through S-phase. This could be determined by conducting a UV survival assay on *psocs* G_1 cells. The involvement of the TLS pathway could also be investigated in cell cycle progression and UV survival in the *psocs* strain. This could be accomplished using genetic analysis, by knocking out components of the TLS pathway, such as the alternative replicative polymerase *RAD30*, or the ubiquitin processing factors *RAD5* or *RAD18*, and identifying mutant phenotypes. Knocking out these factors may alter cell cycle progression or UV survival differently in the *psocs* strain compared to the *pRAD7* strain, which could help reveal the regulatory mechanism of TLS vs NER and the involvement of the Rad7 E3 ligase.

The *psocs* strain is known to exhibit UV sensitivity when *RAD23* is deleted, however it has been shown that Rad23 does not affect the *psocs* G_1-exit phenotype in untreated cells, so cell cycle progression in the *psocs* strain with *RAD23* deleted following UV irradiation was observed. $\Delta rad23$ cells proved

more difficult to test for post-UV cell cycle phenotype as they exhibit a reduced UV survival, unlike the *psocs* strain. This resulted in apparent indefinite G_1 arrest after exposing to $100Jm^{-2}$ UV. After lowering the UV dose from $100Jm^{-2}$ to $20Jm^{-2}$, a similar phenotype was observed as seen in *pRAD7* and *psocs RAD23$^+$* cells. The *psocs Δrad23* strain exhibited faster G_1 exit, although S-phase progression did not occur as quickly as seen for the *psocs* strain, however extensive G_2 arrest and particles with >2N DNA content were observed. The S-phase progression still appears to be faster than the *pRAD7 Δrad23* strain, however the lower UV dose may affect this progression. This could be due to differential regulation of the TLS pathway as discussed previously.

It has been assumed in this chapter that the *psocs* cell cycle phenotype is due to misregulation of a stress-induced cell cycle arrest. In order to confirm this theory, unstressed cells would have to be tested for cell cycle progression. The process of elutriation is the least invasive technique for cells to obtain a synchronised G_1 population. An alternative method is α-factor synchronisation, which involves exposing cells to α mating factor, thus inducing G_1 arrest. Although this omits the mechanical stress the cells must undergo during elutriation, the induced cell cycle arrest causes cells to enter a stationary phase-like G_1 arrest. Observing recovery from α-factor-induced G_1 arrest may help reveal the cell cycle progression occurring in *psocs* cells when recovering from stationary phase. Another method of observing the unperturbed cell cycle in *psocs* strains could be time-lapse microscopy, which would provide detailed monitoring of single cell cycle progression. Although flow cytometric data cannot be obtained to produce a true representation of the unperturbed cell cycle in *psocs* strains, the growth curve presents evidence to suggest that the *psocs* strain does not exhibit significant misregulation of the unperturbed cell cycle.

Considering the two phenotypes observed in the *psocs* strain relating to cell cycle progression, it appears the Rad7-containing E3 ligase has a potentially complex role in stress-responsive cell cycle control. It suggests that cell cycle

regulation by the ligase is dependent on the type of stress the cell encounters. This is visualised in Figure 6.19.

STRESS:	**UV Radiation** (DNA Damage)	**Centrifugation** (Mechanical Stress)	**Stationary Phase** (Starvation Stress)

PHENOTYPE: (*psocs* strain compared to WT)	**Premature Exit** from stress-induced G_1 cell cycle arrest		**Delayed Exit** from stationary phase cell cycle arrest

CONCLUSION:	Rad7 E3 Ligase **promotes maintenance** by **preventing G_1 exit** of stress-induced cell cycle arrest		Rad7 E3 Ligase **promotes exit** from starvation-induced cell cycle arrest

Figure 6.19 – Overview of Observed Phenotypes of *psocs* Strain with Regard to Cell Cycle Progression in Response to Various Stresses.

The different cell cycle phenotypes may suggest that the E3 ligase targets different factors in response to different stresses, or possibly just targets Rad4, which affects various factors, or transcriptional targets according to the type of stress encountered. The control of cell cycle progression by proteasomal proteolysis of regulatory factors has been observed in fission yeast. The DNA replication-licensing factor Cdt1 was found to be degraded in M and G_1 phase in response to DNA damage. This occurred in a Rad3 and Cds1-independent manner (Mec1 and Rad53 homologues), so the degradation was checkpoint-independent. The degradation was dependent upon the Cdt2 and Ddb1-containing CUL4 ligase complex, which is homologous to the Ddb1-Ddb2 ligase complex in humans. This complex is involved in human GG-NER and shares orthologous functions with the *S. cerevisiae* Rad7-Rad16 containing complex. During normal cell cycle progression, Cdt1 functions as a replication-licensing factor, so is degraded in S-phase following initiation of DNA replication to ensure only one round of DNA replication occurs. It was speculated that the degradation of Cdt1 in G_1 phase could contribute to genome stability by preventing S-phase onset and

thus reducing the demand on dNTP pools during DNA repair (Ralph et al. 2006). Although a homologue to Cdt1 does not exist in *S. cerevisiae*, it is possible that a similar mechanism could be occurring whereby the Rad7 E3 ligase is degrading a factor to postpone S-phase onset thus preventing DNA repair and replication happening simultaneously and creating excessive demand upon dNTP pools. However in the case of the *psocs* mutant this appears to be a general stress response as opposed to just a response to DNA damage.

6.4.3 Identification of Genes Responsible for the Premature G_1 Exit of *psocs* Strains

The microarray data obtained in Chapter 4 was examined to identify transcriptional misregulation of genes in the *psocs* strain that could cause or contribute to the *psocs* premature G_1 exit cell cycle phenotype. Very few genes were transcriptionally altered in the *psocs* strain, and the potential genes extracted in Figure 6.13 or Figure 6.15 as most significantly misregulated in the *psocs* strain were poorly characterised or showed an inappropriate expression pattern (not misregulated in a *psocs*-dependent manner). For this reason, it must be concluded that the *psocs* cell cycle phenotype is not a result of altered transcriptional regulation of known cell cycle-regulatory genes. If this was to be pursued further, microarrays could be performed using synchronised cells. This would provide better clarity in revealing cell cycle-specific altered transcription in the *psocs* strain, which can be masked when using asynchronous cells.

6.4.4 Suppression of *psocs* Cell Cycle Phenotypes by Constitutive Activation of RNR

Due to the lack of possible cell cycle-related transcriptional targets identified by global analysis, the role of the RNR pathway in cell cycle control was investigated. The Rad7 E3 ligase has been shown previously to have a possible role in regulating cellular dNTP levels via regulation of the RNR pathway. It was considered that the cell cycle defects identified in this chapter

could be due to misregulation of dNTP levels in *psocs* cells. Constitutive activation of the RNR pathway has been shown previously to suppress the UV sensitivity of the *psocs Δrad23* strain, which appears to occur in a *psocs*-dependent fashion, thus suggesting that the Rad7-containing E3 ligase has a regulatory effect on the RNR pathway. If failure to upregulate dNTP pools in *psocs* strains is the cause of the defective cell cycle progression, constitutive activation of RNR, and thus elevation of cellular dNTP levels should affect the cell cycle defective phenotypes observed in this chapter.

Constitutive activation or expression of the RNR pathway was found to completely suppress the defects in cell cycle progression seen in the *psocs* (and *psocs Δrad23*) strains. This suggests that following progression to early stationary phase, the *psocs* strain cannot elevate dNTP levels effectively in order to reinstate DNA replication and logarithmic growth phase. This could cause the growth defect displayed in Figure 6.16. This could explain how upregulation of dNTP synthesis would reinstate normal stationary phase exit.

The results obtained in this chapter also suggest that misregulation of dNTP levels are responsible for the premature G_1 exit of the *psocs* (and *psocs Δrad23*) strains. Deletion of either *SML1* or *CRT1* completely suppressed the defective G_1 exit phenotype. A study performed in *S. pombe* could provide a possible model for the observed *psocs* G_1 phenotype. The DNA replication licensing factor Cdt1 was found to be degraded in a UPS-dependent manner in response to DNA damage in G_1 in order to delay S-phase progression and reduce dNTP demand while DNA repair was occurring (Ralph et al. 2006). A similar mechanism could be dependent on the Rad7 E3 ligase, whereby degradation of a regulatory factor could prevent onset of DNA replication following DNA damage. However, the premature G_1 exit phenotype is also observed in cells that have not been exposed to DNA damage. It is possible that S-phase delay is a feature of general stress response, and not just DNA damage. The suppression of the premature G_1 exit by deletion of *SML1* or *CRT1* suggests that increasing dNTP levels overrides the regulation controlling S-phase entry. It remains unclear if the G_1 exit is accelerated in

Δ*sml1* and Δ*crt1* strains, which would probably be the most plausible conclusion, as elevation of dNTP levels would be predicted to promote DNA replication. Alternatively, *SML1* or *CRT1* deletion could restore the delayed S-phase entry of the *pRAD7* strain when exposed to centrifugal stress.

It has been shown in this chapter that the Rad7-containing E3 ligase affects cell cycle progression in response to stress and DNA damage. These defects appear to result from defective regulation of cellular dNTP levels as the phenotypes are suppressed by constitutive activation of the RNR pathway.

7 General Discussion and Further Work

The complex co-ordination of different cellular pathways is required to allow eukaryotic cells to adapt and respond to DNA damage. *S. cerevisiae* provides an invaluable model to represent the precise mechanism by which eukaryotic cells cope with DNA damage, and promote cellular survival. This study has revealed new aspects of the complex cellular response to DNA damage involving novel regulatory roles of the Rad7, Rad4 and Rad23 NER factors, and provides an investigative potential for further studies in this research area.

7.1 Evidence of a Functional Interaction Between Abf1 and the 19S Proteasome

The initial aim of this study was to reveal a possible functional interaction between the 19S regulatory complex of the 26S proteasome and the global regulator protein Abf1. It was proposed that the 19S proteasome could be responsible for destabilising Abf1 binding to DNA using the same mechanism as observed for Gal4 (Archer et al. 2008b). This prompted the theory that mutating the proteasome could suppress the DNA binding defect of the *abf1-1* mutant allele (Rhode et al. 1992), thus restoring its activity in such processes as DNA replication and NER. A series of experiments were conducted to observe the mutant strains' phenotypes in order to reveal a genetic interaction between Abf1 and the 19S proteasome.

A physical interaction between the 19S proteasome and Abf1 was identified by Co-IP, however a significant functional interaction could not be observed using mutant alleles and phenotypic analysis of cellular growth and UV sensitivity. A slight suppression of temperature sensitivity in the *sug2-1 abf1-1* strain compared to the *abf1-1* strain might suggest some functional interaction, but the strains had identical logarithmic growth rates and UV survival curves.

The physical interaction, and slight suppression of temperature sensitivity provides scope for further investigation in this area, which could be conducted using alternative Abf1 mutants, such as the C-terminal mutants first characterised by (Miyake et al. 2002). The role of the C-terminal domain of Abf1 is less understood than the DNA-binding N-terminal region, so although C-terminal mutants were not conveniently available at the time of this study, Abf1's C-terminal function remains an intriguing and exciting area of research, which could potentially expand on the results obtained here and reveal a functional interaction with the proteasome. In order to further test the Abf1-19S functional interaction, chromatin immunoprecipitation (ChIP) could be employed, using the *abf1-1/sug2-1* mutants and observing Abf1 binding at specific genomic loci. This could be used to determine the function of Abf1 affected, for example altered binding at ARS could affect its role in DNA replication, whereas altered binding at promoter elements of genes could affect its role in transcriptional regulation. It would also be of interest to analyse the binding dynamics of Abf1 C-terminal mutants as this has not been investigated previously, and may help characterise a possible functional interaction with the 19S proteasome. ChIP analysis could be performed on *abf1* mutants at a local or global level to obtain a genomic overview of differential Abf1 binding, and how it is affected by the 19S proteasome.

An advantage of using genetic techniques with *ABF1* and the *SUG* genes in this study is the allele specificity and variability they exhibit. As discussed previously, many different characterised functional mutant alleles exist for both Abf1 and Sug1/2, which differentially affect distinct cellular processes, such as transcription and DNA repair. It is not until a variety of allelic combinations of the two genes have been tested that a proper conclusion regarding the Abf1-19S proteasome interaction can be drawn. It has been shown in this study that combining *abf1-1* and *sug2-1* in a strain proved to be unstable, and combining *abf1-1* and *sug1-20* appeared to be lethal. Obtaining a variety of mutant backgrounds proved more difficult than first presumed, and it was soon apparent that the task was beyond the scope of this study. It can be seen from the results obtained in Chapter 3 that the *abf1-1 sug2-1* mutant strain does not produce a significant phenotype using the assays performed,

however the positive Co-IP and temperature sensitivity results supports the speculation that Abf1 does functionally interact with the 19S proteasome. Investigation of different combinations of *abf1* and *sug* mutant alleles could help characterise the possible functional interaction between Abf1 and the 19S proteasome. Further investigation in this area was not performed in this study.

7.2 The Rad4-Rad23 Functions in DNA Damage-Responsive Gene Transcription

The role of the Rad4-Rad23 complex in NER has been reported previously in the literature, however it has been suggested more recently that the Rad4-Rad23 complex has a role in the general DNA damage response (Gillette et al. 2006), and that Rad23 has a role in global transcription (Wade et al. 2009). The characterisation of an NER regulatory component involving the Rad7-containing E3 ubiquitin ligase-dependent ubiquitination of Rad4 that requires *de novo* protein synthesis, coupled with the observation that deletion of Rad23 appears to affect *RAD4* transcription, prompted the theory that the Rad4-Rad23 complex may have a role in DNA damage-responsive gene transcription, and that this role was dependent on the Rad7-dependent ubiquitination of Rad4 (Gillette et al. 2006). (Wade et al. 2009) also identified a possible role for Rad23 in global transcription, however Rad4 was thought not to be involved in this function. To investigate the role of the Rad4-Rad23 complex in UV-responsive transcription, global gene expression studies were performed and potential regulatory targets of the Rad4-Rad23 complex were identified (Chapter 4).

Using the Rad7 E3 ligase-defective, UV-sensitive *psocs Δrad23* mutant strain, which does not exhibit post-UV Rad7-mediated Rad4 ubiquitination, misregulated genes in response to UV were identified by comparing to the *pRAD7* and *pRAD7 Δrad23* strains. This comparison was conducted to specifically reveal genes affected by Rad4 ubiquitination in response to DNA damage in the absence of Rad23. The comparison identified four main

pathways that exhibited significantly altered transcription; genes involved in dNTP synthesis, DNA damage-responsive chromatin remodelling, telomere maintenance and proteasome metabolism. All four groups showed downregulation of genes that promote cell integrity and genome stability, which could impact on UV-sensitivity, thus explaining the additional UV-sensitivity of the *psocs Δrad23* strain compared to the *pRAD7 Δrad23* strain.

The misregulation of genes involved in regulating cellular dNTP levels was considered most striking, thus most likely to impact upon cellular survival in response to UV. This pathway is discussed in more detail below, however the investigative potential of the other misregulated genes was also considered.

The array data show reduced upregulation of almost all proteasomal subunits in the *Δrad23* mutants, with some *pRAD7* vs *psocs* variation. This observation may help to characterise the role of upregulation of proteasomal subunits in response to DNA damage. It is known that deletion of *RPN4*, the transcriptional activator of proteasomal and other genes causes increased DNA damage sensitivity, however it was not known whether this is due to reduced transcription of the proteasome or other targets of Rpn4, such as *RAD23*, that caused the DNA damage sensitivity (Gasch et al. 2001). A study was performed using mutants that had defective Rpn4 binding at proteasomal genes, which showed that DNA damage-dependent upregulation of proteasomal transcription does affect DNA damage sensitivity (Wang et al. 2008), so therefore reduced transcriptional induction of the proteasomal genes as observed in the *pRAD7 Δrad23* and *psocs Δrad23* strains could cause the observed increased UV sensitivity. These results suggest that Rad23 has a regulatory role in proteasomal gene expression, however the role of Rad4 ubiquitination does not appear to be significant from comparison between the *pRAD7 Δrad23* and *psocs Δrad23* strains. The role of Rad23 or Rad4 in regulation of proteasomal genes could be examined by ChIP at promoters of proteasomal genes, which would determine occupancy of the complex at the UAS. It is also possible that Rad4 or Rad23 could affect an additional factor, such as Rpn4, so assessment of Rpn4 DNA binding by ChIP

at proteasomal gene promoters in the *psocs/rad23* mutant strains may help reveal this regulatory connection. The role of transcriptional regulation of the proteasome in response to DNA damage remains an interesting concept, which may be regulated by the Rad4-Rad23 complex.

Genes involved in DNA damage response-related chromatin modification including *ASF1* and *RTT109* were also found to exhibit increased downregulated in the *psocs* Δ*rad23* strain in response to UV. Both genes act in chromatin modification to facilitate the DNA repair process (Mello et al. 2002; Recht et al. 2006), and their expression is induced following DNA damage in the *pRAD7* strain. Reduced transcription could cause reduced cellular Asf1/Rtt109, which could result in defects in the DNA damage response, thus causing or contributing to the *psocs* Δ*rad23* UV sensitivity. It is known that deletion of *ASF1* causes increased UV sensitivity (Le et al. 1997), which suggests it has an important role in the DNA damage response. It would be of interest to observe Asf1 protein levels in response to DNA damage in the *psocs* Δ*rad23* strain to deduce whether they are significantly lower than the *pRAD7* and *pRAD7* Δ*rad23* strains, as a result of reduced *ASF1* transcription in the *psocs* Δ*rad23* strain. This could help reveal the importance of Asf1 upregulation in the DNA damage response. ChIP analysis could also be employed to identify if Rad4 or Rad23 bind to the *ASF1* or *RTT109* promoters, and thus affect their DNA damage-responsive transcription.

Downregulation of the previously discussed genes involved in chromatin modification or dNTP synthesis has been shown to result in telomeric shortening (Nyswaner et al. 2008; Toussaint et al. 2005). Other ORFs involved in telomere maintenance also exhibited increased downregulated in the *psocs* Δ*rad23* mutant strain, primarily subtelomeric Y' element ORFs. Although the regulatory role of these elements has not been characterised in strains with functional telomerase, such as the strains employed in this study, it would be of interest to observe the telomeric state of the *psocs* Δ*rad23* strain. If shortened telomeres were revealed, it would help explain the

increased UV-sensitivity of the *psocs* Δ*rad23* strain. Evidence supporting the theory that the *psocs* Δ*rad23* strain may exhibit telomeric instability includes the reduced expression of *CDC8* and the RNR pathway, altered regulation of subtelomeric Y' element ORFs, and downregulaiton of *ASF1* and *RTT109*.

The most striking group to exhibit transcriptional misregulation in the *psocs* Δ*rad23* strain was genes involved in dNTP metabolism. This included the RNR pathway and the dTTP-specific synthesis pathway. Regulation of cellular dNTPs plays an important role in promoting successful DNA synthesis, both during DNA replication in S-phase, and DNA repair in response to DNA damage. Misregulation of dNTP levels can affect genome stability and cause mutagenesis. The RNR genes were found to be expressed at a lower level in the *psocs* Δ*rad23* strain, which could suggest that the strain has lower cellular dNTP levels. Reduced expression of the *CDC8* gene could also affect dNTP levels, by reducing dTTP levels and upsetting the nucleotide balance, thus increasing genome instability. This prompted the theory that constitutive activation or expression of the RNR pathway with the intention of raising cellular dNTP levels could promote genome stability and thus suppress the UV sensitivity phenotype of the *psocs* Δ*rad23* strain.

7.3 The Rad7 E3 Ligase Activity Has a Role in Regulation of the DNA Damage Response via the RNR Pathway

Following the observation that genes involved in dNTP synthesis, particularly the RNR pathway, exhibited reduced transcriptional upregulation in response to DNA damage in the *psocs Δrad23* strain, mutants were created with the RNR pathway constitutively activated or constitutively expressed. This was intended to elevate cellular dNTP pools to an acceptable level to suppress the *psocs Δrad23* strain's increased UV sensitivity, under the suggestion that reduced RNR upregulation in the *psocs Δrad23* strain caused reduced cellular dNTP levels following DNA damage. The repressor of RNR transcription, Crt1, and the inhibitor of the RNR complex, Sml1, were deleted in separate strains. Both mutations have been shown to constitutively elevate cellular dNTP levels (Tang et al. 2009).

It has been shown that constitutive activation of RNR in the *psocs Δrad23 Δsml1* strain can suppress the additional UV sensitivity of the *psocs Δrad23* strain compared to the *pRAD7 Δrad23* strain (Chapter 5), however the UV sensitivity of the *pRAD7 Δrad23* strain was not significantly affected by deletion of *SML1*. This suggests that the Rad7 E3 ligase-mediated Rad4 ubiquitination has a regulatory role in maintenance of cellular dNTP levels. Deletion of *CRT1* in *pRAD7 Δrad23* and *psocs Δrad23* strains also cause suppression of UV sensitivity, but to a greater extent than the *Δsml1* strains, and enhanced the UV survival to above the *pRAD7 Δrad23* level.

The level of suppression of UV-sensitivity varied between RNR mutants, which shows that deletion of *CRT1* suppressed the UV sensitivity to a greater extent than deletion of *SML1*. This could be a direct result of actual cellular dNTP levels, as *Δsml1* strains have been shown to elevate dNTP levels ~2 fold, whereas *Δcrt1* strains have been documented to elevate dNTP levels 3-4 fold (Tang et al. 2009). This could explain the increased suppression of the *Δcrt1* strains compared to the *Δsml1* strains. The actual dNTP level could also explain the incomplete suppression of the UV sensitivity (not suppressed to

the WT level), because dNTP levels are raised by 6-8 fold in response to DNA damage (Chabes et al. 2003). If the *psocs* Δ*rad23* strain exhibits reduced DNA damage-responsive dNTP level increase, then deletion of Crt1 or Sml1 may be able to suppress the UV sensitivity to a certain extent, but not to the UV sensitivity of the *pRAD7* or *psocs* strains as dNTP levels are not elevated high enough for efficient DNA repair.

On the other hand, the increased suppression of UV sensitivity in the Δ*crt1* strains could suggest an additional regulatory interaction. Whereas the only known function of Sml1 is as an inhibitor of RNR, Crt1 is known to repress the transcription of several genes, many of which are involved in the DNA damage response. This may suggest that the constitutive expression of genes other than the RNR pathway may contribute to the increased UV survival in Δ*crt1* strains compared to Δ*sml1* strains. An example of these additional factors could be Hug1, a gene repressed by Crt1 and seen to be misregulated in Chapter 4.3.6. Although *HUG1* is known to be transcriptionally upregulated in response to DNA damage, its function is not yet known (Zaim et al. 2005).

If the Rad7-E3 ligase has a regulatory role in stress/DNA damage-responsive dNTP production, it may affect the activity of the Dun1 kinase, which activates the RNR pathway in S-phase and in response to DNA damage. Dun1 regulation by the Rad4-Rad23 complex and the Rad7 E3 ligase could provide a stress/DNA damage-specific regulatory aspect of the checkpoint and dNTP-regulatory pathway. The Rad4-Rad23 complex has been shown to bind at the *DUN1* promoter in *pRAD7* (WT) cells (Figure 5.6), which suggests that the Rad4-Rad23 complex has a role in regulation of *DUN1* transcription. Therefore, increased *DUN1* transcription regulated by the Rad4-Rad23 complex could increase RNR activation and subsequently upregulate dNTP synthesis in response to stress. To investigate this role further, Rad4-Rad23 occupancy could be examined at the *DUN1* promoter in response to DNA damage, and in the *psocs* mutant strains. This could reveal a DNA damage-dependent regulatory role of the Rad4-Rad23 complex in *DUN1* transcription, and could reveal the role of Rad4 ubiquitination. To identify other possible

regulatory gene targets of the Rad4-Rad23 complex, further ChIP studies could be conducted at promoters of other candidate genes such as *DDR2*, *ASF1*, *RTT109* and *CDC8*. In order to obtain a more global perspective and thus potentially identify all Rad4-Rad23-regulated genes a ChIP-chip study could be performed. This would identify Rad4-Rad23 binding across the genome, and if performed in psocs strains could help further characterise the role of Rad4 ubiquitination in DNA damage-responsive transcription.

It was suggested from the data presented in Chapter 5 that the Rad7 E3 ligase has a regulatory role in maintenance of dNTP levels via regulation of DNA damage-responsive transcription of genes such as *DUN1*. This can be seen from the suppressed UV sensitivity of the *psocs* Δ*rad23* strain when RNR is constitutively activated or expressed, and the binding of the Rad4-Rad23 complex at *DUN1*'s promoter. In order to confirm the data presented here, and to investigate further the regulatory mechanism, the cellular dNTP levels could be measured directly in response to DNA damage in the *psocs* Δ*rad23* strain compared to the *pRAD7* strain using an HPLC technique as used in (Chabes et al. 2003). This would unambiguously reveal the role of the Rad7 E3 ligase in maintenance of cellular dNTP levels.

7.4 The Rad7 E3 Ligase Has a Regulatory Role in Cell Cycle Progression

Under normal growth conditions, dNTP levels are altered in a cell cycle-dependent manner. In order to investigate the regulatory role in maintenance of dNTP levels of the Rad7 E3 ligase, cell cycle progression was observed in *pRAD7* and *psocs* strains. Altered cell cycle progression was initially investigated by conducting a growth curve. If the *psocs* strains exhibit lower dNTP levels, it could exhibit delayed cell cycle progression, most likely caused by defective DNA replication during S-phase, a phenotype observed in a Δ*dun1* strain (Zhao and Rothstein 2002) This was found not to be the case, as logarithmically growing *psocs* and *pRAD7* cells exhibited the same cell cycle duration.

It was observed using cells that had entered early stationary phase, that *psocs* cells exhibit slower growth than *pRAD7* cells when placed in fresh media to return to logarithmic growth phase. This suggested defective stress responsive signalling in the *psocs* strain, which could be a result of decreased dNTP levels. The apparent normal progression of the unperturbed cell cycle suggests that this is a defect in response to stress and not in general cell cycle regulation. Another explanation could be that S-phase is delayed, but the cell cycle 'catches up' in other phases, as seen in the *dun1* mutant strain observed in (Zhao and Rothstein 2002). This defect was suppressed by deleting *SML1*, which suggests it was caused by insufficient dNTP levels. To investigate cell cycle progression further, flow cytometric analysis was performed on the *psocs/rad23* strains, both untreated and in response to DNA damage.

Flow cytometric analysis revealed a different defect in *psocs* strains in cell cycle progression. Rather than exhibiting delayed cell cycle progression, the *psocs* strains displayed premature G_1 exit in G_1-synchronised cells, which only appeared to occur following initial G_1 exit, and following cycles occurred at the same rate in both *psocs* and *pRAD7* strains, with no visible prolonged S-phase. This premature G_1 exit was observed the same in *pRAD7 Δrad23* and *psocs Δrad23* strains. Premature G_1 exit was also displayed in response to UV irradiation, however the *psocs* strain also exhibited rapid progression through S-phase, extended G_2 arrest, and the presence of particles with a >2N DNA content. This cell cycle progression could indicate that defective DNA damage-responsive signalling is occurring in psocs strains. Although the psocs strain does not exhibit significant UV sensitivity, it was suggested that psocs cells could exhibit UV sensitivity at a certain stage of the cell cycle, for example G_1 cells, which could be sensitive due to defective S-phase progression. In an asynchronous cell population this effect could be masked by the majority of the cells not exhibiting UV sensitivity. The apparent accelerated S-phase progression in *psocs* cells could be due to increased activation of a pathway such as translesion synthesis (TLS), which would promote damage bypass rather than accurate repair, thus leading to damage

accumulation and genomic instability in certain cells, but not significantly affecting UV survival.

An alternative explanation of the *psocs* premature G_1 exit phenotype could be the mechanism reported in *S. pombe* by (Ralph et al. 2006), which identified the DNA replication licensing factor Cdt1, that was targeted for ubiquitination in order to delay S-phase initiation to reduce the demand on dNTPs whilst DNA repair occurred. Failure to ubiquitinate Cdt1 resulted in premature onset of S-phase, the phenotype observed in the *psocs* strains. However, the *psocs* strains also exhibited premature G_1 exit in the absence of DNA damage, which may suggest that S-phase delay is a general stress response rather than a response to DNA damage, possibly to allow dNTP synthesis before logarithmic growth phase is resumed. It was assumed that the premature G_1 exit was caused by misregulation of a general stress response, rather than a DNA damage-specific response as it was proposed that non-UV-treated cells were still subjected to stress by centrifugation during elutriation, so also exhibited a checkpoint response.

It was speculated that decreased levels of cellular dNTPs could be the cause of the defective cell cycle progression in *psocs* strains. It has been shown that the Rad7 E3 ligase has a possible role in regulation of cellular dNTP levels via the RNR pathway, so misregulation of dNTP synthesis in psocs strains could also be the cause of the defective cell cycle progression. Cell cycle progression analysis was also performed in the Δ*sml1* and Δ*crt1* strains constructed in Chapter 5 to deduce whether elevation of dNTP levels could suppress the cell cycle progression defects observed in *psocs* strains. It was shown that constitutive activation or expression of RNR, which was reliably assumed to elevate cellular dNTP pools, was able to suppress and therefore alleviate both observed cell cycle defects in the *psocs* strain. In the case of the delayed exit from stationary phase in the *psocs* strains, it could be accepted that, as suggested previously, *psocs* strains have a defective ability to increase dNTP levels in response to stress/DNA damage, so constitutive elevation of dNTP levels could allow normal stationary phase exit of *psocs*

strains. The complete suppression of the phenotype by activating the RNR pathway suggests that insufficient dNTP pools could be the sole cause of the defect.

Suppression of the *psocs* strains' premature G_1 exit phenotype by activating RNR is likely to be a result of elevated dNTP levels. In the case of *S. pombe*, ubiquitination of Cdt1 prevents S-phase onset following DNA damage, thus reducing the dNTP demand (Ralph et al. 2006). If dNTP levels are increased sufficiently, it could be proposed that there would be no need to delay S-phase onset.

The incomplete suppression of the UV sensitivity of *pRAD7 Δrad23* and *psocs Δrad23* strains by deletion of *SML1* or *CRT1* was suggested to be due to insufficient dNTP levels, as deletion of *SML1* is known to increase dNTP levels by 2.5 fold, deletion of *CRT1* is known to increase dNTP levels by 3-4 fold, but DNA damage induces a 6-8 fold increase in cellular dNTP levels (Chabes et al. 2003). The complete suppression of the cell cycle progression defects observed in *Δsml1* and *Δcrt1* cells suggests that the dNTP level increase caused by these mutations allows normal cell cycle progression. If hyper-activation of a pathway such as TLS is the cause of defective cell cycle progression in psocs strains then this could suggest that a threshold dNTP level could be required to decide whether TLS or repair will be activated in response to DNA damage. This could be investigated by introducing TLS pathway mutations into the *psocs* strains, then observing cell cycle progression and dNTP levels in response to DNA damage.

To conclude, the results suggest that the Rad7 E3 ligase has a regulatory role in maintenance of stress or DNA damage-responsive cellular dNTP levels. The *psocs* strain has exhibited increased UV-sensitivity (when *RAD23* is deleted), delayed stationary phase exit and premature G_1 exit when subjected to centrifugal stress or DNA damage. These defects can be suppressed by constitutive activation or expression of the RNR pathway, which is reliably assumed to elevate cellular dNTP levels, which suggests that the Rad7 E3

ligase has a role in elevating dNTP pools in response to stress or DNA damage. The Rad4-Rad23 complex has been shown to bind to the promoter of *DUN1*, which presents a plausible regulatory mechanism for the Rad7 E3 ligase and the RNR pathway.

7.5 Possible Further Experiments and Prospects

To confirm and expand on the results obtained in this study, it would be useful to view the actual cellular dNTP levels in the *psocs* Δ*rad23* strain, and observe the effects of introducing the Δ*sml1* or Δ*crt1* mutations. This could confirm the speculated role of the Rad7 E3 ligase in regulation of cellular dNTP levels, either in response to DNA damage, other stresses or during normal growth. It could also reveal whether there was a uniform decrease in dNTP levels, or if the balance of different dNTP was upset, thus resulting in increased genomic instability and explaining the UV sensitivity of the strain. Disruption of the dNTP balance could suggest that Rad7 E3 ligase affects other genes, such as *CDC8*, which is specific to dTTP production rather than general dNTP synthesis.

To characterise further the transcriptional regulatory role of the Rad23-Rad4 complex, more extensive ChIP experiments could be performed at the *DUN1* promoter, and at other gene promoters identified in Chapter 4. To obtain a more global perspective of this transcriptional role, ChIP-chip could be performed to analyse Rad4-Rad23 binding across the whole genome. These ChIP studies could be performed in response to DNA damage, and in the *psocs* mutant strains in order to detect altered occupancy at gene promoters. The Dun1 kinase is known to be activated following DNA damage to activate the RNR pathway by inhibiting Sml1 and Crt1 (Zhao and Rothstein 2002), therefore if Rad4-Rad23 vacating the promoter causes upregulation of *DUN1* transcription following DNA damage, the RNR complex would be activated further, thus promoting dNTP synthesis. If Rad4-Rad23 was acting as a transcriptional repressor, Rad4 ubiquitination in response to DNA damage could cause a conformational change thus preventing DNA binding of the

Rad4-Rad23 complex and promoting *DUN1* transcription. It is possible that this repressor activity of the Rad4-Rad23 complex could occur at other DNA damage-responsive genes, such as those identified in Chapter 4. Following its ubiquitination, it appears that Rad4 is degraded by the proteasome, however this degradation is not required for its function in NER. Degradation of the human Rad4 homologue XPC is not observed in response to DNA damage (Sugasawa 2006), therefore the role of the degradation of Rad4 remains unknown. It is possible that Rad4 degradation occurs in yeast because *de novo* protein synthesis is not as energetically demanding as it is in human cells. This would suggest that evolutionary pressure has prevented XPC degradation due to energy demands, thus suggesting that Rad4 degradation has no significant regulatory function.

It has been reported that DNA damage promotes nuclear localisation of Rad4, and without DNA damage it remains dispersed throught the cytosol and nucleus (Li et al.). It is plausible that a subset of Rad4-Rad23 in the cell remains bound to gene promoters in the nucleus to repress transcription, and following DNA damage the remainder of the Rad4-Rad23 could localise to the nucleus as observed in (Li et al.), and bind to damaged DNA to recruit NER factors.

Post-translational modification of regulatory factors dramatically increases the complexity of the proteome, and allows factors to adopt different functions without the need for *de novo* protein synthesis. Rad4 may be subjected to post-translational modification to retain the Rad4-Rad23 complex in the cytosol in the absence of DNA damage, or it may be the case that post-translational modification is required for Rad4 to function as a repair factor or transcriptional regulator. It is known that Rad4 becomes ubiquitinated in response to DNA damage, however Rad4 may be subjected to other post-translational modifications such as phosphorylation or SUMO modification in order to participate in specific regulatory tasks. SUMO modification has

previously been documented to affect subcellular localisation of regulatory factors (Hay 2005).

Defective subcellular localisation of Rad4 in the *psocs* Δ*rad23* mutant may be a contributor to its UV sensitivity. It could be conceived that Rad4 ubiquitination could trigger its nuclear localisation, thus allowing it to function in the NER pathway. It is also plausible that Rad23's UBL domain could compensate for the lack of Rad4 ubiquitination in the *psocs* mutant thus suppressing the defect in Rad4 subcellular localisation, and preventing a UV-sensitive phenotype in the *psocs* strain.

The results obtained in this study have further characterised the complex regulatory pathways involved in the DNA damage response in *S. cerevisiae*, by identifying a possible role of the Rad4-Rad23 complex in DNA damage-responsive transcription involving Rad7-dependent Rad4 ubiquitination. This has identified and explored a possible role for the Rad7 E3 ligase in regulation of cellular dNTP levels, which has been shown to affect UV sensitivity and cell cycle progression. Several other potential regulatory target genes of the Rad4-Rad23 complex have been identified, which provides scope for further research in this area to further examine and characterise the subset of DNA damage-responsive genes regulated by the Rad4-Rad23 complex, and implications of their regulation in the DNA damage response.

The participation of NER factors in the overall DNA damage response remains a fascinating and intriguing area of research. This continues to reveal the responses and adaptations cells undergo to cope with the threat of DNA damage, thus maintaining genomic integrity and promoting cell survival. The results presented in this thesis provide scope for further investigation in this area, regarding the role of the Rad4-Rad23 complex in DNA damage-responsive transcription, and as a result of this, regulation of cellular dNTP levels.

Experimental Acknowledgements

References

Abraham, R. T. 2001. Cell cycle checkpoint signaling through the ATM and ATR kinases. *Genes Dev* 15(17), pp. 2177-2196.

Adams, A. K. and Holm, C. 1996. Specific DNA replication mutations affect telomere length in Saccharomyces cerevisiae. *Mol Cell Biol* 16(9), pp. 4614-4620.

Agarwal, R. et al. 2003. Two distinct pathways for inhibiting pds1 ubiquitination in response to DNA damage. *J Biol Chem* 278(45), pp. 45027-45033.

Al-Moghrabi, N. M. et al. 2003. UV-induced de novo protein synthesis enhances nucleotide excision repair efficiency in a transcription-dependent manner in S. cerevisiae. *DNA Repair (Amst)* 2(11), pp. 1185-1197.

Alcasabas, A. A. et al. 2001. Mrc1 transduces signals of DNA replication stress to activate Rad53. *Nat Cell Biol* 3(11), pp. 958-965.

Archer, C. T. et al. 2008a. Physical and functional interactions of monoubiquitylated transactivators with the proteasome. *J Biol Chem* 283(31), pp. 21789-21798.

Archer, C. T. et al. 2008b. Activation domain-dependent monoubiquitylation of Gal4 protein is essential for promoter binding in vivo. *J Biol Chem* 283(18), pp. 12614-12623.

Bailly, V. et al. 1997. Yeast DNA repair proteins Rad6 and Rad18 form a heterodimer that has ubiquitin conjugating, DNA binding, and ATP hydrolytic activities. *J Biol Chem* 272(37), pp. 23360-23365.

Baker, S. P. and Grant, P. A. 2005. The proteasome: not just degrading anymore. *Cell* 123(3), pp. 361-363.

Ball, H. L. et al. 2005. ATRIP binding to replication protein A-single-stranded DNA promotes ATR-ATRIP localization but is dispensable for Chk1 phosphorylation. *Mol Biol Cell* 16(5), pp. 2372-2381.

Baumeister, W. et al. 1998. The proteasome: paradigm of a self-compartmentalizing protease. *Cell* 92(3), pp. 367-380.

Beckman 1989. *The JE-5.0 Elutriation System - Instruction Manual.* Palo Alto, CA 94304: Spinco Division of Beckman Instruments Inc.

Beinoraviciute-Kellner, R. et al. 2005. In vitro selection of DNA binding sites for ABF1 protein from Saccharomyces cerevisiae. *FEBS Lett* 579(20), pp. 4535-4540.

Bergink, S. et al. 2007. Regulation of UV-induced DNA damage response by ubiquitylation. *DNA Repair (Amst)* 6(9), pp. 1231-1242.

Bertolaet, B. L. et al. 2001. UBA domains of DNA damage-inducible proteins interact with ubiquitin. *Nat Struct Biol* 8(5), pp. 417-422.

Blankley, R. T. and Lydall, D. 2004. A domain of Rad9 specifically required for activation of Chk1 in budding yeast. *J Cell Sci* 117(Pt 4), pp. 601-608.

Boyce, R. P. and Howard-Flanders, P. 1964. Release of Ultraviolet Light-Induced Thymine Dimers from DNA in E. Coli K-12. *Proc Natl Acad Sci U S A* 51, pp. 293-300.

Bres, V. et al. 2003. A non-proteolytic role for ubiquitin in Tat-mediated transactivation of the HIV-1 promoter. *Nat Cell Biol* 5(8), pp. 754-761.

Brown, T. A. 1999. *Genomes*. Oxford, UK: BIOS Scientific Publishers Ltd.

Brusky, J. et al. 2000. UBC13, a DNA-damage-inducible gene, is a member of the error-free postreplication repair pathway in Saccharomyces cerevisiae. *Curr Genet* 37(3), pp. 168-174.

Cadet, J. et al. 2005. Ultraviolet radiation-mediated damage to cellular DNA. *Mutat Res* 571(1-2), pp. 3-17.

Callegari, A. J. and Kelly, T. J. 2006. UV irradiation induces a postreplication DNA damage checkpoint. *Proc Natl Acad Sci U S A* 103(43), pp. 15877-15882.

Caron, P. R. et al. 1985. Involvement of helicase II (uvrD gene product) and DNA polymerase I in excision mediated by the uvrABC protein complex. *Proc Natl Acad Sci U S A* 82(15), pp. 4925-4929.

Carr, A. M. 2002. DNA structure dependent checkpoints as regulators of DNA repair. *DNA Repair (Amst)* 1(12), pp. 983-994.

Carter, B. L. and Jagadish, M. N. 1978. The relationship between cell size and cell division in the yeast Saccharomyces cerevisiae. *Exp Cell Res* 112(1), pp. 15-24.

Chabes, A. et al. 2003. Survival of DNA damage in yeast directly depends on increased dNTP levels allowed by relaxed feedback inhibition of ribonucleotide reductase. *Cell* 112(3), pp. 391-401.

Chambers, A. et al. 1990. ARS binding factor 1 binds adjacent to RAP1 at the UASs of the yeast glycolytic genes PGK and PYK1. *Nucleic Acids Res* 18(18), pp. 5393-5399.

Chang, C. et al. 2001. The Gal4 activation domain binds Sug2 protein, a proteasome component, in vivo and in vitro. *J Biol Chem* 276(33), pp. 30956-30963.

Chi, Y. et al. 2001. Negative regulation of Gcn4 and Msn2 transcription factors by Srb10 cyclin-dependent kinase. *Genes Dev* 15(9), pp. 1078-1092.

Chien, C. Y. et al. 2009. The yeast Cdc8 exhibits both deoxythymidine monophosphate and diphosphate kinase activities. *FEBS Lett* 583(13), pp. 2281-2286.

Cho, G. et al. 1995. Structure-function analysis of the DNA binding domain of Saccharomyces cerevisiae ABF1. *Nucleic Acids Res* 23(15), pp. 2980-2987.

Clerici, M. et al. 2001. Hyperactivation of the yeast DNA damage checkpoint by TEL1 and DDC2 overexpression. *Embo J* 20(22), pp. 6485-6498.

Clyne, R. K. and Kelly, T. J. 1997. Identification of autonomously replicating sequence (ARS) elements in eukaryotic cells. *Methods* 13(3), pp. 221-233.

Cohen-Fix, O. and Koshland, D. 1997. The anaphase inhibitor of Saccharomyces cerevisiae Pds1p is a target of the DNA damage checkpoint pathway. *Proc Natl Acad Sci U S A* 94(26), pp. 14361-14366.

Cross, F. R. 1990. Cell cycle arrest caused by CLN gene deficiency in Saccharomyces cerevisiae resembles START-I arrest and is independent of the mating-pheromone signalling pathway. *Mol Cell Biol* 10(12), pp. 6482-6490.

Dantuma, N. P. et al. 2009. The ubiquitin receptor Rad23: at the crossroads of nucleotide excision repair and proteasomal degradation. *DNA Repair (Amst)* 8(4), pp. 449-460.

Datta, A. et al. 2000. Checkpoint-dependent activation of mutagenic repair in Saccharomyces cerevisiae pol3-01 mutants. *Mol Cell* 6(3), pp. 593-603.

Daulny, A. and Tansey, W. P. 2009. Damage control: DNA repair, transcription, and the ubiquitin-proteasome system. *DNA Repair (Amst)* 8(4), pp. 444-448.

de Bettignies, G. and Johnston, L. H. 2003. The mitotic exit network. *Curr Biol* 13(8), p. R301.

DellaVecchia, M. J. et al. 2004. Analyzing the handoff of DNA from UvrA to UvrB utilizing DNA-protein photoaffinity labeling. *J Biol Chem* 279(43), pp. 45245-45256.

DeMarini, D. M. 2004. Genotoxicity of tobacco smoke and tobacco smoke condensate: a review. *Mutat Res* 567(2-3), pp. 447-474.

Demartino, G. N. and Gillette, T. G. 2007. Proteasomes: machines for all reasons. *Cell* 129(4), pp. 659-662.

den Dulk, B. et al. 2005. The Rad4 homologue YDR314C is essential for strand-specific repair of RNA polymerase I-transcribed rDNA in Saccharomyces cerevisiae. *Mol Microbiol* 56(6), pp. 1518-1526.

den Dulk, B. et al. 2006. Rad33, a new factor involved in nucleotide excision repair in Saccharomyces cerevisiae. *DNA Repair (Amst)* 5(6), pp. 683-692.

den Dulk, B. et al. 2008. The NER protein Rad33 shows functional homology to human Centrin2 and is involved in modification of Rad4. *DNA Repair (Amst)* 7(6), pp. 858-868.

Dennis, G., Jr. et al. 2003. DAVID: Database for Annotation, Visualization, and Integrated Discovery. *Genome Biol* 4(5), p. P3.

Diede, S. J. and Gottschling, D. E. 2001. Exonuclease activity is required for sequence addition and Cdc13p loading at a de novo telomere. *Curr Biol* 11(17), pp. 1336-1340.

Diffley, J. F. and Stillman, B. 1988. Purification of a yeast protein that binds to origins of DNA replication and a transcriptional silencer. *Proc Natl Acad Sci U S A* 85(7), pp. 2120-2124.

Dolan, J. W. and Fields, S. 1990. Overproduction of the yeast STE12 protein leads to constitutive transcriptional induction. *Genes Dev* 4(4), pp. 492-502.

Domkin, V. et al. 2002. Yeast DNA damage-inducible Rnr3 has a very low catalytic activity strongly stimulated after the formation of a cross-talking Rnr1/Rnr3 complex. *J Biol Chem* 277(21), pp. 18574-18578.

Downs, J. A. et al. 2000. A role for Saccharomyces cerevisiae histone H2A in DNA repair. *Nature* 408(6815), pp. 1001-1004.

Dulbecco, R. 1949. Reactivation of ultra-violet-inactivated bacteriophage by visible light. *Nature* 163(4155), p. 949.

Durocher, D. et al. 2000. The molecular basis of FHA domain:phosphopeptide binding specificity and implications for phospho-dependent signaling mechanisms. *Mol Cell* 6(5), pp. 1169-1182.

Elledge, S. J. and Davis, R. W. 1990. Two genes differentially regulated in the cell cycle and by DNA-damaging agents encode alternative regulatory subunits of ribonucleotide reductase. *Genes Dev* 4(5), pp. 740-751.

Ellison, V. and Stillman, B. 2003. Biochemical characterization of DNA damage checkpoint complexes: clamp loader and clamp complexes with specificity for 5' recessed DNA. *PLoS Biol* 1(2), p. E33.

Emili, A. 1998. MEC1-dependent phosphorylation of Rad9p in response to DNA damage. *Mol Cell* 2(2), pp. 183-189.

Emili, A. et al. 2001. Dynamic interaction of DNA damage checkpoint protein Rad53 with chromatin assembly factor Asf1. *Mol Cell* 7(1), pp. 13-20.

Evans, T. et al. 1983. Cyclin: a protein specified by maternal mRNA in sea urchin eggs that is destroyed at each cleavage division. *Cell* 33(2), pp. 389-396.

Ezhkova, E. and Tansey, W. P. 2004. Proteasomal ATPases link ubiquitylation of histone H2B to methylation of histone H3. *Mol Cell* 13(3), pp. 435-442.

Fasullo, M. et al. 1999. Radiosensitive and mitotic recombination phenotypes of the Saccharomyces cerevisiae dun1 mutant defective in DNA damage-inducible gene expression. *Genetics* 152(3), pp. 909-919.

Ferdous, A. et al. 2001. The 19S regulatory particle of the proteasome is required for efficient transcription elongation by RNA polymerase II. *Mol Cell* 7(5), pp. 981-991.

Ferdous, A. et al. 2002. A nonproteolytic function of the 19S regulatory subunit of the 26S proteasome is required for efficient activated transcription by human RNA polymerase II. *Biochemistry* 41(42), pp. 12798-12805.

Ferdous, A. et al. 2007. The role of the proteasomal ATPases and activator monoubiquitylation in regulating Gal4 binding to promoters. *Genes Dev* 21(1), pp. 112-123.

Flurin, P. H. et al. 2005. [Arthroscopic repair of full-thickness cuff tears: a multicentric retrospective study of 576 cases with anatomical assessment.]. *Rev Chir Orthop Reparatrice Appar Mot* 91(S8), pp. 31-42.

Fourel, G. et al. 2002. General regulatory factors (GRFs) as genome partitioners. *J Biol Chem* 277(44), pp. 41736-41743.

Friedberg, E. C. 2001. How nucleotide excision repair protects against cancer. *Nat Rev Cancer* 1(1), pp. 22-33.

Friedberg, E. C. 2005a. Suffering in silence: the tolerance of DNA damage. *Nat Rev Mol Cell Biol* 6(12), pp. 943-953.

Friedberg, E. C., Walker G. C. and Siede W. 1995. *DNA Repair and Mutagenesis*. American Society of Microbiology Press, Washington DC.

Friedberg, E. C., Walker G. C. and Siede W. 2005b. *DNA Repair and Mutagenesis (2nd Edition)*. American Society for Microbiology Press, Washington DC.

Friedberg, E. C., Walker G. C. and Siede W. 2006. *DNA Repair and Mutagenesis (2nd Edition)*. American Society for Microbiology Press, Washington DC.

Fromme, J. C. et al. 2004. DNA glycosylase recognition and catalysis. *Curr Opin Struct Biol* 14(1), pp. 43-49.

Fu, Y. et al. 2008. DNA damage-induced gene expression in Saccharomyces cerevisiae. *FEMS Microbiol Rev* 32(6), pp. 908-926.

Fu, Y. and Xiao, W. 2006. Identification and characterization of CRT10 as a novel regulator of Saccharomyces cerevisiae ribonucleotide reductase genes. *Nucleic Acids Res* 34(6), pp. 1876-1883.

Gailus-Durner, V. et al. 1996. Participation of the yeast activator Abf1 in meiosis-specific expression of the HOP1 gene. *Mol Cell Biol* 16(6), pp. 2777-2786.

Gardner, R. et al. 1999. RAD53, DUN1 and PDS1 define two parallel G2/M checkpoint pathways in budding yeast. *Embo J* 18(11), pp. 3173-3185.

Gasch, A. P. et al. 2001. Genomic expression responses to DNA-damaging agents and the regulatory role of the yeast ATR homolog Mec1p. *Mol Biol Cell* 12(10), pp. 2987-3003.

Geymonat, M. et al. 2003. In vitro regulation of budding yeast Bfa1/Bub2 GAP activity by Cdc5. *J Biol Chem* 278(17), pp. 14591-14594.

Ghaemmaghami, S. et al. 2003. Global analysis of protein expression in yeast. *Nature* 425(6959), pp. 737-741.

Giannattasio, M. et al. 2002. A dominant-negative MEC3 mutant uncovers new functions for the Rad17 complex and Tel1. *Proc Natl Acad Sci U S A* 99(20), pp. 12997-13002.

Gietz, R. D. and Woods, R. A. 2002. Transformation of yeast by lithium acetate/single-stranded carrier DNA/polyethylene glycol method. *Methods Enzymol* 350, pp. 87-96.

Gillette, T. G. et al. 2001. The 19S complex of the proteasome regulates nucleotide excision repair in yeast. *Genes Dev* 15(12), pp. 1528-1539.

Gillette, T. G. et al. 2006. Distinct functions of the ubiquitin-proteasome pathway influence nucleotide excision repair. *Embo J* 25(11), pp. 2529-2538.

Glickman, M. H. and Raveh, D. 2005. Proteasome plasticity. *FEBS Lett* 579(15), pp. 3214-3223.

Glotzer, M. et al. 1991. Cyclin is degraded by the ubiquitin pathway. *Nature* 349(6305), pp. 132-138.

Gonzalez, F. et al. 2002. Recruitment of a 19S proteasome subcomplex to an activated promoter. *Science* 296(5567), pp. 548-550.

Goodin, L. J. et al. 1971. Photoreversal of ultraviolet-induced division delay in Saccharomyces cerevisiae. *Radiat Res* 45(2), pp. 440-448.

Gordon, L. K. and Haseltine, W. A. 1982. Quantitation of cyclobutane pyrimidine dimer formation in double- and single-stranded DNA fragments of defined sequence. *Radiat Res* 89(1), pp. 99-112.

Green, E. M. et al. 2005. Replication-independent histone deposition by the HIR complex and Asf1. *Curr Biol* 15(22), pp. 2044-2049.

Greer, S. F. et al. 2003. Enhancement of CIITA transcriptional function by ubiquitin. *Nat Immunol* 4(11), pp. 1074-1082.

Grenon, M. et al. 2001. Checkpoint activation in response to double-strand breaks requires the Mre11/Rad50/Xrs2 complex. *Nat Cell Biol* 3(9), pp. 844-847.

Guterman, A. and Glickman, M. H. 2004. Deubiquitinating enzymes are IN/(trinsic to proteasome function). *Curr Protein Pept Sci* 5(3), pp. 201-211.

Guzder, S. N. et al. 1994. DNA repair gene RAD3 of S. cerevisiae is essential for transcription by RNA polymerase II. *Nature* 367(6458), pp. 91-94.

Guzder, S. N. et al. 2006. Complex formation with damage recognition protein Rad14 is essential for Saccharomyces cerevisiae Rad1-Rad10 nuclease to perform its function in nucleotide excision repair in vivo. *Mol Cell Biol* 26(3), pp. 1135-1141.

Guzder, S. N. et al. 1997. Yeast Rad7-Rad16 complex, specific for the nucleotide excision repair of the nontranscribed DNA strand, is an ATP-dependent DNA damage sensor. *J Biol Chem* 272(35), pp. 21665-21668.

Guzder, S. N. et al. 1998. The DNA-dependent ATPase activity of yeast nucleotide excision repair factor 4 and its role in DNA damage recognition. *J Biol Chem* 273(11), pp. 6292-6296.

Han, J. et al. 2007. Rtt109 acetylates histone H3 lysine 56 and functions in DNA replication. *Science* 315(5812), pp. 653-655.

Hanawalt, P. C. and Haynes, R. H. 1965. Repair Replication of DNA in Bacteria: Irrelevance of Chemical Nature of Base Defect. *Biochem Biophys Res Commun* 19, pp. 462-467.

Hao, B. et al. 2009. Candida albicans RFX2 encodes a DNA binding protein involved in DNA damage responses, morphogenesis, and virulence. *Eukaryot Cell* 8(4), pp. 627-639.

Harm, W. 1979. Relative effectiveness of the 300--320 NM spectral region on sunlight for the production of primary lethal damage in E. coli cells. *Mutat Res* 60(3), pp. 263-270.

Harrison, J. C. and Haber, J. E. 2006. Surviving the breakup: the DNA damage checkpoint. *Annu Rev Genet* 40, pp. 209-235.

Hartwell, L. H. 1991. Twenty-five years of cell cycle genetics. *Genetics* 129(4), pp. 975-980.

Hasty, P. et al. 2003. Aging and genome maintenance: lessons from the mouse? *Science* 299(5611), pp. 1355-1359.

Hay, R. T. 2005. SUMO: a history of modification. *Mol Cell* 18(1), pp. 1-12.

Higgins, D. R. et al. 1983. Isolation and characterization of the RAD3 gene of Saccharomyces cerevisiae and inviability of rad3 deletion mutants. *Proc Natl Acad Sci U S A* 80(18), pp. 5680-5684.

Hiyama, H. et al. 1999. Interaction of hHR23 with S5a. The ubiquitin-like domain of hHR23 mediates interaction with S5a subunit of 26 S proteasome. *J Biol Chem* 274(39), pp. 28019-28025.

Hoege, C. et al. 2002. RAD6-dependent DNA repair is linked to modification of PCNA by ubiquitin and SUMO. *Nature* 419(6903), pp. 135-141.

Howard-Flanders, P. et al. 1966. Three loci in Escherichia coli K-12 that control the excision of pyrimidine dimers and certain other mutagen products from DNA. *Genetics* 53(6), pp. 1119-1136.

Huang da, W. et al. 2009. Systematic and integrative analysis of large gene lists using DAVID bioinformatics resources. *Nat Protoc* 4(1), pp. 44-57.

Huang, M. et al. 1998. The DNA replication and damage checkpoint pathways induce transcription by inhibition of the Crt1 repressor. *Cell* 94(5), pp. 595-605.

Husain, I. et al. 1985. Effect of DNA polymerase I and DNA helicase II on the turnover rate of UvrABC excision nuclease. *Proc Natl Acad Sci U S A* 82(20), pp. 6774-6778.

Ichihashi, M. et al. 2003. UV-induced skin damage. *Toxicology* 189(1-2), pp. 21-39.

Janion, C. 2001. Some aspects of the SOS response system--a critical survey. *Acta Biochim Pol* 48(3), pp. 599-610.

Janion, C. 2008. Inducible SOS response system of DNA repair and mutagenesis in Escherichia coli. *Int J Biol Sci* 4(6), pp. 338-344.

Jelinsky, S. A. et al. 2000. Regulatory networks revealed by transcriptional profiling of damaged Saccharomyces cerevisiae cells: Rpn4 links base excision repair with proteasomes. *Mol Cell Biol* 20(21), pp. 8157-8167.

Jentsch, S. et al. 1987. The yeast DNA repair gene RAD6 encodes a ubiquitin-conjugating enzyme. *Nature* 329(6135), pp. 131-134.

Jiricny, J. 2006. The multifaceted mismatch-repair system. *Nat Rev Mol Cell Biol* 7(5), pp. 335-346.

Johnston, M. 1987. A model fungal gene regulatory mechanism: the GAL genes of Saccharomyces cerevisiae. *Microbiol Rev* 51(4), pp. 458-476.

Ju, D. et al. 2008. Genome-wide analysis identifies MYND-domain protein Mub1 as an essential factor for Rpn4 ubiquitylation. *Mol Cell Biol* 28(4), pp. 1404-1412.

Jun, S. H. et al. 2006. DNA mismatch repair system. Classical and fresh roles. *Febs J* 273(8), pp. 1609-1619.

Kapetanaki, M. G. et al. 2006. The DDB1-CUL4ADDB2 ubiquitin ligase is deficient in xeroderma pigmentosum group E and targets histone H2A at UV-damaged DNA sites. *Proc Natl Acad Sci U S A* 103(8), pp. 2588-2593.

Kelner, A. 1949. Effect of Visible Light on the Recovery of Streptomyces Griseus Conidia from Ultra-violet Irradiation Injury. *Proc Natl Acad Sci U S A* 35(2), pp. 73-79.

Kim, E. M. et al. 2002. Phosphorylation of Rph1, a damage-responsive repressor of PHR1 in Saccharomyces cerevisiae, is dependent upon Rad53 kinase. *Nucleic Acids Res* 30(3), pp. 643-648.

Kodadek, T. No Splicing, no dicing: non-proteolytic roles of the ubiquitin-proteasome system in transcription. *J Biol Chem* 285(4), pp. 2221-2226.

Kondo, T. et al. 2001. Recruitment of Mec1 and Ddc1 checkpoint proteins to double-strand breaks through distinct mechanisms. *Science* 294(5543), pp. 867-870.

Kunkel, T. A. and Erie, D. A. 2005. DNA mismatch repair. *Annu Rev Biochem* 74, pp. 681-710.

Le, S. et al. 1997. Two new S-phase-specific genes from Saccharomyces cerevisiae. *Yeast* 13(11), pp. 1029-1042.

Lecker, S. H. et al. 2006. Protein degradation by the ubiquitin-proteasome pathway in normal and disease states. *J Am Soc Nephrol* 17(7), pp. 1807-1819.

Lee, D. et al. 2005. The proteasome regulatory particle alters the SAGA coactivator to enhance its interactions with transcriptional activators. *Cell* 123(3), pp. 423-436.

Lee, S. J. et al. 2003. Rad53 phosphorylation site clusters are important for Rad53 regulation and signaling. *Mol Cell Biol* 23(17), pp. 6300-6314.

Lee, Y. D. and Elledge, S. J. 2006. Control of ribonucleotide reductase localization through an anchoring mechanism involving Wtm1. *Genes Dev* 20(3), pp. 334-344.

Li, Y. et al. Rad4 regulates protein turnover at a postubiquitylation step. *Mol Biol Cell* 21(1), pp. 177-185.

Lindahl, T. 1993. Instability and decay of the primary structure of DNA. *Nature* 362(6422), pp. 709-715.

Liu, Y. and Xiao, W. 1997. Bidirectional regulation of two DNA-damage-inducible genes, MAG1 and DDI1, from Saccharomyces cerevisiae. *Mol Microbiol* 23(4), pp. 777-789.

Lommel, L. et al. 2002. Proteolysis of a nucleotide excision repair protein by the 26 S proteasome. *Curr Genet* 42(1), pp. 9-20.

Longhese, M. P. et al. 2000. Checkpoint proteins influence telomeric silencing and length maintenance in budding yeast. *Genetics* 155(4), pp. 1577-1591.

Louis, E. J. 1995. The chromosome ends of Saccharomyces cerevisiae. *Yeast* 11(16), pp. 1553-1573.

Luscombe, N. M. et al. 2004. Genomic analysis of regulatory network dynamics reveals large topological changes. *Nature* 431(7006), pp. 308-312.

Malik, S. et al. 2008. Elongating RNA polymerase II is disassembled through specific degradation of its largest but not other subunits in response to DNA damage in vivo. *J Biol Chem* 283(11), pp. 6897-6905.

Marahrens, Y. and Stillman, B. 1992. A yeast chromosomal origin of DNA replication defined by multiple functional elements. *Science* 255(5046), pp. 817-823.

Martinez-Pastor, M. T. et al. 1996. The Saccharomyces cerevisiae zinc finger proteins Msn2p and Msn4p are required for transcriptional induction through the stress response element (STRE). *Embo J* 15(9), pp. 2227-2235.

Masutani, C. et al. 1997. Identification and characterization of XPC-binding domain of hHR23B. *Mol Cell Biol* 17(12), pp. 6915-6923.

Maxwell, P. H. et al. 2004. Ty1 mobilizes subtelomeric Y' elements in telomerase-negative Saccharomyces cerevisiae survivors. *Mol Cell Biol* 24(22), pp. 9887-9898.

Mazur, S. J. and Grossman, L. 1991. Dimerization of Escherichia coli UvrA and its binding to undamaged and ultraviolet light damaged DNA. *Biochemistry* 30(18), pp. 4432-4443.

Mello, J. A. et al. 2002. Human Asf1 and CAF-1 interact and synergize in a repair-coupled nucleosome assembly pathway. *EMBO Rep* 3(4), pp. 329-334.

Melo, J. A. et al. 2001. Two checkpoint complexes are independently recruited to sites of DNA damage in vivo. *Genes Dev* 15(21), pp. 2809-2821.

Michel, B. 2005. After 30 years of study, the bacterial SOS response still surprises us. *PLoS Biol* 3(7), p. e255.

Mimitou, E. P. and Symington, L. S. 2008. Sae2, Exo1 and Sgs1 collaborate in DNA double-strand break processing. *Nature* 455(7214), pp. 770-774.

Min, J. H. and Pavletich, N. P. 2007. Recognition of DNA damage by the Rad4 nucleotide excision repair protein. *Nature* 449(7162), pp. 570-575.

Mitchell, D. L. 1988. The relative cytotoxicity of (6-4) photoproducts and cyclobutane dimers in mammalian cells. *Photochem Photobiol* 48(1), pp. 51-57.

Mitchell, D. L. et al. 1992. Sequence specificity of cyclobutane pyrimidine dimers in DNA treated with solar (ultraviolet B) radiation. *Nucleic Acids Res* 20(2), pp. 225-229.

Mitchell, D. L. and Nairn, R. S. 1989. The biology of the (6-4) photoproduct. *Photochem Photobiol* 49(6), pp. 805-819.

Mitchell, D. L. et al. 1990. Nonrandom induction of pyrimidine-pyrimidone (6-4) photoproducts in ultraviolet-irradiated human chromatin. *J Biol Chem* 265(10), pp. 5353-5356.

Miyake, T. et al. 2002. Identification of a multifunctional domain in autonomously replicating sequence-binding factor 1 required for transcriptional activation, DNA replication, and gene silencing. *Mol Cell Biol* 22(2), pp. 505-516.

Miyake, T. et al. 2004. Genome-wide analysis of ARS (autonomously replicating sequence) binding factor 1 (Abf1p)-mediated transcriptional regulation in Saccharomyces cerevisiae. *J Biol Chem* 279(33), pp. 34865-34872.

Modrich, P. and Lahue, R. 1996. Mismatch repair in replication fidelity, genetic recombination, and cancer biology. *Annu Rev Biochem* 65, pp. 101-133.

Murata, S. et al. 2009. Molecular mechanisms of proteasome assembly. *Nat Rev Mol Cell Biol* 10(2), pp. 104-115.

Nakayama, K. I. and Nakayama, K. 2006. Ubiquitin ligases: cell-cycle control and cancer. *Nat Rev Cancer* 6(5), pp. 369-381.

Nalley, K. et al. 2006. Proteolytic turnover of the Gal4 transcription factor is not required for function in vivo. *Nature* 442(7106), pp. 1054-1057.

Naumovski, L. and Friedberg, E. C. 1983. A DNA repair gene required for the incision of damaged DNA is essential for viability in Saccharomyces cerevisiae. *Proc Natl Acad Sci U S A* 80(15), pp. 4818-4821.

Neecke, H. et al. 1999. Cell cycle progression in the presence of irreparable DNA damage is controlled by a Mec1- and Rad53-dependent checkpoint in budding yeast. *Embo J* 18(16), pp. 4485-4497.

Ng, J. M. et al. 2003. A novel regulation mechanism of DNA repair by damage-induced and RAD23-dependent stabilization of xeroderma pigmentosum group C protein. *Genes Dev* 17(13), pp. 1630-1645.

Niida, H. and Nakanishi, M. 2006. DNA damage checkpoints in mammals. *Mutagenesis* 21(1), pp. 3-9.

Nouspikel, T. 2009. DNA repair in mammalian cells : Nucleotide excision repair: variations on versatility. *Cell Mol Life Sci* 66(6), pp. 994-1009.

Nyswaner, K. M. et al. 2008. Chromatin-associated genes protect the yeast genome from Ty1 insertional mutagenesis. *Genetics* 178(1), pp. 197-214.

O'Neill, T. et al. 2002. Determination of substrate motifs for human Chk1 and hCds1/Chk2 by the oriented peptide library approach. *J Biol Chem* 277(18), pp. 16102-16115.

Olsson, M. and Lindahl, T. 1980. Repair of alkylated DNA in Escherichia coli. Methyl group transfer from O6-methylguanine to a protein cysteine residue. *J Biol Chem* 255(22), pp. 10569-10571.

Orphanides, G. et al. 1999. The chromatin-specific transcription elongation factor FACT comprises human SPT16 and SSRP1 proteins. *Nature* 400(6741), pp. 284-288.

Ozsarac, N. et al. 1997. Regulation of gene expression during meiosis in Saccharomyces cerevisiae: SPR3 is controlled by both ABFI and a new sporulation control element. *Mol Cell Biol* 17(3), pp. 1152-1159.

Paciotti, V. et al. 2000. The checkpoint protein Ddc2, functionally related to S. pombe Rad26, interacts with Mec1 and is regulated by Mec1-dependent phosphorylation in budding yeast. *Genes Dev* 14(16), pp. 2046-2059.

Paciotti, V. et al. 2001. Characterization of mec1 kinase-deficient mutants and of new hypomorphic mec1 alleles impairing subsets of the DNA damage response pathway. *Mol Cell Biol* 21(12), pp. 3913-3925.

Park, E. et al. 1992. RAD25 (SSL2), the yeast homolog of the human xeroderma pigmentosum group B DNA repair gene, is essential for viability. *Proc Natl Acad Sci U S A* 89(23), pp. 11416-11420.

Park, H. D. et al. 1999. Synergistic operation of the CAR2 (Ornithine transaminase) promoter elements in Saccharomyces cerevisiae. *J Bacteriol* 181(22), pp. 7052-7064.

Paull, T. T. et al. 2000. A critical role for histone H2AX in recruitment of repair factors to nuclear foci after DNA damage. *Curr Biol* 10(15), pp. 886-895.

Pearlman, D. A. et al. 1985. Molecular models for DNA damaged by photoreaction. *Science* 227(4692), pp. 1304-1308.

Pegg, A. E. 2000. Repair of O(6)-alkylguanine by alkyltransferases. *Mutat Res* 462(2-3), pp. 83-100.

Peng, G. and Hopper, J. E. 2002. Gene activation by interaction of an inhibitor with a cytoplasmic signaling protein. *Proc Natl Acad Sci U S A* 99(13), pp. 8548-8553.

Perlstein, D. L. et al. 2005. The active form of the Saccharomyces cerevisiae ribonucleotide reductase small subunit is a heterodimer in vitro and in vivo. *Biochemistry* 44(46), pp. 15366-15377.

Petersen, J. and Hagan, I. M. 2005. Polo kinase links the stress pathway to cell cycle control and tip growth in fission yeast. *Nature* 435(7041), pp. 507-512.

Peterson, C. L. and Cote, J. 2004. Cellular machineries for chromosomal DNA repair. *Genes Dev* 18(6), pp. 602-616.

Pickart, C. M. and Cohen, R. E. 2004. Proteasomes and their kin: proteases in the machine age. *Nat Rev Mol Cell Biol* 5(3), pp. 177-187.

Pintard, L. et al. 2004. Cullin-based ubiquitin ligases: Cul3-BTB complexes join the family. *Embo J* 23(8), pp. 1681-1687.

Planta, R. J. 1997. Regulation of ribosome synthesis in yeast. *Yeast* 13(16), pp. 1505-1518.

Prakash, S. et al. 2005. Eukaryotic translesion synthesis DNA polymerases: specificity of structure and function. *Annu Rev Biochem* 74, pp. 317-353.

Prakash, S. and Prakash, L. 2000. Nucleotide excision repair in yeast. *Mutat Res* 451(1-2), pp. 13-24.

Qiu, H. et al. 1993. The Saccharomyces cerevisiae DNA repair gene RAD25 is required for transcription by RNA polymerase II. *Genes Dev* 7(11), pp. 2161-2171.

Radman, M. 1975. SOS repair hypothesis: phenomenology of an inducible DNA repair which is accompanied by mutagenesis. *Basic Life Sci* 5A, pp. 355-367.

Ralph, E. et al. 2006. DNA damage induces Cdt1 proteolysis in fission yeast through a pathway dependent on Cdt2 and Ddb1. *EMBO Rep* 7(11), pp. 1134-1139.

Ramsey, K. L. et al. 2004. The NEF4 complex regulates Rad4 levels and utilizes Snf2/Swi2-related ATPase activity for nucleotide excision repair. *Mol Cell Biol* 24(14), pp. 6362-6378.

Rattray, A. J. and Symington, L. S. 1995. Multiple pathways for homologous recombination in Saccharomyces cerevisiae. *Genetics* 139(1), pp. 45-56.

Rechsteiner, M. and Hill, C. P. 2005. Mobilizing the proteolytic machine: cell biological roles of proteasome activators and inhibitors. *Trends Cell Biol* 15(1), pp. 27-33.

Recht, J. et al. 2006. Histone chaperone Asf1 is required for histone H3 lysine 56 acetylation, a modification associated with S phase in mitosis and meiosis. *Proc Natl Acad Sci U S A* 103(18), pp. 6988-6993.

Reed, S. H. et al. 1999. Yeast autonomously replicating sequence binding factor is involved in nucleotide excision repair. *Genes Dev* 13(23), pp. 3052-3058.

Reed, S. H. et al. 1998. The yeast RAD7 and RAD16 genes are required for postincision events during nucleotide excision repair. In vitro and in vivo studies with rad7 and rad16 mutants and purification of a Rad7/Rad16-containing protein complex. *J Biol Chem* 273(45), pp. 29481-29488.

Reichard, P. et al. 2000. Cross-talk between the allosteric effector-binding sites in mouse ribonucleotide reductase. *J Biol Chem* 275(42), pp. 33021-33026.

Rhode, P. R. et al. 1992. Role of multifunctional autonomously replicating sequence binding factor 1 in the initiation of DNA replication and transcriptional control in Saccharomyces cerevisiae. *Mol Cell Biol* 12(3), pp. 1064-1077.

Richardson, H. et al. 1992. Cyclin-B homologs in Saccharomyces cerevisiae function in S phase and in G2. *Genes Dev* 6(11), pp. 2021-2034.

Rouse, J. and Jackson, S. P. 2002. Lcd1p recruits Mec1p to DNA lesions in vitro and in vivo. *Mol Cell* 9(4), pp. 857-869.

Ruby, S. W. and Szostak, J. W. 1985. Specific Saccharomyces cerevisiae genes are expressed in response to DNA-damaging agents. *Mol Cell Biol* 5(1), pp. 75-84.

Russell, S. J. et al. 2001. Selective chemical inactivation of AAA proteins reveals distinct functions of proteasomal ATPases. *Chem Biol* 8(10), pp. 941-950.

Russell, S. J. and Johnston, S. A. 2001. Evidence that proteolysis of Gal4 cannot explain the transcriptional effects of proteasome ATPase mutations. *J Biol Chem* 276(13), pp. 9825-9831.

Russell, S. J. et al. 1999. The 19S regulatory complex of the proteasome functions independently of proteolysis in nucleotide excision repair. *Mol Cell* 3(6), pp. 687-695.

Russell, S. J. et al. 1996. Isolation and characterization of SUG2. A novel ATPase family component of the yeast 26 S proteasome. *J Biol Chem* 271(51), pp. 32810-32817.

Sabouri, N. et al. 2008. Evidence for lesion bypass by yeast replicative DNA polymerases during DNA damage. *Nucleic Acids Res* 36(17), pp. 5660-5667.

Saeki, Y. et al. 2002. Identification of ubiquitin-like protein-binding subunits of the 26S proteasome. *Biochem Biophys Res Commun* 296(4), pp. 813-819.

Salghetti, S. E. et al. 2001. Regulation of transcriptional activation domain function by ubiquitin. *Science* 293(5535), pp. 1651-1653.

Sancar, G. B. et al. 1995. Promoter elements of the PHR1 gene of Saccharomyces cerevisiae and their roles in the response to DNA damage. *Nucleic Acids Res* 23(21), pp. 4320-4328.

Sanchez, Y. et al. 1996. Regulation of RAD53 by the ATM-like kinases MEC1 and TEL1 in yeast cell cycle checkpoint pathways. *Science* 271(5247), pp. 357-360.

Schauber, C. et al. 1998. Rad23 links DNA repair to the ubiquitin/proteasome pathway. *Nature* 391(6668), pp. 715-718.

Schlecht, U. et al. 2008. Genome-wide expression profiling, in vivo DNA binding analysis, and probabilistic motif prediction reveal novel Abf1 target genes during fermentation, respiration, and sporulation in yeast. *Mol Biol Cell* 19(5), pp. 2193-2207.

Schmidt, M. et al. 2005. Proteasome-associated proteins: regulation of a proteolytic machine. *Biol Chem* 386(8), pp. 725-737.

Schmitt, M. E. et al. 1990. A rapid and simple method for preparation of RNA from Saccharomyces cerevisiae. *Nucleic Acids Res* 18(10), pp. 3091-3092.

Schwob, E. and Nasmyth, K. 1993. CLB5 and CLB6, a new pair of B cyclins involved in DNA replication in Saccharomyces cerevisiae. *Genes Dev* 7(7A), pp. 1160-1175.

Searle, J. S. et al. 2004. The DNA damage checkpoint and PKA pathways converge on APC substrates and Cdc20 to regulate mitotic progression. *Nat Cell Biol* 6(2), pp. 138-145.

Seeberg, E. et al. 1995. The base excision repair pathway. *Trends Biochem Sci* 20(10), pp. 391-397.

Selby, C. P. and Sancar, A. 1993. Transcription-repair coupling and mutation frequency decline. *J Bacteriol* 175(23), pp. 7509-7514.

Setlow, R. B. and Carrier, W. L. 1964. The Disappearance of Thymine Dimers from DNA: an Error-Correcting Mechanism. *Proc Natl Acad Sci U S A* 51, pp. 226-231.

Sharma, V. M. et al. 2007. Histone deacetylases RPD3 and HOS2 regulate the transcriptional activation of DNA damage-inducible genes. *Mol Cell Biol* 27(8), pp. 3199-3210.

Sharp, J. A. et al. 2001. Yeast histone deposition protein Asf1p requires Hir proteins and PCNA for heterochromatic silencing. *Curr Biol* 11(7), pp. 463-473.

Shiozaki, K. et al. 1998. Heat stress activates fission yeast Spc1/Styl MAPK by a MEKK-independent mechanism. *Mol Biol Cell* 9(6), pp. 1339-1349.

Shroff, R. et al. 2004. Distribution and dynamics of chromatin modification induced by a defined DNA double-strand break. *Curr Biol* 14(19), pp. 1703-1711.

Sidorova, J. M. and Breeden, L. L. 1997. Rad53-dependent phosphorylation of Swi6 and down-regulation of CLN1 and CLN2 transcription occur in response to DNA damage in Saccharomyces cerevisiae. *Genes Dev* 11(22), pp. 3032-3045.

Sikorski, R. S. and Hieter, P. 1989. A system of shuttle vectors and yeast host strains designed for efficient manipulation of DNA in Saccharomyces cerevisiae. *Genetics* 122(1), pp. 19-27.

Smith, D. M. et al. 2006. Proteasomes and their associated ATPases: a destructive combination. *J Struct Biol* 156(1), pp. 72-83.

Smolka, M. B. et al. 2005. Dynamic changes in protein-protein interaction and protein phosphorylation probed with amine-reactive isotope tag. *Mol Cell Proteomics* 4(9), pp. 1358-1369.

Soto, T. et al. 2007. Transduction of centrifugation-induced gravity forces through mitogen-activated protein kinase pathways in the fission yeast Schizosaccharomyces pombe. *Microbiology* 153(Pt 5), pp. 1519-1529.

Soulier, J. and Lowndes, N. F. 1999. The BRCT domain of the S. cerevisiae checkpoint protein Rad9 mediates a Rad9-Rad9 interaction after DNA damage. *Curr Biol* 9(10), pp. 551-554.

Spellman, P. T. et al. 1998. Comprehensive identification of cell cycle-regulated genes of the yeast Saccharomyces cerevisiae by microarray hybridization. *Mol Biol Cell* 9(12), pp. 3273-3297.

Stinchcomb, D. T. et al. 1979. Isolation and characterisation of a yeast chromosomal replicator. *Nature* 282(5734), pp. 39-43.

Sturn, A. et al. 2002. Genesis: cluster analysis of microarray data. *Bioinformatics* 18(1), pp. 207-208.

Sugasawa, K. 2006. UV-induced ubiquitylation of XPC complex, the UV-DDB-ubiquitin ligase complex, and DNA repair. *J Mol Histol* 37(5-7), pp. 189-202.

Sugasawa, K. et al. 1997. Two human homologs of Rad23 are functionally interchangeable in complex formation and stimulation of XPC repair activity. *Mol Cell Biol* 17(12), pp. 6924-6931.

Sun, Z. et al. 1998. Rad53 FHA domain associated with phosphorylated Rad9 in the DNA damage checkpoint. *Science* 281(5374), pp. 272-274.

Svejstrup, J. Q. 2007. Contending with transcriptional arrest during RNAPII transcript elongation. *Trends Biochem Sci* 32(4), pp. 165-171.

Swaffield, J. C. et al. 1992. Alterations in a yeast protein resembling HIV Tat-binding protein relieve requirement for an acidic activation domain in GAL4. *Nature* 360(6406), p. 768.

Sweet, D. H. et al. 1997. Role of UME6 in transcriptional regulation of a DNA repair gene in Saccharomyces cerevisiae. *Mol Cell Biol* 17(11), pp. 6223-6235.

Symington, M. J. et al. 1996. Neostigmine but not edrophonium prolongs the action of mivacurium. *Can J Anaesth* 43(12), pp. 1220-1223.

Tang, H. M. et al. 2009. Loss of yeast peroxiredoxin Tsa1p induces genome instability through activation of the DNA damage checkpoint and elevation of dNTP levels. *PLoS Genet* 5(10), p. e1000697.

Taschner, M. et al. A role for checkpoint kinase-dependent Rad26 phosphorylation in transcription-coupled DNA repair in Saccharomyces cerevisiae. *Mol Cell Biol* 30(2), pp. 436-446.

Team, R. D. C. 2010. R: A Language and Environment for Statistical Computing. *R Foundation for Statistical Computing.*

Teng, Y. et al. 2008. Saccharomyces cerevisiae Rad16 mediates ultraviolet-dependent histone H3 acetylation required for efficient global genome nucleotide-excision repair. *EMBO Rep* 9(1), pp. 97-102.

Theis, J. F. and Newlon, C. S. 1997. The ARS309 chromosomal replicator of Saccharomyces cerevisiae depends on an exceptional ARS consensus sequence. *Proc Natl Acad Sci U S A* 94(20), pp. 10786-10791.

Thoma, F. 1999. Light and dark in chromatin repair: repair of UV-induced DNA lesions by photolyase and nucleotide excision repair. *Embo J* 18(23), pp. 6585-6598.

Thrower, J. S. et al. 2000. Recognition of the polyubiquitin proteolytic signal. *Embo J* 19(1), pp. 94-102.

Toker, A. and Cantley, L. C. 1997. Signalling through the lipid products of phosphoinositide-3-OH kinase. *Nature* 387(6634), pp. 673-676.

Toulmay, A. and Schneiter, R. 2006. A two-step method for the introduction of single or multiple defined point mutations into the genome of Saccharomyces cerevisiae. *Yeast* 23(11), pp. 825-831.

Toussaint, M. et al. 2005. Limited TTP supply affects telomere length regulation in a telomerase-independent fashion. *Nucleic Acids Res* 33(2), pp. 704-713.

Traven, A. and Heierhorst, J. 2005. SQ/TQ cluster domains: concentrated ATM/ATR kinase phosphorylation site regions in DNA-damage-response proteins. *Bioessays* 27(4), pp. 397-407.

Traven, A. et al. 2006. Yeast Gal4: a transcriptional paradigm revisited. *EMBO Rep* 7(5), pp. 496-499.

Tremblay, M. et al. 2008. Complementary roles of yeast Rad4p and Rad34p in nucleotide excision repair of active and inactive rRNA gene chromatin. *Mol Cell Biol* 28(24), pp. 7504-7513.

Tringe, S. G. et al. 2006. The WTM genes in budding yeast amplify expression of the stress-inducible gene RNR3. *Genetics* 174(3), pp. 1215-1228.

Truglio, J. J. et al. 2006. Prokaryotic nucleotide excision repair: the UvrABC system. *Chem Rev* 106(2), pp. 233-252.

Tyler, J. K. et al. 1999. The RCAF complex mediates chromatin assembly during DNA replication and repair. *Nature* 402(6761), pp. 555-560.

Usui, T. et al. 2006. Rad50S alleles of the Mre11 complex: questions answered and questions raised. *Exp Cell Res* 312(14), pp. 2694-2699.

van Gool, A. J. et al. 1994. RAD26, the functional S. cerevisiae homolog of the Cockayne syndrome B gene ERCC6. *Embo J* 13(22), pp. 5361-5369.

Venditti, P. et al. 1994. ABFI contributes to the chromatin organization of Saccharomyces cerevisiae ARS1 B-domain. *Biochim Biophys Acta* 1219(3), pp. 677-689.

Verhage, R. A. et al. 1996. Repair of rDNA in Saccharomyces cerevisiae: RAD4-independent strand-specific nucleotide excision repair of RNA polymerase I transcribed genes. *Nucleic Acids Res* 24(6), pp. 1020-1025.

Wade, S. L. et al. 2009. The Snf1 kinase and proteasome-associated Rad23 regulate UV-responsive gene expression. *Embo J* 28(19), pp. 2919-2931.

Walters, K. J. et al. 2002. Structural studies of the interaction between ubiquitin family proteins and proteasome subunit S5a. *Biochemistry* 41(6), pp. 1767-1777.

Wang, H. et al. 2001. Pds1 phosphorylation in response to DNA damage is essential for its DNA damage checkpoint function. *Genes Dev* 15(11), pp. 1361-1372.

Wang, P. J. et al. 1997a. Rnr4p, a novel ribonucleotide reductase small-subunit protein. *Mol Cell Biol* 17(10), pp. 6114-6121.

Wang, X. et al. 2008. Disruption of Rpn4-induced proteasome expression in Saccharomyces cerevisiae reduces cell viability under stressed conditions. *Genetics* 180(4), pp. 1945-1953.

Wang, Z. et al. 1997b. The RAD7, RAD16, and RAD23 genes of Saccharomyces cerevisiae: requirement for transcription-independent nucleotide excision repair in vitro and interactions between the gene products. *Mol Cell Biol* 17(2), pp. 635-643.

Watanabe, C. M. et al. 2002. Transcriptional effects of the potent enediyne anti-cancer agent Calicheamicin gamma(I)(1). *Chem Biol* 9(2), pp. 245-251.

Waters, R. et al. 1993. Inducible removal of UV-induced pyrimidine dimers from transcriptionally active and inactive genes of Saccharomyces cerevisiae. *Mol Gen Genet* 239(1-2), pp. 28-32.

Weber, S. 2005. Light-driven enzymatic catalysis of DNA repair: a review of recent biophysical studies on photolyase. *Biochim Biophys Acta* 1707(1), pp. 1-23.

Weinert, T. A. and Hartwell, L. H. 1988. The RAD9 gene controls the cell cycle response to DNA damage in Saccharomyces cerevisiae. *Science* 241(4863), pp. 317-322.

Werner-Washburne, M. et al. 1993. Stationary phase in the yeast Saccharomyces cerevisiae. *Microbiol Rev* 57(2), pp. 383-401.

Werner-Washburne, M. et al. 1996. Stationary phase in Saccharomyces cerevisiae. *Mol Microbiol* 19(6), pp. 1159-1166.

Willems, A. R. et al. 2004. A hitchhiker's guide to the cullin ubiquitin ligases: SCF and its kin. *Biochim Biophys Acta* 1695(1-3), pp. 133-170.

Wilson, C., Pepper, S. D., Miller, C. J. QC and Affymetrix data.

Wiltshire, S. et al. 1997. An Abf1p C-terminal region lacking transcriptional activation potential stimulates a yeast origin of replication. *Nucleic Acids Res* 25(21), pp. 4250-4256.

Woolstencroft, R. N. et al. 2006. Ccr4 contributes to tolerance of replication stress through control of CRT1 mRNA poly(A) tail length. *J Cell Sci* 119(Pt 24), pp. 5178-5192.

Wu, X. et al. 1999. DNA ligation during excision repair in yeast cell-free extracts is specifically catalyzed by the CDC9 gene product. *Biochemistry* 38(9), pp. 2628-2635.

Xu, Q. et al. 1995. Sug1 modulates yeast transcription activation by Cdc68. *Mol Cell Biol* 15(11), pp. 6025-6035.

Yamada, M. et al. 1998. Y'-Help1, a DNA helicase encoded by the yeast subtelomeric Y' element, is induced in survivors defective for telomerase. *J Biol Chem* 273(50), pp. 33360-33366.

Yang, C. et al. 1999. Conservation of ARS elements and chromosomal DNA replication origins on chromosomes III of Saccharomyces cerevisiae and S. carlsbergensis. *Genetics* 152(3), pp. 933-941.

Yarragudi, A. et al. 2007. Genome-wide analysis of transcriptional dependence and probable target sites for Abf1 and Rap1 in Saccharomyces cerevisiae. *Nucleic Acids Res* 35(1), pp. 193-202.

Yasui, A. et al. 1994. A new class of DNA photolyases present in various organisms including aplacental mammals. *Embo J* 13(24), pp. 6143-6151.

Yu, S. et al. 2004. The yeast Rad7/Rad16/Abf1 complex generates superhelical torsion in DNA that is required for nucleotide excision repair. *DNA Repair (Amst)* 3(3), pp. 277-287.

Yu, S. et al. 2009. ABF1-binding sites promote efficient global genome nucleotide excision repair. *J Biol Chem* 284(2), pp. 966-973.

Zaim, J. et al. 2005. Identification of new genes regulated by the Crt1 transcription factor, an effector of the DNA damage checkpoint pathway in Saccharomyces cerevisiae. *J Biol Chem* 280(1), pp. 28-37.

Zakian, V. A. 1996. Structure, function, and replication of Saccharomyces cerevisiae telomeres. *Annu Rev Genet* 30, pp. 141-172.

Zhang, Z. and Reese, J. C. 2005. Molecular genetic analysis of the yeast repressor Rfx1/Crt1 reveals a novel two-step regulatory mechanism. *Mol Cell Biol* 25(17), pp. 7399-7411.

Zhao, X. et al. 1998. A suppressor of two essential checkpoint genes identifies a novel protein that negatively affects dNTP pools. *Mol Cell* 2(3), pp. 329-340.

Zhao, X. and Rothstein, R. 2002. The Dun1 checkpoint kinase phosphorylates and regulates the ribonucleotide reductase inhibitor Sml1. *Proc Natl Acad Sci U S A* 99(6), pp. 3746-3751.

Zhu, Y. and Xiao, W. 2004. Pdr3 is required for DNA damage induction of MAG1 and DDI1 via a bi-directional promoter element. *Nucleic Acids Res* 32(17), pp. 5066-5075.

Zou, L. and Elledge, S. J. 2003. Sensing DNA damage through ATRIP recognition of RPA-ssDNA complexes. *Science* 300(5625), pp. 1542-1548.

Zou, Y. et al. 2006. Asymmetric positioning of nucleosomes and directional establishment of transcriptionally silent chromatin by Saccharomyces cerevisiae silencers. *Mol Cell Biol* 26(20), pp. 7806-7819.

Appendix I – Growth Media, Solutions and Buffers

Growth Media

All media listed require autoclave sterilisation for 20-30 minutes at 15 psi.

YNDB Minimal Medium (1L)
Yeast Nitrogen Base (without amino acids) – 7.2g
Glucose – 20g
Bacto-Agar (for solid media) – 20g
Appropriate Amino Acid Selection Mix – 0.85g
H_2O to final volume

YPD Complex Medium (1000ml)
Yeast Extract – 10g
Bacto-Peptone – 20g
Glucose – 20g
Bacto-Agar (for solid media) – 20g
H_2O to final volume

Amino Acid Dry Mix – (To Supplement 50L Minimal Media)
Argenine – 1g
Methionine – 1g
Tyrosine – 1.5g
Isoleucine – 1.5g
Lysine HCl – 1.5g
Phenylalanine – 2.5g
Glutamic Acid – 5g
Aspartic Acid – 5g
Valine – 7.5g
Threonine – 10g
Serine – 20g
*Tryptophan – 4g
*Leucine – 5g
*Adenine – 1g
*Uracil – 1g
*Histidine – 3g

*Essential amino acids can be omitted to produce selective media
Ensure Dry Mix is thoroughly mixed before use.

Stock Solutions and Buffers

All stock solutions are sterilised by autoclave unless otherwise stated

SDS-PAGE and Western Blotting

Yeast Dialysis Buffer (1L)
    1M Hepes-KOH – 20ml
    0.5M EDTA – 20ml
    $MgSO_4$ – 1.2g
    Glycerol – 100ml
    H_2O to final volume
    *DTT – 5ml
    *Proteinase Inhibitors – 10ml
        *Add immediately before use

10x TBST (1L)
    1M Tris-Base (pH 8.0) – 100ml
    NaCl – 87.66g
    Tween 20 – 5ml
    H_2O to final volume

10x SDS Running Buffer (1L)
    Tris-Base – 30.3g
    Glycine – 144.2g
    SDS – 10g
    H_2O to final volume
        Adjust pH to 8.3

Western Transfer Buffer (2L)
    Tris-Base – 6.06g
    Glycine – 22.6g
    SDS – 0.3g
    Methanol – 400ml
    H_2O to final volume

Western Membrane Stripping Solution (100ml)
    2-Mercaptoethanol – 694μl
    SDS – 2g
    1M Tris-HCl pH 6.7 – 62.5ml
    H_2O to final volume

RNA Extraction and Northern Blotting

RNA Lysis Buffer (1L)
Tris-Base – 1.21g
0.5M EDTA – 20ml
SDS – 5g
H_2O to final volume

10x FA Gel Buffer (500ml)
3-[N-Morpholino]propanesulfonic acid (MOPS) – 20.9g
3M NaAc – 8.2ml
0.5M EDTA – 10ml
RNase-free H_2O to final volume
Adjust pH to 7.0

20x SSC (1L)
NaCl – 175.3g
Na Citrate.$2H_2O$ – 88.2g
H_2O to final volume
Adjust pH to 7.0

2x Binding and Washing (BW) Buffer (100ml)
NaCl – 11.6g
1M Tris-HCl pH 8.0 – 1ml
0.5M EDTA – 0.2ml

Hybridisation Solution (250ml)
BSA – 2.5g
1M Phosphate Buffer – 125ml
20% SDS – 87.5ml
0.5M EDTA – 0.5ml
H_2O to final volume

1M Phosphate Buffer
71g Na_2HPO_4
(or 89g $Na_2HPO_4.2H_2O$
or 134g $Na_2HPO_4.7 H_2O$)
4ml 85% H_3PO_4
H_2O to final volume

1M DTT (Dithiothreitol) (20ml)
Dissolve 3.09g DTT in 20ml 0.01M Sodium Acetate (pH 5.2)
Filter-sterilise (do not autoclave)

Chromatin Extraction

ChIP lysis Buffer (1L)

1M HEPES-KOH pH 7.5 – 50ml
5M NaCl – 28ml
0.5 EDTA – 2ml
10% Triton X-100 – 100ml
5% Na-deoxycholate – 20ml
1mM PMSF, 1mM Benzamidine (100x stock)
10μg/ml Aprotinin, 1μg/ml Leupeptin (100x stock)
1μg/ml Pepstatin (100x stock) – 10ml of each
H_2O to final volume

Other Stock Solutions and Buffers

Sodium Citrate Buffer (1L)

Na_3Citrate – 12.9g
Adjust pH to 7.0

10x TE (100ml)

1M Tris-HCl pH 7.5 – 10ml
0.5M EDTA pH 8.0 – 4ml
H_2O to final volume

10x LiAc (100ml)

LiAc – 10.9g
H_2O to final volume
Adjust to pH 7.5

Phosphate-Buffered Saline (PBS) (1L)

NaCl – 8g
KCl – 0.2g
Na_2HPO_4 – 1.44g
(or $Na_2HPO_4.2H_2O$ – 1.8g)
H_2O to final volume
Adjust pH to 7.4

DNA Lysis Buffer (1L)
   Urea – 240g
   NaCl – 11.7g
   EDTA – 5g
   SDS – 5g
   H_2O to final volume

50x TAE (1L)
   Tris Base – 242g
   NaAc.$3H_2O$ – 136g
   0.5M EDTA – 200ml
   H_2O to final volume
         Adjust pH to 7.2

0.5M EDTA (Ethylenediaminetetraacetic acid) (1L)
   EDTA.Na_2.$2H_2O$ – 186.7g
   H_2O to final volume
               Adjust pH to 8.0

Appendix II – UV Survival Data

Chapter 2 UV Survival (Figure 3.8)

Strain	UV Dose (Jm⁻²)	Count 1	Count 2	Count 3	Mean Count	Standard Deviation	% Survival
WT	0	271	292	279	280.7	10.6	100.0
	10	222	269	245	245.3	23.5	87.4
	20	165.5	158.5	187	170.3	14.9	60.7
	30	85	73.6	97	85.2	11.7	30.4
	40	49.8	51.4	45	48.7	3.3	17.4
	80	32	35.1	33.1	33.4	1.6	11.9
abf1-1	0	265	222	245	244.0	21.5	100.0
	10	236	204	204	214.7	18.5	88.0
	20	122	130.5	124.5	125.7	4.4	51.5
	30	52.4	67.4	79.4	66.4	13.5	27.2
	40	14.9	15	16.7	15.5	1.0	6.4
	80	1.9	2	2.1	2.0	0.1	0.8
abf1-1 sug2-1	0	238	245	240	241.0	3.6	100.0
	10	186	175	168	176.3	9.1	73.2
	20	112	107	100	106.3	6.0	44.1
	30	58.4	52.6	60	57.0	3.9	23.7
	40	22.7	20.5	19.2	20.8	1.8	8.6
	80	1.7	1.5	1.3	1.5	0.2	0.6

Chapter 4 UV Survival (Figure 4.8)

Media	UV Dose (Jm⁻²)	Count 1	Count 2	Mean Count	Standard Deviation	% Survival
PBS	0	100.0	100.0	100.0	0.0	100.0
	50	30.0	28.7	29.3	0.8	29.3
	100	2.22	6.6	4.4	3.1	4.4
	150	0.33	1.0	0.7	0.5	0.7
	200	0.00	0.1	0.04	0.1	0.04
Minimal Media	0	100.0	100.0	100.0	0.0	100.0
	50	66.0	63.6	64.8	1.7	64.8
	100	42.1	41.1	41.6	0.7	41.6
	150	15.2	32.3	23.8	12.1	23.8
	200	11.3	15.6	13.4	3.0	13.4

Chapter 5 UV Survival (Figure 5.3, Figure 5.4 and Figure 5.5)

Strain	UV Dose (Jm⁻²)	Count 1	Count 2	Count 3	Mean Count	Standard Deviation	% Survival
pRAD7	0	256	253	229	246.0	14.8	100.0
	5	239	247	267	251.0	14.4	102.0
	10	241	234	234	236.3	4.0	96.1
	15	221	209	197	209.0	12.0	85.0
	20	207	201	244	217.3	23.3	88.3
psocs	0	127	151	132	136.7	12.7	100.0
	5	117	145	119	127.0	15.6	92.9
	10	123	134	138	131.7	7.8	96.3
	15	140	136	148	141.3	6.1	103.4
	20	100	102	110	104.0	5.3	76.1
pRAD7 Δrad23	0	172	158	148	159.3	12.1	100.0
	5	70	62	74	68.7	6.1	43.1
	10	12	13	9	11.3	2.1	7.1
	15	2.05	3	1.98	2.3	0.6	1.5
	20	0.989	0.102	0.754	0.6	0.5	0.4
psocs Δrad23	0	77	93	85	85.0	8.0	100.0
	5	14.1	13	30.9	19.3	10.0	22.7
	10	2.08	1.25	3.5	2.3	1.1	2.7
	15	0.104	0.081	0.085	0.1	0.01	0.11
	20	0.0122	0.0148	0.0094	0.0	0.00	0.01

Strain	UV Dose (Jm⁻²)	Count 1	Count 2	Count 3	Mean Count	Standard Deviation	% Survival
pRAD7 Δrad23 Δsml1	0	108	123	104	111.7	10.0	100.0
	5	94	58	97	83.0	21.7	74.3
	10	17	16	26	19.7	5.5	17.6
	15	3.15	4.85	5.1	4.4	1.1	3.9
	20	0.257	0.461	0.31	0.3	0.1	0.3
psocs Δrad23 Δsml1	0	99	153	104	118.7	29.8	100.0
	5	78	74	60	70.7	9.5	59.6
	10	3.07	11.1	5.79	6.7	4.1	5.6
	15	2.87	1	2.12	2.0	0.9	1.7
	20	0.241	0.29	0.44	0.3	0.1	0.3

Strain	UV Dose (Jm⁻²)	Count 1	Count 2	Count 3	Mean Count	Standard Deviation	% Survival
pRAD7 Δrad23 Δcrt1	0	305	278	295	292.7	13.7	100.0
	5	313	289	281	294.3	16.7	100.6
	10	147	139	114	133.3	17.2	45.6
	15	39	43	54	45.3	7.8	15.5
	20	21	23	15	19.7	4.2	6.7
psocs Δrad23 Δcrt1	0	194	226	216	212.0	16.4	100.0
	5	131	140	160	143.7	14.8	67.8
	10	88	63	84	78.3	13.4	36.9
	15	16.2	28	25	23.1	6.1	10.9
	20	3.81	8.54	3.3	5.2	2.9	2.5

Appendix III – Budding Index Analysis

To be viewed in conjunction with Chapter 0 Flow Cytometry Data

A3.1   *pRAD7* ( ) & *psocs* ( ) (No UV)

(Figure 6.6)
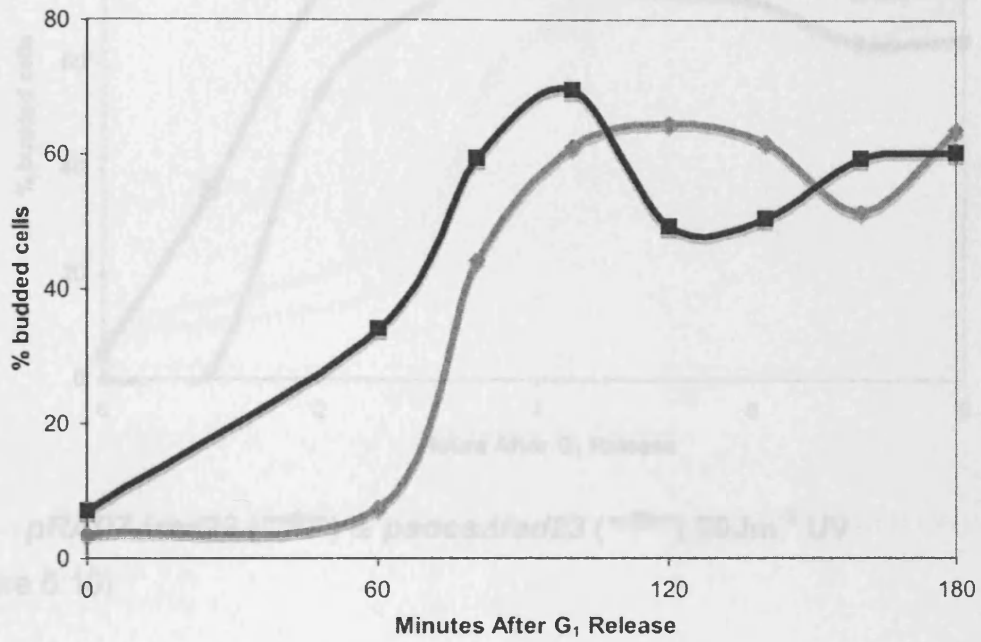
A3.2   *pRAD7 Δrad23* ( ) & *psocs Δrad23* ( ) (No UV)

(Figure 6.7)
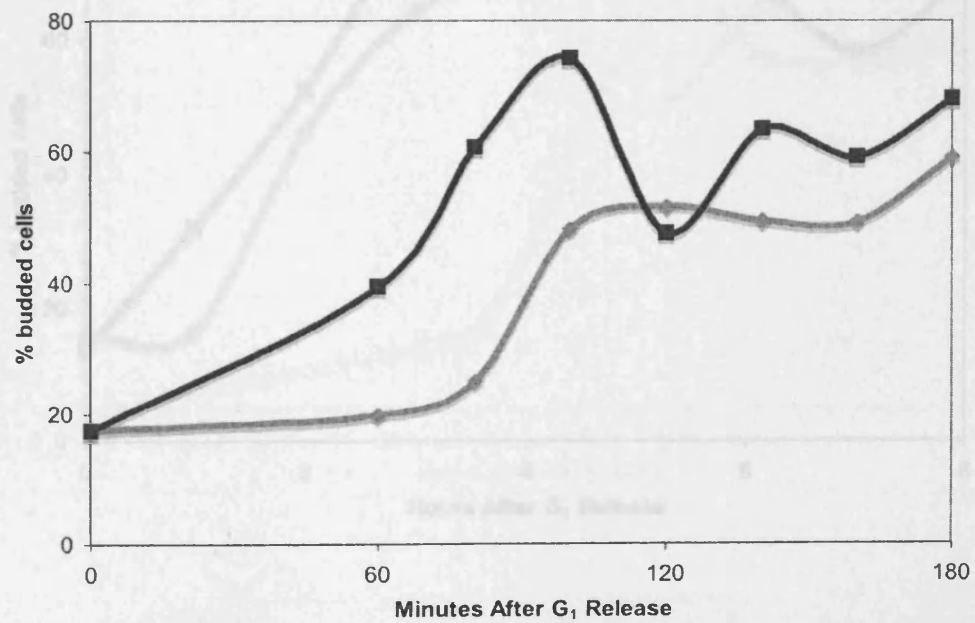
A3.3 *pRAD7* (━━━) & *psocs* (━■━) 100Jm^{-2} UV

(Figure 6.8)
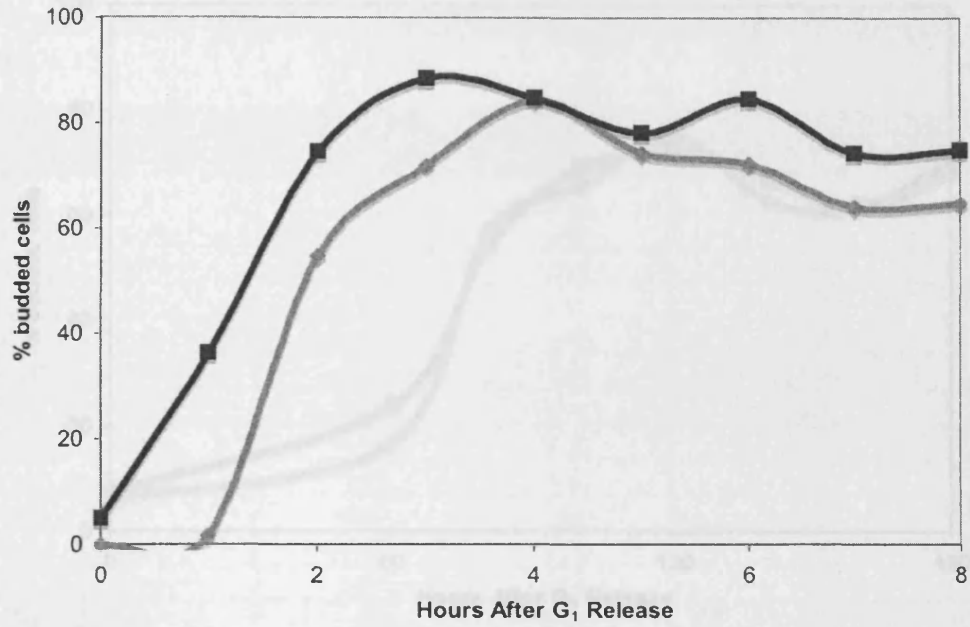
A3.4 *pRAD7Δrad23* (━━━) & *psocsΔrad23* (━■━) 20Jm^{-2} UV
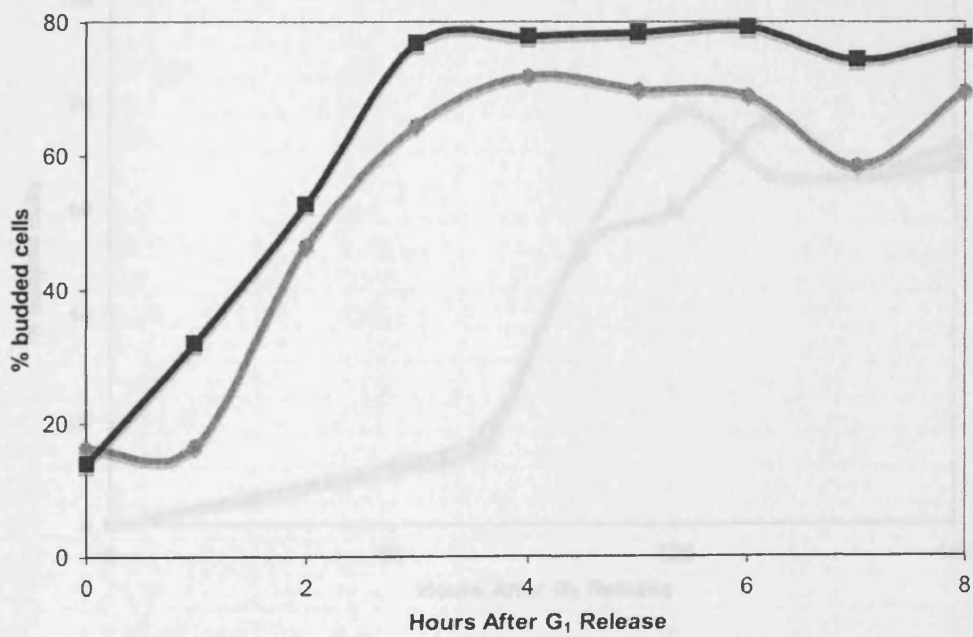
(Figure 6.10)

A3.5 *pRAD7Δrad23Δsml1* () & *psocsΔrad23Δsml1* () (No UV)
(Figure 6.17)
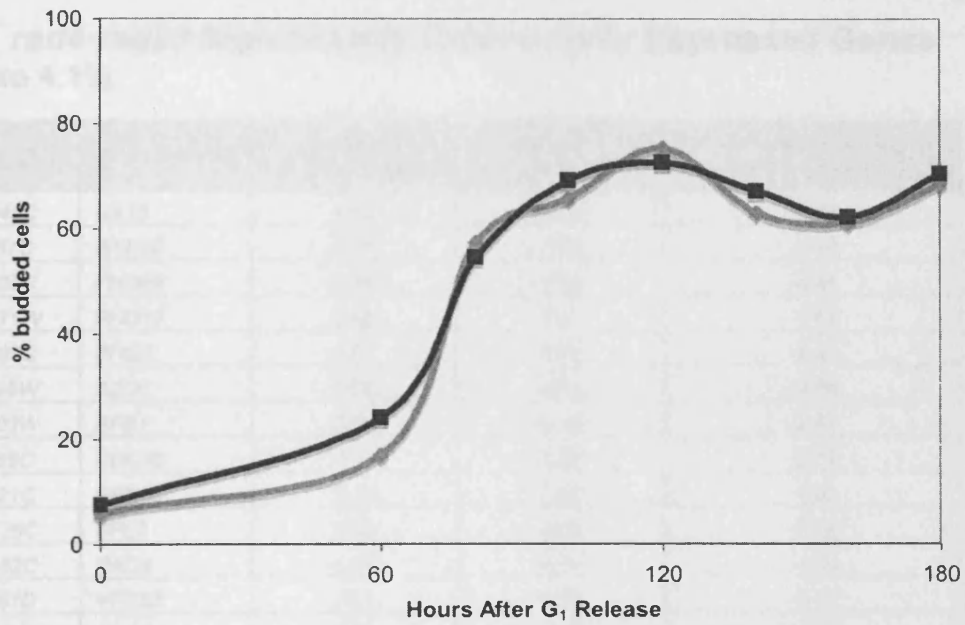
A3.6 *pRAD7Δrad23Δcrt1* () & *psocsΔrad23Δcrt1* () (No UV)
(Figure 6.18)
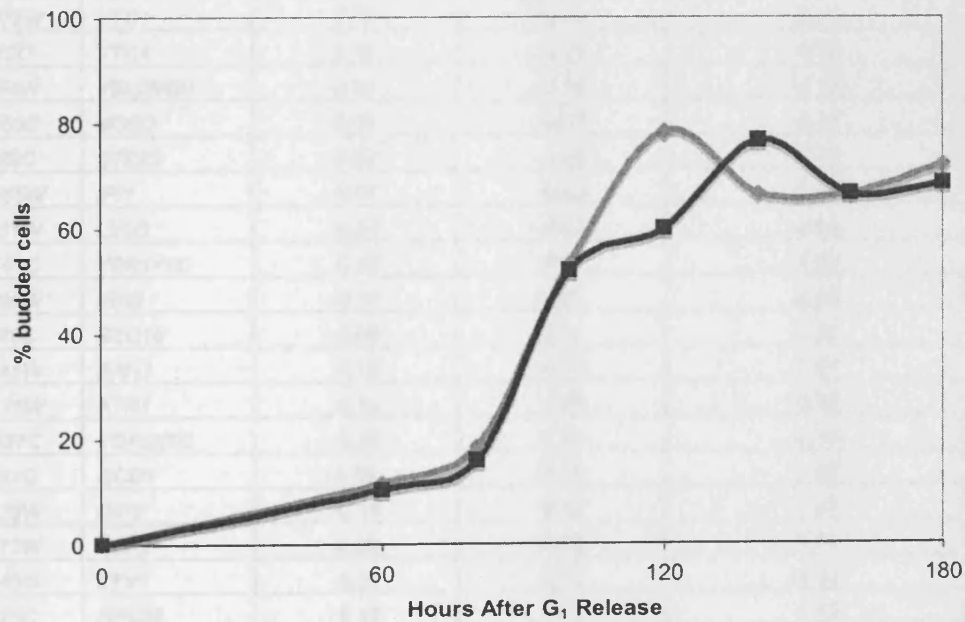
Appendix IV – Gene Lists From Microarray Data

(See also electronic Appendix IV CD with full gene lists and .CEL files)

A4.1 *rad4-rad23* Significantly Differentially Expressed Genes
(Figure 4.13)

Gene ORF	Gene Symbol	*Δrad4*/WT (Fold-Change)	*Δrad23*/WT (Fold-Change)	*Δrad4Δrad23*/WT (Fold-Change)
YDR345C	HXT3	0.02	-5.29	-7.47
YEL037C	RAD23	0.11	-5.05	-5.79
YML123C	PHO84	0.45	-0.03	-4.41
YAR071W	PHO11	0.88	0.35	-1.61
YBR093C	PHO5	0.67	0.09	-2.00
YJR105W	ADO1	0.05	-0.02	-2.64
YAL003W	EFB1	0.07	0.10	-2.47
YLR229C	CDC42	-0.12	0.02	-2.20
YLR421C	RPN13	-0.26	0.00	-1.98
YHR136C	SPL2	0.40	0.06	-3.05
YER162C	RAD4	-0.54	0.74	-1.64
YLR261C	VPS63	0.11	0.24	-1.17
YJR072C	NPA3	0.20	0.16	-1.09
YPL019C	VTC3	0.14	0.15	-1.11
YLR420W	URA4	0.19	0.18	-0.75
YJL193W	YJL193W	0.18	0.22	-0.75
YJL131C	YJL131C	0.22	0.13	-0.67
YJR003C	YJR003C	0.25	0.11	-0.77
YER072W	VTC1	0.12	0.01	-0.71
YJL012C	VTC4	0.12	-0.02	-0.78
YBL054W	YBL054W	0.11	-0.10	-0.73
YNR053C	NOG2	0.01	-0.17	-0.78
YLR389C	STE23	-0.07	-0.09	-0.75
YHR085W	IPI1	-0.07	-0.23	-0.68
YLR451W	LEU3	-0.04	-0.23	-0.66
YBR141C	YBR141C	-0.02	-0.11	-0.60
YLR096W	KIN2	-0.11	0.07	-0.80
YLR166C	SEC10	-0.08	0.07	-0.91
YNL141W	AAH1	-0.18	-0.09	-0.67
YML116W	ATR1	-0.14	0.08	-0.65
YOR287C	YOR287C	-0.12	0.01	-0.66
YLR291C	GCD7	0.06	0.10	-1.69
YLR129W	DIP2	-0.14	0.12	-1.47
YKL172W	EBP2	0.00	0.06	-1.32
YKL143W	LTV1	-0.09	0.14	-1.23
YLR325C	RPL38	-0.10	0.05	-1.12
YJL096W	MRPL49	0.00	0.00	-1.13
YJR104C	SOD1	0.04	0.03	-1.18
YKL060C	FBA1	-0.14	-0.08	-1.22
YKL207W	YKL207W	-0.11	-0.04	-1.25
YJL063C	MRPL8	0.08	-0.18	-1.56

Gene ORF	Gene Symbol	Δrad4/WT (Fold-Change)	Δrad23/WT (Fold-Change)	Δrad4Δrad23/WT (Fold-Change)
YLR063W	YLR063W	-0.01	-0.18	-1.36
YPL263C	KEL3	-0.33	0.10	-0.97
YJL062W	LAS21	-0.08	-0.24	-1.03
YDR281C	PHM6	-0.15	-0.21	-1.17
YKR067W	GPT2	-0.20	-0.06	-1.03
YLR357W	RSC2	-0.18	-0.12	-1.04
YML086C	ALO1	-0.27	-0.14	-1.38
YKR099W	BAS1	-0.24	-0.24	-1.28
YKL002W	DID4	-0.31	-0.30	-1.24
YPL198W	YPL198W	-0.42	-0.08	-1.27
YFL014W	HSP12	-0.48	-1.72	0.88
YML058W	YML058W	-0.18	-0.59	1.24
YKL163W	PIR3	0.18	-0.11	1.28
YGR043C	YGR043C	0.01	-0.22	1.31
YMR196W	YMR196W	-0.12	-0.27	1.06
YNL160W	YGP1	-0.35	-0.37	0.67
YGL121C	GPG1	-0.25	-0.32	0.70
YOR202W	HIS3	-0.08	-0.30	0.60
YOR028C	CIN5	-0.02	-0.23	0.65
YGR256W	GND2	-0.13	-0.30	0.71
YJL116C	NCA3	-0.47	-0.52	0.64
YOL053C	DDR2	-0.59	-0.35	0.75
YIL066C	RNR3	-0.17	-0.65	0.40
YPR160W	GPH1	-0.73	-0.85	0.44
YER158C	YER158C	-0.25	-0.70	-0.11
YBR067C	TIP1	-0.10	-0.69	-0.11
YJL079C	PRY1	-0.31	-0.85	-0.06
YGR032W	GSC2	-0.26	-0.69	0.08
YBR282W	MRPL27	-0.46	-0.62	-0.14
YDL124W	YDL124W	-0.70	-0.21	0.14
YCR061W	YCR061W	-0.62	-0.42	-0.29
YIL162W	SUC2	-0.65	-0.39	-0.19
YDR204W	COQ4	-0.66	-0.41	-0.20
YPR129W	SCD6	-0.71	-0.51	-0.26
YOR253W	NAT5	-0.62	-0.33	-0.34
YFL031W	HAC1	-0.75	-0.25	-0.38
YDL067C	COX9	-0.76	-0.39	-0.39
YCL033C	YCL033C	-0.67	-0.28	-0.06
YDR007W	TRP1	-0.65	-0.22	-0.14
YMR286W	MRPL33	-0.61	-0.16	-0.26
YDL125C	HNT1	-0.65	-0.17	-0.26
YDL219W	DTD1	-0.64	-0.21	-0.25
YPR159W	KRE6	-0.75	-0.44	-0.04
YOL058W	ARG1	0.06	-1.64	-0.45
YBR072W	HSP26	-0.41	-1.59	-0.09
YNL279W	PRM1	-0.19	-1.16	-0.22
YBR040W	FIG1	-0.16	-1.18	-0.39
YHR018C	ARG4	-0.12	-1.06	-0.44
YHL028W	WSC4	-0.20	-1.07	-0.46

Gene ORF	Gene Symbol	Δrad4/WT (Fold-Change)	Δrad23/WT (Fold-Change)	Δrad4Δrad23/WT (Fold-Change)
YJR109C	CPA2	0.27	-0.60	-0.05
YCL025C	AGP1	0.03	-0.68	-0.11
YER069W	ARG5,6	0.11	-0.69	-0.16
YNR044W	AGA1	0.10	-0.82	-0.22
YCR089W	FIG2	0.06	-0.86	-0.26
YGL117W	YGL117W	0.14	-0.73	-0.49
YIL123W	SIM1	-0.88	-0.90	-0.75
YOR302W	YOR302W	-0.47	-0.99	-0.96
YJR147W	HMS2	-0.32	-0.54	-0.90
YPL250C	ICY2	-0.19	-0.87	-0.83
YAR066W	YAR066W	-0.15	-0.70	-0.75
YKR093W	PTR2	-0.11	-0.60	-0.65
YAR068W	YAR068W	-0.06	-0.59	-0.69
YGR079W	YGR079W	-0.11	-0.57	-0.77
YKL029C	MAE1	-0.01	-0.34	-0.60
YOR107W	RGS2	0.00	-0.47	-0.62
YER056C	YER056C	-0.29	-0.21	-0.64
YJL078C	PRY3	-0.36	-0.26	-0.63
YKL208W	CBT1	-0.22	-0.21	-0.74
YOR316C	COT1	-0.26	-0.17	-0.82
YLR032W	RAD5	-0.27	-0.26	-0.81
YCL036W	GFD2	-0.33	-0.31	-0.84
YNR053C	NOG2	-0.36	-0.27	-0.86
YBR267W	REI1	-0.29	-0.34	-0.79
YHR048W	YHR048W	-0.17	-0.37	-0.64
YHR070W	TRM5	-0.36	-0.40	-0.72
YLR073C	YLR073C	-0.29	-0.42	-0.66
YER119C	AVT6	-0.69	-0.65	-0.35
YCR065W	HCM1	-0.60	-0.60	-0.33
YPL058C	PDR12	-0.56	-0.62	-0.37
YPR034W	ARP7	-0.75	-0.55	-0.50
YOR383C	FIT3	-0.73	-0.60	-0.52
YLR136C	TIS11	-0.67	-0.58	-0.48
YDL222C	FMP45	-0.54	-0.82	-0.35
YBR247C	ENP1	-0.44	-0.73	-0.56
YER175C	TMT1	-0.44	-0.75	-0.42
YML047C	PRM6	-0.26	-0.70	-0.39
YDR534C	FIT1	-0.32	-0.62	-0.60
YBR157C	ICS2	-0.33	-0.67	-0.50
YGL125W	MET13	-0.39	-0.62	-0.54
YDL170W	UGA3	-0.19	-0.69	-0.54
YIL015C	YIL014C-A	-0.20	-0.55	-0.60
YBL051C	PIN4	-0.70	-0.40	-0.54
YFL031W	HAC1	-0.64	-0.43	-0.64
YER125W	RSP5	-0.63	-0.52	-0.62
YBR145W	ADH5	-0.45	-0.49	-0.73
YNL190W	YNL190W	-0.51	-0.49	-0.71
YBR254C	TRS20	-0.45	-0.31	-0.61
YBR105C	VID24	-0.40	-0.36	-0.65

Gene ORF	Gene Symbol	Δrad4/WT (Fold-Change)	Δrad23/WT (Fold-Change)	Δrad4Δrad23/WT (Fold-Change)
YDR075W	PPH3	-0.52	-0.26	-0.65
YEL017C	PMP2	-0.51	-0.37	-0.64
YOR204W	DED1	-0.52	-0.32	-0.71
YHR143W	YHR143W	-0.51	-0.36	-0.70
YOR315W	YOR315W	-0.63	-0.31	-0.69
YBR219C	YBR219C	-0.78	1.48	0.59
YCR021C	HSP30	1.08	1.86	0.29
YJL188C	BUD19	0.62	0.24	0.21
YKL022C	CDC16	0.64	0.21	0.25
YKL025C	PAN3	0.75	0.34	0.30
YKL024C	URA6	0.74	0.30	-0.04
YMR011W	HXT2	0.22	1.30	0.54
YMR081C	ISF1	0.66	1.25	0.52
YER067W	YER067W	0.73	1.06	-0.07
YMR316W	DIA1	0.36	0.91	0.11
YHL036W	MUP3	0.40	0.73	0.16
YOL014W	YOL014W	0.54	0.98	0.24
YFL067W	YFL067W	0.03	0.79	0.21
YBR056W	YBR056W-A	0.17	0.74	0.17
YKR075C	YKR075C	0.12	0.78	0.15
YJR158W	YJR158W	0.23	0.68	0.28
YDR277C	MTH1	0.20	0.75	0.31
YAR064W	YAR064W	0.28	0.63	0.15
YOR268C	YOR268C	0.14	0.60	0.16
YGR142W	BTN2	0.73	1.20	1.68
YLR327C	RBF9	0.32	1.17	1.56
YKL123W	YKL123W	0.55	0.53	0.80
YJL144W	YJL144W	0.35	0.67	0.84
YLR264C	YLR264C-A	0.56	0.64	0.54
YDL021W	GPM2	-0.06	-0.05	0.90
YPL223C	GRE1	-0.15	-0.04	1.00
YGR070W	ROM1	0.03	0.15	0.95
YDR070C	FMP16	-0.01	0.07	0.78
YMR175W	SIP18	-0.04	0.17	0.82
YMR169C	ALD3	0.07	-0.08	0.78
YIL136W	OM45	0.03	-0.03	0.64
YBR053C	YBR053C	0.10	0.07	0.63
YGR130C	YGR130C	0.08	0.06	0.63
YHR087W	YHR087W	0.13	0.01	0.64
YER037W	PHM8	0.27	0.07	0.63
YBR006W	UGA2	0.29	0.14	0.77
YIL101C	XBP1	0.15	0.12	0.81
YDR258C	HSP78	0.40	0.30	0.64
YIL065C	FIS1	0.22	0.23	0.61
YNR002C	FUN34	0.25	0.24	0.61
YPL240C	HSP82	0.17	0.28	0.66
YGR146C	YGR146C	0.21	0.29	0.68
YOR120W	GCY1	0.26	0.36	1.11
YKL093W	MBR1	0.21	0.34	0.79

Gene ORF	Gene Symbol	Δrad4/WT (Fold-Change)	Δrad23/WT (Fold-Change)	Δrad4Δrad23/WT (Fold-Change)
YLR108C	YLR108C	0.18	0.29	0.94
YHL048W	COS8	0.11	0.58	0.87
YDR171W	HSP42	0.10	0.47	0.79
YHR092C	HXT4	0.13	0.65	0.70
YHR054C	YHR054C	0.23	0.49	0.64
YDR216W	ADR1	-0.15	0.40	0.81
YGR243W	FMP43	-0.07	0.63	0.57
YDR342C	HXT7	-0.07	0.60	0.69
YHL048W	COS8	-0.08	0.46	0.60
YDR034W	YDR034W-B	0.01	0.38	0.65
YDL020C	RPN4	0.07	0.28	0.71
YDR018C	YDR018C	0.00	0.20	0.71
YLL039C	UBI4	-0.16	0.22	0.63
YBR183W	YPC1	-0.05	0.21	0.61
YDR343C	YDR343C	-0.05	0.99	0.94
YGL263W	COS12	0.15	0.70	1.57
YPR158W	YPR158W	-0.12	0.41	1.26

243

A4.3 *psocs-rad23* Significantly Differentially Expressed Genes
(Figure 4.17)

Gene ORF	Gene Symbol	*psocs* un /*pRAD7* un (Fold-Change)	*pRAD7Δrad23* un /*pRAD7* un (Fold-Change)	*psocsΔrad23* un /*pRAD7* un (Fold-Change)
YEL021W	URA3	-0.13	4.33	4.10
YEL037C	RAD23	-0.26	-4.67	-5.00
YJL153C	INO1	0.25	-3.24	-3.10
YOL154W	ZPS1	0.14	-2.99	-1.67
YJR052W	RAD7	-3.00	-0.75	-3.15
YGL258W	YGL258W	0.26	-1.76	-1.84
YHL016C	DUR3	-0.05	-1.51	-1.49
YGL125W	MET13	0.10	-1.74	-1.23
YCL025C	AGP1	0.03	-1.75	-1.31
YGL258W	YGL258W	0.38	-1.55	-1.55
YOR387C	YOR387C	0.30	-1.51	-1.47
YDR502C	SAM2	0.29	-2.15	-0.95
YEL073C	YEL073C	-0.21	-1.74	-0.85
YBR177C	EHT1	-0.15	-1.67	-0.63
YDR497C	ITR1	-0.27	-1.50	-0.59
YBR145W	ADH5	-0.21	-1.41	-0.72
YJR073C	OPI3	0.26	-1.52	-0.93
YJL052W	TDH1	-0.01	-1.12	-0.86
YJL048C	UBX6	0.04	-1.09	-0.74
YFL021W	GAT1	-0.08	-1.30	-0.81
YER091C	MET6	0.03	-1.22	-0.74
YNL169C	PSD1	0.21	-1.19	-0.61
YDL039C	PRM7	-0.66	-0.52	-1.38
YDL038C	YDL038C	-0.57	-0.65	-1.27
YDL037C	BSC1	-0.54	-1.25	-1.19
YGR032W	GSC2	-0.10	-0.65	-1.25
YBR105C	VID24	-0.17	-0.77	-1.15
YBL042C	FUI1	-0.03	-0.79	-1.33
YJL088W	ARG3	-0.36	-1.00	-0.84
YHL045W	YHL045W	-0.35	-1.00	-0.85
YLR237W	THI7	-0.34	-0.63	-0.81
YER081W	SER3	-0.31	-0.78	-0.91
YKR039W	GAP1	-0.14	-1.01	-0.86
YER069W	ARG5,6	-0.10	-1.09	-1.04
YPR194C	OPT2	-0.09	-0.91	-1.07
YPL277C	YOR389W	-0.09	-0.98	-0.97
YER073W	ALD5	-0.05	-0.79	-0.91
YOR107W	RGS2	-0.14	-0.81	-0.84
YGL117W	YGL117W	0.05	-1.33	-1.19
YGL256W	ADH4	0.20	-1.30	-1.32
YKL216W	URA1	0.02	-1.10	-1.28
YOL126C	MDH2	-0.04	-0.99	-1.35
YLL053C	YLL053C	-0.15	-1.08	-1.14
YLL052C	AQY2	-0.13	-1.09	-1.19
YOR338W	YOR338W	-0.23	-1.14	-1.23
YNL142W	MEP2	-0.28	-1.21	-1.08

Gene ORF	Gene Symbol	*psocs* un /*pRAD7* un (Fold-Change)	*pRAD7Δrad23* un /*pRAD7* un (Fold-Change)	*psocsΔrad23* un /*pRAD7* un (Fold-Change)
YER088C	DOT6	0.15	-0.40	-0.73
YPL177C	CUP9	0.15	-0.47	-0.81
YHR044C	DOG1	-0.16	-0.06	-0.76
YNL065W	AQR1	0.02	-0.14	-0.61
YKL043W	PHD1	-0.41	-0.44	-0.60
YHR049W	FSH1	-0.35	-0.52	-0.62
YBR114W	RAD16	-0.34	-0.62	-0.55
YPR065W	ROX1	-0.23	-0.61	-0.51
YOR306C	MCH5	-0.20	-0.53	-0.75
YIL119C	RPI1	-0.04	-0.57	-0.68
YOR203W	YOR203W	-0.04	-0.52	-0.69
YGR108W	CLB1	-0.09	-0.45	-0.68
YOL140W	ARG8	-0.16	-0.49	-0.61
YNL141W	AAH1	-0.19	-0.44	-0.62
YJL056C	ZAP1	0.46	-0.64	-0.35
YGR055W	MUP1	-0.06	-1.35	-0.31
YGR157W	CHO2	0.19	-1.15	-0.22
YHR123W	EPT1	0.03	-1.15	-0.19
YGL077C	HNM1	-0.05	-1.14	-0.31
YER026C	CHO1	-0.22	-1.09	-0.40
YPR158W	YPR158W	-0.24	-0.99	-0.25
YHR123W	EPT1	0.02	-0.96	-0.40
YGR254W	ENO1	-0.02	-0.93	-0.33
YOR375C	GDH1	-0.02	-0.87	-0.37
YLR133W	CKI1	0.17	-0.95	-0.42
YLR303W	MET17	0.10	-0.87	-0.40
YHR067W	YHR067W	0.12	-0.84	-0.42
YOR383C	FIT3	0.11	-0.83	-0.37
YGR161C	RTS3	-0.03	-0.60	-0.46
YPL264C	YPL264C	-0.03	-0.61	-0.39
YIR017C	MET28	0.04	-0.73	-0.43
YHR094C	HXT1	-0.04	-0.72	-0.49
YHL020C	OPI1	-0.01	-0.67	-0.47
YOR344C	TYE7	0.00	-0.69	-0.51
YLR132C	YLR132C	0.23	-0.70	-0.43
YJR008W	YJR008W	0.21	-0.72	-0.41
YGL255W	ZRT1	0.14	-0.66	-0.45
YBR256C	RIB5	0.12	-0.61	-0.57
YDL198C	YDL198C	0.08	-0.61	-0.50
YKL120W	OAC1	0.10	-0.63	-0.51
YOL108C	INO4	0.08	-0.64	-0.51
YBR029C	CDS1	0.11	-0.72	-0.55
YOR130C	ORT1	0.09	-0.67	-0.54
YPR167C	MET16	0.10	-0.70	-0.59
YNL104C	LEU4	0.12	-0.72	-0.62
YHL040C	ARN1	-0.15	-0.83	-0.64
YGR121C	MEP1	-0.15	-0.88	-0.52
YOR302W	YOR302W	-0.10	-0.84	-0.55
YPR138C	MEP3	-0.05	-0.75	-0.58

Gene ORF	Gene Symbol	psocs un /pRAD7 un (Fold-Change)	pRAD7Δrad23 un /pRAD7 un (Fold-Change)	psocsΔrad23 un /pRAD7 un (Fold-Change)
YGR281W	YOR1	-0.08	-0.78	-0.61
YOL058W	ARG1	-0.09	-0.79	-0.58
YNL044W	YIP3	-0.13	-0.66	-0.63
YOL059W	GPD2	-0.14	-0.64	-0.59
YGR224W	AZR1	0.01	-0.64	-0.57
YPR145W	ASN1	-0.02	-0.63	-0.55
YOR389W	YOR389W	-0.04	-0.62	-0.57
YOR202W	HIS3	0.01	-0.63	-0.65
YNL129W	NRK1	-0.03	-0.65	-0.61
YLR168C	YLR168C	0.16	-0.67	-0.75
YJR109C	CPA2	0.16	-0.83	-0.77
YER175C	TMT1	0.11	-0.90	-0.73
YPL058C	PDR12	0.24	-0.84	-0.68
YOL119C	MCH4	-0.01	-0.74	-0.77
YOL143C	RIB4	-0.06	-0.84	-0.76
YHL022C	SPO11	0.07	-0.82	-0.71
YHR071W	PCL5	0.02	-0.80	-0.66
YMR246W	FAA4	0.00	-0.77	-0.69
YDR123C	INO2	0.12	-0.82	-0.56
YHR018C	ARG4	0.04	-0.83	-0.61
YMR062C	ECM40	0.05	-0.88	-0.62
YKL158W	APE2	0.08	-0.61	0.12
YBR147W	YBR147W	-0.21	-0.61	0.06
YER056C	YER056C	-0.31	-0.62	-0.35
YER086W	ILV1	-0.27	-0.69	-0.23
YER057C	HMF1	-0.37	-0.60	-0.19
YDR499W	LCD1	-0.14	-0.61	-0.30
YKL182W	FAS1	0.01	-0.68	-0.23
YER185W	YER185W	-0.05	-0.60	-0.20
YPL231W	FAS2	0.00	-0.62	-0.14
YGL184C	STR3	0.12	-0.64	-0.26
YJR133W	XPT1	0.02	-0.65	-0.36
YMR006C	PLB2	0.04	-0.62	-0.29
YIL144W	TID3	-0.69	0.07	-0.02
YHR063W	YHR063W	-0.72	0.05	-0.01
YHR183W	GND1	-0.78	0.13	0.23
YDR171W	HSP42	-0.52	-0.08	0.65
YDR432W	NPL3	-0.64	-1.02	0.14
YDL060W	TSR1	-0.80	-0.40	-0.01
YDR075W	PPH3	-0.48	-0.68	-0.31
YDR006C	SOK1	-0.49	-0.68	-0.25
YDR007W	TRP1	-0.58	-0.77	-0.25
YDR238C	SEC26	-0.61	-0.67	0.09
YDR172W	SUP35	-0.67	-0.54	0.04
YDR399W	HPT1	-0.51	-0.62	-0.06
YDL092W	SRP14	-0.47	-0.73	-0.02
YDR533C	HSP31	-0.51	-0.72	-0.12
YDL155W	CLB3	-0.50	-0.72	-0.09
YDR139C	RUB1	-0.41	-0.60	0.04

Gene ORF	Gene Symbol	psocs un /pRAD7 un (Fold-Change)	pRAD7Δrad23 un /pRAD7 un (Fold-Change)	psocsΔrad23 un /pRAD7 un (Fold-Change)
YDR333C	YDR333C	-0.49	-0.63	0.03
YCR077C	PAT1	-0.45	-0.61	-0.01
YFL031W	HAC1	0.64	0.24	0.19
YKL206C	YKL206C	0.31	0.22	-0.64
YGL205W	POX1	-0.11	0.70	-0.01
YLR214W	FRE1	0.08	1.12	1.03
YHR137W	ARO9	0.00	1.28	1.06
YER011W	TIR1	-0.04	1.21	0.98
YGL263W	COS12	0.02	1.48	0.87
YDR342C	HXT7	-0.03	1.40	1.11
YDR343C	YDR343C	0.02	1.54	1.11
YGL037C	PNC1	-0.02	1.28	1.30
YFR053C	HXK1	-0.05	1.42	1.38
YDR380W	ARO10	0.00	1.73	1.42
YMR011W	HXT2	-0.19	1.64	1.28
YDR305C	HNT2	0.31	0.17	0.69
YCR061W	YCR061W	0.08	0.42	0.85
YJL164C	TPK1	-0.05	0.36	0.89
YPR160W	GPH1	-0.04	0.46	0.87
YPR002W	PDH1	-0.15	0.47	0.98
YGR248W	SOL4	-0.09	0.42	0.62
YLR149C	YLR149C	-0.11	0.65	0.72
YER142C	MAG1	-0.11	0.63	0.72
YGL047W	ALG13	-0.10	0.55	0.63
YEL011W	GLC3	-0.15	0.60	0.62
YKR011C	YKR011C	-0.07	0.52	0.76
YPL240C	HSP82	-0.20	0.52	0.72
YDR111C	ALT2	0.07	0.57	0.61
YBR183W	YPC1	0.05	0.63	0.60
YKL121W	YKL121W	-0.04	0.61	0.55
YER044C	YER044C	0.00	0.60	0.56
YDR358W	GGA1	-0.05	0.56	0.62
YOL053C	DDR2	-0.03	0.54	0.64
YJL217W	YJL217W	-0.03	0.59	0.64
YGR008C	STF2	-0.03	0.62	0.65
YOL048C	YOL048C	-0.05	0.62	0.67
YJL212C	OPT1	0.11	0.31	0.76
YJL196C	ELO1	0.16	0.30	0.61
YJL163C	YJL163C	0.08	0.32	0.62
YCR061W	YCR061W	0.06	0.27	0.64
YNL037C	IDH1	0.07	0.27	0.62
YLR270W	DCS1	0.18	0.47	0.72
YLR218C	YLR218C	0.01	0.39	0.63
YLR258W	GSY2	0.08	0.41	0.66
YEL039C	CYC7	0.09	0.37	0.69
YKL195W	YKL195W	0.10	0.48	0.65
YDL022W	GPD1	0.07	0.47	0.62
YLR304C	ACO1	0.05	0.52	0.70
YGL104C	VPS73	0.02	0.45	0.73

247

Gene ORF	Gene Symbol	psocs un /pRAD7 un (Fold-Change)	pRAD7Δrad23 un /pRAD7 un (Fold-Change)	psocsΔrad23 un /pRAD7 un (Fold-Change)
YMR250W	GAD1	0.03	0.49	0.76
YOR374W	ALD4	-0.24	0.22	0.65
YDL214C	PRR2	-0.02	0.18	0.62
YIL155C	GUT2	-0.04	0.30	0.64
YGL010W	YGL010W	-0.05	0.25	0.70
YMR105C	PGM2	-0.13	0.22	0.70
YHR087W	YHR087W	-0.27	0.73	0.74
YPL061W	ALD6	-0.45	0.88	0.87
YKL096W	YKL096W	-0.08	1.01	1.29
YCL042W	GLK1	-0.13	0.77	1.39
YCL040W	GLK1	-0.19	0.87	1.08
YLL026W	HSP104	0.07	0.96	1.02
YDL241W	YDL241W	0.09	0.93	0.93
YNR001C	CIT1	0.08	0.89	0.91
YML100W	TSL1	0.07	0.83	1.03
YLR267W	BOP2	-0.03	0.90	1.00
YML128C	MSC1	-0.05	0.81	1.06
YKL163W	PIR3	0.17	1.12	0.80
YIR043C	YIR043C	0.39	1.14	0.82
YGR109C	CLB6	0.00	1.09	0.53
YBR040W	FIG1	0.01	1.14	0.59
YJR048W	CYC1	0.26	0.64	0.92
YOR027W	STI1	0.39	0.81	0.94
YLR202C	YLR202C	0.23	0.69	0.55
YHL048W	COS8	0.25	0.66	0.54
YDR435C	PPM1	0.24	0.60	0.56
YKL151C	YKL151C	0.17	0.59	0.67
YBR126C	TPS1	0.06	0.62	0.71
YBR056W	YBR056W	0.10	0.61	0.69
YOR298C	MBF1	0.23	0.62	0.71
YOR292C	YOR292C	0.28	0.62	0.67
YKR077W	YKR077W	0.20	0.79	0.55
YCL061C	MRC1	0.17	0.77	0.45
YBR302C	COS2	0.12	0.77	0.42
YBR073W	RDH54	0.11	0.71	0.38
YOR074C	CDC21	0.10	0.73	0.40
YHL035C	VMR1	0.20	0.70	0.43
YBR071W	YBR071W	0.23	0.68	0.48
YLR130C	ZRT2	0.23	0.68	0.35
YDR055W	PST1	0.28	0.70	0.37
YNL102W	POL1	0.20	0.74	0.38
YLL039C	UBI4	0.00	0.75	0.89
YKL067W	YNK1	0.11	0.67	0.83
YHR138C	YHR138C	-0.04	0.66	0.73
YHL030W	ECM29	-0.03	0.70	0.71
YDR516C	EMI2	0.02	0.67	0.75
YLR216C	CPR6	0.04	0.74	0.76
YJL218W	YJL218W	-0.01	0.76	0.72
YER067W	YER067W	-0.01	0.73	0.80

248

Gene ORF	Gene Symbol	*psocs* un /pRAD7 un (Fold-Change)	pRAD7Δrad23 un /pRAD7 un (Fold-Change)	psocsΔrad23 un /pRAD7 un (Fold-Change)
YDL130W	YDL130W	-0.04	0.74	0.79
YDR070C	FMP16	-0.14	0.76	0.85
YBL064C	PRX1	-0.07	0.81	0.72
YOL014W	YOL014W	-0.08	0.77	0.77
YOL158C	ENB1	-0.04	0.83	0.81
YLR297W	YLR297W	0.15	0.86	0.66
YAR007C	RFA1	0.13	0.83	0.67
YKR091W	SRL3	0.20	0.75	0.70
YBR149W	ARA1	0.17	0.79	0.74
YDL018C	ERP3	0.15	0.71	0.76
YDL169C	UGX2	0.14	0.68	0.70
YPR026W	ATH1	0.17	0.67	0.71
YNL115C	YNL115C	0.12	0.68	0.67
YOL122C	SMF1	0.16	0.95	0.77
YCL064C	CHA1	0.08	0.80	0.75
YPL014W	YPL014W	0.07	0.86	0.77
YMR145C	NDE1	0.09	0.82	0.83
YHR140W	YHR140W	-0.03	0.84	0.50
YCL024W	KCC4	0.07	0.89	0.46
YER015W	FAA2	0.02	0.89	0.48
YKL109W	HAP4	0.03	0.91	0.59
YHR092C	HXT4	0.05	0.90	0.54
YMR179W	SPT21	0.08	0.87	0.54
YLR284C	ECI1	-0.01	0.83	0.66
YGR243W	FMP43	-0.04	0.86	0.59
YPR184W	GDB1	-0.09	0.74	0.62
YLR056W	ERG3	0.00	0.77	0.62
YML075C	HMG1	0.03	0.73	0.67
YKL142W	MRP8	0.29	0.73	0.26
YJL192C	SOP4	0.28	0.75	0.13
YBL035C	POL12	0.14	0.64	0.31
YDL110C	YDL110C	-0.09	0.62	0.46
YCR021C	HSP30	-0.18	0.61	0.46
YOR195W	SLK19	-0.09	0.63	0.28
YER070W	RNR1	-0.03	0.60	0.26
YDL003W	MCD1	-0.04	0.62	0.26
YDR097C	MSH6	-0.04	0.65	0.29
YOR144C	ELG1	-0.02	0.62	0.32
YDL164C	CDC9	-0.10	0.67	0.39
YOR074C	CDC21	-0.03	0.63	0.37
YOL123W	HRP1	-0.06	0.63	0.34
YIL160C	POT1	-0.02	0.74	0.25
YMR199W	CLN1	0.01	0.66	0.25
YOL090W	MSH2	0.01	0.70	0.38
YFL062W	COS4	0.04	0.67	0.31
YNL202W	SPS19	0.03	0.67	0.36
YNL336W	YNL336W	0.03	0.64	0.37
YMR101C	SRT1	0.03	0.63	0.34
YPR120C	CLB5	0.05	0.70	0.35

Gene ORF	Gene Symbol	psocs un /pRAD7 un (Fold-Change)	pRAD7Δrad23 un /pRAD7 un (Fold-Change)	psocsΔrad23 un /pRAD7 un (Fold-Change)
YPL153C	RAD53	0.07	0.72	0.31
YMR076C	PDS5	0.04	0.75	0.29
YER096W	SHC1	-0.08	0.75	0.39
YLR103C	CDC45	0.00	0.80	0.42
YBR070C	ALG14	-0.01	0.76	0.45
YNL082W	PMS1	0.03	0.62	0.44
YML059C	NTE1	-0.01	0.65	0.42
YDR144C	MKC7	0.01	0.71	0.53
YNL312W	RFA2	0.03	0.69	0.55
YBR041W	FAT1	0.01	0.70	0.55
YMR119W	ASI1	0.01	0.69	0.54
YLR183C	TOS4	0.05	0.72	0.47
YML132W	YML132W	0.08	0.72	0.51
YNL280C	ERG24	0.02	0.68	0.47
YLR454W	FMP27	0.06	0.66	0.46

A4.4 Significantly Differentially Expressed Genes in Response to UV, ONLY in *psocs Δrad23* Strain
(Figure 4.20 and Figure 4.21)

Probe ID	Gene ORF	Gene Symbol	fc psocs un /pRAD7 un	fc pRAD7Δrad23 un /pRAD7 un	fc psocsΔrad23 un /pRAD7 un	fc pRAD7 15 /pRAD7 un	fc psocs 15 /psocs un	fc pRAD7Δrad23 15 /pRAD7Δrad23 un	fc psocsΔrad23 15 /psocsΔrad23 un	fc pRAD7 60 /pRAD7 un	fc psocs 60 /psocs un	fc pRAD7Δrad23 60 /pRAD7Δrad23 un	fc psocsΔrad23 60 /psocsΔrad23 un
5724_at	YEL021W	URA3	-0.18	0.29	0.08	-0.08	0.20	0.10	0.14	-0.17	0.01	0.01	0.48
5753_at	YEL037C	RAD23	0.08	0.17	0.18	-0.40	-0.41	-0.42	-0.54	0.29	0.12	-0.09	-0.32
11185_at	YJL153C	INO1	0.05	0.14	0.29	-0.28	-0.23	-0.17	-0.56	0.55	0.45	0.67	-0.10
8726_at	YOL154W	ZPS1	-0.06	0.15	0.08	2.14	2.21	1.61	1.48	3.26	3.38	2.78	3.53
10981_at	YJR052W	RAD7	-0.04	0.13	0.09	2.23	2.22	1.68	1.62	3.26	3.37	2.89	3.64
5255_s_at	YGL258W	YGL258W	0.01	0.39	0.63	0.45	0.51	0.03	-0.19	1.17	1.14	0.00	0.03
4546_at	YHL016C	DUR3	0.19	0.18	-0.26	0.19	-0.04	0.00	0.44	-0.30	-0.33	0.01	0.31
5117_at	YGL125W	MET13	0.11	0.07	0.27	-0.08	-0.03	0.09	-0.05	0.29	0.15	-0.17	-0.33
6907_at	YCL025C	AGP1	0.00	0.77	0.62	-0.23	-0.13	-0.22	-0.30	0.29	-0.04	-0.29	-0.48
5254_i_at	YGL258W	YGL258W	0.19	0.39	-0.06	0.40	0.15	0.24	0.66	-0.29	-0.33	0.18	0.38
8141_at	YOR387C	YOR387C	-0.13	0.04	0.22	-0.39	-0.26	-0.26	-0.38	-0.23	-0.24	-0.67	-0.90
5971_at	YDR502C	SAM2	0.06	-0.15	0.20	0.07	0.01	0.17	-0.14	0.60	0.53	0.35	-0.11
5811_at	YEL073C	YEL073C	-0.01	0.05	0.23	-0.14	0.09	-0.19	0.01	0.03	-0.07	-0.05	-0.59
7179_at	YBR177C	EHT1	0.08	0.18	-0.21	0.25	0.17	0.10	0.58	-0.11	0.03	0.31	0.69
5966_at	YDR497C	ITR1	-0.05	-0.23	-0.24	0.31	0.32	0.18	0.29	0.48	0.63	1.01	1.16
7236_at	YBR145W	ADH5	0.02	-0.37	-0.14	-0.30	-0.21	-0.17	-0.38	-0.02	0.09	0.00	-0.77
10957_at	YJR073C	OPI3	0.07	0.21	0.23	0.01	0.06	-0.03	-0.04	0.00	-0.24	-0.39	-0.63
11060_at	YJL052W	TDH1	0.14	-0.30	-0.51	-1.32	-1.26	-0.79	-0.66	-1.28	-1.29	-0.94	-1.45
11065_at	YJL048C	UBX6	0.03	0.04	0.00	0.55	0.40	0.61	0.71	1.31	1.30	1.71	1.97
5409_at	YFL021W	GAT1	-0.17	0.05	-0.39	0.65	0.87	0.33	0.80	0.73	1.10	1.06	1.78
5620_at	YER091C	MET6	0.14	0.38	-0.31	0.00	-0.09	-0.10	0.61	-0.10	-0.07	0.35	0.72
9044_at	YNL169C	PSD1	0.08	-0.61	0.12	-0.71	-0.69	-0.22	-0.90	-0.45	-0.65	-0.47	-1.39
6513_at	YDL039C	PRM7	0.22	0.54	-0.14	0.62	0.38	0.25	0.97	1.22	1.17	0.86	1.83
6514_at	YDL038C	YDL038C	0.31	0.22	-0.64	0.60	0.17	0.37	1.31	1.22	1.11	1.18	2.01
6515_at	YDL037C	BSC1	0.08	0.40	-0.38	-0.38	-0.47	-0.40	0.26	-1.01	-1.09	-1.46	-0.66
4959_at	YGR032W	GSC2	0.10	0.48	0.65	0.28	0.16	-0.28	-0.39	1.84	1.79	0.55	0.50

Probe ID	Gene ORF	Gene Symbol	fc *psocs* un /pRAD7 un	fc *pRAD7Δrad23* un /pRAD7 un	fc *psocsΔrad23* un /pRAD7 un	fc *pRAD7 15* /pRAD7 un	fc *psocs 15* /psocs un	fc *pRAD7Δrad23 15* /pRAD7Δrad23 un	fc *psocsΔrad23 15* /psocsΔrad23 un	fc *pRAD7 60* /pRAD7 un	fc *psocs 60* /psocs un	fc *pRAD7Δrad23 60* /pRAD7Δrad23 un	fc *psocsΔrad23 60* /psocsΔrad23 un
7241_at	YBR105C	VID24	0.07	0.27	0.37	0.00	0.02	-0.13	-0.08	0.78	0.69	0.29	0.11
7410_at	YBL042C	FUI1	0.06	-0.09	0.07	-0.75	-0.60	-0.40	-0.63	-1.52	-1.77	-2.06	-2.13
11114_at	YJL088W	ARG3	0.06	-0.44	0.05	-0.64	-0.51	-0.21	-0.44	-0.33	-0.44	-0.67	-0.98
3193_at	YHL045W	YHL045W	-0.18	-0.16	0.11	0.95	0.95	0.58	0.34	-0.08	0.06	2.01	1.02
10085_at	YLR237W	THI7	0.07	-0.14	0.25	-0.45	-0.43	-0.41	-0.79	0.54	0.32	0.20	-0.15
5654_at	YER081W	SER3	0.09	-0.25	0.09	0.40	0.29	0.15	-0.13	1.22	0.97	0.76	0.54
10511_at	YKR039W	GAP1	0.26	-1.52	-0.93	0.46	0.16	0.70	1.12	-0.10	0.04	1.91	0.90
5642_at	YER069W	ARG5,6	0.15	0.38	-0.32	0.08	-0.05	-0.04	0.88	0.42	0.24	-0.58	0.37
7546_at	YPR194C	OPT2	-3.00	-0.75	-3.15	-0.50	-0.42	-0.25	-0.35	0.53	-0.03	0.07	-0.72
8019_s_at	YPL277C	YOR389W	0.03	0.08	0.34	0.06	0.08	0.26	0.03	0.57	0.34	0.21	-0.32
5646_at	YER073W	ALD5	0.03	-0.05	0.36	0.27	0.22	0.51	0.24	1.70	1.59	1.37	0.96
8444_at	YOR107W	RGS2	0.09	-0.31	0.28	0.61	0.40	0.74	0.26	1.69	1.64	1.46	0.87
5125_at	YGL117W	YGL117W	-0.01	-0.01	0.32	0.24	0.33	0.39	0.17	1.36	1.36	0.97	0.68
5257_at	YGL256W	ADH4	0.02	0.05	0.35	0.30	0.34	0.54	0.31	0.87	0.82	0.36	0.19
10796_at	YKL216W	URA1	0.12	-0.11	-0.29	0.02	-0.15	-0.05	0.28	-0.39	-0.46	-0.43	0.23
8663_at	YOL126C	MDH2	0.05	0.37	0.39	-0.07	0.01	-0.08	-0.19	0.02	-0.25	-0.35	-0.73
10377_at	YLL053C	YLL053C	-0.02	-0.23	0.05	-0.17	-0.14	0.34	-0.05	-0.84	-1.08	-1.30	-1.53
10378_at	YLL052C	AQY2	0.09	0.25	-0.39	-0.28	-0.26	-0.43	0.46	-0.31	-0.34	-0.64	-0.07
8228_at	YOR338W	YOR338W	0.02	-0.09	0.08	-0.77	-0.65	-0.65	-0.91	-0.44	-0.36	-0.84	-1.11
9026_at	YNL142W	MEP2	0.15	-0.51	-0.12	-0.35	-0.35	-0.24	-0.47	-0.20	-0.20	-0.60	-0.92
5617_at	YER088C	DOT6	-0.09	0.01	0.25	-0.07	0.04	0.20	-0.06	-0.02	-0.19	-0.10	-0.65
7938_at	YPL177C	CUP9	0.09	-0.14	0.05	-0.12	-0.17	0.11	-0.10	0.13	-0.12	-0.47	-0.54
4473_i_at	YHR044C	DOG1	0.08	0.32	0.62	1.48	1.29	1.06	0.90	2.46	2.46	1.95	1.79
8923_at	YNL065W	AQR1	0.02	0.06	0.29	-0.69	-0.55	-0.73	-0.85	0.32	0.22	-0.24	-0.49
10609_at	YKL043W	PHD1	0.16	0.30	0.61	0.31	0.25	0.44	0.15	0.79	0.59	0.74	0.13
4478_at	YHR049W	FSH1	0.11	0.31	0.76	-0.70	-0.74	-0.70	-0.86	-0.41	-0.73	-0.52	-1.60
7250_at	YBR114W	RAD16	-0.03	-0.07	0.04	-0.13	-0.08	0.04	-0.14	0.45	0.45	0.07	-0.27
7685_at	YPR065W	ROX1	0.11	-0.41	0.09	-0.43	-0.36	-0.12	-0.61	-0.02	-0.12	0.15	-0.81
8241_at	YOR306C	MCH5	0.07	-0.21	0.28	-0.29	-0.24	-0.09	-0.41	-0.21	-0.21	0.25	-1.05
4192_at	YIL119C	RPI1	-0.10	0.27	0.57	0.71	0.94	0.40	0.06	1.64	1.71	1.24	0.93

Probe ID	Gene ORF	Gene Symbol	fc psocs un /pRAD7 un	fc pRAD7Δrad23 un /pRAD7 un	fc psocsΔrad23 un /pRAD7 un	fc pRAD7 15 /pRAD7 un	fc psocs 15 /psocs un	fc pRAD7Δrad23 15 /pRAD7Δrad23 un	fc psocsΔrad23 15 /psocsΔrad23 un	fc pRAD7 60 /pRAD7 un	fc psocs 60 /psocs un	fc pRAD7Δrad23 60 /pRAD7Δrad23 un	fc psocsΔrad23 60 /psocsΔrad23 un
8360_at	YOR203W	YOR203W	-0.03	0.34	0.56	0.73	0.90	0.36	0.10	1.65	1.69	1.22	0.98
4898_at	YGR108W	CLB1	0.10	-0.20	0.43	0.41	0.31	0.55	0.03	1.06	1.02	1.28	0.44
8694_at	YOL140W	ARG8	-0.04	-0.33	0.02	-0.73	-0.60	-0.53	-0.84	0.22	0.18	-0.20	-0.73
9027_at	YNL141W	AAH1	0.10	0.17	0.25	0.20	0.13	0.27	0.19	0.79	0.60	0.34	0.17
11101_at	YJL056C	ZAP1	0.06	-0.06	0.06	-0.66	-0.70	-0.68	-0.72	-0.41	-0.55	-0.89	-1.25
4936_at	YGR055W	MUP1	0.01	-0.36	0.22	-0.36	-0.33	0.03	-0.60	0.10	-0.05	-0.10	-0.77
4858_at	YGR157W	CHO2	0.12	-0.13	0.11	-0.12	-0.27	0.10	-0.23	0.01	-0.20	-0.05	-0.64
4416_at	YHR123W	EPT1	0.23	-0.34	0.21	-0.40	-0.58	-0.11	-0.49	0.85	0.69	0.36	-0.73
5074_at	YGL077C	HNM1	-0.03	-0.06	-0.12	0.16	0.21	0.24	0.35	-0.06	0.12	0.42	0.54
5681_at	YER026C	CHO1	0.17	0.10	0.21	0.05	-0.08	0.04	0.15	0.74	0.69	0.28	0.03
7602_at	YPR158W	YPR158W	0.27	-0.37	0.15	-0.64	-0.72	-0.31	-0.75	-0.39	-0.61	-0.61	-1.40
4417_at	YHR123W	EPT1	0.16	-0.52	0.28	-0.82	-0.72	-0.25	-0.99	-0.28	-0.39	-0.06	-1.04
4729_i_at	YGR254W	ENO1	0.03	-0.44	0.13	-0.51	-0.50	-0.12	-0.72	-0.29	-0.27	-0.66	-1.24
8174_at	YOR375C	GDH1	0.18	-0.17	0.11	-0.57	-0.60	-0.39	-0.68	-0.04	-0.17	0.03	-0.65
10207_at	YLR133W	CKI1	0.01	0.15	0.25	0.91	0.90	1.01	0.93	2.42	2.60	2.15	3.12
10018_at	YLR303W	MET17	0.01	0.14	-0.08	-0.66	-0.75	-0.86	-0.70	-0.60	-0.51	-0.16	0.02
4448_at	YHR067W	YHR067W	-0.01	0.30	0.08	1.23	0.97	0.87	1.06	1.35	1.42	1.77	2.00
8182_at	YOR383C	FIT3	-0.04	-0.57	-0.68	-0.11	-0.05	-0.42	-0.16	-1.02	-0.77	-0.66	-0.31
4862_at	YGR161C	RTS3	0.04	-0.01	0.17	0.53	0.47	0.56	0.51	0.71	0.83	0.31	0.08
8031_at	YPL264C	YPL264C	-0.04	0.30	0.64	1.27	0.82	0.83	0.53	2.75	2.90	1.92	2.12
4098_at	YIR017C	MET28	0.00	-0.05	-0.06	0.44	0.33	0.40	0.50	0.89	0.99	1.48	1.54
4430_at	YHR094C	HXT1	-0.10	0.40	0.05	0.65	0.68	0.54	0.75	2.11	2.19	2.06	2.81
4542_at	YHL020C	OPI1	0.00	0.16	0.26	0.21	0.14	-0.08	-0.07	1.06	1.15	0.57	0.41
8188_at	YOR344C	TYE7	-0.10	-0.21	-0.06	-0.07	0.16	0.16	-0.02	-0.37	-0.12	-0.02	0.25
10206_at	YLR132C	YLR132C	-0.06	-0.04	0.07	0.14	0.30	0.31	0.31	-0.04	0.20	0.47	0.57
11030_at	YJR008W	YJR008W	-0.20	-0.06	-0.12	-0.04	0.04	0.06	-0.01	0.42	0.66	0.93	1.05
5258_at	YGL255W	ZRT1	-0.04	-0.72	-0.49	-1.03	-0.90	-0.67	-1.06	-0.86	-0.80	-1.35	-1.46
7121_at	YBR256C	RIB5	0.06	0.08	0.01	0.10	0.00	0.08	0.12	-0.76	-0.83	-0.17	-0.12
6665_at	YDL198C	YDL198C	-0.04	-0.26	-0.44	0.21	0.28	0.40	0.76	0.04	0.20	0.36	0.80
10709_at	YKL120W	OAC1	0.28	-0.01	-0.57	-0.64	0.11	-0.32	0.12	1.70	1.94	-2.12	-0.45

253

Probe ID	Gene ORF	Gene Symbol	fc psocs un /pRAD7 un	fc pRAD7Δrad23 un /pRAD7 un	fc psocsΔrad23 un /pRAD7 un	fc pRAD7 15 /pRAD7 un	fc psocs 15 /psocs un	fc pRAD7Δrad23 15 /pRAD7Δrad23 un	fc psocsΔrad23 15 /psocsΔrad23 un	fc pRAD7 60 /pRAD7 un	fc psocs 60 /psocs un	fc pRAD7Δrad23 60 /pRAD7Δrad23 un	fc psocsΔrad23 60 /psocsΔrad23 un
8680_at	YOL108C	INO4	0.03	0.22	-0.10	0.57	0.36	0.31	0.58	0.77	0.76	0.90	1.42
7342_at	YBR029C	CDS1	-0.11	0.36	0.39	0.50	0.49	0.03	0.08	1.47	1.61	0.91	0.79
8422_at	YOR130C	ORT1	0.03	-0.05	0.39	0.71	0.55	0.39	0.09	1.84	1.76	0.72	0.65
7565_at	YPR167C	MET16	-0.01	-0.02	-0.18	0.06	-0.05	0.02	0.11	-0.67	-0.62	-0.16	-0.03
8973_at	YNL104C	LEU4	-0.02	0.18	0.15	0.74	0.73	0.62	0.80	0.89	0.92	1.27	1.50
4568_at	YHL040C	ARN1	-0.11	0.30	0.38	0.43	0.42	0.12	0.17	1.33	1.35	0.73	0.70
4866_at	YGR121C	MEP1	-0.10	0.13	0.02	0.41	0.46	0.40	0.49	0.77	1.02	1.01	1.46
8236_at	YOR302W	YOR302W	-0.01	-0.23	0.09	0.84	0.62	0.56	0.20	0.77	0.84	1.20	1.20
7626_at	YPR138C	MEP3	0.26	-1.76	-1.84	-0.53	-0.49	0.06	0.18	-1.53	-1.74	0.57	0.54
4711_at	YGR281W	YOR1	0.14	-0.66	-0.45	-0.97	-0.82	-0.32	-0.35	-0.81	-1.14	-1.30	-1.67
8593_at	YOL058W	ARG1	-0.04	0.24	0.48	0.34	0.28	0.12	-0.06	1.39	1.41	0.86	0.67
3949_i_at	YNL044W	YIP3	-0.06	-0.28	-0.09	-0.02	0.13	-0.19	-0.09	-0.67	-0.62	-0.35	0.21
8592_at	YOL059W	GPD2	-0.14	0.34	-0.22	-0.17	-0.13	-0.31	0.10	-0.61	-0.31	-0.92	0.13
4790_at	YGR224W	AZR1	-0.14	0.04	0.59	0.82	0.60	0.57	0.13	1.76	1.75	1.17	0.91
7588_at	YPR145W	ASN1	0.08	0.07	0.49	-0.33	-0.37	-0.36	-0.66	0.05	0.00	0.10	-0.59
8144_g_at	YOR389W	YOR389W	-0.31	0.22	-0.14	-0.30	-0.32	-0.35	-0.20	-1.78	-1.70	-1.29	-1.08
8359_at	YOR202W	HIS3	-0.19	-0.30	0.21	-0.25	-0.18	-0.10	-0.56	0.34	0.28	-0.08	-0.36
8993_at	YNL129W	NRK1	0.17	0.35	0.08	0.32	0.14	0.03	0.40	-0.02	0.01	0.38	0.60
10148_at	YLR168C	YLR168C	-0.06	0.12	0.12	-0.10	-0.03	-0.19	-0.18	0.78	0.85	0.29	0.12
10902_at	YJR109C	CPA2	0.09	0.37	0.69	4.06	3.72	3.51	3.28	4.90	4.67	4.84	5.26
5523_at	YER175C	TMT1	-0.01	0.01	-0.30	0.20	0.28	0.25	0.47	0.25	0.45	0.46	0.97
7831_at	YPL058C	PDR12	-0.16	-0.34	-0.29	-0.53	-0.38	-0.37	-0.46	-0.84	-0.71	-1.17	-1.61
8669_at	YOL119C	MCH4	-0.04	-0.41	0.01	-0.41	-0.17	-0.13	-0.68	0.47	0.80	0.06	-0.48
8691_at	YOL143C	RIB4	0.31	0.17	0.69	0.79	0.17	0.29	0.05	1.14	0.79	0.64	0.40
4540_at	YHL022C	SPO11	-0.20	-0.18	0.39	0.76	0.70	0.69	0.26	1.88	1.74	1.36	1.19
4452_at	YHR071W	PCL5	-0.11	0.28	-0.20	-0.13	-0.11	-0.18	0.11	-0.73	-0.61	-0.14	0.00
9386_at	YMR246W	FAA4	-0.07	0.09	-0.04	0.39	0.35	0.24	0.43	0.35	0.58	0.84	1.06
6358_at	YDR123C	INO2	-0.03	0.34	0.34	0.34	0.42	0.00	0.08	1.55	1.47	0.98	0.94
4537_at	YHR018C	ARG4	-0.66	-0.52	-1.38	-2.60	-1.71	-1.53	-1.16	-2.72	-2.12	-3.02	-1.86
9592_at	YMR062C	ECM40	-0.21	-0.14	-0.27	0.36	0.41	0.03	0.21	0.26	0.26	0.84	0.98

254

Probe ID	Gene ORF	Gene Symbol	fc psocs un /pRAD7 un	fc pRAD7Δrad23 un /pRAD7 un	fc psocsΔrad23 un /pRAD7 un	fc pRAD7 15 /pRAD7 un	fc psocs 15 /psocs un	fc pRAD7Δrad23 15 /pRAD7Δrad23 un	fc psocsΔrad23 15 /psocsΔrad23 un	fc pRAD7 60 /pRAD7 un	fc psocs 60 /psocs un	fc pRAD7Δrad23 60 /pRAD7Δrad23 un	fc psocsΔrad23 60 /psocsΔrad23 un
10715_at	YKL158W	APE2	-0.12	-0.02	-0.21	-0.19	-0.07	0.08	0.17	-0.62	-0.41	-0.03	0.00
7193_at	YBR147W	YBR147W	-0.06	0.34	0.32	-0.34	-0.14	-0.30	-0.27	0.23	0.14	-0.29	-0.38
5669_g_at	YER056C	YER056C	-0.37	-0.31	0.53	1.27	1.28	0.81	0.10	2.08	2.17	1.33	1.38
5614_at	YER086W	ILV1	0.01	-0.07	-0.19	-0.78	-0.65	-0.38	-0.18	-1.33	-1.33	-3.16	-1.96
5672_at	YER057C	HMF1	-0.08	-0.08	0.19	1.45	1.38	0.91	0.81	3.86	3.83	1.18	3.21
5968_at	YDR499W	LCD1	0.11	-0.19	0.09	-0.07	-0.28	-0.24	-0.40	0.82	0.91	0.24	-0.01
10781_at	YKL182W	FAS1	0.03	-0.17	0.07	-0.14	-0.10	-0.12	-0.35	0.63	0.53	0.13	-0.21
5534_at	YER185W	YER185W	0.08	0.42	0.85	0.67	0.56	0.10	-0.07	3.22	3.16	2.00	1.45
7973_at	YPL231W	FAS2	0.06	0.27	0.64	0.56	0.52	0.16	-0.04	2.79	2.79	1.30	1.38
5196_at	YGL184C	STR3	-0.35	0.20	0.48	-0.79	-0.40	-1.07	-1.53	0.21	0.32	-0.86	-0.75
10881_at	YJR133W	XPT1	0.07	-0.02	0.07	0.22	0.24	0.27	0.21	0.29	0.26	0.87	1.29
9628_at	YMR006C	PLB2	-0.09	-0.19	-0.14	0.49	0.53	0.66	0.84	1.68	2.04	1.29	2.84
4257_at	YIL144W	TID3	-0.21	-0.06	-0.04	0.75	1.06	-0.40	0.64	0.31	0.59	0.29	1.05
4330_at	YHR063W	YHR063W	-0.08	-0.18	-0.03	0.19	0.16	0.24	0.04	0.02	0.07	0.44	0.64
4343_at	YHR183W	GND1	-0.21	-0.61	0.06	1.38	1.14	1.03	0.74	0.40	0.93	1.89	1.33
6317_at	YDR171W	HSP42	-0.17	-0.77	-1.15	-0.93	-0.65	-0.42	-0.07	-0.04	0.23	-0.43	0.66
6038_at	YDR432W	NPL3	0.01	0.07	0.30	-0.53	-0.52	-0.52	-0.71	-0.25	-0.41	-0.71	-1.30
6538_at	YDL060W	TSR1	0.23	0.33	0.40	1.10	0.82	0.60	0.75	2.39	2.43	1.87	1.75
6399_at	YDR075W	PPH3	0.02	-0.19	-0.21	0.34	0.27	0.25	0.43	0.48	0.58	1.08	1.09
6467_at	YDR006C	SOK1	-0.24	-0.43	0.12	-0.04	0.07	0.02	-0.73	0.49	0.58	1.18	0.75
6468_at	YDR007W	TRP1	0.14	0.30	0.33	0.40	0.33	0.27	0.23	1.48	1.36	1.98	2.75
6249_at	YDR238C	SEC26	0.15	-0.14	0.33	-0.03	-0.05	0.05	-0.28	0.48	0.39	0.36	-0.20
6318_at	YDR172W	SUP35	-0.07	0.35	0.40	0.48	0.51	0.16	0.05	1.41	1.40	0.89	0.72
6050_at	YDR399W	HPT1	-0.08	0.06	-0.14	0.09	0.15	-0.11	0.20	-0.19	-0.10	0.10	0.49
6594_at	YDL092W	SRP14	-0.13	-0.16	-0.15	0.34	0.47	0.40	0.42	1.30	1.43	1.83	2.01
5957_at	YDR533C	HSP31	0.13	-0.21	0.30	-0.58	-0.70	-0.39	-0.93	0.13	0.05	-0.03	-1.09
6620_at	YDL155W	CLB3	-0.16	-0.01	0.17	-0.27	-0.14	-0.26	-0.50	-0.40	-0.33	-1.00	-1.02
6330_at	YDR139C	RUB1	0.08	0.13	-0.09	0.19	0.13	0.00	0.14	-0.30	-0.35	-0.84	-0.94
6119_at	YDR333C	YDR333C	-0.25	0.03	0.25	1.50	1.67	1.00	0.88	1.93	2.05	1.34	1.30
6818_at	YCR077C	PAT1	-0.15	0.47	0.98	-0.42	-0.25	-0.23	-0.76	-0.37	-0.27	-0.74	-1.18

Probe ID	Gene ORF	Gene Symbol	fc psocs un /pRAD7 un	fc pRAD7Δrad23 un /pRAD7 un	fc psocsΔrad23 un /pRAD7 un	fc pRAD7 15 /pRAD7 un	fc psocs 15 /psocs un	fc pRAD7Δrad23 15 /pRAD7Δrad23 un	fc psocsΔrad23 15 /psocsΔrad23 un	fc pRAD7 60 /pRAD7 un	fc psocs 60 /psocs un	fc pRAD7Δrad23 60 /pRAD7Δrad23 un	fc psocsΔrad23 60 /psocsΔrad23 un
3942_at	YFL031W	HAC1	0.21	0.40	-0.03	-0.48	-0.59	-0.03	0.36	-2.04	-1.87	-1.03	-0.94
10760_at	YKL206C	YKL206C	-0.04	-0.29	-0.24	-0.11	-0.16	0.09	0.28	-0.38	-0.45	0.17	0.24
5220_at	YGL205W	POX1	-0.22	-0.31	0.34	-0.98	-0.75	-1.25	-1.90	-0.09	-0.31	-0.97	-1.43
10106_at	YLR214W	FRE1	0.12	0.28	0.55	0.76	0.70	0.31	0.03	1.75	1.04	1.37	1.24
4386_at	YHR137W	ARO9	0.02	0.15	0.37	0.58	0.44	0.21	-0.07	0.13	-0.33	1.16	0.35
5711_at	YER011W	TIR1	0.09	0.42	0.43	0.31	0.20	-0.12	-0.05	1.22	1.15	0.63	0.59
5297_at	YGL263W	COS12	0.04	0.06	0.27	1.45	1.43	0.98	0.84	2.25	1.67	2.46	2.25
6128_f_at	YDR342C	HXT7	-0.05	0.19	0.42	0.91	0.80	0.51	0.27	3.04	2.73	2.38	2.59
6129_f_at	YDR343C	YDR343C	-0.02	-0.25	0.15	0.04	0.03	-0.10	-0.21	-0.17	-0.52	-0.44	-1.21
5025_at	YGL037C	PNC1	0.00	-0.01	0.42	0.45	0.33	-0.08	-0.35	1.19	0.91	0.98	0.47
5307_at	YFR053C	HXK1	-0.04	0.18	0.31	0.19	0.23	0.16	0.07	1.19	1.00	0.61	0.51
6077_at	YDR380W	ARO10	-0.02	-0.28	0.21	-0.36	-0.24	-0.07	-0.56	0.70	0.46	0.36	-0.21
9633_at	YMR011W	HXT2	-0.25	0.02	0.25	1.66	1.89	1.14	0.87	2.44	2.54	2.03	1.86
6182_f_at	YDR305C	HNT2	0.09	-0.08	0.25	0.31	0.35	0.12	-0.28	1.07	0.83	0.63	0.31
6846_at	YCR061W	YCR061W	-0.04	0.14	0.26	0.72	0.69	0.22	-0.01	0.87	0.50	1.17	0.96
11174_at	YJL164C	TPK1	0.01	-0.30	0.04	0.27	0.07	0.01	-0.34	0.46	0.04	0.57	0.04
7604_at	YPR160W	GPH1	0.06	0.33	0.29	2.68	2.71	2.05	2.17	2.70	2.84	2.76	3.35
7754_at	YPR002W	PDH1	-0.10	-0.25	0.13	-0.55	-0.28	-0.63	-0.93	-0.56	-0.86	-0.75	-1.21
4768_at	YGR248W	SOL4	-0.01	-0.07	0.35	-0.17	-0.14	-0.01	-0.47	-0.34	-0.35	-0.76	-0.96
10179_at	YLR149C	YLR149C	-0.01	-0.18	-0.06	-0.45	-0.37	-0.52	-0.57	0.67	0.79	0.39	-0.02
5582_at	YER142C	MAG1	-0.04	-0.99	-1.35	-0.35	-0.21	-0.82	-0.52	-0.51	-0.48	-0.13	0.60
5060_at	YGL047W	ALG13	0.06	0.25	0.19	0.00	-0.20	0.23	0.23	1.69	1.63	1.83	2.30
5735_at	YEL011W	GLC3	0.02	-0.17	-0.13	0.28	0.22	0.12	0.32	0.03	0.11	0.62	0.63
10574_at	YKR011C	YKR011C	-0.09	-0.04	-0.16	-1.92	-1.82	-1.60	-1.86	-1.93	-2.22	-2.25	-2.80
8010_i_at	YPL240C	HSP82	-0.04	0.06	-0.05	0.17	0.15	0.23	0.32	-0.86	-0.97	-0.26	-0.24
6346_at	YDR111C	ALT2	0.11	0.16	0.14	0.46	0.35	0.28	0.35	0.25	0.30	-0.34	-0.40
7184_at	YBR183W	YPC1	0.10	-0.07	0.06	-0.51	-0.55	-0.29	-0.63	-0.74	-1.00	-1.20	-1.40
10708_at	YKL121W	YKL121W	-0.06	0.18	0.51	1.03	0.92	0.73	0.37	1.32	1.29	1.49	1.26
5699_at	YER044C	YER044C	-0.04	0.15	0.21	-0.21	-0.15	-0.46	-0.38	-0.22	-0.26	-0.80	-0.91
6099_at	YDR358W	GGA1	-0.19	-0.34	0.12	0.64	0.70	0.38	-0.01	1.38	1.15	0.67	0.33

256

Probe ID	Gene ORF	Gene Symbol	fc psocs un /pRAD7 un	fc pRAD7Δrad23 un /pRAD7 un	fc psocsΔrad23 un /pRAD7 un	fc pRAD7 15 /pRAD7 un	fc psocs 15 /psocs un	fc pRAD7Δrad23 15 /pRAD7Δrad23 un	fc psocsΔrad23 15 /psocsΔrad23 un	fc pRAD7 60 /pRAD7 un	fc psocs 60 /psocs un	fc pRAD7Δrad23 60 /pRAD7Δrad23 un	fc psocsΔrad23 60 /psocsΔrad23 un
8599_at	YOL053C	DDR2	0.11	-0.01	0.21	1.91	1.97	1.51	1.28	3.86	3.72	3.46	3.84
11255_at	YJL217W	YJL217W	0.08	0.18	0.48	1.46	1.39	1.11	0.69	2.38	2.01	2.46	2.08
4980_at	YGR008C	STF2	0.01	0.44	0.30	0.43	0.37	0.25	0.28	4.08	3.96	3.73	3.21
8604_at	YOL048C	YOL048C	-0.06	0.05	0.33	0.41	0.44	0.26	0.14	1.12	0.70	0.85	0.50
11260_at	YJL212C	OPT1	-0.02	-0.05	0.19	-0.23	-0.12	-0.12	-0.46	0.17	-0.10	0.20	-0.44
11230_at	YJL196C	ELO1	0.18	0.29	0.45	1.63	1.51	1.02	1.05	2.00	2.09	1.55	1.35
11175_at	YJL163C	YJL163C	0.00	0.00	-0.13	-0.13	-0.08	-0.06	-0.09	-1.33	-1.55	-0.76	-0.69
6847_g_at	YCR061W	YCR061W	-0.03	-0.09	-0.19	-0.30	-0.29	-0.37	-0.11	-1.75	-1.77	-1.22	-1.05
8904_at	YNL037C	IDH1	0.00	0.05	0.27	-0.11	-0.07	-0.14	-0.37	0.96	0.84	0.67	0.26
10075_at	YLR270W	DCS1	0.12	0.10	0.24	0.21	0.11	-0.02	0.12	0.55	0.56	0.12	-0.13
10110_at	YLR218C	YLR218C	0.11	-0.10	0.16	-0.30	-0.31	-0.35	-0.49	0.00	-0.27	-0.59	-0.77
10060_at	YLR258W	GSY2	0.16	0.39	0.09	0.36	0.25	-0.01	0.35	1.03	1.05	1.38	1.69
5751_at	YEL039C	CYC7	-0.07	-0.01	0.26	0.04	0.20	0.22	-0.05	0.68	0.71	0.32	-0.13
10767_at	YKL195W	YKL195W	0.15	-0.20	0.19	-0.53	-0.55	-0.33	-0.61	0.16	-0.04	0.39	-0.49
6485_at	YDL022W	GPD1	-0.17	-0.15	-0.41	-1.79	-1.48	-1.27	-1.18	-1.16	-1.17	-1.21	-1.01
10019_at	YLR304C	ACO1	-0.16	-0.60	-0.55	-1.18	-1.27	-1.00	-1.16	-1.82	-1.95	-1.82	-2.53
5093_at	YGL104C	VPS73	-0.03	-0.06	0.40	0.54	0.52	0.47	0.22	1.20	1.06	1.25	0.49
9388_at	YMR250W	GAD1	0.05	0.09	0.32	-0.16	-0.01	-0.28	-0.40	0.47	0.45	0.10	-0.32
8173_at	YOR374W	ALD4	0.15	-0.51	-0.22	-1.31	-1.32	-1.05	-1.26	-0.57	-0.88	-0.94	-1.27
6694_at	YDL214C	PRR2	-0.05	0.38	0.15	4.20	3.98	3.40	3.66	5.21	5.53	4.71	6.16

A4.5 More Severely Differentially Expressed Genes in Response to UV in *psocs Δrad23* Strain (compared to *pRAD7 Δrad23* strain) (Figure 4.22 and Figure 4.23)

Probe ID	Gene ORF	Gene Symbol	fc psocs un /pRAD7 un	fc pRAD7Δrad23 un /pRAD7 un	fc psocsΔrad23 un /pRAD7 un	fc pRAD7 15 /pRAD7 un	fc psocs 15 /psocs un	fc pRAD7Δrad23 15 /pRAD7Δrad23 un	fc psocsΔrad23 15 /psocsΔrad23 un	fc pRAD7 60 /pRAD7 un	fc psocs 60 /psocs un	fc pRAD7Δrad23 60 /pRAD7Δrad23 un	fc psocsΔrad23 60 /psocsΔrad23 un
6915_at	YCL064C	CHA1	0.08	0.80	0.75	0.59	0.01	-0.73	-0.62	-0.35	-0.42	-1.00	-2.36
3834_s_at	YLL067C	YBL111C	0.24	-0.31	0.28	-0.57	-0.66	-0.34	-0.82	0.49	0.35	-0.17	-1.33
3187_s_at	YHL050C	YBL111C	0.23	-0.34	0.21	-0.40	-0.58	-0.11	-0.49	0.85	0.69	0.36	-0.73
11260_at	YJL212C	OPT1	0.11	0.31	0.76	-0.70	-0.74	-0.70	-0.86	-0.41	-0.73	-0.52	-1.60
7666_at	YPR090W	YPR089W	0.00	0.08	0.04	-0.11	-0.06	-0.09	-0.01	-0.27	-0.34	-0.85	-0.56
10716_at	YKL157W	APE2	0.00	0.06	0.20	0.09	0.15	0.25	0.12	0.25	0.12	-0.02	0.10
3646_s_at	YNL339C	YNL339C	0.27	-0.37	0.15	-0.64	-0.72	-0.31	-0.75	-0.39	-0.61	-0.61	-1.40
10981_at	YJR052W	RAD7	-3.00	-0.75	-3.15	-0.50	-0.42	-0.25	-0.35	0.53	-0.03	0.07	-0.72
7058_at	YBR285W	YBR285W	-0.09	-0.19	-0.14	0.49	0.53	0.66	0.84	1.68	2.04	1.29	2.84
8400_at	YOR153W	PDR5	-0.02	-0.25	0.15	0.04	0.03	-0.10	-0.21	-0.17	-0.52	-0.44	-1.21
7422_at	YBL075C	SSA3	0.14	0.30	0.33	0.40	0.33	0.27	0.23	1.48	1.36	1.98	2.75
10760_at	YKL206C	YKL206C	0.31	0.22	-0.64	0.60	0.17	0.37	1.31	1.22	1.11	1.18	2.01
8663_at	YOL126C	MDH2	-0.04	-0.99	-1.35	-0.35	-0.21	-0.82	-0.52	-0.51	-0.48	-0.13	0.60
5654_at	YER081W	SER3	-0.31	-0.78	-0.91	0.93	0.85	1.10	1.45	0.28	0.71	1.79	2.53
7130_g_at	YBR220C	YBR219C	-0.01	-0.08	-0.10	0.02	0.03	0.09	0.23	-0.92	-0.74	-0.86	-0.69
10447_s_at	YKL198C	PTK1	0.02	-0.37	-0.14	-0.30	-0.21	-0.17	-0.38	-0.02	0.09	0.00	-0.77
10653_at	YKL086W	SRX1	-0.17	0.05	-0.39	0.65	0.87	0.33	0.80	0.73	1.10	1.06	1.78
9904_at	YLR413W	YLR413W	-0.16	-0.60	-0.55	-1.18	-1.27	-1.00	-1.16	-1.82	-1.95	-1.82	-2.53
10982_at	YJR053W	BFA1	0.01	-0.44	0.04	-0.41	-0.47	-0.55	-0.96	0.67	0.50	-0.42	-1.12
11360_at	YAL048C	YAL048C	0.01	-0.36	0.22	-0.36	-0.33	0.03	-0.60	0.10	-0.05	-0.10	-0.77
9912_at	YLR421C	RPN13	-0.03	-0.06	0.40	0.54	0.52	0.47	0.22	1.20	1.06	1.25	0.49
4324_s_at	YHR218W	YBL111C	0.13	-0.27	0.23	-0.17	-0.36	0.16	-0.41	0.73	0.70	-0.05	-0.70
4287_s_at	YHR209W	YHR209W	-0.10	0.40	0.05	0.65	0.68	0.54	0.75	2.11	2.19	2.06	2.81
3183_f_at	YIL177C	YBL113C	0.04	0.14	-0.19	0.70	0.30	0.07	0.50	0.53	0.60	-0.43	0.10
9108_at	YNL241C	ZWF1	0.14	-0.13	0.33	0.36	0.20	0.26	-0.08	1.50	1.22	0.78	0.16
11298_at	YAR042W	SWH1	0.11	-0.41	0.09	-0.43	-0.36	-0.12	-0.61	-0.02	-0.12	0.15	-0.81

Probe ID	Gene ORF	Gene Symbol	fc psocs un /pRAD7 un	fc pRAD7Δrad23 un /pRAD7 un	fc psocsΔrad23 un /pRAD7 un	fc pRAD7 15 /pRAD7 un	fc psocs 15 /psocs un	fc pRAD7Δrad23 15 /pRAD7Δrad23 un	fc psocsΔrad23 15 /psocsΔrad23 un	fc pRAD7 60 /pRAD7 un	fc psocs 60 /psocs un	fc pRAD7Δrad23 60 /pRAD7Δrad23 un	fc psocsΔrad23 60 /psocsΔrad23 un
11230_at	YJL196C	ELO1	0.16	0.30	0.61	0.31	0.25	0.44	0.15	0.79	0.59	0.74	0.13
11366_at	YAL043C	PTA1	0.02	-0.14	0.14	0.06	-0.03	0.05	-0.17	-0.11	-0.10	0.31	-0.25
8575_at	YOL032W	YOL032W	0.06	0.33	0.29	2.68	2.71	2.05	2.17	2.70	2.84	2.76	3.35
11026_at	YJR004C	SAG1	0.12	-0.11	-0.29	0.02	-0.15	-0.05	0.28	-0.39	-0.46	-0.43	0.23
11020_i_at	YJL001W	PRE3	0.03	-0.05	0.36	0.27	0.22	0.51	0.24	1.70	1.59	1.37	0.96
5608_at	YER123W	YCK3	0.08	0.07	0.49	-0.33	-0.37	-0.36	-0.66	0.05	0.00	0.10	-0.59
3736_s_at	YLR467W	YLR467W	0.16	-0.52	0.28	-0.82	-0.72	-0.25	-0.99	-0.28	-0.39	-0.06	-1.04
7298_at	YBR075W	YBR074W	-0.07	0.58	0.26	0.24	0.15	-0.02	0.14	-0.47	-0.48	-0.80	-0.45
9335_at	YMR286W	MRPL33	-0.02	-0.05	0.19	-0.23	-0.12	-0.12	-0.46	0.17	-0.10	0.20	-0.44
8470_at	YOR088W	YVC1	-0.07	0.00	0.00	-0.03	0.10	-0.14	-0.09	0.44	0.12	-0.13	0.20
7423_at	YBL074C	AAR2	0.15	-0.14	0.33	-0.03	-0.05	0.05	-0.28	0.48	0.39	0.36	-0.20
6513_at	YDL039C	PRM7	-0.66	-0.52	-1.38	-2.60	-1.71	-1.53	-1.16	-2.72	-2.12	-3.02	-1.86
5421_i_at	YFL067W	YFL067W	-0.17	-0.21	-0.19	-0.12	0.10	-0.10	-0.14	-0.17	-0.10	-0.02	0.28
11136_at	YJL111W	CCT7	-0.09	0.01	0.25	-0.07	0.04	0.20	-0.06	-0.02	-0.19	-0.10	-0.65
6847_g_at	YCR061W	YCR061W	0.06	0.27	0.64	0.56	0.52	0.16	-0.04	2.79	2.79	1.30	1.38
3737_s_at	YLR467W	YLR467W	0.03	-0.44	0.13	-0.51	-0.50	-0.12	-0.72	-0.29	-0.27	-0.66	-1.24
8811_at	YNR053C	NOG2	-0.09	0.12	-0.20	-1.33	-1.14	-1.07	-1.16	-2.01	-2.33	-2.39	-2.46
10341_at	YLL002W	RTT109	-0.01	0.05	0.23	-0.14	0.09	-0.19	0.01	0.03	-0.07	-0.05	-0.59
5988_at	YDR474C	JIP4	0.04	0.04	0.01	-0.41	-0.20	-0.54	-0.34	0.52	0.78	-1.17	-0.40
10446_s_at	YKL199C	YKL199C	0.07	-0.36	-0.29	0.00	-0.04	-0.04	-0.08	0.11	0.22	0.11	-0.44
11322_at	YAL001C	TFC3	0.14	0.35	0.00	-0.07	-0.17	-0.24	0.16	0.12	0.04	-0.92	-0.29
11013_at	YJL008C	CCT8	0.03	0.08	0.34	0.06	0.08	0.26	0.03	0.57	0.34	0.21	-0.32
3791_s_at	YLL067C	YBL111C	0.18	-0.17	0.11	-0.57	-0.60	-0.39	-0.68	-0.04	-0.17	0.03	-0.65
10081_at	YLR234W	TOP3	0.05	0.14	0.29	-0.28	-0.23	-0.17	-0.56	0.55	0.45	0.67	-0.10
9293_at	YML058W	HUG1	0.01	0.44	0.30	0.43	0.37	0.25	0.28	4.08	3.96	3.73	3.21
4892_at	YGR102C	YGR102C	0.03	0.22	-0.10	0.57	0.36	0.31	0.58	0.77	0.76	0.90	1.42
5576_at	YER135C	YER135C	0.01	0.10	0.51	0.08	0.00	0.07	-0.48	-0.03	-0.03	-0.11	-0.63
7822_at	YPL067C	YPL067C	0.02	-0.33	0.02	-0.21	0.01	-0.12	-0.45	-0.69	-0.79	-0.70	-1.21
8404_at	YOR157C	PUP1	0.00	-0.01	0.42	0.45	0.33	-0.08	-0.35	1.19	0.91	0.98	0.47
5775_at	YEL059C	SOM1	-0.01	0.01	-0.30	0.20	0.28	0.25	0.47	0.25	0.45	0.46	0.97

259

Probe ID	Gene ORF	Gene Symbol	fc psocs un /pRAD7 un	fc pRAD7Δrad23 un /pRAD7 un	fc psocsΔrad23 un /pRAD7 un	fc pRAD7 15 /pRAD7 un	fc psocs 15 /psocs un	fc pRAD7Δrad23 15 /pRAD7Δrad23 un	fc psocsΔrad23 15 /psocsΔrad23 un	fc pRAD7 60 /pRAD7 un	fc psocs 60 /psocs un	fc pRAD7Δrad23 60 /pRAD7Δrad23 un	fc psocsΔrad23 60 /psocsΔrad23 un
6619_at	YDL156W	YDL156W	0.05	-0.09	0.30	-0.48	-0.29	-0.15	-0.86	-0.10	0.00	-0.18	-0.67
3184_s_at	YIL177C	YRF1-1	0.08	-0.53	-0.22	-0.56	-0.64	0.17	-0.37	-0.16	-0.35	0.04	-0.18
11210_at	YJL173C	RFA3	0.08	0.29	0.50	0.45	0.30	0.67	0.37	0.95	0.61	0.99	0.42
9873_at	YLR426W	YLR426W	0.14	0.30	0.26	0.21	0.05	-0.11	0.02	0.33	0.30	0.20	0.07
7394_at	YBL013W	FMT1	0.10	-0.22	0.03	-0.37	-0.37	-0.37	-0.54	-0.27	-0.19	-0.28	-0.75
8724_at	YOL155C	YOL155C	0.06	0.25	0.19	0.00	-0.20	0.23	0.23	1.69	1.63	1.83	2.30
10717_at	YKL156W	RPS27A	0.03	0.02	0.16	-0.08	-0.06	0.05	-0.14	-0.78	-1.29	-0.87	-1.34
11348_at	YAL019W	FUN30	-0.07	-0.04	0.05	-0.99	-0.85	-0.55	-0.81	-1.37	-1.55	-1.46	-1.92
10299_at	YLR047C	YLR047C	0.06	-0.15	0.20	0.07	0.01	0.17	-0.14	0.60	0.53	0.35	-0.11
10022_at	YLR307W	CDA1	-0.18	0.29	0.08	-0.08	0.20	0.10	0.14	-0.17	0.01	0.01	0.48
8030_at	YPL265W	DIP5	-0.22	-0.31	0.34	-0.98	-0.75	-1.25	-1.90	-0.09	-0.31	-0.97	-1.43
8610_at	YOL042W	NGL1	-0.10	-0.25	0.13	-0.55	-0.28	-0.63	-0.93	-0.56	-0.86	-0.75	-1.21
7549_g_at	YPR196W	MAL33	0.12	0.16	0.02	0.46	0.34	0.42	0.47	0.41	0.50	0.40	0.72
8303_at	YOR237W	HES1	-0.15	0.09	-0.04	-0.01	0.10	0.05	0.15	-0.09	0.03	0.05	0.50
11134_at	YJL115W	ASF1	0.07	0.40	0.46	0.03	0.09	-0.02	-0.22	0.90	0.71	0.92	0.43
3948_s_at	YKL198C	PTK1	-0.01	-0.34	-0.15	-0.19	-0.35	-0.09	-0.27	0.11	0.15	0.10	-0.35
10181_at	YLR151C	PCD1	-0.14	0.17	0.19	0.25	0.44	0.41	0.03	1.58	1.68	1.58	2.03
6690_at	YDL218W	YDL218W	-0.02	-0.06	0.17	-0.02	0.09	0.09	0.01	0.59	0.76	0.74	1.19
5188_at	YGL191W	COX13	-0.10	0.13	0.02	0.41	0.46	0.40	0.49	0.77	1.02	1.01	1.46
9711_at	YML088W	UFO1	-0.07	-0.01	0.26	0.04	0.20	0.22	-0.05	0.68	0.71	0.32	-0.13
9996_at	YLR327C	RBF9	-0.05	0.38	0.15	4.20	3.98	3.40	3.66	5.21	5.53	4.71	6.16
11221_at	YJL206C	NCE101	0.04	-0.03	0.18	0.36	0.30	0.65	0.33	0.73	0.53	0.74	0.28
4075_at	YIR039C	YPS6	0.01	0.15	0.25	0.91	0.90	1.01	0.93	2.42	2.60	2.15	3.12
4725_f_at	YGR122C	YGR122C	0.17	-0.03	-0.06	0.03	0.03	0.07	0.21	0.11	-0.15	0.12	0.12
5789_at	YEL046C	GLY1	-0.16	-0.34	-0.29	-0.53	-0.38	-0.37	-0.46	-0.84	-0.71	-1.17	-1.61
7754_at	YPR002W	PDH1	-0.15	0.47	0.98	-0.42	-0.25	-0.23	-0.76	-0.37	-0.27	-0.74	-1.18
5536_at	YER187W	YER187W	-0.14	0.34	-0.22	-0.17	-0.13	-0.31	0.10	-0.61	-0.31	-0.92	0.13
10750_at	YKL169C	YKL169C	0.03	0.16	-0.17	0.35	0.30	0.12	0.48	0.43	0.45	0.53	0.97
10986_at	YJR057W	CDC8	-0.04	0.17	0.41	-0.03	0.08	0.28	-0.17	0.28	0.05	0.18	-0.25
11046_at	YJL021C	BBC1	0.11	0.17	0.31	0.06	-0.14	0.01	-0.08	0.86	0.84	-0.27	-0.25

260

Probe ID	Gene ORF	Gene Symbol	fc psocs un /pRAD7 un	fc pRAD7Δrad23 un /pRAD7 un	fc psocsΔrad23 un /pRAD7 un	fc pRAD7 15 /pRAD7 un	fc psocs 15 /psocs un	fc pRAD7Δrad23 15 /pRAD7Δrad23 un	fc psocsΔrad23 15 /psocsΔrad23 un	fc pRAD7 60 /pRAD7 un	fc psocs 60 /psocs un	fc pRAD7Δrad23 60 /pRAD7Δrad23 un	fc psocsΔrad23 60 /psocsΔrad23 un
10856_at	YJR154W	YJR154W	0.02	-0.34	-0.02	-0.61	-0.36	-0.15	-0.45	-0.06	-0.05	0.02	-0.56
10621_at	YKL031W	YKL031W	-0.07	-0.07	-0.32	-0.12	0.09	-0.30	0.12	-0.47	-0.28	-0.43	0.00
8679_at	YOL109W	ZEO1	-0.02	0.19	0.30	0.05	0.04	-0.23	-0.43	0.02	-0.47	-0.02	-0.44
7812_at	YPL078C	ATP4	0.00	0.18	0.01	0.61	0.49	0.42	0.47	1.05	1.19	1.17	1.59
9800_s_at	YML133C	YBL111C	0.15	-0.20	0.19	-0.53	-0.55	-0.33	-0.61	0.16	-0.04	0.39	-0.49
9180_at	YNL304W	YPT11	-0.12	-0.02	0.18	-0.16	-0.14	-0.27	-0.53	0.18	0.19	0.17	-0.25
9928_at	YLR393W	ATP10	0.05	0.09	0.32	-0.16	-0.01	-0.28	-0.40	0.47	0.45	0.10	-0.32
6961_g_at	YCL065W	YCL065W	0.00	0.05	-0.20	0.19	0.00	-0.01	0.16	0.10	0.17	0.46	0.40
6934_at	YCL041C	YCL041C	0.07	-0.02	0.07	0.22	0.24	0.27	0.21	0.29	0.26	0.87	1.29
7807_at	YPL036W	PMA2	-0.16	-0.54	-0.07	-0.25	0.02	0.15	-0.35	-0.44	-0.47	-0.47	-0.89
6054_at	YDR403W	DIT1	0.00	0.02	-0.14	0.01	-0.06	-0.03	0.12	0.16	0.22	0.21	0.62
8630_at	YOL067C	RTG1	-0.01	-0.18	-0.06	-0.45	-0.37	-0.52	-0.57	0.67	0.79	0.39	-0.02
11351_at	YAL016W	TPD3	0.13	0.02	0.37	0.37	0.32	0.37	0.04	0.46	-0.27	0.62	-0.11
7789_at	YPL054W	LEE1	-0.07	0.00	0.13	0.31	0.40	0.24	0.09	1.04	1.40	1.13	1.54
10624_at	YKL072W	STB6	-0.06	-0.12	0.01	-0.81	-0.55	-0.51	-0.60	-0.78	-0.85	-0.79	-1.20
10651_at	YKL088W	YKL088W	0.01	-0.30	0.02	-0.15	-0.04	-0.24	-0.43	-0.11	0.04	-0.21	-0.62
7488_at	YBL098W	BNA4	0.16	0.49	0.18	0.19	0.15	0.11	0.49	-0.29	-0.45	-0.26	0.15
11021_f_at	YJL001W	PRE3	0.09	-0.31	0.28	0.61	0.40	0.74	0.26	1.69	1.64	1.46	0.87
9624_at	YMR002W	YMR002W	0.00	0.05	0.27	-0.11	-0.07	-0.14	-0.37	0.96	0.84	0.67	0.26
4212_g_at	YIL099W	SGA1	-0.05	0.22	0.14	0.30	0.46	0.31	0.26	1.43	1.53	1.24	1.93
8021_at	YPL274W	SAM3	0.08	-0.54	-0.09	-0.39	-0.34	0.10	0.10	0.08	0.03	0.00	-0.40
9392_at	YMR253C	YMR253C	0.06	-0.23	0.06	0.39	0.38	0.48	0.19	0.90	0.51	0.73	0.33
10532_at	YKR061W	KTR2	-0.15	0.09	-0.30	0.30	0.48	0.27	0.53	0.00	0.31	0.13	0.53

A4.6 Top 100 Differentially Regulated Genes in *psocs* Untreated Strain (Figure 6.12 and Figure 6.13)

Probe ID	Gene ORF	Gene Symbol	fc *psocs* un /p*RAD7* un	fc p*RAD7Δrad23* un /p*RAD7* un	fc *psocsΔrad23* un /p*RAD7* un
10981_at	YJR052W	RAD7	-3.00	-0.75	-3.15
6538_at	YDL060W	TSR1	-0.80	-0.40	-0.01
4343_at	YHR183W	GND1	-0.78	0.13	0.23
4330_at	YHR063W	YHR063W	-0.72	0.05	-0.01
4257_at	YIL144W	TID3	-0.69	0.07	-0.02
6318_at	YDR172W	SUP35	-0.67	-0.54	0.04
6513_at	YDL039C	PRM7	-0.66	-0.52	-1.38
3942_at	YFL031W	HAC1	0.64	0.24	0.19
6038_at	YDR432W	NPL3	-0.64	-1.02	0.14
6249_at	YDR238C	SEC26	-0.61	-0.67	0.09
6468_at	YDR007W	TRP1	-0.58	-0.77	-0.25
6025_at	YDR465C	RMT2	-0.58	-0.50	-0.09
6514_at	YDL038C	YDL038C	-0.57	-0.65	-1.27
6395_at	YDR071C	PAA1	-0.56	-0.27	0.09
6535_at	YDL063C	YDL063C	-0.55	-0.39	-0.28
6455_s_at	YDR039C	ENA2	-0.55	-0.25	0.08
4399_at	YHR149C	SKG6	-0.55	0.33	0.18
6958_s_at	YCL067C	HMLALPHA2	-0.55	-0.50	0.01
6316_at	YDR170C	SEC7	-0.55	-0.45	0.01
6515_at	YDL037C	BSC1	-0.54	-1.25	-1.19
4342_at	YHR182W	YHR182W	-0.54	0.03	0.03
4978_at	YGR052W	FMP48	-0.54	-0.51	-0.53
4187_at	YIL077C	YIL077C	-0.54	0.19	0.01
6537_f_at	YDL061C	RPS29B	-0.53	-0.60	-0.03
4199_at	YIL112W	HOS4	-0.53	0.00	-0.07
6827_at	YCR037C	PHO87	-0.52	-0.24	-0.09
6317_at	YDR171W	HSP42	-0.52	-0.08	0.65
6120_at	YDR334W	SWR1	-0.51	-0.48	0.07
6107_at	YDR365C	ESF1	-0.51	-0.60	-0.20
6050_at	YDR399W	HPT1	-0.51	-0.62	-0.06
6329_at	YDR139C	RUB1	-0.51	-0.42	-0.02
5957_at	YDR533C	HSP31	-0.51	-0.72	-0.12
6178_at	YDR304C	CPR5	-0.51	-0.53	0.25
6049_at	YDR398W	UTP5	-0.50	-0.45	-0.18
6618_at	YDL157C	YDL157C	-0.50	-0.24	0.27
6620_at	YDL155W	CLB3	-0.50	-0.72	-0.09
6456_at	YDR041W	RSM10	-0.50	-0.41	0.08
5965_at	YDR496C	PUF6	-0.49	-0.27	-0.13
6467_at	YDR006C	SOK1	-0.49	-0.68	-0.25
6119_at	YDR333C	YDR333C	-0.49	-0.63	0.03
5685_at	YER030W	YER030W	-0.49	-0.51	0.02
6399_at	YDR075W	PPH3	-0.48	-0.68	-0.31
6396_at	YDR072C	IPT1	-0.48	-0.39	-0.20
6521_at	YDL031W	DBP10	-0.47	-0.01	-0.24
6594_at	YDL092W	SRP14	-0.47	-0.73	-0.02
5668_at	YER056C	YER056C	-0.47	-0.38	-0.33

Probe ID	Gene ORF	Gene Symbol	fc psocs un /pRAD7 un	fc pRAD7Δrad23 un /pRAD7 un	fc psocsΔrad23 un /pRAD7 un
6245_at	YDR234W	LYS4	-0.47	-0.31	-0.23
6246_at	YDR235W	PRP42	-0.47	-0.23	-0.01
11101_at	YJL056C	ZAP1	0.46	-0.64	-0.35
6094_at	YDR397C	NCB2	-0.46	-0.36	-0.12
6760_g_at	YCL057C	YCL057C-A	-0.46	-0.31	0.10
6176_at	YDR302W	GPI11	-0.45	-0.34	0.14
6523_at	YDL029W	ARP2	-0.45	-0.39	0.16
6818_at	YCR077C	PAT1	-0.45	-0.61	-0.01
7828_at	YPL061W	ALD6	-0.45	0.88	0.87
6244_at	YDR233C	RTN1	-0.45	0.04	0.01
6313_at	YDR167W	TAF10	-0.45	-0.01	-0.04
6175_at	YDR301W	CFT1	-0.44	-0.35	-0.08
6886_at	YCR009C	RVS161	-0.44	-0.55	0.05
6327_at	YDR137W	RGP1	-0.44	-0.14	0.03
6604_at	YDL126C	CDC48	-0.44	-0.17	0.24
6325_at	YDR135C	YCF1	-0.44	0.32	0.20
6454_g_at	YDR038C	ENA5	-0.43	-0.20	0.10
6177_at	YDR303C	RSC3	-0.43	-0.48	-0.15
6314_at	YDR168W	CDC37	-0.43	0.02	0.10
6092_at	YDR395W	SXM1	-0.43	0.01	-0.02
6173_at	YDR299W	BFR2	-0.43	0.12	-0.10
6248_at	YDR237W	MRPL7	-0.42	-0.41	0.04
7041_s_at	YBR267W	REI1	-0.42	-0.25	-0.24
6673_at	YDL190C	UFD2	-0.42	-0.29	0.08
6381_at	YDR101C	ARX1	-0.42	-0.03	-0.33
6688_at	YDL219W	DTD1	-0.42	-0.51	0.21
11133_at	YJL116C	NCA3	-0.42	0.49	0.12
6315_at	YDR169C	STB3	-0.42	-0.40	-0.10
8018_i_at	YPL277C	YPL277C	0.41	-0.07	-0.03
6330_at	YDR139C	RUB1	-0.41	-0.60	0.04
7888_at	YPL137C	YPL137C	-0.41	0.05	0.12
5752_at	YEL038W	UTR4	-0.41	-0.26	0.12
6323_at	YDR133C	YDR133C	-0.41	0.14	0.18
10609_at	YKL043W	PHD1	-0.41	-0.44	-0.60
6605_at	YDL125C	HNT1	-0.41	-0.34	0.14
6398_at	YDR074W	TPS2	-0.40	-0.25	0.50
7459_s_at	YBL083C	ALG3	-0.40	-0.26	0.00
6591_at	YDL095W	PMT1	-0.40	-0.08	0.09
5813_at	YEL071W	DLD3	-0.40	-0.19	0.37
6174_at	YDR300C	PRO1	-0.40	0.17	0.11
6033_at	YDR427W	RPN9	-0.40	0.24	0.34
6451_at	YDR036C	EHD3	-0.39	0.15	0.16
6190_at	YDR270W	CCC2	-0.39	-0.49	0.04
9885_at	YLR438W	CAR2	0.39	-0.02	0.16
8545_at	YOR027W	STI1	0.39	0.81	0.94
6102_at	YDR361C	BCP1	-0.39	0.09	-0.10
5616_at	YER087C	SBH1	-0.39	-0.49	0.04
5969_at	YDR500C	RPL37B	-0.39	-0.49	0.03
4078_i_at	YIR043C	YIR043C	0.39	1.14	0.82

Probe ID	Gene ORF	Gene Symbol	fc psocs un /pRAD7 un	fc pRAD7Δrad23 un /pRAD7 un	fc psocsΔrad23 un /pRAD7 un
6522_at	YDL030W	PRP9	-0.39	-0.21	-0.09
6466_at	YDR005C	MAF1	-0.38	-0.43	-0.04
4411_at	YHR118C	ORC6	-0.38	0.03	-0.18
6606_at	YDL125C	HNT1	-0.38	-0.31	0.14

A4.7 Significantly Differentially Expressed Genes from Spellman 800 List In *psocs* Untreated Strain (Figure 6.14 and Figure 6.15)

Probe ID	Gene ORF	Gene Symbol	fc psocs un /pRAD7 un	fc pRAD7Δrad23 un /pRAD7 un	fc psocsΔrad23 un /pRAD7 un
8988_at	YNL134C	YNL134C	0.21	0.51	0.60
6424_at	YDR055W	PST1	0.28	0.70	0.37
8480_at	YOR052C	YOR052C	-0.25	0.02	0.25
7321_at	YBR053C	YBR053C	0.23	0.33	0.40
5750_at	YEL040W	UTR2	-0.31	-0.15	-0.01
8779_at	YNR067C	DSE4	0.21	0.25	0.45
5544_at	YER150W	SPI1	-0.35	-0.01	0.40
10078_at	YLR273C	PIG1	0.29	0.48	0.49
3646_s_at	YNL339C	YNL339C	0.27	-0.37	0.15
3792_s_at	YLL066C	YBL113C	0.08	0.21	0.10
3834_s_at	YLL067C	YBL111C	0.24	-0.31	0.28
6603_at	YDL127W	PCL2	-0.22	-0.15	0.04
3187_s_at	YHL050C	YBL111C	0.23	-0.34	0.21
3184_s_at	YIL177C	YRF1-1	0.08	-0.53	-0.22
6462_at	YDR001C	NTH1	-0.37	0.31	0.05
10502_at	YKR077W	YKR077W	0.20	0.79	0.55
4399_at	YHR149C	SKG6	-0.55	0.33	0.18
7294_at	YBR071W	YBR071W	0.23	0.68	0.48
5952_at	YDR528W	HLR1	-0.26	0.10	-0.01
8975_at	YNL102W	POL1	0.20	0.74	0.38
7832_at	YPL057C	SUR1	0.25	0.26	0.26
6591_at	YDL095W	PMT1	-0.40	-0.08	0.09
6593_at	YDL093W	PMT5	-0.38	-0.41	0.11
9044_at	YNL169C	PSD1	0.21	-1.19	-0.61
5546_at	YER152C	YER152C	-0.21	-0.33	0.04
5746_at	YER001W	MNN1	0.20	0.32	0.00
5602_at	YER118C	SHO1	-0.27	-0.31	0.13
6618_at	YDL157C	YDL157C	-0.50	-0.24	0.27
6171_at	YDR297W	SUR2	-0.33	-0.02	-0.26
4257_at	YIL144W	TID3	-0.69	0.07	-0.02
7999_at	YPL250C	ICY2	0.34	-0.53	-0.21
6008_at	YDR448W	ADA2	-0.33	-0.10	-0.06
5748_at	YEL042W	GDA1	-0.31	0.13	-0.03
11097_at	YJL060W	BNA3	0.27	0.28	0.17
6176_at	YDR302W	GPI11	-0.45	-0.34	0.14
4396_at	YHR146W	CRP1	-0.20	-0.06	-0.12
10977_at	YJR048W	CYC1	0.26	0.64	0.92

7400_at	YBL052C	SAS3	-0.26	-0.60	-0.10
4884_i_at	YGR138C	TPO2	0.28	-0.01	-0.57
8030_at	YPL265W	DIP5	-0.22	-0.31	0.34
8543_at	YOR025W	HST3	0.25	-0.13	-0.16
7614_at	YPR128C	ANT1	-0.25	-0.13	0.22
9885_at	YLR438W	CAR2	0.39	-0.02	0.16
5216_at	YGL209W	MIG2	0.36	-0.18	-0.20
7831_at	YPL058C	PDR12	0.24	-0.84	-0.68
6038_at	YDR432W	NPL3	-0.64	-1.02	0.14
10609_at	YKL043W	PHD1	-0.41	-0.44	-0.60
8249_at	YOR313C	SPS4	0.22	-0.02	0.13
8684_at	YOL150C	YOL150C	-0.20	-0.37	-0.49
6894_at	YCL038C	ATG22	-0.22	0.15	0.15
10608_at	YKL044W	YKL044W	-0.30	-0.57	-0.45
7840_at	YPL095C	YPL095C	0.21	0.40	-0.03
6513_at	YDL039C	PRM7	-0.66	-0.52	-1.38
6515_at	YDL037C	BSC1	-0.54	-1.25	-1.19
5585_at	YER145C	FTR1	-0.28	0.26	0.13
7828_at	YPL061W	ALD6	-0.45	0.88	0.87
6602_at	YDL128W	VCX1	-0.33	-0.22	0.01
6830_at	YCR042C	TAF2	-0.33	-0.51	-0.13
7322_at	YBR054W	YRO2	0.36	-0.03	-0.42

265

Appendix V – Growth Curve Optical Density (OD$_{600}$) Values

Growth Curve Data From Chapter 3 (Figure 3.7)

Figure 3.7 1. Growth at 25°C

Time (Hours)	WT	abf1-1	abf1-1 sug2-1	sug2-1
0	0.100	0.100	0.100	0.100
1	0.143	0.113	0.137	0.135
2	0.191	0.122	0.156	0.164
3	0.256	0.143	0.177	0.238
4	0.302	0.184	0.186	0.282
5	0.390	0.197	0.224	0.371
6	0.461	0.224	0.248	0.446
7	0.541	0.269	0.267	0.519
8	0.599	0.289	0.289	0.572

Figure 3.7 2. Growth at 30°C

Time (Hours)	WT	abf1-1	abf1-1 sug2-1	sug2-1
0	0.100	0.100	0.100	0.100
1	0.116	0.133	0.118	0.166
2	0.168	0.153	0.133	0.236
3	0.269	0.159	0.151	0.341
4	0.372	0.190	0.186	0.429
5	0.440	0.215	0.204	0.525
6	0.519	0.220	0.221	0.585
7	0.558	0.250	0.243	0.649
8	0.609	0.284	0.252	0.713

Figure 3.7 3. Growth at 37°C

Time (Hours)	WT	abf1-1	abf1-1 sug2-1	sug2-1
0	0.100	0.100	0.100	0.100
1	0.184	0.099	0.117	0.161
2	0.251	0.101	0.092	0.203
3	0.391	0.079	0.119	0.328
4	0.525	0.104	0.113	0.401
5	0.624	0.086	0.107	0.463
6	0.755	0.107	0.116	0.523
7	0.860	0.112	0.110	0.602
8	0.924	0.110	0.110	0.663

Growth Curve Data From Chapter 6

(Figure 6.2, Figure 6.3 and Figure 6.16)

Figure 6.2 – Growth From Early Stationary Phase Cultures

Time (Hours)	pRAD7	psocs
0	0.100	0.100
1	0.102	0.108
2	0.130	0.129
3	0.194	0.187
4	0.255	0.232
5	0.311	0.269
6	0.505	0.405
7	0.650	0.530
8	0.813	0.735
9	1.330	0.874
10	2.580	1.777
12	4.360	3.367
13	4.950	4.027
14	5.190	4.427

Figure 6.3 – Growth From Logarithmic Phase Cultures

Time (Hours)	pRAD7	psocs
0	0.100	0.100
1	0.102	0.102
2	0.115	0.116
3	0.158	0.153
4	0.217	0.210
5	0.320	0.304
6	0.468	0.454
7	0.685	0.661
8	0.943	0.917
9	1.965	1.899
10	2.735	2.669
12	3.415	3.329
13	3.815	3.729

Figure 6.16 – Growth From Early Stationary Phase Cultures

Time (Hours)	pRAD7 Δrad23 Δsml1	psocs Δrad23 Δsml1	pRAD7 Δrad23 Δcrt1	psocs Δrad23 Δcrt1
0	0.100	0.100	0.100	0.100
1	0.090	0.097	0.104	0.117
2	0.128	0.131	0.146	0.167
3	0.211	0.210	0.224	0.222
4	0.303	0.277	0.29	0.290
5	0.389	0.338	0.386	0.378
6	0.595	0.559	0.604	0.586
7	0.761	0.677	0.753	0.739
8	1.166	0.921	1.071	1.316
9	1.386	1.218	1.461	1.376
10	2.926	2.598	2.821	2.626
12	4.506	4.388	4.391	4.186
13	4.856	4.828	4.881	4.786
14	4.906	4.878	4.931	4.866

Appendix VI – Plasmid Stability Data

(Table 6.2)

Cell Counts on YPD and HIS- plates

pRAD7 Strain

	0h	4h
YPD - 1	191	418
YPD - 2	185	451
YPD - 3	208	305
Mean	194.7	391.3
HIS - 1	165	248
HIS - 2	154	223
HIS - 3	185	225
Mean	168.0	232.0

% HIS$^+$	86.3	59.3

psocs Strain

	0h	4h
YPD - 1	372	1089
YPD - 2	408	1106
YPD - 3	567	999
Mean	449.0	1064.7
HIS - 1	347	734
HIS - 2	385	731
HIS - 3	358	689
Mean	363.3	718.0

% HIS$^+$	80.9	67.4

Appendix VII – qPCR Data

Figure 4.5

Number of qPCR Cycles Shown for *RAD7* and *ACT1* (control)

Relative Expression Values calculated using:

$$\text{Relative Expression} = 2^{((ACT1 \text{ mean cycles}) - (RAD7 \text{ mean cycles}))}$$

	pRS314-RAD7	pRS314-socs	pRS313-RAD7	pRS313-socs
ACT1 - 1	25.6	26.5	25.0	24.9
ACT1 - 2	25.2	25.3	25.0	25.0
ACT1 - 3	25.5	26.0	25.0	24.8
Mean	25.4	25.9	25.0	24.9
RAD7 - 1	18.6	20.3	18.8	19.3
RAD7 - 2	18.7	20.4	18.9	19.4
RAD7 - 3	18.5	19.8	18.7	19.2
Mean	18.6	20.2	18.8	19.3

Relative Expression Values	114.0	54.4	73.5	48.5
	1	0.48	1	0.66

Figure 5.6

Number of qPCR Cycles Shown for *DUN1* Promoter Input and IP.

Ratio Values calculated using: IP mean / Input mean

	Input	IP	Input Mean	IP Mean	Input Adjusted	IP Adjusted	IP/Input	SD
pRAD7	4.95E-03	2.85E-04	5.40E-03	2.42E-04	0.488	1.938	**3.972**	1.715
	5.31E-03	2.41E-04						
	5.95E-03	1.98E-04						
Δrad4Δrad23	1.11E-02	1.34E-04	1.11E-02	1.25E-04	1	1	1	
	1.14E-02	1.15E-04						
	1.08E-02							

Appendix VIII - PCR Primers

All oligonucleotide primers were synthesised by Eurofins MWG Operon (Germany).

Chapter 3.2.2 (Figure 3.3)
Primers to Amplify *pRS306 URA3* gene, with homology to *ABF1* 3'
Region (**Bold** indicates homology to *pRS306* plasmid)

F	GCA ATT GCG CCA ACG TAA CGA CGT TAC CAA TGG GCA AGT CTA CGA AGA AGC **GCA GAT TGT ACT GAG AGT GC**
R	CCA TAA TGA ACC ACA TCA AAA GCC TGA CTT CTA TTG GCG GGG TAA GTA ACC **CCT GAT AGA CGG TTT TTC G**

Primers to Amplify *ABF1* Gene, Including 5' and 3' UTRs

F	GGA TGG ACA AAT TAG TCG TG
R	CTT CAA ACC CGA ACC CTT G

Primers to Amplify 388bp Region Incorporating *abf1-1* Mutation Site

F	GGA TGG ACA AAT TAG TCG TG
R	GCT AAC CTT ATT ATT ACT GCC

Primers to Amplify *sug2-1* Mutation Site

F	CTC CAG CGT CTG GTA TTG TGG
R	CG GCC TCA TTT GGC AAT GGG

271

Chapter 5.2.4 (Figure 5.2)
Primers to Amplify 252bp region of *SML1* ORF for Northern Analysis

F	(5' Biotin-Labelled) CAA CAA CAA GCC CCT TCC AC
R	CGA CCT TAC CCT GGT TGA AC

Primers to Amplify 419bp region of *CRT1* ORF for Northern Analysis

F	(5' Biotin-Labelled) GGT CCA AGT AAC GGA TCT TC
R	GGT ATT GGT ACG TTT GGC AG

Chapter 5.3.4 (Figure 5.6)
Primers to Amplify Promoter region of *DUN1* for ChIP

F	(5' Biotin-Labelled) *AAAAAA* CAG GAT GAA TCC AAA GCT CTA
R	AAA CGC TGC AAT TCT AAT GAG